Assessment of rock mass decay in artificial slopes

Beoordeling van de degradatie van gesteentemassa's in kunstmatige hellingen

Proefschrift

ter verkrijging van de graad van doctor
aan de Technische Universiteit Delft,
op gezag van de Rector Magnificus prof. dr. ir. J.T. Fokkema,
voorzitter van het College voor Promoties,
in het openbaar te verdedigen op
vrijdag 1 september 2006 om 10:00 uur

door Marco HUISMAN
mijnbouwkundig ingenieur

geboren te Gouderak

Dit proefschrift is goedgekeurd door de promotor:
Prof. dr. J.D. Nieuwenhuis

Samenstelling promotiecommissie:

Rector Magnificus	Voorzitter
Prof. dr. J.D. Nieuwenhuis	Technische Universiteit Delft, promotor
Prof. dr-ing. M. Alber, M.Sc.	Ruhr-Universität Bochum
Prof. dr. M.H. De Freitas	Imperial College London
Prof. dr. ir. A.A.A. Molenaar	Technische Universiteit Delft
Prof. dr. ir. F. Molenkamp	Technische Universiteit Delft
Dr. H.R.G.K. Hack	ITC
Dr. J. Rupke	Universiteit van Amsterdam / ITC

Dr. H.R.G.K. Hack en Dr. J. Rupke hebben als begeleiders in belangrijke mate aan de totstandkoming van het proefschrift bijgedragen.

Dit onderzoek is gefinancierd door het ITC, de Universiteit van Amsterdam (Alpine Geomorphology Research Group) en de Technische Universiteit Delft.

ISBN 90-6164-246-9
ITC dissertation number 137

(Vladimir) ***That passed the time.***

(Estragon) ***It would have passed in any case.***

(Vladimir) ***Yes, but not so rapidly.***

– Samuel Beckett, *Waiting for Godot*

Contents

Summary

"A narrator should not supply interpretations of his work; otherwise he would have not written a novel, which is a machine for generating interpretations." – Umberto Eco, *Postscript to The Name of the Rose.*

This research investigates the decay of rock masses underlying slopes, and seeks to quantify the relations of such decay with time and geotechnical parameters of the slope and rock mass.

Decay can greatly affect the geotechnical properties of rocks within engineering timescales, and may induce a rapid change in mass strength, from initial rock-like properties to soil-like properties in a weathered state., as well as a notable decrease of slope stability. Several rock types are known to have a high susceptibility to such decay within engineering timescales, most notably mudstones and gypsum-bearing formations.

The adjustment of rock masses to more surface related chemical and physical factors and processes has been considered. Three main processes involved in the temporal decay of slopes in engineering timescales are:

- Relaxation or redistribution of stress and strain following excavation by man or due to natural processes, leading to loss of structural integrity. This may lead to deformation and further exposure of the rock material to atmospheric influences.
- Weathering of the slope material:
  The rock material is altered physically or chemically in-situ, which causes weakening of both the material and the mass as a whole; this is associated with a decrease in block size, an increase in the frequency of discontinuities, and an increase in permeability.

- (Subsequent) erosion of the slope material:
  Weathered material, or unweathered material which is loosened by weathering and/or erosion of other parts, is transported away from its original location, destroying the relict fabric of the rock mass structure.

Following primary relaxation after excavation, the decay of a rock mass is a process seeking equilibrium between weathering and erosion whilst under the influence of on-going stress and strain redistribution in the form of secondary relaxation. The outcome of the decay process and the effects that the decay has on the geotechnical properties of the resulting rock mass, and thus, ultimately, the slope stability is determined by the extent to which such equilibrium is actually reached. Through conceptual modelling of these decay processes, three main situations have been distinguished:

- Imbalance favouring erosion (i.e. weathering-delimited).
- Equilibrium between weathering and erosion.
- Imbalance favouring weathering (i.e. erosion-delimited).

A data set obtained by twelve years of fieldwork has been used to assess and quantify the time-related decay of rock masses, and to analyse the influence of various parameters on the rate of decay through weathering. This encompassed Triassic formations of the Germanic facies type, notably Middle Muschelkalk, Upper Muschelkalk, and Keuper. A close relationship has been found between weathering intensity rates, the slope aspect and the prevailing wind directions during rainfall events, with a notable influence of damage to the rock mass by the applied excavation method. The exact relation differs from one geotechnical unit to another depending on the principal weathering processes that act on each unit. These relations can be used to predict weathering intensity rates and therefore also the weathering degree as a function of time. With the use of a probabilistic slope stability assessment method, predictions for future slope stability can also be made.

Marco Huisman

Samenvatting

"Een verteller moet geen interpretaties verschaffen van zijn eigen werk; anders had hij geen roman geschreven, een instrument om interpretaties te genereren." – Umberto Eco, *Naschrift bij De Naam van de Roos.*

Het onderzoek waarvan dit proefschrift het resultaat vormt is gericht op de degradatie van gesteentemassa's die in hellingen ontsloten zijn, met als doel om de tijdsafhankelijke degradatie van dergelijke gesteentemassa's, die van grote invloed kan zijn op de hellingsstabiliteit, nader te kwantificeren. Tevens is de invloed van diverse geotechnische randvoorwaarden op de degradatie onderzocht. Degradatie door toedoen van processen als verwering en erosie kan de geotechnische eigenschappen van het gesteente sterk beïnvloeden, en dat zelfs in de relatief korte tijdsschaal die bij geotechnische werken van belang is. De degradatie kan leiden tot een snelle achteruitgang in sterkte van de gesteentemassa, en een verandering van gesteente-achtige karakteristieken naar gedrag als dat van ongeconsolideerde grond in een verweerde toestand. Diverse gesteentetypen zijn zeer gevoelig voor deze degradatie; dit geldt met name voor klei- en gipshoudende zwakke gesteenten.

De deelprocessen van degradatie zijn het gevolg van de aanpassing van een gesteentemassa aan oppervlak-gerelateerde chemische en mechanische factoren en processen. Onderscheid wordt gemaakt tussen:

- Relaxatie na ontgraven, waarbij een herverdeling plaatsvindt van vervormingen en spanningen door de gesteentemassa. Dit veroorzaakt onder meer verplaatsingen langs discontinuiteïten en een verdere blootstelling van de gesteentemassa aan invloeden uit de atmosfeer.

- Verwering van het gesteente, waarbij het materiaal in-situ wordt aangetast door (een combinatie van) chemische en mechanische processen. Dit verzwakt zowel het materiaal als de massa, en gaat samen met een afname van de blokgrootte in de massa, en een toename van het aantal discontinuïteiten en waterdoorlatendheid.
- Erosie van materiaal van de helling, waarbij verweerd of onverweerd materiaal wordt losgemaakt uit de helling en wordt getransporteerd, met als resultaat dat het raamwerk van de gesteentemassa wordt verbroken.

Na de initiële ontspanning streeft degradatie naar een evenwicht tussen erosie en verwering. In hoeverre een evenwicht wordt bereikt bepaalt het resultaat van de degradatie en uiteindelijk ook de invloed van degradatie op de hellingsstabiliteit. Drie mogelijkheden worden onderscheden:

- Een onbalans ten faveure van erosie, waarbij de degradatie wordt beperkt door de snelheid van verwering.
- Evenwicht tussen erosie en verwering.
- Een onbalans ten faveure van verwering, waarbij de degradatie wordt beperkt door de snelheid van erosie.

Met behulp van een dataset, die de neerslag vormt van twaalf jaar veldwerk, is de tijdsafhankelijke degradatie van verschillende formaties gekwantificeerd, tezamen met de invloed daarop van diverse geotechnische parameters. Het onderzoek heeft zich gericht op formaties uit het Trias, te weten de Midden-Muschelkalk, Boven-Muschelkalk en Keuper. Een goede relatie is gevonden tussen de snelheid van verandering van verweringsintensiteit, de orientatie van de helling en de overheersende windrichtingen tijdens neerslagsituaties, waarbij ook invloed van de opbreking van het gesteente als gevolg van de ontgraving zichtbaar is. De precieze relatie verschilt per geotechnische eenheid, en hangt af van de primaire verweringsprocessen die in elke eenheid een rol spelen. Met behulp van deze relaties kunnen de verweringsintensiteit en de hellingstabiliteit voorspeld worden als tijdsafhankelijke variabelen.

Marco Huisman

Acknowledgements

"Himalayan climbing is about putting one foot in front of another and breathing whilst doing so. Keep doing this and you'll make it." – Roger Baxter-Jones, *Shisha Pangma – The alpine-style first ascent of the South-West Face.*

The English mountaineer George Leigh Mallory once famously replied to the question *"Why climb Everest?"*: *"Because it's there"*. It is tempting to describe this research as a veritable mountain which I had to climb and, like Mount Everest in Mallory's days, the topic already existed for quite some time. David Price, of whom I had the privilege to be a student, Jan Nieuwenhuis, Robert Hack and Jan Rupke – they were working on the problem of susceptibility to weathering and rock mass decay in road cuts well before I was. Thanks to you all for giving me the opportunity to tackle this peak, and for pointing out the route that I was supposed to be climbing every now and then.

Jan Sevink of the University of Amsterdam must be thanked for his review of the data analysis. With Michael Alber in the committee we close a circle since Michael's visit to us several years ago, and it is my pleasure to have him present at the public defence. This also applies to Michael De Freitas whose thorough review gave me some useful thoughts and new insights.

All the help and advice I received from my previous colleagues of the former Division of Engineering Geology at ITC was greatly appreciated – Hans van Noord, Senol Ozmutlu, Niek Rengers, Siefko Slob, Rob Soeters, and Wolter Zigterman. Thanks also to Radko Kühnel – *děkuju* for sharing your knowledge, Radko. If there is one person to mention and say thanks to for the support of ITC in general, it is definitely Martin Hale, but the help of

Loes Colenbrander and Andries Menning in finalizing this thesis should also not go unnoticed. With respect to my employer Bluewater Energy Services, I would particularly like to thank Richard Leeuwenburgh, for allowing me this distraction from subsea activities.

I received wonderful assistance from Wim Verwaal and Arno Mulder of the Delft University of Technology, who helped me through all the tricky bits of sampling and laboratory testing. Laurent Gareau, Salomon Kroonenberg, Michiel Maurenbrecher, Keith Turner and Peter Verhoef provided more-than-useful feedback in our discussions, apart from making excellent fieldwork partners in Spain! Ruud Ephraim and Karl-Heinz Wolf were of great help in the tedious work of microscopic analysis and XRF/XRD interpretation.

I should also thank the very international group of students who worked on this subject during my research and who suffered my scrutiny: Guru Prasad Adhikari, Binod Chapagain, Indra Chhetri, Diana Franco Rodriguez, Eddy Hernandez, Geert de Jong, and Wiebke Tegtmeier.

Thanks also to my parents and brother, for your care and support. And, of course, mountaineering is never complete without Lisa climbing up there with me – and this enterprise has been no exception to that.

What I write here is the account I believe to be true.

- Hekataios of Milete, *Genealogiai*

1 Introduction

"...I mean to paint for you as best I can, which is but poorly, which is but a rude man's art, the sound of water on stone, the fool's dream of the hard giving way to the soft..." – Richard Flanagan, *Gould's Book of Fish*.

1.1 The research

The problem of infrastructure works that become unsafe with time due to decay of rock and soil masses in artificial and natural slopes is a well-known feature in every part of the world. Some road cuts stand up for a century with sometimes even no apparent loss of safety, whereas some will already show failures during construction. Some will fail after one year, some after ten, some after seventy-five. The question is: why this difference?

Early failures are not all explained by improper design or engineering, just as the fact that many road cuts are only expected to serve for about fifty to seventy-five years does not mean that the century-old ones have only benefited from costly overdesign.

Apart from straightforward improper design and engineering as far as these are based on existing knowledge and experience, the answer to the question above is that there are processes acting on the slope that may cause a significant decrease in geotechnical strength and slope stability, yet are poorly understood, only marginally quantified, and often simply neglected in slope design because of this. These decay processes are relaxation after stress release, and loss of rock mass quality due to weathering and erosion. Many economically hazardous and potentially life-threatening mass movements in artificial as well as natural slopes are caused or facilitated by decay of soil and rock under the influence of such processes (e.g. Hencher

and McNicholl, 1995; Nieuwenhuis, 1991a/b; Nieuwenhuis, 2002). This time-related decay of soil and rock affects all engineering structures that involve natural, in-situ materials, but is most easily recognized in artificial slopes on which the study at hand focuses.

For the safe construction of a road cut with respect to its envisaged engineering lifetime, it is therefore of vital importance to incorporate in the initial design not only the present-day geotechnical characteristics, but also the dominant time-related processes that control the engineering behaviour of soil and rock masses in time as well as the rate of decay of the rock mass quality. These processes can be governed by external (e.g. atmosphere) as well as internal factors (lithological, physical and chemical). The involved processes may act on a micro-scale of millimetres or less. Still, on the macro-scale of natural and artificial slopes that ranges from metres to tens or hundreds of metres, these processes acting on various geotechnical units combine to affect the stability of the slope itself in the positive or, more often than not, the negative sense.

The understanding of the generally slow processes that determine the decay of soil and rock masses, and their impact on slope stability, is required for sustainable development in civil and environmental engineering [1]. Governmental planning departments throughout the world now give more and more special attention to these phenomena and, hence, to sustainable development. Interest in slow processes of decay of soil and rock is also shown by insurance and civil engineering companies to predict and to limit future economic and environmental risks due to civil engineering and infrastructure works.

Proper prediction of the future engineering behaviour of soil and rock masses is of the utmost importance for safe design and construction of civil

[1] *A main objective of the policy of various international organizations – a recent example was the United Nations International Decade of Natural Disaster Reduction (IDNDR), 1990-2000 (Rengers et al., 2001).*

engineering structures (e.g. Price, 1993 and 1995), by facilitating the early recognition of engineering geological problems. It will also provide a means to incorporate suitable safety margins for a certain civil engineering structure within the planning stage and execution of the construction, without exaggerating safety factors and thus unnecessarily increasing the costs.

To be able to conduct a slope stability hazard assessment, which incorporates the time-related development of the slope stability within practical economical and temporal restraints, first of all the number of geotechnical characteristics to be investigated and the associated number of parameters to be measured has to be limited. This applies to both natural and artificial slopes; in artificial slopes an extra difficulty in the form of a decrease of mass quality due to excavation is encountered. Natural slopes subjected to rapid erosion of the slopes themselves or rapid deepening of adjacent valleys may show similar decay of rock mass quality. In artificial slopes, decay is the rule rather than the exception. In both natural and artificial slopes, it is important to have insight into the complex of external and internal processes acting from outside or inside the rock or soil masses.

1.2 Problem definition

1.2.1 Background

The concept of rock mass decay includes a wide range of diagenesis (weathering[2]) and erosion processes with widely varying rates and effects, as well as loss of structure due to stress and strain redistribution. The combination of these processes often leads to a significant weakening of a

[2] *Diagenesis is any modification of rock material from its initial stage (volcanic or sedimentary rock). These modifications may strengthen (through compression, precipitation recrystallization) or weaken (through extension, solution, alteration, low quality precipitates) the rock mass. In this thesis, modifications leading to degradation of a rock mass are considered under the comprehensive term "weathering".*

rock mass in terms of geotechnical applications. It should however be noted that in some cases the rock mass quality may actually improve locally by weathering related processes (e.g. case hardening by precipitation of duricrusts).

The research at hand deals with decay affecting rock masses underlying natural and especially artificial slopes during periods in the order of 50 to 100 years after exposure of the rock mass to the atmosphere. This means that the amount of decay that is to be expected strongly depends on the susceptibility of the rock mass to the various decay processes that occur in today's environment. However, the history of the rock mass in question on a geological timescale should also be appreciated, since that will define the starting point for the current-day decay processes to work on (e.g. Nieuwenhuis, 1991a/b).

Conceptually, the decay of a rock mass in geotechnical terms following the initial stress release after excavation can be described as a process seeking equilibrium between weathering and erosion as well as on-going stress and strain redistribution. The extent to which such equilibrium is actually reached influences the outcome of the decay process and the effects that the decay has on the geotechnical properties of the resulting rock mass. Three main possibilities can be distinguished:

- Imbalance favouring erosion.
- Equilibrium between weathering and erosion.
- Imbalance favouring weathering.

During the considered time spans of 50 to 100 years a given rock mass exposed to the atmosphere may change from one of the possible situations listed above to another. This will be the case even if no changes in the decay environment occur; slopes that initially show an imbalance favouring weathering are likely to tend towards equilibrium between weathering and erosion. Depending on the prevailing weathering and erosion rates such equilibrium may or may not be reached in the time spans considered. The

balance between weathering and erosion is, however, a delicate one; this issue will be addressed in detail in paragraph 2.7.

1.2.2 Scope

Determining the decay of geotechnical parameters in time is difficult in most subsurface infrastructural engineering works. However, in slope processes a good monitoring of processes and parameters is possible as the material and processes are for a large part visible – an important difference with structures as tunnels and foundations. The visibility of the material in slopes allows determining and monitoring the behaviour of the material in a relatively easy way. Therefore this research is restricted to slopes of the following types:

- Rock faces, either artificial or natural, from which the height and slope angle can be established in detail in the past and at present. Heights of these slopes are in the order of 1 up to 100 m.
- (Geotechnical) soil slopes, also with heights up to 100 m.

The height is necessarily a limit as for larger slopes usually the variation in different materials also increases. Slope movements, which are not triggered by internal processes related to the cut itself but rather by "foreign" influences, either natural (such as earthquakes, or subsidence due to karst formation) or man-induced (such as subsidence over mine works), are not considered in this research.

1.2.3 Research objectives

The objective of the research is to determine the relation between time and decay of rock and (geotechnical) soil masses. The future decay of rock and soil masses exposed in infrastructure works and the subsequent decrease of the quality of geotechnical parameters in the future can be quantified more reliably, thus leading to the possibility of adapting design parameters and reducing costs through lowering the degree of uncertainty. Secondly the better possibilities to determine future behaviour of rock and soil masses may allow for more quantified slope hazard analysis and for narrowing the gap between earth sciences and civil engineering.

1.3 Data sources

The classification data set used in this research was gathered during engineering geological mapping fieldworks in the Falset area by the author, students and staff from ITC and the Delft University of Technology, in the period of 1990 until 2004. Previous compilations of available data were made by Kouokam (1993), Hack (1998), Chapagain (2001), Hernandez (2002) and De Jong (2003). In Appendix H, the method of data gathering and the resulting data set are described further.

1.4 Research area

The primary data set used for this research consists of classifications made in an area surrounding the town of Falset, stretching over the *comarcas* (administrative regions) of Priorat, Baix Camp and Ribera d'Ebre, which all form part of Catalunya in northeastern Spain (Figure 1).

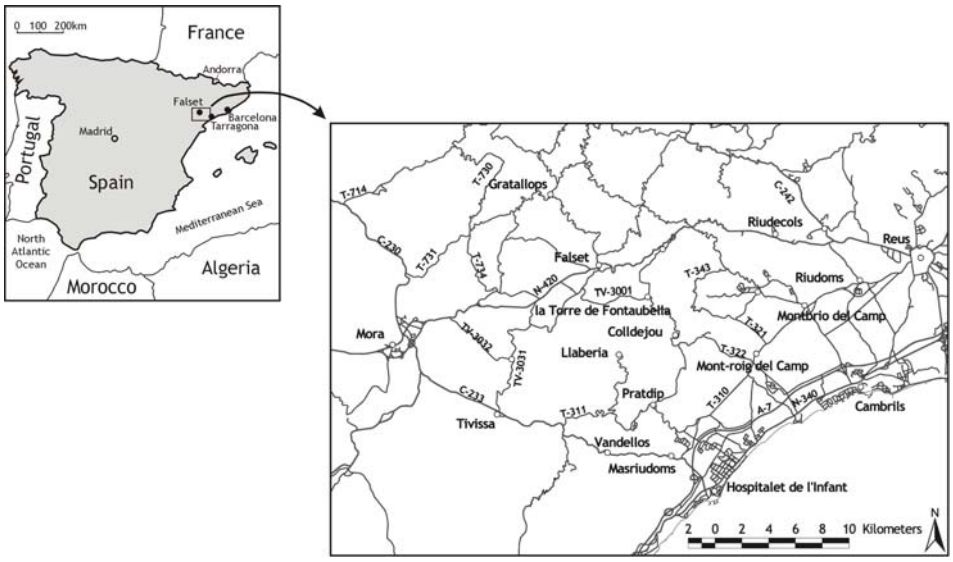

Figure 1 – The research area around Falset in Catalunya, northeastern Spain.

In the research area, the southwest-northeast orientated Catalanides mountain range, also known as the El Camp Mountain Front (Masana, 1994), separates the coastal plains to the southwest of Reus from the Ebro river basin around Mora d'Ebre (Figure 2). The Catalanides rise up to about 1000m above sea level; the town of Falset itself lies on the western side of the range at an altitude of 350m asl.

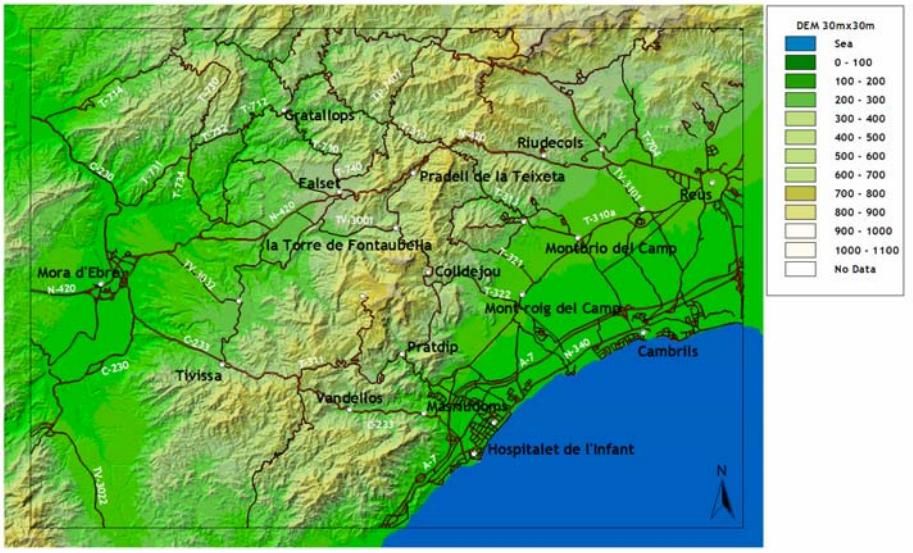

Figure 2 - Topography and main roads of the Falset research area.

The area is underlain by a sedimentary sequence of Devonian through Quaternary age. Igneous rocks occur, intruded into Carboniferous formations as granodiorite bodies and aplitic dykes. The majority of the intrusions are from Carboniferous to Permian age and possibly associated with the Hercynian orogeny; minor intrusive phases occurred during the Alpine orogeny. The data set used in this study has been collected in the Triassic sediments of the Middle Muschelkalk. The Triassic rocks correspond with the Germanic facies type, characterized by massive or very thickly bedded sandstones with basal conglomerate beds (Buntsandstein), followed by thickly bedded limestones and dolomites (Lower Muschelkalk), sandy clayey siltstone with gypsum content (Middle Muschelkalk), limestones and dolomites with marly intercalations (Upper Muschelkalk),

and a sequence of shales and siltstones, in the lower part interbedded with limestones and dolomites (Keuper). On top of the Keuper, as the youngest and stratigraphically uppermost formation in this Triassic series, undifferentiated dolomites occur. A description of the geological and geotechnical units in the area is given in Appendix A.

The climate in the area is characterized by dry, hot summers and moderate winters. Precipitation is highest during the autumn. The wind usually blows from the northwest; this wind, locally called the *mestral* or *sere*, is strongest in autumn and winter and may then occasionally reach wind speeds up to 100 km/h. In the summer a sea breeze locally known as the *marinada* is common. The topography of the area in combination with the prevailing wind directions leads to the formation of several microclimates, and in broad terms three sub-areas can be distinguished on the basis of the local climate. An overview of the climate characteristics for these three sub-areas is presented in Table 1. Today's climate of the area is discussed in detail in Appendix B.

Table 1 - Basic climatic data for the Falset area.

		Ebro basin	Catalanides	Coastal plains
Mean annual temperature	[°C]	14 - 16	12 - 14	15 - 17
Mean annual precipitation	[mm]	400 - 550	600 - 750	500 - 650
Mean annual evapotranspiration	[mm]	700 - 1000	600 - 850	700 - 850

Extensive agricultural use is made of the soft soils and weathered rocks in the valleys, and the coastal plain. The more mountainous areas that are underlain by stronger sandstone or limestone rock masses are mainly covered with small bushes and forests. A number of small villages and towns are found near the fertile areas, and are connected by a system of roads and tracks. Many road cuts in the area have been constructed or renewed in the first half of the 20th century using several excavation techniques. Since 1988 new roads have been constructed, and some of the older roads have been realigned; at several locations construction works are carried out at present.

Throughout this thesis, several slopes are used to serve as examples with the processes and effects discussed in the text. These slopes are described in Box 1 and Appendix G.

Box 1 - Case study slopes

Out of the 426 individual classifications that were used for this research (described in Appendix H), four slopes that show a variety of processes are used as examples in the following chapters illustrating the processes and theories described in the text. The locations of these four slopes are given in Figure 3. Appendix G shows oblique photographs of these slopes.

Figure 3 - Locations of case study slopes in the Falset area.

Gavadà – Keuper shales
A small road leading from the C-233 at the Coll de Fatxes to the south, past the farm locally known as Geinessies towards the settlement of Gavadà and the Coll d'Aumet, was reconstructed and widened in 1999, and a number of small road cuts had to be made. Since the road approximately follows the boundary between Upper Muschelkalk and Keuper for some distance, this reconstruction provided the rare opportunity to see and watch relatively intact Keuper shales and their decay. A small cut around N4543330/E314815[3] was investigated in detail for this.

➲

[3] *All coordinates reported in this thesis are in UTM projection (UTM zone 31, northern hemisphere), Hayford Ellipsoid, European Datum (ED50).*

Masriudoms – Middle Muschelkalk siltstones
At the western edge of the village of Masriudoms around N4543282/E322140, a road cut comprising two opposite slopes was excavated in Middle Muschelkalk siltstones in 1992, during reconstruction of the C-233 road that leads from Hospitalet de l'Infant to Mora de l'Ebre. The slope on the north side of the road has an orientation towards 198°, whereas the south slope is orientated towards 020°.
The slopes were excavated with excavators and scrapers since blasting is not required in this relatively weak formation. The as-built slope angles were between 50° and 60°, comparable to other excavations made in the same unit during this reconstruction project along the C-233, and excavations made between 1988 and 1990 along the N-420 near Pradell de la Teixeta. The old road alignment in use until 1992 circumvented a small hill; the new road cuts straight through this, exposing the Middle Muschelkalk of which it is made. Both slopes have had very much the same weathering history until the time of excavation; the historic development until 1992 in terms of hydrology, surface cover influencing infiltration, vegetation cover influencing groundwater pH, surface erosion and associated stress release et cetera has been similar. The same holds true for the lithology; at distances like this, with both slopes at the same stratigraphical level due to the near-horizontal bedding, no major lithological differences influencing weathering and erosion behaviour are to be expected in this formation. The two slopes can therefore be used to compare the differences in weathering and erosional development since excavation, that exist because of differences in slope orientation.

La Torre de Fontaubella – Upper Muschelkalk ("Cindarto slope")
The so-called "Cindarto-slope" has been the subject of a detailed site investigation study by Cindarto (1992). The slope is located along the TV-3001 between La Torre de Fontaubella and Marçà, at N4554790/E318020 and is excavated in Upper Muschelkalk limestones. The road cut had been a liability for block slide failure ever since its excavation in the 1950/1960's because of a day-lighting bedding plane with dip angle of 37° that is dipping directly towards the road. In 1991 such a failure indeed occurred. In the following years the slope was investigated in detail. The geometry was recorded using triangulations and over the years several rock mass characterisations and classifications were made, and samples were taken for laboratory testing.

Hostal – Keuper shales and limestones
This slope is located along the N-420 road, at location N4557925/E320500. The slope length and height are 225m and 40m, respectively. It faces approximately east (110°) and was constructed with an average slope angle of 70°. The initial excavation for realignment of the N-420 was made in 1988; since then, the slope geometry has changed considerably because of erosion and mass movement of weak layers and rock fall as well as periodic re-excavation works.
The slope consists of marls, limestones and dolomites of the Keuper formation. The Keuper sequence in this area is typically represented by red and greenish shales, with regular intercalations of dolomite and limestone. These harder layers may have a considerable thickness, as in the study slope, with the thickest dolomitic limestone bank measuring about seven metres.

1.5 Classification methods

The basis for the decay analysis of the slopes in this study is the Slope Stability Probability Classification (SSPC) system, which was designed and validated specifically in the research area (Hack, 1998). Since its development, the SSPC system has also been used outside of Spain as well; studies have been made in Bhutan (Chhetri, 2005), the United States (Knott, 2004), New Zealand (Lindsay et al., 2000), Costa Rica (Sigaran, 2005), the Philippines, and South Africa. The classification involves a description of the rock material and rock mass properties according to the British Standard BS5930 (1981), together with a more elaborate description of the discontinuities. The SSPC method can be described as a three-step classification system and considers three rock masses (Hack et al., 2003):

a) The rock mass in the exposure: the "exposure rock mass" (ERM).
b) The rock mass in an unweathered and undisturbed condition prior to excavation: the "reference rock mass" (RRM).
c) The rock mass in which the existing or new slope is to be situated: the "slope rock mass"" (SRM).

First, rock mass parameters of importance are described and characterized in an exposure resulting in the "exposure rock mass"; this is the actual field classification and represents a natural outcrop or pre-existing cut in the area of the future excavation. This exposure rock mass is then converted into a theoretical rock mass, of which the properties are corrected for local influences such as weathering and the disturbance due to the excavation method. This theoretical mass is termed the "reference rock mass" (RRM) and respresents a (hypothetical) rock mass that is unweathered and unaffected by excavation. The actual stability assessment is made in the "slope rock mass" (SRM). This is derived from the "reference rock mass" (RRM) by correction of the parameters of the "reference rock mass" with the slope specific parameters. Slope specific parameters are correction parameters for the influence of future weathering within the engineering lifetime of the slope and for the influence of the method of excavation to be used (Hack et al., 2003).

In the SSPC, the stability of a (future) slope in the slope rock mass is determined in two different analyses: orientation dependent or orientation independent. The first is related to the orientation of the discontinuities and the slope and considers sliding and toppling, the second considers slope failure that is not related to discontinuities.

1.6 Outline of thesis

Following the introduction in chapter 1, chapter 2, "Rock mass decay in geo-engineering", describes the essence of the research: the effects and consequences of rock mass decay in geo-engineering, particularly in slopes, and the way in which it can be perceived, described and quantified. This chapter emphasizes on how the interaction of different decay processes (notably erosion and weathering) affects excavated slopes, and the potential results that may be derived from the combination of processes.

Observations on primary decay processes in the investigated engineering geological units in the research area are described in chapter 3, "Observations on decay processes in slopes". The seven units that have been regarded for this research show various forms of decay. As it will be apparent later on in the thesis, today's climate in the area can explain the observations made on weathering intensity and weathering rates.

Chapter 4, "Conceptual model for weathering and erosion", defines the interaction of erosion and weathering in slopes in terms of a numerical model. The results of this are compared to the qualitative description of the underlying phenomena in chapter 2.

Following the conceptual modelling of chapter 4, chapter 5, "Time-dependent weathering intensity: empirical results" gives an analysis of empirical data shows the relevance of local climate for the anticipated rates of change in weathering intensity. Since it is the weathering intensity that influences slope stability in the stability assessment as incorporated in the SSPC system, observed trends can be applied to the prediction of slope stability development through rock mass decay.

In chapter 6, "Applications and limitations", the practical implications and applications of the research results are discussed. Conclusions and recommendations follow in chapter 7.

In the appendices, several topics are discussed, starting with Appendix A, "Geology of Falset research area". In Appendix B, "Climate", the current climate conditions in the research area are discussed that are related to observations on rock mass decay in chapter 5. Appendices C and D, "Weathering processes" and "Erosion processes", present background information on weathering and (wet) erosion. Some previously existing models and theories that describe rock mass decay, or its isolated underlying processes, are described in Appendix E, "Weathering and erosion models in literature". Appendix F, "Data simulation and bootstrapping", describes the statistical procedure used to evaluate the observations on weathering in chapter 5. Several case study slopes that are used throughout the thesis to provide examples with the text are presented in Appendix G. Finally, Appendix H contains an overview of the data set used for this research.

Following the appendices, the literature references are included as well as an overview of symbols and abbreviations, a glossary of technical terms, a keyword index, and the author's curriculum vitae.

Key figures in the thesis are:

- Figure 14 (page 55), which explains the definition of weathering rates as followed in this thesis;
- Figure 15 (page 60), which shows the difference between actual decay development, the description according to classification systems, and the idealized concept;
- Figure 18 (page 64), Figure 19 (page 66), and Figure 20 (page 67), that summarize the possible decay situations that arise from the balance between erosion and weathering penetration rates;

- Figure 49 (page 115), that relates conceptual modelling results to the situations described in Figure 18, Figure 19, and Figure 20 (see above);
- Figure 51 (page 123) to Figure 57 (page 126), that give apparent weathering intensity rates for the various engineering geological units as derived from the data set through a bootstrap analysis.

2 Rock mass decay in geo-engineering

"The problem with the future is that it keeps turning into the present." – Bill Waterson, *Calvin & Hobbes: Attack of the deranged mutant killer monster snow goons.*

2.1 Effects and consequences of rock mass decay in slopes

Decay in general and more specifically weathering of rock masses exposed in slopes can greatly affect the geotechnical properties of those rocks within engineering timescales, and even induce a rapid change of rock material from initial rock-like properties to soil-like properties (e.g. Gökceoğlu et al., 2000). The influence of weathering on geotechnical properties of rocks and soils and its engineering significance has been investigated in a wide range of materials and environments (e.g. Chandler and Apted, 1988; Fookes and Hawkins, 1988; Chigira and Oyama, 1999; Ehlen, 1999; Gupta and Rao, 2000). Several case studies show the importance of chemical and physical weathering in the behaviour of geotechnical constructions and the relation between weathering processes and instability phenomena (e.g. Chigira et al., 2002); this not only applies to constructions on in-situ materials such as road cuts (e.g. Francis, 1987), but also to constructions such as bridges made of natural stone (e.g. Jiang and Esaki, 2002).

The importance of understanding and acknowledging the decay processes that result in such changes lies not only in stabilizing existing slopes along infrastructure, or optimizing the design of future slopes; Smyth and Royle (2000) indicate that the importance goes beyond this and also affects urban development and human safety in settlements. In recent history, examples

abound where slope instability has caused tremendous economical damage as well as loss of life (e.g. Brabb and Harrod, 1989). Any new insight into the processes that cause slopes to become unstable with time may help to limit future hazards. The study at hand is however limited to decay in road cuts. This in itself is an all-too-common problem in geotechnical engineering and many examples of slope failures due to decay exist. As an example, Calcaterra et al. (1998) describe mass movements that have occurred in weathered slates in the Sierra de Collcerola, northwest of Barcelona: *"many of these failures involved slopes cut along recent infrastructures: debris flows, wedge and plane failures, generally surficial, occurred more frequently"*.

The engineering significance that the particular degree of weathering at a given moment in time has on the geotechnical behaviour of a rock mass is a subject on which several researchers have worked. In most cases, published results deal with masses with relatively high weathering intensities, such as residual soils (e.g. Vaughan et al., 1988), but some deal with chemical weathering and its influence on intact rock (e.g. Williams and McNamara, 1992). In general, the problem of rock mass decay within engineering time has been a subject of investigation for several decades. In an early paper, Fookes et al. (1971) already addressed the influence of a given degree or intensity of weathering on the engineering behaviour of a number of rock types, rather than going into weathering and decay occurring within engineering time-spans. They did describe the problem however, defining weatherability as *"the susceptibility of rock to short term weathering"* and stating that this aspect can prove to be of considerable importance in engineering. It was already acknowledged that *"several kinds of alteration are possible and a material which is an end product of weathering under one set of conditions may become raw material for renewed weathering if conditions change"* (Fookes et al., 1971), a statement which essentially describes the possibility of significant decay after excavation of slopes and exposure of the involved rocks to the environment. These problems are further addressed in Fookes and Sweeney (1976), describing the practical engineering problems that can arise if the rock mass underlying a slope is exposed, and the remedial works that may be required to limit the

consequences of rock mass decay. Later, Fookes et al. (1988) published a key paper designating the importance of weathering and rock mass decay in geotechnical engineering.

In the series of papers by Fookes et al. mentioned above, the idea is followed that a change in thermodynamic conditions from the environment of formation to the present day atmosphere and its associated general climate type are determining weathering and also weatherability. This point of view is by now overtaken by newer insights that indicate the reasons for weathering to be more complex[4] (e.g. Pope et al., 1995; Trudgill, 2000). Still, the problems that arise from the decay continue to be a major concern. Price (1995) considers weathering as *"one of the greatest sources of potential difficulties in geotechnical engineering"* because it may:

1. Considerably modify material and mass engineering properties;
2. Result in a distribution of these modifications in a way which is very difficult to forecast;
3. Produce variations in the distribution of mass properties which cannot be readily dealt with by calculation techniques;
4. Modify material and mass engineering properties after the engineering work has been completed.

Nicholson (2003) has also investigated in detail a fifth consequence of weathering and decay in general, namely the effects on morphology due to erosion and gravitationally induced transport:

[4] *For example, as Pope et al. (1995) describe, the difference between the environment of formation of a rock mass and the environment to which it may be exposed today may not be the governing driving force behind weathering and in many cases will not be directly related to weathering susceptibility. Think for example of weathering-resistant granites that were formed under high pressure and temperature, and weathering-susceptible shales that were formed under conditions much more in resemblance with today's atmosphere.*

5. Morphological consequences in the form of boundary modification (receding crest / build-up of debris at toe and their effects on infrastructure, such as partial or complete blocking of roads and stability problems in roads or civil constructions lying above the receding slope), aesthetic impact (effects on the overall appearance of the slope landform), conservation impact (effects on sites of social or cultural interest, and hydrological changes in the physical and/or chemical weathering front.

The fourth point including its geotechnical consequences forms the subject of this thesis, and an example of its importance is given in Box 2. Insight into the relevant processes and a prediction of the amount of decay and its bearing on the stability of a slope should ideally be appreciated and incorporated already in design stages. The importance of accurate site description including expected future developments in geotechnical engineering was further emphasized by Hutchinson (2001), who states that such a site description should not limit itself to present-day circumstances, but should also reflect on expected behaviour in the future in as far as that is relevant to the project at hand. The relevance of insight into the processes of weathering and rock decay is not limited to the field of geotechnical engineering alone; land conservation (e.g. leaching) and mineral exploration (e.g. laterite development) also have high stakes in weathering research. And even on a global scale weathering plays its part, having a direct relationship with the Earth's climate[5] (Dupré et al. 2003) albeit mostly on a completely different time scale than for its role in engineering.

The second and third point are addressed in a paper by Hencher and McNicholl (1995) and in the Ph.D. thesis of Nicholson (2001a) and related papers (Nicholson and Nicholson, 2000; Nicholson and Lumsden, 2000; Nicholson, 2001b; Nicholson, 2003), and should not go unaccounted; the

[5] *It is interesting to note that although weathering is usually assumed to be the result of a particular climate, it may on a different and far longer timescale also affect and change that same climate by its products, notably carbondioxide (CO_2).*

highly inhomogeneous rock profiles that can result from weathering (be it long-term or short-term) are posing serious problems to the geotechnical engineer. Next to decay in time (point 4), this may lead to hazardous and unforeseen complications as early as the excavation stages. Since weathered rock profiles may be very complex and irregular, the resulting variability cannot usually be predicted using standard methods of geological interpolation and extrapolation (Hencher and McNicholl, 1995).

2.2 Decay processes and their engineering significance

2.2.1 General

As Kühnel (2002) stated, *"rock degradation begins by weakening of the rock and ends with its disintegration and total decay"*; a study into rock mass decay should ideally address this complete range of processes.

Three main processes that are involved in the temporal decay of slopes in engineering timescales are:

- **Relaxation** or redistribution of stress and strain, leading to loss of structural integrity:

  Primary relaxation will occur directly following excavation, in the course of days to months. As a result, discontinuities are slightly opened giving access to water. The normal stress on discontinuity planes decreases, and usually so does the friction resistance (an important long-term exception to the latter is formed by cases in which growth of crystals in the opened discontinuity effectively cements the surrounding material). This primary relaxation is the direct result of excavation itself, and is of influence on weathering and erosion through the above mentioned processes.

  What will be called secondary relaxation in this thesis will occur after excavation due to the effects of weathering and erosion. Due to ongoing changes in material strength, density and volume, slope angle and slope morphology, stress-strain redistribution will be a continuing process even after the primary effects of major stress release during excavation have dissipated.

Box 2 – Decrease of friction angle by rock mass decay, Cindarto slope

The 1991 slide that affected the Cindarto slope occurred on a bedding plane with an inclination of 36°-37° towards the road. Sections with a smaller dip angle were not affected (Figure 4).

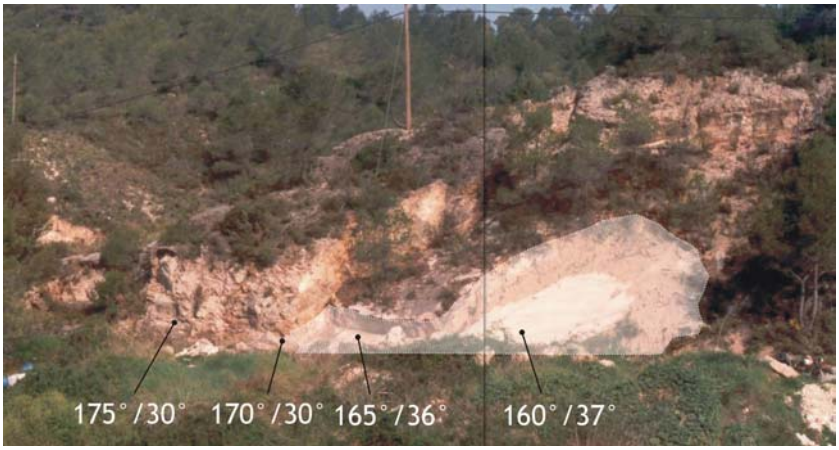

Figure 4 - The Cindarto slope in 1993, showing the area affected by the 1991 slide. Original photo by A. ten Katen.

In 1991, the bedding planes were found to contain some clay infill (Cindarto, 1992). This was at that time no more than a thin dusting on the bedding plane surface resulting from weathering. In 2002 parts of the outcropping bedding planes, and especially the bedding plane that acted as sliding plane in 1991, were found to contain a significantly thicker slightly plastic layer of approximately 8mm. Material analysis using XRF/XRD testing indicated a montmorillonite content in this layer of approximately 3% by volume, and a total clay content including non-swelling clays of approximately 14%. Apart from the plastic layer, the discontinuity walls were weathered to a depth of about 3mm (see Box 6, page 61).

In 1991 and 1992 shear box tests have been done on the bedding planes (Cindarto, 1992). The shear box friction angle from these tests is 45°, with no (apparent) cohesion. The clay infill on the bedding surface (which was very thin; 1-2 mm) as observed in the field was lost during the sawing and sample preparation and not present during the actual shear box testing. Block samples incorporating the plastic layer observed in 2002 were taken in 2003 and tested in the shear box with the plastic layer as the slide plane. The average friction angle was now 27°. A small apparent cohesion was found of 14 kPa (Huisman et al., 2004).

The decrease of rock mass strength properties is considerable, and with ongoing decay further slope stability problems may be expected. If the plastic layer extends underneath the potential sliding blocks with the thickness found in the outcrop, the safety factor of the remaining part of the slope in dry conditions will be 0.88 and the SSPC stability probability for sliding only 2%.

A common outcome of such secondary relaxation is the effect known as creep, a process which is only quantified with difficulty. The stress-strain redistribution during secondary relaxation will itself influence the type and intensity of the weathering and erosion processes occurring in a slope as well as the equilibrium between the two.

- **Weathering** of the slope material:
  In-situ, the rock material is altered physically or chemically, causing weakening of both the material and the mass as a whole. This is associated with a decrease in block size, an increase in the frequency of discontinuities, a reduction of the shear strength along discontinuities, and an increase in permeability.
- (Subsequent) **erosion** of the slope material:
  Weathered material, or unweathered material that is loosened by weathering and/or erosion of surrounding parts of the rock mass, is transported away from its original location, destroying the rock mass structure.

These processes are mostly restricted to a relatively shallow zone in the rock mass close to the slope surface, and such shallow surface processes are usually not taken into account in slope stability assessments that commonly address deep-seated instability. Rock mass decay is not always recognized as a significant process, it is difficult to quantify, and its mechanisms are not well understood (Nicholson and Lumsden, 2000).

2.2.2 Relaxation

2.2.2.1 Primary relaxation

Primary relaxation occurs soon after excavation of a slope, with time generally counted in days to months. This primary relaxation (as opposed to long-term secondary relaxation) is what is classically described with terms as rebound (Ollier, 1975). Excavation of rock masses reduces the overburden stress in the underlying strata, thereby leading to elastic relaxation and expansive recovery (Wetzel and Einsele, 1991; Nicholson and Lumsden, 2000). An important consideration in slope excavation is that not only the

overburden stress is decreased, but also the horizontal stress confining the rock mass underlying the slope. Therefore stress distribution may become anisotropic.

Because of this primary relaxation of the rock masses and the resulting volume increase, several simultaneous effects occur that are interrelated and partially enhance each other. Principal effects are that porosity and permeability of the rock material are increased due to the formation of microcracks in cemented material; flowpaths of running water are changed; and the normal stress on discontinuity planes is decreased leading to a considerable increase in their aperture. The aperture may further be affected by shear displacements that can occur as a result of a decrease of the confining stress (Yeo et al., 1998). However, the effects of relaxation go further than these. Other effects include shear displacement along discontinuities leading to non-fitting and breaking of asperities; rotation of blocks; unbalanced elastic expansion of intact blocks that introduce shear stress and consequent fracturing of intact rock.

As a result, several important changes occur in the rock mass characteristics:

- Most often, both the effective friction angle and the cohesion of the discontinuities are decreased due to non-fitting of discontinuities and shearing of asperities. Together with a reduction of the normal stress on discontinuity planes, this destabilises the rock mass in question. In combination with the steepening of the existing topography by excavation, this can lead to irreversible deformation of the rock mass.
- As a result of increasing aperture (due to decreasing confining stress) and shear displacement along discontinuities, the hydraulic conductivity of discontinuities is increased, and water circulation and penetration is enhanced (Wetzel and Einsele, 1991; Indraratna et al., 1999; Vicente Silvestre et al., 2002). As Indraratna et al. (1999) demonstrated, aperture of the discontinuities is (next to

roughness of the discontinuity walls) one of the primary factors influencing the flow rate of percolating water.

This effect renders the rock mass more accessible to weathering agents, increasing the potential for chemical weathering (e.g. solution) and physical weathering (e.g. slaking by wetting and drying). The effects of the presence of water and the processes that occur where the rock mass is wetted thus extends further into the rock mass. As a result of enhanced water circulation, the relative humidity in the unsaturated zone may also fluctuate more frequently, again promoting chemical and physical weathering.

The overall increase in volume that results from the combination of reversible (elastic) and irreversible deformation of the rock mass and material following excavation leads to outward displacements. The relevance of this for geo-engineering is apparent; a recent case example in the research area is described in Box 3. Resulting deformations cannot be readily described by analytical models because of their complexity; numerical studies have been made however, such as reported by Feng et al. (2003), giving generally good agreement between numerical prediction and field measurements at the Three Gorges shiplock construction.

2.2.2.2 Secondary relaxation

Even if primary relaxation has more immediate and generally larger effects on slope stability than long-term secondary relaxation, the second may be more hazardous from a geotechnical point of view since the effects become apparent only some time after excavation and completion, when remedial measures are costly if at all possible. Furthermore the effects are ongoing and hard to predict.

Secondary relaxation involves much the same effects as primary relaxation described in the previous paragraph. Relaxation and stress and strain redistribution are caused by changes in material and mass characteristics due to weathering (e.g. density, material strength, material elasticity) and removal of material and changes in the slope morphology by erosion.

Box 3 – Relaxation in metamorphic rocks: N-420 realignment

Around 1990 one of the main roads in the research area, the N-420 that runs from Cordoba to Tarragona, was slightly realigned for most of the stretch between Reus and Falset, in order to accommodate the increasing traffic. One part of approximately 4 kilometers long, between the Coll Teixeta and the Coll Negre close to the village of Riudecols, was not reconstructed at that time, mainly because of the difficult geotechnical nature of the site (Franco Rodriguez, 2001). At the end of 1999, reconstruction of this last remaining part commenced (Figure 5), and this was completed in 2002. During construction, severe slope stability problems made re-excavation works necessary.

Figure 5 - The view West from Coll Negre towards Coll Teixeta showing the realignment works, September 2000. The slope on the right is "D16".

The newly constructed part of the alignment cuts through Carboniferous sedimentary and metamorphic rocks with several intrusive dykes. Three units are distinguished:

Pizarra gris	Grey slate with some intercalations of sandstone (arenisca gris); degree of weathering (BS5930, 1981) varying from slightly to completely, block size and shape very small to large tabular.
Arenisca gris	Grey sandstone with intercalations of slate (pizarra gris); degree of weathering (BS5930, 1981) varying from slightly to completely, block size and shape very small to large tabular.
Porfido granitico	Grey-white to yellow granodiorite; degree of weathering (BS5930, 1981) varying from fresh to residual soil, block size and shape apart from residual soils medium/large blocky to columnar.

The units are highly inhomogeneous with respect to the degree of weathering. Both the Carboniferous rocks and the intrusives may occur as fresh to slightly weathered material as well as completely weathered material or residual soil, and this may even occur within a couple of meters. ➲

Even apart from the differential weathering, the stability of the slopes in the new alignment is negatively influenced by a combination of factors. The Carboniferous rocks have a small block size caused by the dense cleavage and the large number of joint sets (4 to 5 easily recognizable), and a low friction angle on the cleavage and joint planes of 20° to 35°. This combined with the relaxation following excavation has led to several stability problems. Most of the slopes were designed and in first instance excavated with slope angles of around 45-50°. However, as is apparent from slopes in similar geotechnical units in the area, a slope angle of more than approximately 30° will lead to instability phenomena.

These problems became apparent during the early stages of construction, only about half a year after excavation. For a number of slopes an additional geotechnical study was made and remedial measures have been taken, such as changing the slope gradients. Figure 6 shows the extent of this re-design for one of the slopes, slope "D16" (visible in the foreground in Figure 5).

Figure 6 – Slope "D16" as initially excavated, in September 2000 (left), and after re-excavation, in May 2001 (right).

The re-excavation of slope "D16" became necessary after a large failure in its bottom right section under the first berm visible in Figure 6 (left photo), and deformation of the existing road above the cut, which was still in use at the time of construction. The decrease of the slope angle also meant that the existing road had to be re-aligned as well; in Figure 6 the small new cut made for this is visible in the right-hand photo. Even following re-excavation, deformations did occur although this has not yet led to failures of the scale experienced in 2000 (Figure 7).

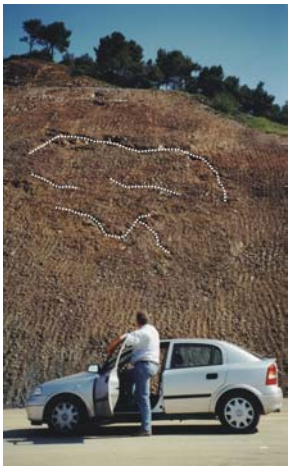

Figure 7 - Cracks appearing in slope "D16" after re-excavation (May 2001).

The time scale on which secondary relaxation operates is thus similar to that of weathering and erosion, and one or more magnitudes larger than that of primary relaxation. In descriptions of long-term slope deformation, creep is often described and in fact this is one of the effects that secondary relaxation may have.

In the long run secondary relaxation may well affect large volumes of the rock mass underlying the slope. A good example of this is shown in Figure 8, with a slope cut in meta-silt- and -sandstones with slatey cleavage of Carboniferous age, near the town of Falset in the research area. The original slope was 5m high and excavated with a 75° slope angle in 1991. Small failures that were not directly related to plane or wedge sliding started occurring shortly after excavation due to primary relaxation. Due to weathering of discontinuity planes and ongoing secondary relaxation, the slope above the original excavation was affected by failures as well, and the slope receded backwards. In 1995 a gravity type support wall was constructed, but above that the slope has been receding further until the present day, affecting a large area behind the original cut and necessitating regular maintenance and cleaning of the road.

Since secondary relaxation is directly caused by weathering and erosion, and in turn also influences the intensity and rate of weathering and erosion processes occurring in a slope, the quantified influence of secondary relaxation on slope stability is hard if not impossible to isolate from pure weathering and erosion effects. Note that the data on weathering effects in this thesis is derived from slope stability classifications and will thus inevitably include effects of secondary relaxation.

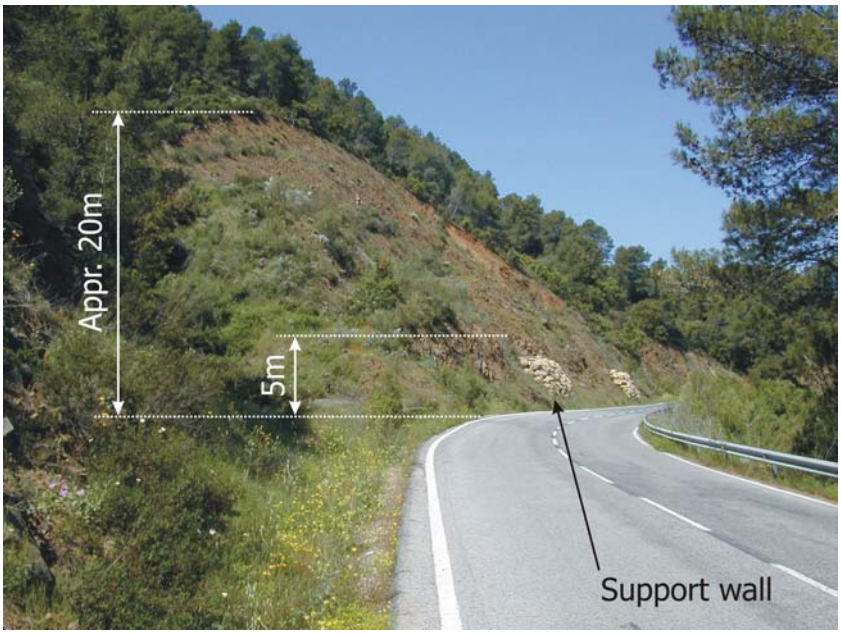

Figure 8 - Receding slope due to secondary relaxation, along T710 road near Falset. Photo by W. Verwaal (2004).

2.2.3 Weathering

Weathering, its processes and effects will be discussed elaborately in paragraphs 2.3-2.6. In an engineering geological context, Price (1995) defined the effects of weathering as *"the irreversible response of soil and rock materials and masses to their natural or artificial exposure to the near-surface geomorphological or engineering environment"*. Conditions controlling weathering in artificial slopes fall into three categories (e.g. Bland and Rolls, 1998):

a) **Internal**: Rock and soil material and mass properties such as porosity, permeability, discontinuities, and material composition.
b) **External**: Parameters related to the weathering environment such as climate, topography, chemistry of weathering solutions, hydrology, and vegetation.
c) **Geotechnical**: Slope design parameters such as aspect, slope angle, height, method of excavation, and drainage measures.

Both the internal and external parameters are functions of time and may have considerably changed from conditions in the past during the history of the site. To some extent, geotechnical parameters such as the slope geometry are possibly changing in the course of time, too - for example if the profile of an existing slope is modified.

In most cases, weathering causes a decrease of the intact rock strength, an increase in the number of discontinuities, the formation of mechanical discontinuities from zones or layers of weakness in the previously intact material, and a decrease of the shear and tensile strength along the discontinuities. Weathering processes in general are often subdivided into mechanical, chemical and biological processes. This is a convenient but not necessarily realistic simplification of the complex processes involved in weathering (Pope et al., 1995). Furthermore, as Trudgill (2000) described, biological weathering is in fact a combination of mechanical and chemical weathering and is therefore no separate phenomenon. In Appendix C, a basic description of various weathering processes is given.

Weathering affects not only the rock material, but also and (for stability, more importantly) the discontinuities present in the rock mass. Weathering will affect rock masses from the slope surface and discontinuities into the material and because of this, the material strength of discontinuity walls will be reduced compared to that of the adjacent rock material further away from the discontinuities (Fookes and Weltman, 1989a/b). In the beginning stages of weathering the walls will be weakened to a depth less than the height of asperities, steps or other roughness components of the discontinuity, and the ultimate shear strength will be governed still by the unweathered material strength that needs to be overcome before asperities can shear through and large displacement can occur. When the weathering penetration depth exceeds the discontinuity roughness, the shear strength will reduce significantly[6], as will the slope stability (Figure 9).

[6] *It should be noted that precipitation of dissolved minerals in the discontinuities can also cause an increase in discontinuity strength through cementation.*

From a slope stability perspective, it is therefore perhaps more important to relate the amount of weathered material not only to the total volume (as in classification systems such as the British Standard BS5930), but also and especially to the part of the material that determines deformation behaviour (the discontinuity walls to a depth equal to the roughness).

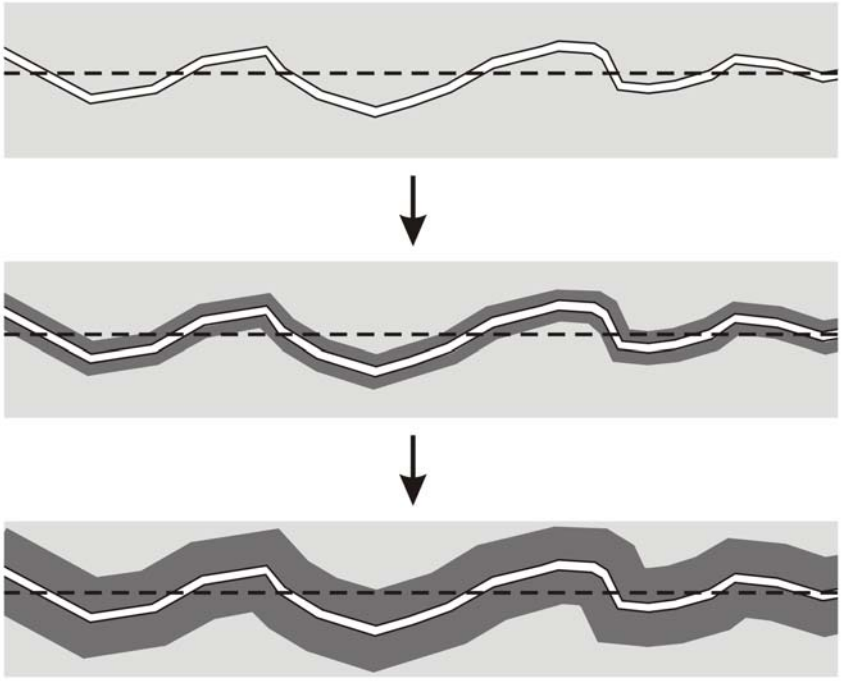

Figure 9 – Three stages of discontinuity wall weathering. Initially, the shear strength along the dotted line is governed by the unweathered material strength (top). When weathering progresses into the material (dark grey), the shear strength is at first still determined partially by the unweathered material strength (middle) but when the penetration depth exceeds the discontinuity roughness, the weathered strength fully determines discontinuity shear strength (bottom).

For the rock material, the most profound effect of weathering is commonly an increase of porosity, in combination with mineral alteration. The porosity increase may be due to an increase of fracture frequency and/or fracture aperture, or to an increase of the pre-existing void volume; all lead to

weakening of the material. Hence, weathered rocks are often open textured, weakly bonded and/or microfractured (Hencher and McNicholl, 1995).

The weakening of intergranular bonds is the main reason for decay of rock materials in both chemical and mechanical weathering processes (Kühnel, 2004). Such intergranular bonds are controlled by factors as the nature and properties of the constituents, their interrelation (interlocking), and the type of interfaces.

Rearrangement of the fabric occurs during any alteration. The mechanical interface strength is considered to be the most important factor for durability under weathering influences. The intergranular bonds are weakened in time by weathering under the influence of mechanical and chemical processes that lead to a variety of destructive reactions, which are usually associated with changes of volume. Bulk volume in general is affected by this, but more important are the molecular volumes of the material constituents (Kühnel, 2004) and the associated small strains that occur throughout the material fabric. The susceptibility of a material to decay through weathering is predetermined by the reactivity of the mineral constituents, access to reactive liquids and gases, and biogenic factors (Kühnel, 2004).

2.2.4 Erosion

Although the processes erosion and (mechanical) weathering have several similarities, a clear distinction can be made. “Erosion” describes the process of material transport, whereas (mechanical) “weathering” describes a process of material change. In this sense, erosion is mostly a phenomenon with a relatively large “mass” scale, whilst both mechanical and chemical weathering are processes with a relatively small “material” scale, primarily affecting in-situ materials. During erosion, weathering of the material being eroded may occur.

Erosion will often act on the products of weathering, removing these from their original location and thus exposing “new” material to weathering. In

such a context, erosion is only one contributor to the overall process of decay. However, especially in soils or weak rock masses, erosion by sheet wash, rill and gully erosion may be the primary decay processes with sometimes little influence of weathering. It is also important to realize that erosion sets a boundary condition for weathering of the rock mass; this is addressed in detail in paragraph 2.7 and Chapter 4.

Erosion affects all soil and rock masses, but the effect is more pronounced in unconsolidated soils and very weak rocks or rock masses with many discontinuities and a small block size. This may mean rocks and rock masses that are weak in a fresh, unweathered state, and rocks that have weakened as a result of weathering. A number of erosion studies trying to quantify the erosion process have been reported, most of which include experimental research on rill and interrill erosion using simulated rainfall both as laboratory tests on prepared or undisturbed soil samples (e.g. Nieuwenhuis, 1991a/b; Parker et al., 1995; Bryan and Rockwell, 1998; Gabbard et al., 1998; Fan and Wu, 2001; Raff et al., 2004) and field tests on selected plots (e.g. Regüés et al., 1995; Cerdà and García-Fayos, 1997; Battany and Grismer, 2000; Xie et al., 2002). Runoff- and infiltration tests have learned that these processes are determined by (amongst other factors) slope angle, surface roughness, discharge over the slope, moisture content of slope material, length of the slope, and the presence of macropores (Shakya and Chander, 1998; Stomph et al., 2001). Many studies are concerned with land erosion from an agricultural point of view and are therefore directed at small slope angles (horizontal or sub-horizontal). Attention has been given to erosion on steeper slopes though, such as by Barton and Coles (1984) and Hutchinson (1998).

Not surprisingly, a common result of the erosion studies is that rates of erosion are found to be higher at times of increased rainfall. Above certain rainfall thresholds that depend on material and mass characteristics, climate and slope geometry, erosion may cause substantially increased incidence of slope failures (Fookes and Weltman, 1989a/b; Franks, 1999; Lineback Gritzner, 2001; Gabeta et al., 2004; Fornis et al., 2005). This is,

however, a very general conclusion and the various factors that influence erosion and its effects have an intricate and complex balance.

Wet erosion, or soil transport by overland flow, is often regarded as a process in which two points are common in most models:

- Some critical shear stress acting on the soil surface needs to be exceeded before erosion can take place
- If and when this critical value is exceeded, soil erosion is proportional to the excess shear stress, with a proportionality constant that represents the soil erosion susceptibility (sometimes termed "erodibility").

In unconsolidated soils or very weak rock slopes with (relict) discontinuities that are affected by erosion, slope development is also strongly influenced by the presence, persistence and orientation of those discontinuities (Barton and Coles, 1984; Zhang et al., 2000).

The shear stress applied by overland flow is usually taken as being the product of the unit weight of water, the depth of flow for shallow flow, and a friction factor for the slope surface. Although both the critical shear stress and the soil erodibility will vary in reality, many theoretical studies assume constant values. When variations in these parameters are taken into account, it can be concluded that (Govindaraju, 1998):

- When the mean critical shear stress is relatively small compared to the maximum critical shear stress, it is commonly exceeded by the applied shear stress. In such a case, using a simplified deterministic model with average values for critical shear stress and soil erodibility will generally lead to an overestimate of the peak rates of sediment loss.
- When the mean critical shear stress is relatively high compared to the minimum critical shear stress, a deterministic model using that mean value may predict very little soil loss by rainsplash alone. This will result in underestimating the soil loss from the hillslope that will in fact occur at the locations where the actual critical shear stress is relatively low, and exceeded by the applied shear stress.

Not only spatial but also temporal variations of soil properties and composition play a role in the development of erosion profiles and its components (e.g. partitioning between rill and interrill or surface and subsurface processes, threshold hydraulic conditions for rill incision, rill network configuration and hillslope sediment delivery; Bryan, 2000) and this further complicates the problem.

Bryan and Rockwell (1998) already found that soil erodibility for a given slope angle can change dramatically over short time periods during rainstorms as a result of changing soil moisture conditions. The same authors concluded that infiltration conditions on the slope surface also strongly influence erodibility and erosion character, rill incision and sediment transport. The erodibility can significantly increase if a hydraulic impedance exists close to the slope surface causing a perched water table to develop. A similar observation was made by Zhang et al. (2000) who found that relict discontinuities subparallel to the slope surface gave rise to perched water tables. This influence is unlikely to be significant for two extreme kinds of soils: on the one hand those that have a high erodibility regardless of moisture conditions, on the other those that are extremely resistant to erosion. Not only the static moisture conditions influence erosion, seepage is also an important factor. Rill and gully formation are enhanced if seepage occurs (Gabbard et al., 1998).

In general, most of the properties that determine soil erodibility, such as soil aggregation and shear strength, and hydrological conditions, are strongly influenced by climatic factors such as rainfall distribution, frost action, and daytime temperature changes. These influences show systematic seasonal variation. Small variations of parameters such as soil water conditions, organic composition, microbiological activity, cementation, clay bonding, duricrust formation, and the structural effect of applied stresses can influence and change erodibility on far shorter time scales, for example between and during individual rainstorms (Bryan, 2000).

The timescale on which decay in general and erosion in particular is studied is important in relation to the continuity of erosion processes. In slope development, decay often acts in sudden, episodic events driven by gravity: rockfall, toppling of undercut blocks (see Box 4), slumps, et cetera. On the timescale in which these events occur, overall decay will not act as a continuous process [7]; only when regarding longer time intervals, an approximately continuous slope development can be observed. When decay is regarded as a continuous process, the episodic influence of such events will generate a certain amount of scatter in the observation data.

2.3 Weathering: current know-how

2.3.1 General

The durability of a rock material is a complex function of internal material features, including fabric, physical and chemical stabilities of coexisting mineral phases, their mutual interrelation, surface properties and inner strain. Rock mass decay results from the interaction of these internal features with varying external conditions and biogenic activity (Kühnel, 2002), and is furthermore influenced by mass characteristics, geotechnical factors and boundary conditions.

A clear differentiation should be made between the intensity and the rate of weathering (e.g. Bland and Rolls, 1998). Weathering *intensity* refers to the degree of decomposition at one particular moment in time, whereas the weathering intensity *rate* (ideally) refers to the amount of change in this weathering intensity per unit time (although the term is used also to describe just a certain amount of change).

[7] *For example, small slumps may expose comparatively fresh material that was buried underneath the slump material. On a detailed timescale, observations before and after such a slump event would indicate an improvement of the slope material's geotechnical quality (in terms of weathering) but rather rapid erosion. Only when making observations in longer time intervals, the influence of such episodic events is averaged out.*

Box 4 – Differential weathering and erosion in the Hostal slope

Several decay processes act upon the rock mass exposed in the Hostal slope, as outlined in Table 2. With an eye on slope stability problems, the processes listed in Table 2 result in some washing of shales onto the road and into a ditch, which in itself is not troublesome. A hazardous effect of this erosion is, however, the undercutting of dolomitic limestone banks. In these layers a joint set is present running almost parallel to the slope face (orientation 128°) with a dip of 80°. The undercutting (see Figure 10) results in toppling; the large size of the toppling blocks presents a potentially hazardous situation with the road nearby.

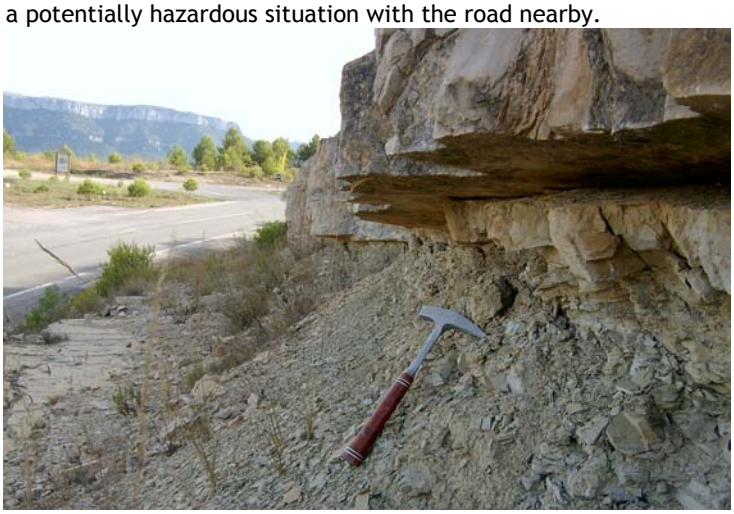

Figure 10 - Differential weathering and erosion have led to undercutting of limestone blocks in the Hostal slope (September 2004). View towards west.

In Table 2 a differentiation should be made between "objective" natural causes for the relative instability of the slope (such as climate), and "subjective" man-made causes. The subjective causes are of course the ones that can be influenced in a design or construction stage, whereas the objective causes more or less follow from given site conditions. When looking at hazard mitigation, the subjective causes are thus the first to be appraised:

- Slope location: One important objective cause for the problems is the presence of shale layers in the slope. Linked to this is the subjective cause of the slope location: by making the choice that the road would cut into the hillside at this site, the whole problem of differential erosion and weathering was introduced in the first place. At the specific site no alternatives exist without shale layers, and it would require a drastic realignment of the whole road to avoid the shales being exposed in a cut.
- Slope orientation: this results from the existing topography and the desired road alignment. As will be shown in paragraph 5.2, the orientation influences the amount and rate of decay of the shales since it affects wetting-drying cycles as well as the amount of heating and cooling. The differences between ultimate physical states will be greater in sun-exposed slopes, with more pronounced wetting-drying cycles. Furthermore the orientation and slope angle determine (in combination with the local dip ➲

and strike of strata) the apparent dip angles in the exposure, which influence stability and erodibility.

- Slope angle: this parameter is, within financial restrictions, a free choice in the design and has a bearing on the decay of both shales and limestones because of factors as stress distribution and water runoff velocity.
- Shales: nearby natural slopes in shales all have an angle of approximately 35°, which seems to be the highest angle at which slopes in the shales are still stable. An artificial cut in the shales exceeding this slope angle leads to rapid erosion, sliding, and a receding slope, resulting in undercutting of the otherwise resistant limestones and dolomites.
- Limestones / dolomites: the toppling failure observed in several layers could be avoided by choosing a lower slope angle.
- Considering the site geology, a differential slope angle in the limestone/dolomite and the shale layers should have been chosen. Although this would not have prevented all the problems, it would certainly have improved the situation.
- Method of excavation: the method of excavation has an important influence on the initial decay and most likely also on the weathering rates after excavation. The study slope was excavated by blasting, which has caused fragmentation of the shales, in turn increasing the erodibility and instability of these layers. Apart from this, there is indication of overblasting in the limestone / dolomite layers which has led to a decrease of the discontinuity spacing and an increase in the vulnerability for toppling.

This example clearly shows the interrelation of weathering and erosion processes.

Table 2 - Decay processes recognized in the study slope. The underlined factors directly result from the slope design.

Unit	Process	Affected by:
Shales	Wetting and drying as well as heating and cooling of shales lead to disintegration into ever smaller flaky particles (Box 8, page 83).	Rainfall; Temperature differences; *Slope orientation.*
	Erosion of flaky particles leads to a decrease in slope angle of layers in this unit (Figure 10); the ultimate slope angle is approximately 35° (observations from nearby natural slopes).	Amount of disintegration; Surface runoff; *Slope angle;* *Method of excavation.*
Dolomitic limestones	Undercutting of the otherwise competent dolomitic limestone banks resulting from decay of underlying shale layers may cause toppling (Figure 10).	Spacing, orientation and dip of joint sets; Decay and mass movement of shales; *Slope orientation and angle;* *Method of excavation.*

2.3.2 Weathering intensity

Assessment of weathering *intensity* is possible through:

a) Verbally descriptive approach
   - This is commonly a description according to a standardized classification system, such as the BS5930 (1981/1999). Weathering intensity classification has been part of dedicated classification systems that address sub-surface and surface excavation stability such as the MRMR (Laubscher, 1990), the Q-system (Barton et al., 1974) and the SSPC (Hack, 1996/1998). Laubscher's system is important since it was the first to include adjustment percentages for various parameters in the system including intact rock strength, RQD and joint condition on the basis of expected weathering intensity. The SSPC adapts descriptions of weathering intensity from the British Standard BS5930 (1981) and also includes statistically derived adjustment factors for mechanical parameters based on the observed and expected weathering intensity.

b) Measures of mechanical index properties
   - A detailed overview of possibilities to assess weathering intensities by (index) testing is given by Martin (1986). This usually takes the form of a strength estimate – by simple means[8], such as by using hands, pocket knives, or geological hammers, or by more complicated devices as Schmidt hammers[9], or even seismic equipment. It should be noted

[8] *A special reference is made to Hack and Huisman (2002) who deal with estimating the intact rock strength of a rock mass by simple means.*

[9] *For the use of Schmidt hammers, refer to Katz et al. (2000) who describe some problems and accuracy issues in determining rock properties with the use of a Schmidt hammer. A case study is given in Sjöberg and Broadbent (1991). In this paper, Schmidt hammer rebound values correlated well with the degree of rock weathering but that of course depends on the effects that the dominant weathering*

that however useful a strength estimate might be for engineering purposes, it does not necessarily relate to the *intensity* of weathering, since that parameter relates to a *change* in properties from some parent material rather than some *absolute value* of that property[10].

The slake durability test, which is often used to quantify slaking properties of mudstones, also falls into this category. Generally, the results of such index tests are useful to predict the field performance of different rock types in a qualitative manner, but they often cannot be used to predict the quantitative behaviour of mudstones under field conditions (although correlations between slake durability and field performance do exist, such as published by Dick and Shakoor (1995) and Shakoor (1995). However, since slaking is an important decay process in rocks that are subject to wetting and drying cycles and susceptible to slaking, this method has good potential to quantify the

processes have; seemingly, in this case, material strength decrease was significant with increasing degree of weathering. A different approach was followed by Tang (1998) who related the Schmidt hammer strength index to the weathering susceptibility of a material, rather than to the weathering intensity.

[10] To give an example in absolute terms: a moderately weathered granite is likely to be stronger both as a material and as a mass than a slightly weathered shale; this difference between the intensity of weathering and the geotechnical consequences of weathering should be made, and cannot be made clearly enough. A further complexity in this respect is that weathering may actually lead to a (local) increase of strength, for example by case hardening (e.g. Winkler, 1994; Bland and Rolls, 1998). It should also be considered that a slope in a highly weathered rock mass that behaves as a unconsolidated soil may show a different failure mode (e.g. rotational) than that same rock mass in a less weathered state (e.g. sliding or toppling), with different stability indices. This has been observed in the Falset area in several new road cuts made during the 2000-2002 realignment of the N-420.

susceptibility to decay in such rocks (e.g. Lee and De Freitas, 1988).

Hack (1998), Hack and Huisman (2002) and Nicholson (2001a) have demonstrated that material tests can have severe limitations in predicting mass performance, especially when discontinuities influence the mass behaviour. This should be noted when applying index testing.

- A different category are measurements in which the value of some property other than material strength is determined that changes as a result of weathering. Parameters that are often used for this are the moisture content (e.g. Matsukura and Takahashi, 1999), porosity (e.g. Nicholson, 2001a), and fracture intensity (Fookes et al., 1971). Usually weathering involves an increase in porosity and fracture frequency (and thus a decrease in fracture spacing). Therefore a description of, for example, the fracturing intensity may be an adequate way of describing the effect weathering has had on a rock mass. It should however be realized that the porosity and fracture intensity or spacing may not be the result of weathering (i.e. a change from the parent material or mass) but an original sedimentary feature. Therefore porosity and fracture spacing indices, although presenting an alternative for classifying the geotechnical quality of a rock mass, should not be used as pure weathering intensity indicators.

c) Measures of intensity based on chemical indices
   - In absolute terms, the composition of the weathered material may be compared to that of the unweathered parent material – supposing of course that the latter is known.
   - An indirect method is to use a ratio of resistant minerals such as quartz and other minerals present in the parent material which are not resistant, and removed by

weathering (e.g. Irfan and Dearman, 1978; Gupta and Rao, 2001; Guan et al., 2002; Kim and Park, 2003).

- Both methods tend to be specifically suited for one and the same parent material. They are especially useful in cases of primary igneous rocks in a wet tropical climate.

2.3.3 Weathering intensity rate

Weathering intensity *rates* may be estimated from geological materials (e.g. when used as construction materials), in-situ observations, mass-balances for catchment areas, or from laboratory tests (which often give ambiguous results when regarded quantitatively). Weathering intensity rates determined in the laboratory do show a variation between minerals, and they are also influenced by the particular mineral structure, the solution used in the experiments, and the mineral surface area. Whether the weathering rates as determined in laboratory tests accurately describe in-situ behaviour is doubtful.

Bland and Rolls (1998) note that *"most studies have shown that chemical weathering rates in the field, as measured by the mass balance method, are one to three orders of magnitude slower than those determined by laboratory investigations"*. Several possible reasons exist for this, such as temperature differences between field and laboratory, and insulation of mineral grains by surface coating as well as reduced contact between water and minerals in field situations. Hydraulic factors are believed to be the most important factors influencing the differences between chemical weathering rates as determined in the laboratory and the field (Bland and Rolls, 1998).

2.4 Time and spatial scales of weathering research

2.4.1 General

Studies into weathering intensity, weathering intensity rates, and rock mass decay can generally be divided into three different time scales, in which the spatial scale changes with the time scale of the investigation (Figure 11).

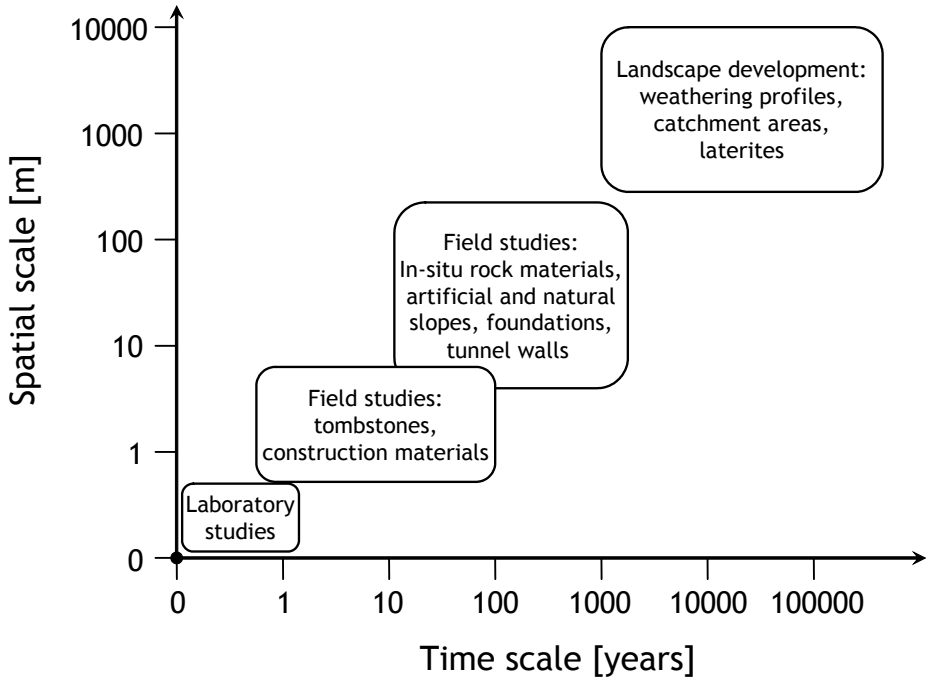

Figure 11 – Approximate time and spatial scales of weathering research.

2.4.2 Geological time scale / landscape spatial scale

On a geological time scale, weathering takes place in the course of the geomorphological development of a landscape during some 10000 years or more, interacting with changes in climate and tectonics. Many examples of studies into such landscape development through weathering are reported (e.g. Hodson et al., 1998; Stonestrom et al., 1998; Bouchard and Jolicoeur, 2000; Le Pera and Sorriso-Valvo, 2000; Stewart et al., 2001; Millot et al., 2002). These mainly deal with chemical weathering, which is characterized by sequential reaction between percolating groundwater and rock-forming minerals (Chigira and Oyama, 1999), and its products. A significant part of these studies is directed at laterite development (Boeglin and Probst, 1998; Freyssenet and Farah, 2000). From a geotechnical viewpoint, a number of investigations on this subject has been carried out on a slope scale (e.g.

Barton and Coles, 1984; Grainger and Harris, 1986; Gardner and Walsh, 1996). Gardner and Walsh (1996) focus on the development of a weathering profile through chemical weathering in natural slopes in the Middle Hills of Nepal, where gneisses have weathered by acid hydrolysis under temperate and subtropical conditions. As a result, residual soil and saprolite layers of several meters thick can be formed, having a significant influence on slope stability. In an active region like this part of the Himalayas, the situation is often complicated by the rapid uplift that results in a mixture of materials with different degrees of weathering.

Generally, weathering profiles developed in different climates and physical settings are highly variable in structure, in mineralogy, in the local biosphere and in the compositions of the soil, gas, and water phases (Curtis, 2003).

2.4.3 Historical time scale / site spatial scale

The researches on a historical timescale deal with larger rock blocks (e.g. tombstones or construction materials) or in-situ rock masses in tunnels or slopes, and are ideally combined with a geomorphological site appraisal to investigate the influence of the surroundings on slope decay and stability (Rupke et al., 1988). The studies on a geological timescale usually encompass far larger in-situ bodies of rock, usually deep weathering profiles or whole catchment areas, and really deal with landscape development at a different spatial scale than the site development that is regarded on a historical scale.

On a site scale, weathering and erosion can have significant effects within a time span generally ranging from a year up to one or several centuries, or sometimes even millenia. Examples are the decay of natural features such as cliffs (e.g. Barton and Coles, 1984) and natural slopes (Nieuwenhuis, 1991a/b), but also the decay of construction materials in monuments, buildings, and especially tombstones - sometimes exotically so, as in the case of the royal tomb of Egyptian farao Seti I (Wüst and McLane, 2000).

On a slope scale, primary investigations into geotechnical decay of rock masses in road cuts using results obtained with the SSPC system were published by Woldearegay and Onrust (2002). Field studies have especially focussed on tombstones, which have been investigated in a range of climates and weathering settings. Results have however not been conclusive. The rate of surface retreat, which is usually taken as an approximation of the weathering intensity rate, has however been found to be proportional to the precipitation intensity and mean annual rainfall at study locations (Neil, 1989). The rate of surface retreat is furthermore found to decrease with a decrease in the decline of ion concentration of the precipitation, which may give significantly different results between rural and urban areas, as well as coastal and inland areas (Neil, 1989; Inkpen and Jackson, 2000).

Orientation effects are ambiguous, even in one and the same material type; as Williams and Robinson (2000) reported, no clear trend was found between weathering rates and tombstone orientation, which was thought to be due to differences in the local microclimate. Temperature differences seem to play a minor role in the studies reported in the literature, but it has to be said that most studies have very little temperature variation in the data sets, and furthermore most studies are conducted in temperate regions where temperatures do not reach extreme values. It is likely that temperature effects would become clearer in more extreme environments, and if data from areas with different climate types would be compared.

Details of the decay of construction materials in buildings and monuments are given in abundance by Winkler (1994), Dubelaar et al. (1997), Kuchitsu et al. (1999), Kühnel and Tshibangu Katshi (1999), Taylor-Firth and Laycock (1999), Viles (2000), Trudgill et al. (2001), and Jiang and Esaki (2002); tombstone studies are reported by Neil (1989), Robinson and Williams (1996), Matsukura and Hirose (1999), and Williams and Robinson (2000), to mention some. In most of these studies on materials, loss of material on surface per unit time is taken as an indicator for weathering and reported “weathering rates” in fact often signify rates of surface material loss and retreat.

2.4.4 Laboratory time scale / sample spatial scale

During laboratory tests, small rock samples are typically subjected to experiments of limited duration (days to weeks, generally) under well-defined and controlled conditions, that try to emulate in-situ weathering processes as close as possible. Well-known examples are slaking tests on mudstones (e.g. Santi, 1995; Cantón et al., 2001; Nicholson, 2001b; Pejon and Zuquette, 2002), salt action tests (e.g. Goudie, 1999; Robinson and Williams, 2000; Nicholson, 2001b) and freeze-thaw testing (e.g. Goudie, 1999; Nicholson and Nicholson, 2000; Nicholson, 2001b).

Studies into rock material weathering in the laboratory abound in the literature; a general overview is given by Viles (2000), who describes both laboratory tests and case studies on rock used as construction material in buildings. Most laboratory tests aim at isolating a specific process and investigating the influence of that process on the rock material of interest. Ideally the simulated process in the laboratory induces similar changes in the material (and similar stresses) as long term weathering in situ does (Trudgill and Viles, 1998). Unfortunately this is seldomly achieved. Hydraulic conditions are often different, and to be effective on laboratory time scales processes are usually also accelerated, amongst others by decreasing the sample size and simultaneously increasing the contact area available for reaction. Thus, many laboratory results are not *quantitatively* reproducible in the field, with laboratory weathering intensity rates being several orders of magnitude higher than those in-situ (e.g. Bland and Rolls, 1998; Hodson et al., 1998; White and Brantley, 2003). Although the *qualitative* results found in the laboratory often confirm field observations, this is not always so; as White and Brantley (2003) observed, even the relative rates at which silicate minerals weather in the laboratory are sometimes different than in-situ rates observed in the field. As an example, the case of plagioclase and K-feldspar is mentioned, which have similar laboratory rates but may show differing in-situ weathering rates with plagioclase weathering faster than K-feldspar (White and Brantley, 2003), depending on hydrochemistry, environment, and climate.

It should also be noted that samples of dimensions typically tested in the laboratory represent the main *material* of a unit rather than the rock *mass*, and as with almost all geotechnically relevant types of rock behaviour, important differences exist between the potential weathering of rock *masses* and that of rock *materials*. Mass characteristics such as the frequency and aperture of discontinuities may be more important to the ultimate resistance to weathering than material characteristics. Materials that are in themselves resistant to weathering but are incorporated in a weak mass may for example show a more rapid and intense decay than less resistant materials embedded in an unbroken rock mass.

Despite these discrepancies between laboratory and field observations, laboratory testing remains a widely applied tool in investigating and quantifying decay of rocks by weathering. Processes simulated in the laboratory typically include:

- Slaking (e.g. Santi, 1995; Cantón et al., 2001; Czerewko and Cripps, 2001; Nicholson, 2001b; Pejon and Zuquette, 2002) – slaking is often investigated for mudstones, since it is in those rocks that slaking is the dominant decay process. Weathering resulting from the wetting-drying cycles simulated in slaking tests typically leads to the formation of fine debris called *pelitoclasts*, a process termed *pelitoclastesis* by Wetzel and Einsele (1991). The number of wetting–drying cycles has the greatest influence on weathering (Cantón et al., 2001).
- Salt action (e.g. Goudie, 1999; Nicholson, 2001b) – salt action is particularly interesting for the durability of construction materials that will be subjected to a chemical environment with either periodic changes in the salinity of any water present (e.g. road construction materials), or a major difference between the salinity of the site at which the material is used, and that of the site where it was quarried (e.g. salt-water breakwater dams). Winkler (1994) presents several examples of both situations and the resulting decay.

  The response of rock materials to salt crystallization is sometimes used as an indicator for the behaviour under freeze-thaw conditions,

but Goudie (1999) showed that resistance to salt is a poor predictor of resistance to frost, with rocks responding differently to salt and freeze-thaw action.

- Freeze-thaw (e.g. Goudie, 1999; Nicholson and Nicholson, 2000; Nicholson, 2001b) – freeze-thaw testing is usually undertaken for construction materials that will be used in wet conditions and temperate climates with frequent diurnal fluctuations of the temperature around 0°C. Results of freeze-thaw tests done by Nicholson and Nicholson (2000) suggest that comparatively strong rocks such as crystalline limestone broke up preferentially along pre-existing lines of weakness such as, microfractures, mineral veins, and stylolites, whereas comparatively weak rocks tend to break up in a random fashion.

An alternative to laboratory testing is the type of field study of weathering using small rock samples and measuring surface material loss as reported by Matsukura and Hirose (1999). Although this solves the problem of how to simulate actual field conditions, a disadvantage of this approach is that various processes may act simultaneously and conditions are not well controlled, while the limitations in interpretation of results presented by the sample scale remain.

Next to physical testing, modelling of small-scale time related processes has become of interest in recent years. The assessment and both analytical and numerical modelling of material change, crystal growth, cracking and fabric evolution has become a subject of interest (e.g. Nova, 1997; Bauluz et al., 2000; Amenta, 2001; Jessel et al., 2001) and several efforts have been made to link those processes to physical characteristics of the rock material and mass (e.g. Azzoni et al., 1996; Chertkov and Ravina, 2000; Kemeny, 2004).

2.5 Intensity of weathering and its change in time: perception, definition and quantification

A rock and soil material or mass will show a certain response to the particular combination of weathering-controlling conditions at the site of its exposure. The intensity and rate of this response is the *"susceptibility of a rock mass to further weathering in the future"* (Hack, 1998). This concept is frequently addressed by "the" weathering rate of a rock material or mass. However, the use of a weathering rate as is common in the literature on this subject (e.g. Matsukura and Hirose, 1999; Inkpen and Jackson, 2000; Williams and Robinson, 2000; Trudgill et al., 2001), usually defined in terms of material loss per area per unit time, suggests that this parameter is constant with respect to time. Physically, this seems unlikely. When decay is regarded as the reaction of a rock mass to an imbalance in its state and the prevailing internal, external and geotechnical conditions, it seems likely that the weathering intensity rate is related to the magnitude of the driving forces of decay, and therefore the degree of imbalance. In other words, weathering intensity rates may be expected to decrease with time, as the state of the rock mass becomes more and more in equilibrium with its surroundings. This was already shown by Colman (1981) and verified recently during field tests by White and Brantley (2003).

The question of how to define weathering intensity rates, and by doing so how to quantify susceptibility to weathering, depends primarily on how the intensity of weathering at a specific moment in time can actually be quantified. The change of this intensity per unit time is then in its most strict definition the weathering intensity rate. As pointed out above, it is preferred to define a parameter describing the susceptibility to weathering in such a way that it only depends on the existing set of weathering parameters, and not on time itself. Such a variable can be used not only to quantify the rate of the decay process active in a slope at one particular moment in time, but also to extrapolate the present-day situation into the future, thus predicting the weakening of a rock or soil mass and ultimately

the resulting decrease of slope stability within the planned engineering lifetime of a slope.

A common method to quantify weathering is to use a ratio of sound and unsound constituents; one example of this is found in Irfan and Dearman (1978) who expressed a micropetrographical index for a weathered Cornwall granite as the ratio of sound and unsound constituents. Other researchers such as Ruxton (1968, cited by Colman, 1981) have used largely similar parameters to define the decay of materials, rather than masses (see Appendix E). Although such an approach indeed gives an objective measure for the intensity of weathering, or at least the changes brought about in the original material, it has the disadvantage of being totally dependent on the decay process. Results for a different parent material, a different weathering environment and so on cannot be compared and in that respect it is a very specific parameter which is a good *quantitative* measure for one specific combination of material and weathering environment, but a poor *qualitative* measure to compare different materials, or different environments (and therefore sites). Furthermore its use is limited to cases where chemical weathering prevails over mechanical weathering (or where mechanical weathering is absent), so that a change in material composition indeed is an indicator of the overall weathering process. In geo-engineering, any study into rock mass decay in time for use in slope stability issues will commonly have to address different sites, settings, weathering processes, materials and masses and, therefore, the merits of such specific parameters as mineral indices are limited[11]. This is one of the reasons why classification systems are still often preferred over these measurable parameters for geo-engineering applications.

In such classification systems, the intensity of weathering is usually quantified using standardized "classes" or "degrees" of weathering, to each

[11] *Such parameters as defined by Irfan and Dearman (1978) are however useful in the assessment of the quality of construction materials and similar applications, or in specific situations where the variability of materials is minimal.*

of which belongs a specific combination of observations on the intensity of weathering (see the Geological Society Engineering Group Working Party Report, 1995); a well-known example is the British Standard classification of BS5930 (1981/1999; see also Dearman, 1995). An alternative would be a rating system such as proposed by Laubscher (1990) and Price (1993); these are however not yet standardized.

In the SSPC classification system used in this study (Hack, 1998), the degree of weathering is quantified with the parameters *WE* (for the exposure rock mass) and *SWE* (for the slope rock mass); *WE* and *SWE* are values smaller than or equal to one, representing the decrease in strength properties by weathering. The parameter is assigned to the different weathering degrees of the British Standard BS5930 (1981) according to Table 3 (after Hack and Price, 1997). Parameter values of *WE* have been determined based on laboratory and field testing (Hack, 1998). It is important to note that *WE* is not "just" a measure for the weathering degree on the actual surface of the slope. It is in fact representing the state of the zone of weathered rock on and near the surface that determines slope stability, and is assigned in accordance with the weathering degree that is of engineering significance with respect to slope stability[12]. The parameter WE_{init}-WE_t (with WE_{init} the initial degree of weathering and WE_t the degree of weathering at some time *t*) is then a measure for the change in weathering.

When regarding the subdivision of weathering intensity into classes, one touches upon the subject of the limited objectivity of the observations on which the classification is based. This is a complex problem in itself, since the personal interpretation by the observer of the specific combination of properties that a material or mass should have to fall within a class according to the standards (see Box 5) is invariably linked to the question in what way observers actually perceive slopes. An observer generally does not

[12] *Next to the intensity of weathering, the depth over which weathering has penetrated into the rock mass exposed in the slope is an important factor for the slope stability. This will be dealt with in paragraph 2.6.*

build his or her judgement of slopes on the two-dimensional surface of the exposed rock, but rather describes the features of the uppermost "skin" of the rock mass. This three-dimensional volume would be in the order of millimetres thick in most limestones and dolomites, and in the order of centimetres thick or more in the case of weak rock formations (that commonly have a much more irregular surface). Therefore the classification is inevitably some sort of average over the conditions found in that particular weathered uppermost layer. The extent (in depth) of this zone on which an observation is based would usually decrease in more competent materials with less mechanical decay. It should be noted that the thickness of the zone on which the classification is based is not necessarily the same as the depth over which weathering has penetrated the rock or soil mass (paragraph 2.6).

Table 3 - *WE*-values for different weathering degrees (validated for the Falset research area).

Degree of weathering in slope (BS5930, 1981)	*WE* [-] (SSPC)
Unweathered	1.00
Slightly weathered	0.95
Moderately weathered	0.90
Highly weathered	0.62
Completely weathered	0.35

Box 5 – Variation in weathering classification

Using a reference group of 14 students, the variation in classification results for the weathering intensity was investigated in May 2002 at two locations: a roadcut of approximately 50 years old in thinly bedded Upper Muschelkalk limestones in the town of Tivissa, and the Gavadà Keuper slope, at the time exposed for 3 years. Both outcrops are very homogeneous and in both cases, the exposed unit show very little variation in the lateral direction. Each student performed two full SSPC classifications at each slope, independent of other students.

The results of both outcrops show variation in the observed weathering intensities, quantified with the WE parameter (see Table 3); the distribution of observed intensities is given in Figure 12. In both cases, observed intensities varied by three classes, ranging from fresh to moderately weathered for the Tivissa slope and moderate to completely weathered for the Gavadà slope. For the Gavadà slope, a clear peak is found with more than 70% of the observations noting "highly weathered" and a small percentage in the surrounding intensity classes. In the Tivissa slope however, the slightly and moderately weathered classes contain almost an equal number of observations.

This does not mean that either the WE-quantification method easily leads to false results, or that weathering classification is ambiguous; it has already been said that WE is assigned in accordance with the weathering degree that is of engineering significance with respect to slope stability and that may well be somewhere between two classes. This will in fact only show with larger data sets; individual classifications would give only slight or moderate degrees of weathering, whereas larger data sets effectively convert the discrete WE classification system into a more continuous one. However, there is a certain subjectivity of the observer involved in making observations, of which the weathering intensity is just one example. It is interesting to study the distribution of observed weathering classes along the Gavadà exposure (Figure 13). From the observed distribution it may be concluded that the variability is not related to the location at which the observation is made, but that there really is a personal variation instead.

In the statistical analysis conducted further in this thesis (see paragraph 5), use is made of the amount of data to indicate trends that would not show on the basis of individual observations. The personal subjectivity will however inevitably introduce scatter in the observed trends. This influence may also be quantified using data simulation (paragraph 5.2.3, page 130).

➲

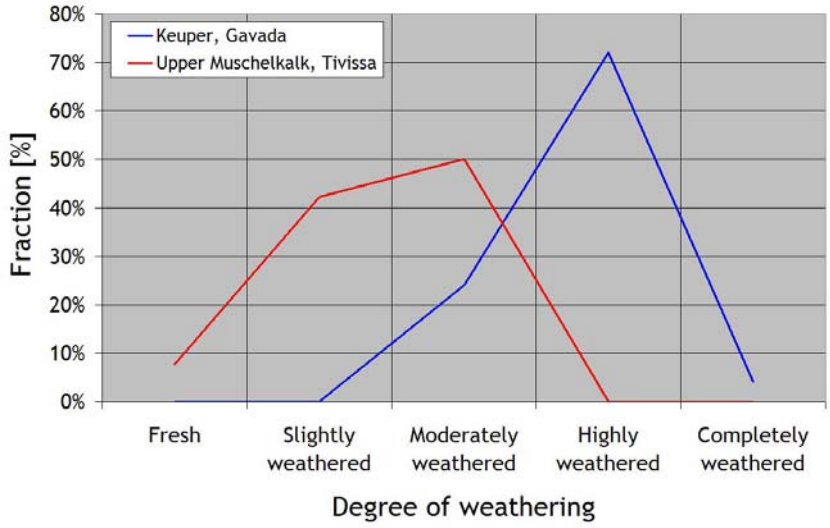

Figure 12 - Distribution of weathering intensity classifications, Tivissa and Gavadà.

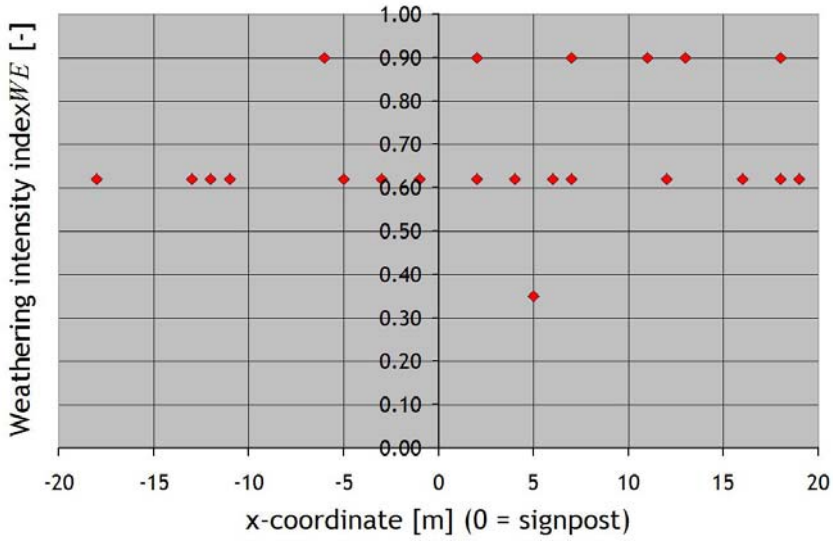

Figure 13 - Distribution of observed *WE*-values along the Gavadà slope.

The personal interpretation and subjective judgement intrinsic in weathering classifications are important grounds for treating weathering classification data probabilistically. The uncertainty resulting from the classification reflects itself in a probability distribution with non-zero variance for the weathering data (e.g. *WE*, see Table 3 and paragraph F.4.1 in Appendix F), rather than a single discrete value. In a wider sense, such variability is introduced not only because of subjectivity of the person who made the classification, but also because of intrinsic variability of the data itself as well as variation introduced by conceptual errors in the appreciation of the data's behaviour in the real world (Ayalew, 2000).

The probabilistic approach of classification-based weathering quantification followed in this research attempts to filter out some of the scatter that is introduced by the uncertainty resulting from influences as described above. Researchers such as Nicholson (2001a) found that outside of carefully controlled laboratory environments, the influences of weathering parameters is at best hard to establish, to an important extent because of such scatter. Results of this study indicate however that if uncertainty is appreciated as an inevitable part of the data and even as part of the information it provides, a probabilistic evaluation can yield results that show trends and details that remain hidden in a deterministic approach. Of course, even such a probabilistic approach may not circumvent the problem of incomplete assessment of the depth to which weathering extends.

Any definition of the *weathering intensity rate* should describe the ratio of the change in the state of weathering and (a function of) the time required for that change. The words “a function of” are included here to address the possibility that the definition of weathering intensity rate is not according to a linear time-scale; it may for example be based on a logarithmic time scale. Ideally, it would be possible to quantify this change dynamically in time – this is to say that the change, and the rate of change, can be defined at any moment. In the real world of slopes, this would mean that the state of weathering of a particular unit in a particular slope would have to be described during a number of years, and the change from each observation

to the next divided by the elapsed time (or a function of it) would give this "dynamic" weathering intensity rate.

However, most often no time series of weathering observations in one unit and in one slope would be available. For few slopes in the database used in this research time series *are* available, but most data only consist of single and independent observations. When only one observation of the state of weathering is made in a particular unit in a particular slope, the dynamic rate cannot be determined anymore. An alternative is the apparent rate, quantified by the change in weathering *from the initial state* divided by a function of the total exposure time.

The principal difference between the apparent and dynamic rates is plotted in Figure 14, with hypothetical data for *WE*. The apparent rate at a certain time is defined as the slope of the chord through the data point and the origin, whereas the dynamic rate is defined as the slope of the tangent in that point. As will be discussed later, most classifications used for this research are not part of a time series of measurements (that would allow determining the dynamic weathering rate), but form individual or discontinuous measurements (that only allow determining the apparent weathering rate). Supposing that weathering is not a linear process in time, neither the apparent nor the dynamic weathering rates will be constant over the exposure time if defined simply as in Figure 14.

If an appropriate scale is chosen for the time axis, the line through the data points in Figure 14 may be transferred into a straight one. If that is achieved, the apparent and dynamic rates become constant over time, and will therefore be useful indicators of weathering susceptibility. It has been found that for the research area a logarithmic time scale is the most appropriate for this, as will be shown later in chapter 5. This corresponds to previous results reported in the literature (see paragraph E.1, Appendix E). Therefore a logarithmic time scale is adopted in this thesis to define the weathering intensity rates.

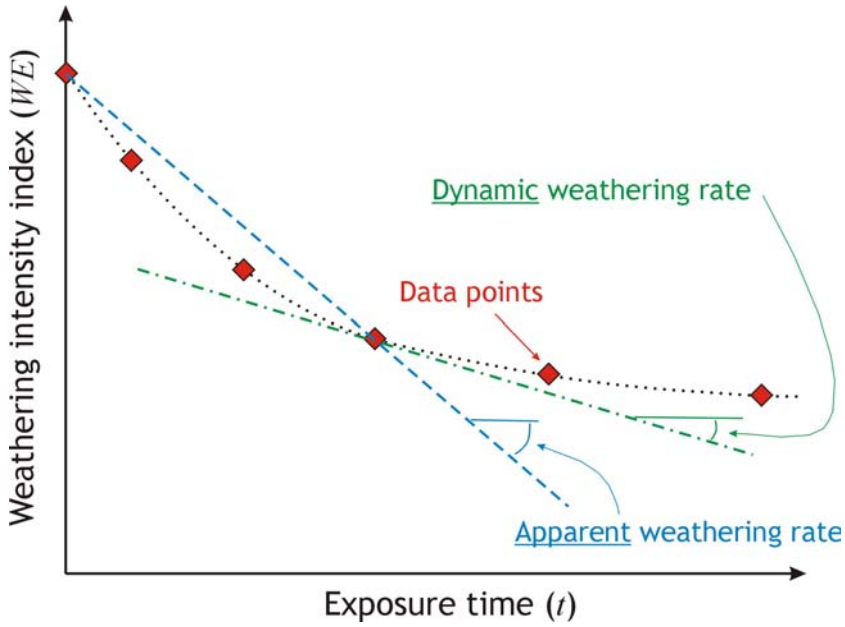

Figure 14 - Definition of apparent and dynamic weathering intensity rates. Note that *WE* decreases as the degree of weathering increases.

The logarithmic time scale results in an approximately linear relationship of the logarithm of time with the parameter WE_{init}-WE_t that quantifies the change in weathering intensity, at least in terms of the apparent weathering intensity rate. This gives the following definitions for the apparent and dynamic weathering intensity rates (with 10-based logarithms):

Apparent weathering intensity rate:

$$R_{WE}^{app} = \frac{WE_{init} - WE_t}{\log(1+t)} \tag{1}$$

Dynamic weathering intensity rate:

$$R_{WE}^{dyn} = \frac{\Delta WE}{\Delta \log(1+t)} \approx \frac{WE_{t-\Delta t} - WE_t}{\log(1+t) - \log(1+(t-\Delta t))} \tag{2}$$

2.6 Penetration of weathering

The parameter *WE* represents the weathering intensity of the rock mass that is actually determining slope stability. Generally, the intensity of weathering will change in depth, with a weathering front penetrating into the rock mass underlying a slope. Therefore, it is expected that the weathering degree gradually decreases with depth. Hence the question of which *WE* to assign to the rock mass does then not only depend on the intensity of weathering itself, with all the involved considerations as described in paragraph 2.5, but also on what penetration depth of a particular weathering degree is of engineering significance with respect to slope stability[13].

The latter consideration implies that ideally, the value of *WE* that corresponds to the weathering degree which should be assigned to (a unit in) a rock mass underlying a slope, decreases simultaneously with the decrease in engineering strength properties that play a role in slope stability. In reality, this is not the case, since the weathering degree can only be described as one out of a limited number of options (see paragraph 2.5). Therefore, even when the classification describes the engineering-wise appropriate weathering degree perfectly, the outcome will be a discontinuous transition from one weathering degree to another at a specific time, rather than a continuous process. When added uncertainty resulting from personal bias or intrinsic variability plays a role, this discontinuous character of the development will actually be less pronounced, but of course episodic interruptions of the process (e.g. sudden erosion events such as falling blocks, etc.) will also disrupt the ideal picture.

[13] *In this study, WE is considered as an appropriate representative for engineering applications that deal with slope stability. In cases where the bearing capacity of foundations, stability of underground excavations etc. are considered, the appropriate WE may be different from the WE value for slope stability.*

This is not to say that weathering degrees taken from engineering classifications are just a "good guess". They are the best data that can actually be derived, but it is important to note that momentary observations can at first sight be disturbed by episodic and discontinuous steps in the slope development. On average, and with enough observations, the underlying process will become apparent, but individual observations may be potentially misleading. This leads to the conclusion that a probabilistic approach to rock mass decay is probably the most promising, as the statistic variation of large data sets can then be best interpreted.

Coming back to the subject of weathering penetration, several characteristics of the weathered zone are of importance and intrinsically included in the engineering judgement of what is the appropriate weathering degree to be assigned to an outcrop:

a) What is the rate of penetration of a weathering front into the rock mass (either along discontinuities, or into the rock material)?
b) How can a significant penetration depth of that weathering front be defined?
c) What is the variation of the weathering degree over that penetration depth?

Little is known about the answers to these questions, at least in quantitative terms. It seems accepted (e.g. Heimsath et al., 1997) that the penetration rate of a weathering front decreases with increasing penetration depth – that is to say, weathered material which is not simultaneously being eroded, acts as a protective cover over the unweathered part of a rock mass and in most cases diminishes the rates at which the decay processes occur[14].

[14] *Again, the complexity of the involved processes has to be considered with respect to this remark. It is quite possible that a cover of loose slope waste such as scree, with a higher porosity than the in-situ material it is covering, may retain more water after rainfall than that in-situ rock and enhance the potential for chemical weathering. In rock types where chemical weathering processes are dominant, this would lead to higher weathering rates for scree-covered sections of the slope profile. In rock types*

As long as this cover remains undisturbed by erosion, the weathering front penetrates at a continuously decreasing rate when regarded on a linear time scale. Since this is the result of weathering alone, this can be called the *reference weathering penetration rate*. A sensitive situation results if at the same time the weathered cover is being eroded (partially or completely). This can lead to an equilibrium between weathering and erosion, or tend towards a prevailing of one of these processes (addressed in detail in paragraph 2.7). In that case, the penetration rate of a weathering front is for any given penetration depth smaller than in a situation without erosion, and the term *slope weathering penetration rate* can be used to describe it[15].

Of course, it is most attractive for modelling purposes to work with constant values for these rates, rather than decreasing functions that would be found when using a linear time scale. Again, this may be achieved by adjusting the time scale according to the nature of the process, so that both rates would be constant on that adjusted time scale (and hence, that the penetration depth would change on that adjusted time scale following a linear relation). The starting hypothesis for the modelling in later parts of this thesis results in what is approximately a logarithmic timescale (see chapter 5, paragraph 5.1) and Appendix E, paragraph E.2). Schematic models that are of a more limited practical use (Appendix E, paragraph E.4) do show that the balance between erosion and weathering may be more complicated than a logarithmic transformation.

The answer to the second question, "how can a significant penetration depth of a weathering front be defined", depends on the scale of and background to the regarded case. Since this research is aimed at engineering application and tries to capture the rock mass decay which is of engineering significance

where cyclic physical weathering processes are dominant (most notably slaking), increased water retention may however lead to a decrease in weathering rates for scree-covered sections, and a shift towards chemical weathering processes.

[15] *Terminology of "reference" and "slope" penetration rates is analogous to the SSPC system's definitions of reference rock mass and slope rock mass (paragraph 1.5).*

to slope stability, "the" penetration depth of weathering should be that depth at which the rock mass characteristics are changed by weathering to such an extent that the influence on rock mass deformation and stability in slopes has become noticeable and, to use the word again, significant. This is a rather general and abstract statement, but it is important to note that changes on a microscopic scale, changes in the mineralogical matrix, changes in porosity, and even changes in the homogeneity and "intactness" of the material (e.g. opening of microcracks) do not necessarily correspond to the changes that define the penetration depth of weathering in the engineering sense as regarded here. An example of that is given by Adhikari (2002) who found microcracks in sub-horizontal limestone layers in an Upper Muschelkalk outcrop near Tivissa. The cracks had formed parallel to the bedding planes during the exposure time of the slope (approximately 50 years) and extended several centimetres into the rock mass (Adhikari, 2002). However, these cracks had no overall effect on the stability of this slope. Still, rock mass disintegration starts at the smallest scale (e.g. Kühnel, 2002; Nicholson, 2001a) and even such microcracks may influence the slope development in time.

Regarding the third question – the variation of the weathering degree or rather the effects that weathering has had – another yet unquantified problem is addressed. At the actual weathering front, rock material that is not (yet) influenced by the weathering environment since the time of excavation is in contact with rock that has been influenced by that weathering environment. It is likely that this in reality is not a sharp boundary, but rather a diffusive transition zone; in any case, the weathering front is the location where "weathered" rock and "unweathered" rock meet[16] (see Box 6).

[16] *The weathering degree of the weathered rock in the immediate vicinity of the weathering front will be almost equal to that of the unweathered rock, and from the front towards the surface the intensity of weathering will increase, probably continuously. Since the weathering degree according to BS5930 as well as in terms of WE is defined in stepped classes, the probable gradual change in actual weathering*

The above leads to the conclusion that an appropriate slope weathering classification with the SSPC in terms of *WE* will be episodic. At some moment a particular *WE* value will be representative for the engineering behaviour of that slope, and with continuing decay, after some time a lower *WE* value (see Table 3, page 50) will have to be assigned when that value becomes descriptive for the slope behaviour. Therefore, the classification will be stepped in time, whereas the underlying process of decay will be principally continuous – although this is in itself made erratic by the episodic influences of occurrences such as, localized failures, rainstorms, inhomogeneities in the rock mass, variations in the hydrological and erosion conditions, etcetera). This principle is visualized in Figure 15 from the onset of weathering. Note that real decay development may actually involve an increase of a decay index such as *WE*, when weathered parts fail, are eroded, or in any other way removed from the slope, thus exposing fresher material.

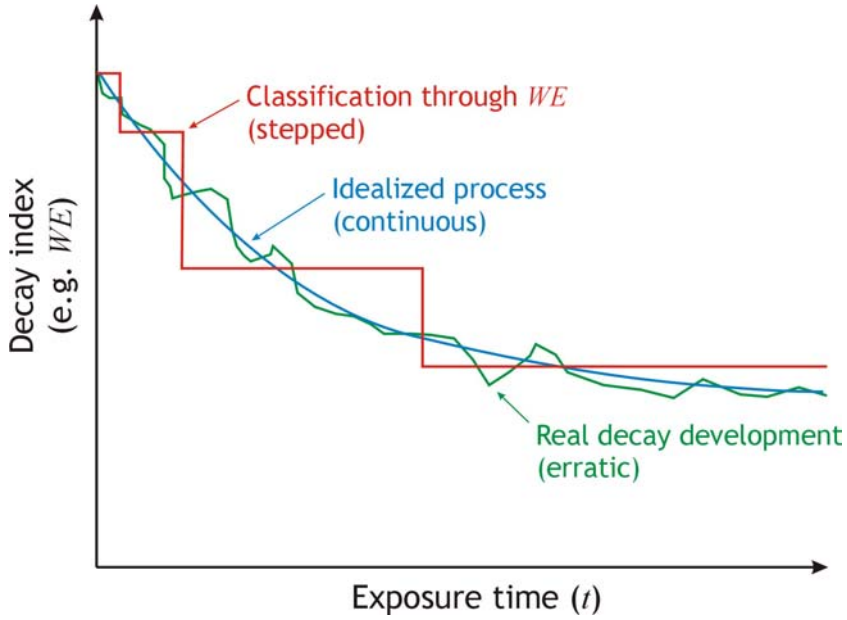

Figure 15 – Slope decay development in time.

intensity (defined as the ratio of the value of some property after weathering and its initial value) will be step-wise in terms of weathering degree.

Box 6 – Weathering front observed in discontinuity walls, Cindarto slope

The bedding plane which acted as sliding plane for the 1991 slide was found to contain a considerable infill of softening material in the still standing part of the slope only ten years later; furthermore, the walls on either side of the discontinuity plane were affected by weathering and clearly discoloured. Figure 16 shows a cross-section through a cut sample taken in 2003 (taken at the 170°/30° dip measurement, see Figure 4, page 20) where both this softening layer and the discoloured discontinuity walls are visible. The picture is displayed such that the bedding plane stands vertical, with the lower discontinuity wall on the left.

Figure 17 shows a thin section made through the left (i.e. bottom) discontinuity wall of Figure 16. The weathering front, seen in Figure 16 as a discoloured zone, is visible at approximately 3mm (3000 µm) from the discontinuity wall. In this case, the weathering front is a rather sharp boundary, with a marked change in both particle size and opaqueness.

Figure 16 - Cross-section through bedding plane of the Cindarto slope. Scale in millimetres.

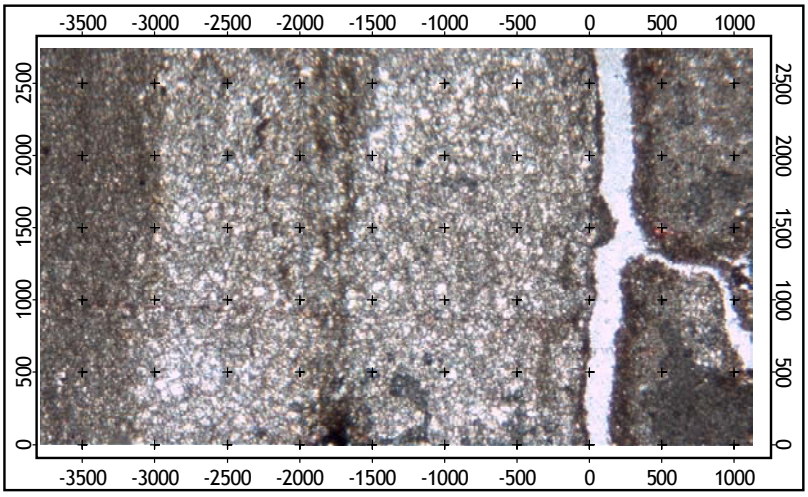

Figure 17 - Overview of thin section through the bottom discontinuity wall of Figure 16. The discontinuity edge is at (0,0). Scale in micrometres.

2.7 Decay: the combined action of weathering and erosion

The combined processes of weathering and erosion will cause decay of any rock mass exposed in a slope, with the mechanical issue of stress release and stress-strain redistribution as catalysts. The relative rates of erosion and weathering determine how the rock mass actually develops and as will be shown in Chapter 4, the ratio of those rates can change within a single slope as a function of both space (i.e. at different locations in the slope) and time.

The primary parameters that determine how the combined processes of erosion and weathering affect a slope are the relative rates of penetration of each process into the rock mass, following excavation of the slope. Erosion may affect both weathered and unweathered material, although erosion rates in weakened weathered material will tend to be highest. If an erosion front is regarded as penetrating the initially excavated rock mass, the penetration rate can be compared to the penetration of a weathering front from the surface into the rock mass. Since the surface of the slope changes with time, due to erosion, the two processes are closely linked. A number of possible situations can be distinguished based on the ratio between erosion and weathering penetration rates, as shown in Figure 18 - Figure 20. It should be noted again that different parts of a single slope can be in different decay situations, and that the situation, in which a specific part of the slope is, might also change in time[17]. This will be demonstrated quantitatively in chapter 4. In the following pages the development of a slope profile on the basis of balance between erosion and weathering will be discussed.

[17] *For simplicity, Figure 18 - Figure 20 are schematic representations. All sketched slopes are in one and the same situation throughout their height, excluding weathering penetration from the ground surface above the slope. In reality, weathering and erosion penetration may not be equal throughout the slope, and weathering profiles predating excavation may also be present. The latter will often result in slopes that are more weathered at their crest than at their toe.*

Figure 18 represents the case where erosion predominates over weathering, and the slope decay is consequently delimited by the rate of erosion. In this case, penetration of a weathering front into the rock mass in the present day is either absent (situations A1 and A2), or slower than erosion (situations B1 and B2). If no weathered zone resulting from previous stages in the slope's decay and no "old" weathering mantle predating the slope excavation is present, the process is clearest (situations A1 and B1). In A1, no weathering occurs and the slope decay is based on erosion and resulting slope retreat alone. Since there is no weathered zone, the degree of weathering as observed in the rock surface is constant and equal to the degree of weathering in the bulk of the rock mass.

In the case of a constant degree of weathering the dynamic weathering intensity rate (see paragraph 2.5) as observed in the slope surface will be zero, whereas the apparent weathering intensity rate will decrease in time. However, if there *is* a weathered zone present at the onset of such a situation (situation A2), either due to previous stages or old weathering, the weathered material will be eroded first. The degree of weathering in the slope surface will actually decrease if the decay situation does not change[18] after the weathered zone is completely eroded. The dynamic weathering intensity rate will change sign and this may also apply to the apparent weathering intensity rate.

[18] *It is very well possible that the penetration rate of erosion decreases considerably after removal of the weathered zone. Additionally, the penetration rate of weathering will probably increase during removal of the weathered zone since weathering penetration rate is likely to be inversely proportional to the existing depth of weathering. This will be elaborated on in Chapter 4. The ratio of erosion and weathering penetration rates is therefore likely to change and the decay situation may change as a result.*

Imbalance favouring erosion	Only erosion, no weathering	**Situation A1** No old weathering mantle or weathering zone from previous stage present	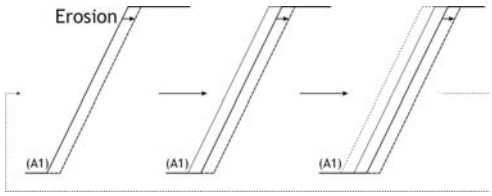
		Situation A2 Old weathering mantle or weathering zone from previous stage present[19]	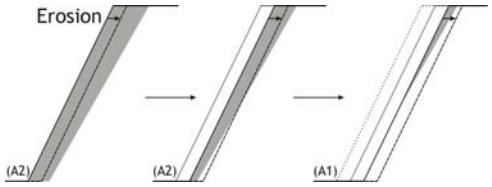
	Some weathering, but erosion penetrates faster than weathering	**Situation B1** No old weathering mantle or weathering zone from previous stage present	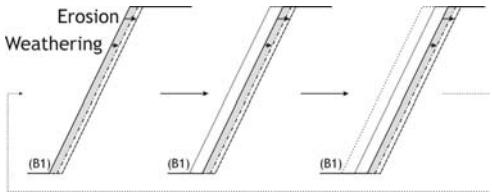
		Situation B2 Old weathering mantle or weathering zone from previous stage present	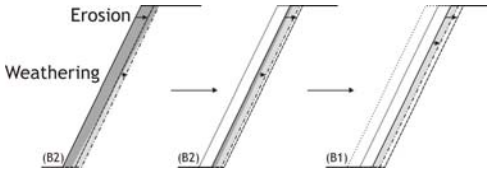

Figure 18 – Decay situations that can exist when erosion penetrates the rock mass faster than weathering. Grey areas indicate weathered material (dark grey: result of previous stage; light grey: result of sketched step).

[19] *In A2 a pre-existing weathering profile is assumed. Since the excavation involves steepening the existing topography, the old weathering mantle will likely be deeper at the top than at the toe of the slope as shown in the drawing.*

Any weathering penetration that occurs during a certain time is obliterated by erosion if weathering does occur at a penetration rate smaller than that of the erosion, and no weathered zone is present (situation B1). Again, the degree of weathering as observed in the rock surface is constant, the dynamic weathering intensity rate is zero, and the apparent weathering intensity rate decreases in time. In situation B2 a weathered zone *is* present. This, as in situation A2, will be removed by erosion and under the assumption that the slope will afterwards continue to decay according to this stage, the observed weathering degree in the slope surface will again decrease and become equal to that of the rock mass bulk when the weathering depth has become zero.

If erosion penetrates into the rock mass with a rate equal rate to that of weathering, there is equilibrium (situations C1 and C2, Figure 19) and the weathering penetration depth remains constant. It is in this case most likely[20] that the observed degree of weathering in the slope surface remains constant as well and therefore that the dynamic weathering intensity rate is zero and the apparent weathering intensity rate decreases in time. The situations in which a weathered zone at the beginning of the stage is present or absent do not differ principally.

The third possibility is of course when weathering penetrates faster into the rock mass than erosion and the rock mass decay is weathering delimited (Figure 20). If erosion does occur but at a slower penetration rate than weathering, the degree of weathering as observed in the slope surface will increase as will the weathering penetration depth (situation D1 and D2). Since part of the weathering penetration is simultaneously being eroded, the apparent weathering intensity rate is not as high as possible in situation E1 and E2 (see below); in this study, this apparent weathering intensity rate is termed the *apparent slope weathering intensity rate*.

[20] *Since it is not necessarily true that the degree of weathering at the surface is directly related to the weathering penetration depth, this cannot be proven.*

Equilibrium between weathering and erosion	Erosion and weathering penetrate into the rock mass at equal rates	**Situation C1** No old weathering mantle or weathering zone from previous stage present	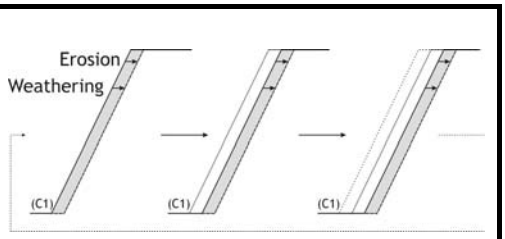
		Situation C2 Old weathering mantle or weathering zone from previous stage present	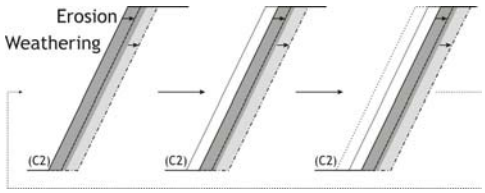

Figure 19 – Decay situations that can exist when erosion and weathering penetrate the rock mass at equal rates. Grey areas indicate weathered material (dark grey: result of previous stage; light grey: result of sketched step).

The apparent slope weathering intensity rate may be constant (and larger than zero), but may also increase or decrease depending on the relative amounts of weathering and erosion in a certain time span. If the weathering degree on the slope surface is linear on a $\log(1+t)$ timescale, the apparent rate as defined in Equation (1) is constant in time for a particular material. If the weathering degree on surface changes linearly with $(\log(1+t))^n$, the apparent weathering intensity rate as defined in Equation (1) decreases with $n<1$ and increases with $n>1$. Again, the presence of a weathering zone at the start of this situation does not make a principal difference.

In situations E1 and E2 the weathering penetration rate is the highest possible since no erosion affects the material being weathered. The apparent and dynamic weathering intensity rates can therefore be termed the *apparent* and *dynamic reference weathering intensity rates*, respectively; if the assumption of a $\log(1+t)$ timescale in Equations (1) and (2) is correct,

both are constant. The depth of weathering and weathering degree at the surface again increase in time.

Imbalance favouring weathering	Some erosion, but weathering penetrates faster than erosion	**Situation D1** No old weathering mantle or weathering zone from previous stage present	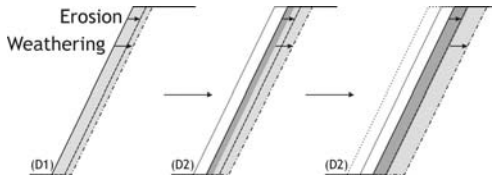
		Situation D2 Old weathering mantle or weathering zone from previous stage present	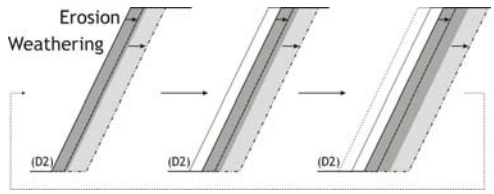
	Only weathering, no erosion	**Situation E1** No old weathering mantle or weathering zone from previous stage present	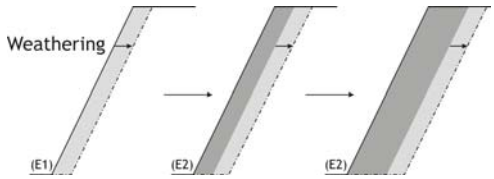
		Situation E2 Old weathering mantle or weathering zone from previous stage present	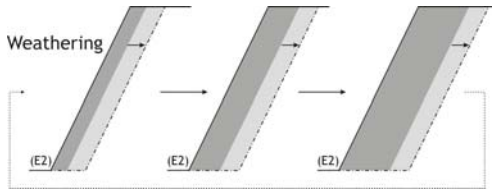

Figure 20 – Decay situations that can exist when weathering penetrates the rock mass faster than erosion. Grey areas indicate weathered material (dark grey: result of previous step; light grey: result of sketched step).

2.8 Factors controlling decay processes

The complexity of rock mass decay processes and the delicate balance between different decay processes that determines the outcome of their combined action has already been pointed at. For weathering itself (paragraph 2.5), influencing factors can be subdivided into internal, external and geotechnical parameters. The dominant parameters are presented in Table 4. Especially the consideration that both weathering and erosion are influenced by the local climate is generally accepted as a matter of fact. Field investigations show the close relation between local climate and its cyclic variations, and the resulting decay processes in exposed rock masses (e.g. Regüés et al., 1995; Cantón et al., 2001).

In contrast with this, the answer to the question of how the "local climate" should be defined is not a matter of fact. The common viewpoint has long been that mesoscale climate is in control of geographical variability in weathering (Pope et al., 1995), with the "weathering environment" typically defined in terms of parameters such as mean annual temperature and precipitation.

A classical example of this is presented in Figure 21, in which four principal climate zones are recognized (periglacial, temperate, arid, and humid tropical) that are supposed to govern weathering processes and rates – assigning, as an example, the same basic driving force for weathering to the Falset area in eastern Spain as to the UK and Sumatra. This simplification has helped to identify principal factors in weathering and to recognize the importance of climatic influences. In recent years however, it has been realized that the climate on a localized and even microscopic scale is what really influences weathering and erosion; as stated by Pope et al. (1995) *"the intuitively grounded theories linking troposheric mesoscale climates and weathering are oversimplified"*.

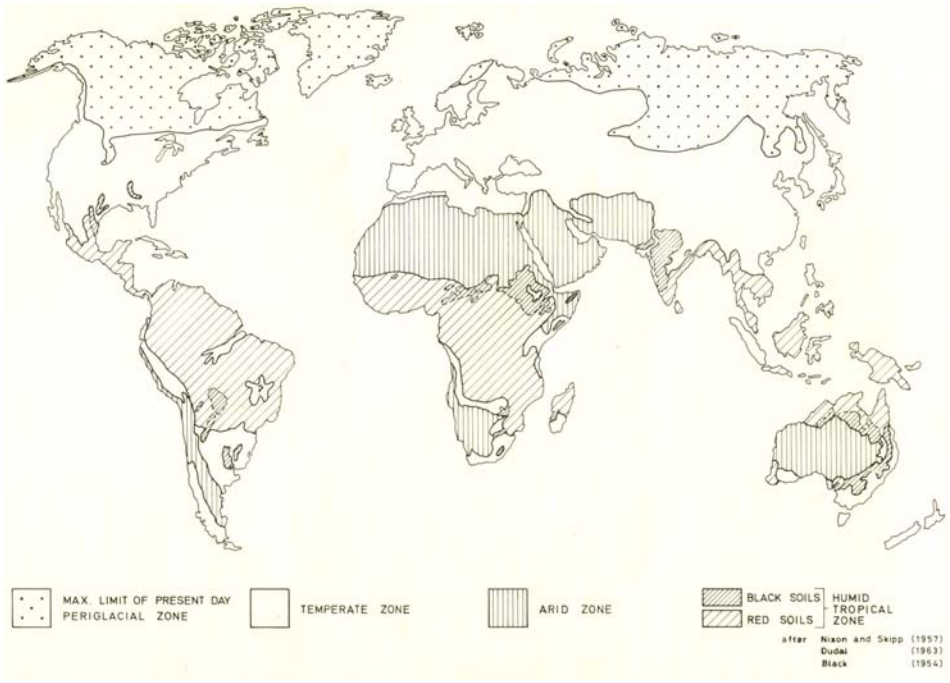

Figure 21 - Generalised map showing the distribution of four principal climatic zones (from Saunders and Fookes, 1970).

Table 4 - Factors controlling decay processes.

	Parameter	Influence
Internal	Material composition	The influences and significance of chemical weathering processes is largely determined by the type of materials present in association with the site-specific conditions Minerals composing rock masses are differently affected by weathering. For example, some minerals are unstable under surface conditions with low stress levels or the influence of water or temperature when exposed. The presence of (even small) amounts of swelling clays greatly increases the weathering susceptibility.
	Material fabric	The material fabric also determines the means of access for weathering agents. As an example, void space in the material that is accessible for water increases weathering susceptibility. In weak materials, the material fabric also directly influences erodibility.
	Influences of water	The specific influences of water greatly depend on the material composition. For example, in the presence of soluble components (e.g. gypsum), prolonged availability of water and water retention enhance decay; in the presence of slaking components (e.g. swelling clays), periodic changes in water content enhance decay. The availability of reactants for chemical reactions depends partially on the composition of the water phase (reactants may also be derived from the solid materials in the rock, or from gas phases).

	Parameter	Influence
	Permeability	Permeability influences the penetration depth of inflowing atmospheric water as well as the rate of groundwater flow. In general, an increase in permeability is associated with an increase in decay rates.
	Discontinuities (aperture, orientation, persistence, permeability)	The discontinuities determine rock mass strength, as well as the permeability and other hydrologic properties of the rock mass. In combination with the slope orientation and angle, their orientation determines the inflow conditions for infiltration of overland flow.
External	Climate	Climate conditions (temperature, precipitation, evaporation) are for a large part responsible for determining decay conditions in specific sites. In the past average climatic condition were thought to be determining but present insights show that micro-conconditions on a slope are of far more influence than originally thought. This is discussed in detail in the main text.
	Morphology	The local topography and in a more general sense the site morphology influence stress levels in slopes, overland flow discharge, inflow conditions, groundwater flow et cetera. The morphology directly above the slope will furthermore influence weathering penetration rates.
	Hydrology	In combination with the internal parameters listed above, hydrological conditions influence both type and rate of prevalent decay processes, both in terms of weathering and erosion.
	Chemistry of rain- and groundwater (acidity and alkalinity, redox potential, oxidizing or reducing environment)	The chemical properties of rain- and groundwater determine for a large part the available resources for chemical reactions and hence the prevalent chemical weathering processes. They are influenced by air pollution (e.g. Winkler, 1997), proximity to the sea (Neil, 1989; Inkpen and Jackson, 2000), and local factors such as vegetation cover on the slope itself and the hillside above.
	Biochemical influences	The influence of biochemical factors such as lichens is complex, and is described in the main text in more detail.
	Geological history	The development of weathering profiles in the geological past influences the slope development in present time; this was already shown in paragraph 2.7. This is true both in terms of observed weathering intensity, and mechanical development, since historical weathering and associated weakening reduce slope stability. It has to be noted that the weathering environment in the geological past may have been very different from today.
Geotechnical	Slope orientation, geometry and height	These parameters determine the intersection of the slope with the local morphology and geology, and thereby influence the boundary conditions for decay processes. Furthermore, the slope aspect determines the exposure to the prevalent wind directions as well as to solar radiation; type and amount of vegetation cover is in its turn a derivative of this.
	Excavation damage	Opening of existing discontinuities, and cracks and discontinuities formed during excavation, determine internal parameters such as aperture or “open-ness” of discontinuities, permeability, et cetera.
	Remedial measures	Any remedial measures incorporated in the slope design determine decay processes, their rates, intensity and effects (see paragraph 6.3).
	Land use	Agricultural land use influences weathering processes as shown by Semhi et al. (2000). For example, the use of fertilizers may very well influence natural weathering-erosion processes. This however plays no role of improtance in the road cuts that are the subject of this study.

The same point has been made by Smith et al. (2000) who found complex and even intense weathering features in highly arid environment in southern Tunisia, pointing out that the simplification of weathering into regional-scale predictions for weathering behaviour as based on such general parameters as mean rainfall and average temperature does not provide enough detail and does not appreciate the variability of weathering processes within one region. On a slope scale, Nicholson (2001a) also found that very local variations (on a slope face itself) in exposure to flowing water, rainfall, sunlight etc. caused noticeable variations in the development, intensity and rate of decay processes. In addition to this the vegetation cover has an important role in determining the chemical environment of a particular site, thus influencing chemical weathering processes.

The above notions lead to the following conclusions:

a) The generalisation of localized observations of decay processes (including their intensity and rates) is impaired by their exact relation with the local environment (local referring to the combination of environmental factors acting on the exact spot at which the observation was made).
b) Representative averages for the intensity and rates of observed decay processes for whole slopes can be matched to the local environmental factors acting on the slope as a whole.
c) Climate data should be related to site-specific conditions (e.g. average slope orientation) when relating it to such representative averages.
d) Inevitably, point observations will show a scatter. This is not only due to the fact that environmental influences may well vary within one single slope (Nicholson, 2001a) but also because variations in the rock mass exposed in a slope exist (e.g. variations in internal factors such as lithology and strength, and geotechnical factors such as aspect, excavation damage, etc.). Even when individual engineering geological units in the rock mass are considered, some natural variation in such factors will exist.

The influence of biochemical factors such as lichens on weathering rates is a good indication of the complexities involved in defining influencing parameters for weathering and the nature of their influence. On one hand, the presence of lichens on rock surfaces is found to increase rock weathering rates by a factor of up to 16 (Stretch and Viles, 2002); similar results were obtained by Aghamiri and Schwartzman (2002) showing the significance of biotic enhancement of chemical weathering. On the other hand, Garcia-Vallès et al. (2003) found that a coat of lichens that is sometimes present on the face of Cappadocian tuff walls apparently reduces the penetration of water and thus the moisture content within the rock, protecting the rock from alteration and decay, and effectively decreasing the weathering intensity rate.

Some parallel exists in the tombstone problem (Robinson and Williams, 1996; Williams and Robinson, 2000) where ambiguous influences of the tombstone orientation with respect to prevailing wind directions were found. If one single parameter is filtered out from all the parameters that influence weathering in a given setting (e.g. presence of lichens, orientation), it seems that the resulting conclusions on that parameter's influence are restricted to the isolated study cases only and extrapolation to other settings may lead to false predictions. Essentially, this is also what has been found by Nicholson (2001a) when trying to extrapolate laboratory test results to field settings with complex and rather undefined conditions. This problem can be bypassed to some extent by analyzing large data sets and incorporating the resulting variability in the actual analysis.

The ultimate culmination of decay problems is slope instability. In this respect, the role of water has long been considered predominant. This notion is often correct, but is has been interpreted so for the wrong reasons. Hack (1998) indicated that contrary to accepted ideas, water pressures are not necessarily a trigger for instability and slope failures in rock, and may in fact be of secondary importance only – a point supported by the findings of a recent paper by Jaboyedoff et al. (2004), who monitored the movement of unstable rock blocks and rainfall. Delay times between the end of rainfall

events and movement of monitored discontinuities indicated that slow processes instead play an important role, such as weakening and softening of discontinuity walls due to wetting. Water pressures that would quickly dissipate in the studied cases (with open discontinuities) cannot be considered as a trigger after the observed delay times. Other observations included that weathering intensity rates of discontinuities increased with both water content and water circulation, and the occurrence of montmorillonite in the gouge present in the discontinuities of the studied rocks led to an increase in the suction and thus an increase in the shear strength when unsaturated, and conversely a decrease in the shear strength when saturated.

3 Observations on decay processes in slopes

"The world is full of obvious things which nobody by any chance ever observes." – Sir Arthur Conan Doyle, *The Adventures of Sherlock Holmes: The Hound of the Baskervilles*.

3.1 Introduction

Even in short time spans of some years, rock mass decay shows itself in the units that are most susceptible to weathering with notable erosion, pelitoclastesis, and discolourisation. Still, also the units that are assumed to have a far greater resistance to weathering and subsequent erosion show a myriad of decay processes.

The different time-scales at which those processes have occurred in the past, and are still occurring today, bring about a complicated overall picture. Separating the superimposed results of weathering and erosion processes is necessary to identify the dominant processes and indicate which properties of the rock mass are determining the effect that weathering and erosion have in engineering time-scales.

Different rock *materials* will generally be affected by a range of different decay processes when subjected to one and the same "weathering environment", defined by a particular combination of external and geotechnical decay paramaters (see paragraph 2.5). The combination of decay processes that act on the various materials present in the rock *mass* exposed in a slope will result in overall rock mass decay. This rock mass decay ultimately affects general behaviour and therefore the stability of the slope as a whole.

In this chapter, overall decay processes observed to act on the various studied engineering geological units in the research area are discussed.

3.2 Decay processes - Keuper

As one of the most "weatherable" formations in the research area, the Keuper series is of particular interest to this study. Two litho-units are discernable in the Keuper: one succession consisting of shales, clays, and thinly to very thinly bedded dolomitized limestones, and one succession with medium-bedded dolomitized limestones that are interbedded with shales[21].

Whereas the latter unit is relatively resistant to decay, in general one rarely encounters a "good" outcrop of the first unit, the Keuper shales ("good" meaning that the geotechnical properties can be observed in some detail and that the intact rock mass is not covered by soil or and/or vegetation). This in itself is already an indication that this lithology rapidly breaks down when exposed in road cuts and other artificial slopes.

In recent years the major excavations in this unit have been along the N-420 between Coll Teixeta and Falset; construction of this section took place between 1989 and 1990, after which some slopes have been modified to cope with stability problems. The slopes in this section are between 10 and 20 metres high and were initially constructed with a slope angle of approximately 65-70°. The only other recent excavations have been cut along a minor road leading from the C-233 at the Coll de Fatxes between Vandellós and Tivissa towards the south past the village of Gavadà. In 1999 this road, which was barely more than a track before, was widened and paved, and several small road cuts of about 2 to 3 metres high were made. With exposures of Keuper shales being so rare, this has been an important opportunity to study the decay of Keuper shales, and the Gavadà study slope is located here (see Appendix G). In Figure 22 three consecutive stages

[21] *Although this latter unit is described as part of the Keuper, some discussion exists as to whether it may actually belong to the Upper Muschelkalk. This thesis follows the conventions of the relevant IGME geological maps.*

in the development of the Gavadà slope are given in the form of photographs of the middle section of the slope, showing the notable decay and pelitoclastesis in the first five years following excavation.

The decay behaviour of the shale unit is predominantly determined by the presence of clays (approximately 25% by volume), including montmorillonite. In the Gavadà study slope these clays occur interbedded with thin to very thin dolomite layers. On a *material* scale, the clays and these dolomite layers show different decay processes. The dolomites are visibly affected by solution giving a characteristic appearance as if the rock is covered by cobwebs (Figure 23). The shale shows pelitoclastesis and in dry periods clear desiccation cracks that are the result of cyclic wetting and drying and the associated swelling and shrinking strains. Other processes such as hydrolysis may well occur simultaneously but the effects of these are not dominantly visible.

Cyclic wetting and drying of the shale is the main process when looking at *rock mass* decay (see Box 7); on the slope scale, the decay of the clays is the major component of decay especially in engineering timescales. Observations in this and similar slopes strongly indicate that as long as the more competent and more resistant materials present in a rock mass do not form the main framework of that rock mass, mass decay is steered by the weaker, less resistant material which does form the main framework (see, for example, the results presented in 5.2).

To some extent this is also true for rock masses in which weathering of less resistant materials causes stability problems in the more competent materials. In such cases it is the *result* of decay of the weak parts which affects the strong parts: for example, undercutting of competent layers after weathering and erosion of less competent layers, as in the Hostal slope described in Box 4, page 35. However, in the case of Keuper shales and clays such as studied at Gavadà it is the *process* of decay in the weak parts which also affects the strong parts: the swelling of the clay-rich layers results in stresses that break up the thin dolomite layers. Thus, the break-up of

competent layers in the second case takes place simultaneously with the decay of the weaker parts, whereas it follows the decay of the weaker parts in the first case. There is however only a fine line between these two cases and in inhomogeneous rock masses, the weakest materials present will always be a cause for concern as to the geotechnical behaviour of the mass as a whole.

a.

b.

c.

Figure 22 - The study slope at Gavadà, in Keuper shales with intercalated dolomite beds (N4543330/E314815) in May 2000 (a), May 2001 (b), and May 2004 (c).

The strains due to swell-shrink cycles (see Box 7) together with the breaking up of material bonds at the microscopic scale (Kühnel, 2002) lead to a slaking and loosening of material at the surface, which is then easily eroded. In the few years after its excavation, the Gavadà slope has already lost a significant amount of material because of this; this will be discussed later in Box 10 in chapter 4 (page 104).

The amount of retreat has been more or less similar over the entire slope, even though the rock mass is heterogeneous. Some slumps have occurred due to undercutting of dolomite banks (Figure 24), distorting the homogeneous nature of the slope retreat somewhat, but the slope face in 2004 is still remarkably planar[22]. Linear erosion is starting to develop however, and shallow grooves are visible (Figure 22). In this and similar weak materials, such grooves often form in the depressions left by excavation equipment that concentrate water flow. Further developed rill and gully erosion effects are also observed in slopes along the N-420 where the same shale outcrops.

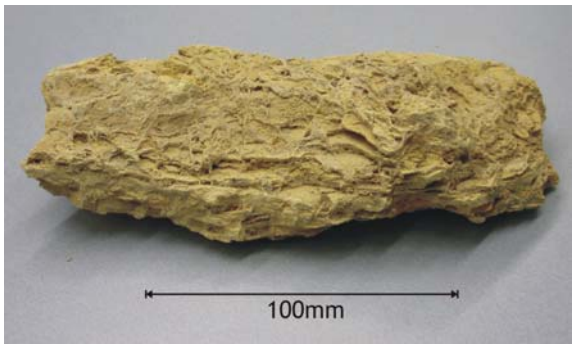

Figure 23 - Cobweb-like dissolution features in dolomite sample from Gavadà study slope.

Figure 24 - Small slump in Gavadà slope (May 2004).

[22] *This indicates that the episodic components of the slope development by decay (refer back to Figure 15 on page 60) occur and repeat themselves at such a small time scale that they are not apparent in yearly or bi-yearly observations as performed for this research.*

Box 7 – Swelling / shrinking of the shales in the Gavadà slope

With the methodology described by Pejon and Zuquette (2002), swell-shrink tests have been conducted on Keuper shale samples from the Gavadà slope, taken at a depth of approximately 30cm below the slope surface. XRF/XRD tests revealed a total clay mineral content of 25% by volume. The main clay mineral present is illite (21% by volume), but swelling capacity is determined mainly by the montmorillonite content of approximately 4% by volume. The swelling/shrinking behaviour is associated with considerable slaking. Laboratory tests on these shales show a second cycle slake durability shales of only 17% ("low durability", Dick and Shakoor, 1995).

During wetting, the sample is submerged until constant strain is obtained; during drying, the water is let out and the sample is dried under atmospheric conditions until the original water content is reached. Figure 25 shows the results of eight repeated wetting-drying cycles on one sample. Since all strains are relative to the original sample height, it is obvious that for each cycle the final sample height at the end of the drying period was less than the original sample height. This is explained by the distruction of the internal material fabric during the first swell cycle, and the associated irreversible decrease of porosity at a given water content that results in a shrinking strain during the first cycle which is double that of the swell strain.

The depth at which the sample was taken ascertains that no previous in-situ wetting-drying cycles have acted on the tested material. The slope material has been found to be wet up to a maximum of 10cm from the slope surface, hence well above the depth of the sample. Therefore Cycle 1 indeed represents the first such cycle acting on this material. After the completion of the first cycle and the associated disruption of the material fabric, strains during swell and shrink have on average an equal magnitude, of + or - 2.2% relative to the sample height at the start of each wetting or drying step.

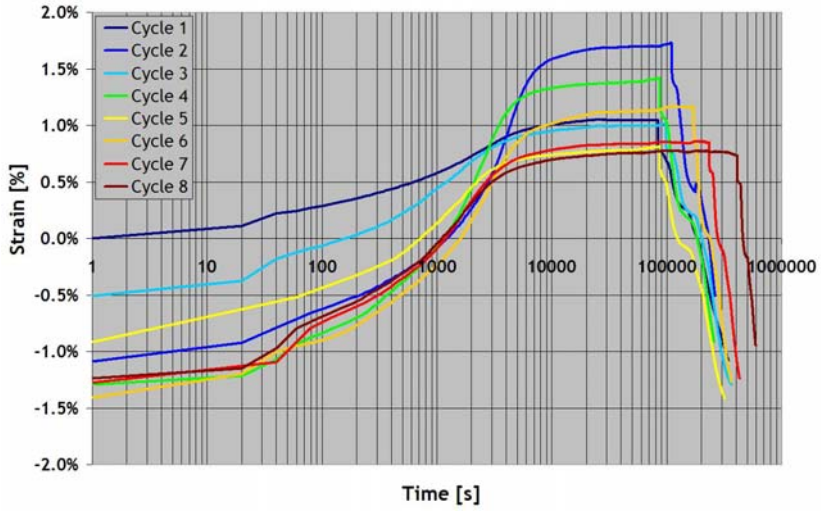

Figure 25 - Swell-shrink test results. Strains relative to original sample height.

The material eroded from the Gavadà slope is collected in a ditch which is connected through a culvert with a small circular pond known as the Toll the Geinessies (Figure 26). This pond contains water for a large part of the year, but during summer it runs dry, revealing at its bottom the finest fraction of the erosion products of the slope.

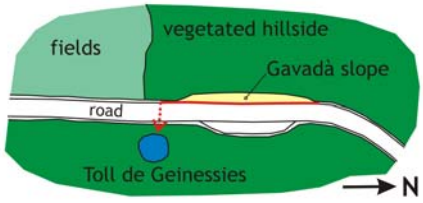

Figure 26 - Sketch map of the Gavadà site. Red line: ditch and culvert.

Figure 27 shows the material bottom of this pond in early September (2004), when it is completely dry. Desiccation cracks are present throughout the deposited material. By measuring the accumulated width of these cracks in a certain section length, a shrinking strain of approximately 4 to 5% is found. The higher values for the strain in the pond bottom sediments are attributed to the fact that the material here consists of the finest fraction with a higher clay content and strong desiciccation in summer.

Figure 27 - Desiccation cracks in the dry bottom of the Toll de Geinessies (September 2004).

The volumetric changes caused by swelling and shrinking strains in slopes such as at Gavadà are surprisingly large even in short time spans. Two holes were left by sample tubes in May 2000, with a diameter of 40 mm and a depth into the slope of approximately 150 mm; one of these did indeed disappear within one year. Six months later, in September 2000, both holes were still visible in the slope. In May 2001 the right hole was not present anymore (Figure 28). In part this was caused by surface retreat due to the rapid erosion of the weak material exposed in this slope. The part of the hole which was not eroded was closed by the surrounding material converging into the small hole. In the left hole this could also be seen in the decreased diameter and non-circular cross-section in 2001. In 2002, the left hole had disappeared as well.

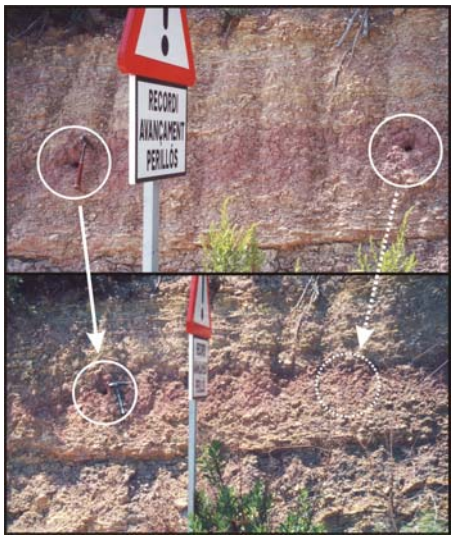

Figure 28 - Sample holes in the Gavadà slope: May 2000 (above) and May 2001 (below).

In several slopes along the N-420 harder shales are encountered[23]. The intact rock strength (IRS) of these shales is higher than that of the more clayey materials outcropping at Gavadà (12.5–50 MPa vs. 5-12.5 MPa). Additionally the blocks that are constituting the mass are better defined, with more persistent joints. It is the block size in this material which is the first and most obvious impression of weathering (described further in Box 8). This decrease in block size caused by decay is confined to the outer part of the rock mass. The loss of coherence associated with it can lead to severe stability problems due to undercutting, as differential erosion in the Hostal study slope shows (described earlier in Box 4, page 35).

The Keuper limestone unit consists mainly of dolomitized limestones, that are similar in constitution to those of the Upper Muschelkalk (see López-Gómez et al., 1993). The limestones in the Keuper series are however often found interbedded with weaker shales. Results discussed in paragraph 5.2 indicate that mass decay in the Keuper limestone unit is largely controlled by the presence of those weaker materials[24]. Material weathering processes however are largely similar to those observed in the Upper Muschelkalk limestones (see paragraph 3.4).

[23] *Results presented in 5.2 indicate that apparent weathering intensity rates are however similar to those of the shales as encountered in the Gavadà slope, with no apparent relation in this unit between intact rock strength and apparent weathering intensity rate.*

[24] *With lower apparent weathering rates for the limestones than for the shales, but with similar preferential directions.*

Box 8 – Desintegration of shales in the Hostal slope: decrease of block size

Figure 29 shows the Hostal slope with a number of shale layers indicated. The lowermost shale layer encountered in the sequence exposed in the slope has a grey-blue colour, and is overlain directly by a more greenish shale layer. Higher up in the sequence other layers of this greenish shale occur.

Figure 29 - The Hostal slope with the various shale layers visible. Photo by W. Verwaal, May 2002.

Both the blue and green shales show considerable weathering and erosion, leading to undercutting of the dolomite layers (Box 4, page 35). The effect of weathering is most noticeable as an increase of the discontinuity frequency, and thus a decrease of the block size. For the green shales, the size of the flaky shale particles at the surface is measured in millimetres up to centimetres.

When excavating a small depth below the surface, it is found that the block size increases rapidly. At 5 to 10 cm underneath the surface, the block size is approximately 2 to 4 cm, and the rock mass becomes increasingly stronger and more difficult to excavate. The blue shales show the same increase in block size with an increase in depth from the surface. In Figure 30 and Figure 31 samples taken at 2cm and 10cm below surface are displayed. Not only does the block size increase with an increase in depth, the angularity of the larger particles increases as well.

A further difference is the colour. The superficial material is greenish to reddish grey, the material deeper in the rock mass grey. This suggests oxidation of iron near the surface, a process which is also associated with volume increase (around 10% - Kühnel, 2003).

➲

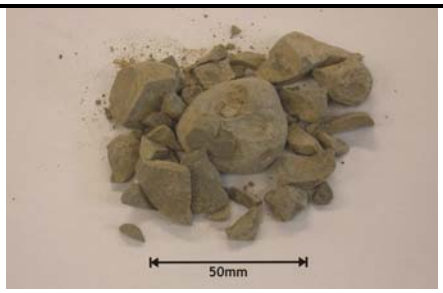

Figure 30 – "Green shales" of the Hostal slope, sample taken 2cm below surface. Note the roundness of the blocks.

Figure 31 – "Green shales" of the Hostal slope, sample taken 10cm below surface. Note the larger block size and the increased angularity

Slake durability testing done on the different shales gave as first cycle slake durability values 30% ("very low durability" – Goodman, 1980) for the blue shales, and 98% ("high durability" – Goodman, 1980) for the green shales. Methylene Blue Adsorption (MBA) test results give MBA adsorption values of 1.58 g/100g and 0.99 g/100g for the blue and green shales, respectively. This indicates a higher swelling potential of the clay constituents of the blue shales, which corresponds to their lower slake durability.

Dick and Shakoor (1995) and Shakoor (1995) have related the 2nd cycle slake durability to indicative undercutting rates. The durability results found on the Hostal slope shales indicate likely undercutting rates of 2-3 cm/yr for the green shales, to 5-10 cm/yr for the blue shales. These values should be considered indications only, since slope height is not incorporated and this is likely to play a role. Furthermore, the slake durability is a material index property and mass field behaviour may differ from this.

At the Gavadà study slope (refer to Appendix G) a similar situation is found as in the Hostal slope shales; within 10 cm from the slope surface, the irregular pattern of disintegrated weak material covering the slope turns into a weak rock with clearly distinguishable discontinuity sets, with a block size of approximately 4 to 5 cm.

3.3 Decay processes - Middle Muschelkalk

In the Middle Muschelkalk series two litho-units are distinguished based on the dominant material types: "siltstone" and "gypsum" (examples in Figure 33 and Figure 34, respectively). The siltstone does also contain gypsum but not more than half of the material, and usually the gypsum forms the cement in this unit that contains 25-30% by volume clay minerals.

Typically, rocks or geotechnical soils such as the Middle Muschelkalk siltstone units can present considerable volume change and breakdown when in contact with water (Pejon and Zuquette, 2002). A combination of three factors has been found to be responsible for their weathering (Cantón et al., 2001):

- Repeated cycles of wetting–drying and associated swelling and shrinkage of small amounts of swelling clays. The presence of even small amounts of swelling clay in certain positions in the texture of the rock can promote swelling and breakdown (Kühnel and Tshibangu Katshi, 1997; Pejon and Zuquette, 2002; Kühnel, 2002) and the durability of clay-bearing rocks is strongly influenced by the type and amount of clay minerals, most notably the amount of expandable clay minerals (Gökceoğlu et al., 2000).
- Dissolution–crystallisation of relatively soluble minerals, gypsum being the most abundant within this category. This is associated with volume changes and resulting internal stresses that can lead to microfracturing by weakening intergranular binding and subsequently reducing strength properties (Kühnel et al., 1994).
- In addition to mineralogical composition the presence of geologically-induced cracks and fissures that affect the structural integrity and give access to weathering agents is relevant.

The first two of the factors listed above are accompanied by volume changes, a common characteristic of reactions and transformations of unstable minerals (Kühnel and Tshibangu Katshi, 1997; Kühnel, 2004). Build-up or release of inner strains during such volume changes lead to formation and propagation of microfissures. All the involved processes may be accelerated by biological involvement. Subsequent erosion rates are controlled by the weathering intensity and penetration rates of the mudstones (Regüés et al., 1995).

Of the three factors mentioned above, the cyclic wetting and drying is the strongest influence on weathering. Wetzel and Einsele (1991) state that *"above the groundwater table, the weathering of mudstones low in carbonate*

and organic matter is controlled mainly by the frequency and intensity of changes in relative humidity within the unsaturated rock (leading to shrinkage and swelling)". Such weathering which results from drying-wetting cycles leads to the formation of what Wetzel and Einsele (1991) term pelitoclasts, fine debris resting on the foot of the slope (Figure 32). Field investigations by Cantón et al. (2001) have confirmed that weathering intensity rates in mudstones in south-eastern Spain were proportional to the number of rainfall events during the sampling periods. This also corresponded to laboratory findings, namely, that in such mudstones it is the number and frequency of wetting–drying cycles that has the greatest influence on weathering intensity rates (Cantón et al., 2001).

Figure 32 - Middle Muschelkalk siltstones along C-233 near Masriudoms. Rill and gully erosion have developed in the face above the scree cover. Excavated in 1992.

Furthermore, studies on badland areas in the Vallcebre basin (Pyrenees) reported by Regüés et al. (1995) suggested that in the setting of that study, erosion rates were controlled by the weathering intensity rate. The same research showed the importance of changes in the seasonal weather pattern.

The morphological development of the area is characterized by regolith formation during seasons with lowest precipitation rates and regolith depletion by storm rainfall erosion during seasons with highest precipitation rates and intense rainfall events. In fact, this seasonal influence and the resulting differences in geomorphological development from one season to the other, with its associated modification of the characteristics and appearance of the surface regolith, can be so strong that *"they raise serious questions about the validity of observations or experiments carried out in only one season"* (Regüés et al., 1995). Meisina (2004) shows the same importance of swelling-shrinking potential for slope stability and the influences of seasonal weather changes. Because of strong shrinking of mudstones in the dry season and associated formation of desiccation cracks, rain water penetrates easily through the cracks into the subsoil. The result of this is a rapid response on precipitation events in the wet season and softening of the clay surrounding the fissures, thus adversely affecting the slope stability of dried materials with such swelling-shrinking capacity. Although the above reported observations were made in natural slopes, the same considerations apply to artificial slopes as well as earth fills such as dikes and dams.

The Middle Muschelkalk siltstones form the most rapidly disintegrating rock mass in the research area, and show an even higher susceptibility to weathering than the Keuper shales. They are however better exposed than the Keuper especially because a number of large and recent road cuts exist along the major roads C-233 from Hospitalet del'Infante to Tivissa, and N-420 from Réus to Falset. Figure 33 shows as an example a slope along the N-420 which has been excavated in 1989/1990 with an initial slope angle of about 70°. Weathering and erosion have brought this down to 40° in 2004; the slope face, which is affected by rill development, is mostly covered by vegetation fifteen years after excavation. Other road cuts in this unit also suffer from gully erosion developing after only several years (Figure 32, page 86; see also Box 9). The toes of such slopes are usually covered with scree although this may in part be actively removed during road maintenance and ditch cleaning.

Slaking is an important decay process in this unit, and cyclic wetting and drying affects the siltstones forming desiccation cracks that lead to the pelitoclastesis, of which the scree cover is the result. A second weathering process is dissolution of the gypsum; especially in the gypsum subunit, this can be clearly recognized, and water flow traces are often visible. In the siltstone unit, which also contains gypsum, dissolution of the gypsum cement will lead to an additional weakening of the material next to the slaking through cyclic wetting and drying.

Gypsum formations are primarily affected by chemical weathering, with dissolution of the gypsum component. This process may lead to severe geotechnical hazards (e.g. Hawkins, 1979; Cooper and Waltham, 1999). Auvray et al. (2004) have investigated the decay process of gypsum that was extracted from two underground mines in France. Even in those underground settings, where no direct impact of rainwater occurred, the effects of chemical weathering were apparent as the presence of traces of dissolution.

The weathering of the Middle Muschelkalk units is therefore the result of the superimposed effects of slaking and dissolution, with the relative importance of each process determined by the principal component of the unit (siltstone or gypsum).

Figure 33 - Road cut in Middle Muschelkalk siltstones along the N-420 near Pradell de la Teixeta, excavated in 1989/1990 (May 2003).

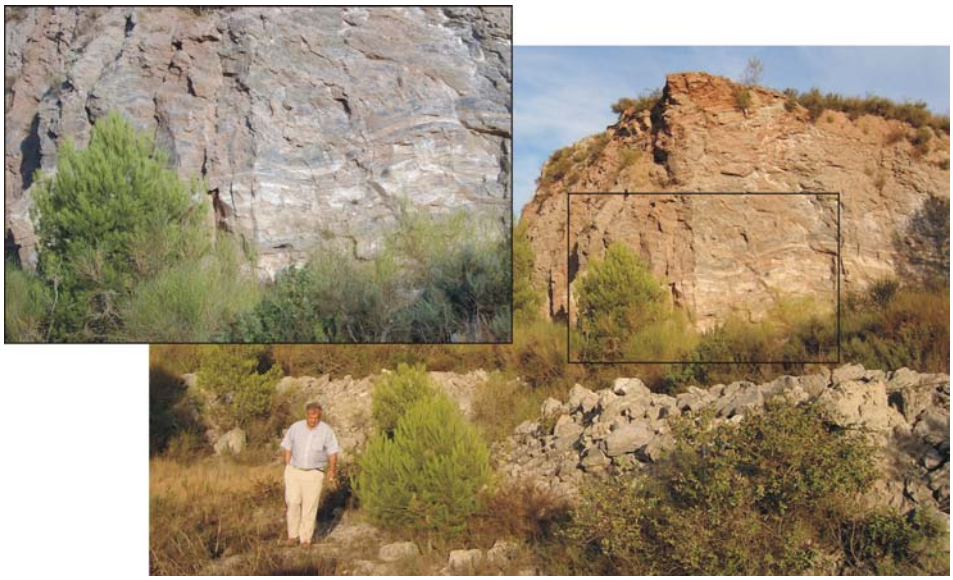

Figure 34 - Gypsum quarry in Middle Muschelkalk, near Pradell de la Teixeta (September 2004).

Box 9 – Rill erosion in the Masriudoms slopes

In both slopes of the Masriudoms site (refer to Appendix G), rill erosion is a prominent decay process, and a first interesting difference between the two slopes in this respect is the development of the average slope angle through the years, with the south-facing slope on the north side of the road showing a slightly higher overall erosion rate than the north-facing slope on the south side, resulting in a slightly lower slope angle at present in the north side slope (38° vs. 41°, measured May 2004). This small difference in erosion rate is not surprising in light of the area's climate as described in Appendix B, with the observed trend for the wind to tend to turn to the southeast, with a simultaneous increase in wind velocity, in times of rain, a trend which is even more pronounced with increasing precipitation intensity.

As Selby (1993) indicates (see also Appendix D), the kinetic energy associated with the impact of raindrops that causes rainsplash erosion increases rapidly with rainfall intensities of a magnitude recorded in the area. Rainsplash adversely affects the surface of slopes in soils by enhancing weathering (notably slaking) and decreasing strength parameters (such as cohesion and internal friction), besides having notable erosion effects of its own at high rainfall intensities (>25 mm/hr) (Roose, 1996). The influence of rainsplash leads to an increase of the susceptibility to flow erosion. With the north side slope being more exposed to the prevailing wind direction during rainfall and associated rainsplash, and the south side slope more sheltered from it, rainsplash and flow (rill) erosion are indeed likely to affect the north slope more than the south slope.

Although the average slope angle in both slopes has been continuously decreasing since the time of excavation, indicating that the slope angle as excavated is not sustainable in this unit, there had been no observed single-event slides or failures until May 2004, when a section of the north-facing south side slope failed (see Figure 35). This event turned the continuous progress of the mass-wasting in this slope into an episodic one, at least for the considered time interval and this section of the slope.

Figure 35 - The south slope at Masriudoms, in April 1997 (left, photo by F. de Boer) and September 2004 (right). The left hand part of the visible section failed in May 2004. Note the base of the electricity pole for reference.

➲

With an Optech Ilris 3D laserscanner, measurements were taken of a part of the slope in May 2004, giving a point cloud with x, y and z-coordinates and reflection intensity for each of the reflection points (Figure 36, see Slob and Hack (2004) for a description of this LIDAR method).

Figure 36 - The rectangle indicates the scanned section of the slope (left), with the resulting point cloud (right).

The resulting point cloud can be compared to the initial slope surface, which in this case was planar. By calculating the retreat of the slope in a horizontal direction for each reflection point, an erosion contour plot can be made. The results for a planar initial slope with a 50° slope angle are given in Figure 37; positive values indicate material accumulation, negative values indicate erosion.

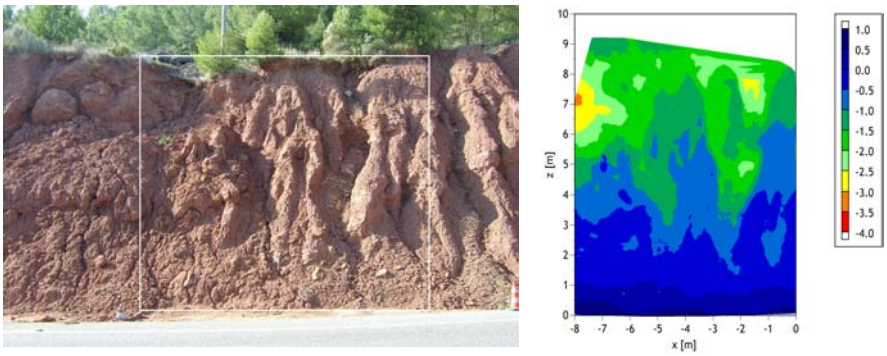

Figure 37 - The rectangle indicates the scanned section of the slope (left), the right figure gives the erosion contours calculated from the May 2004 LIDAR data. Intervals in metres.

The rill erosion is recognizable in the contour plot, with the erosion contours curving from parallel to the slope toe, to perpendicular to the slope toe. The back scar of the slump is visible in the top left of the contour plot of the scan data.

3.4 Decay processes - Upper Muschelkalk

The limestones of the Upper Muschelkalk series are often dolomitized (López-Gómez et al., 1993). In general, these limestones are sound from a slope stability point of view; very little material weakening is observed in slopes during periods of approximately 100 years, with hardly any change in weathering degree since the time of excavation. However, weathering on discontinuities is observed; an example of this and the effects it may have on slope stability were discussed in Box 2 (page 20) and Box 6 (page 61). This is believed to be caused mainly by hydrolysis.

Because of the low primary permeability, weathering in limestone units as the Upper Muschelkalk formation is enhanced by penetration of water into the rock mass through discontinuities. These may be orientated such that they dip into the slope, favourable for water access from the slope face itself, or such that they dip out of the slope, favourable for water percolation from the hillside behind the slope. The latter condition can coincide with a slope condition close to limiting equilibrium for sliding failure and this is the case in which the effects of weathering can lead to sliding of blocks and wedges through only a slight decrease of shear resistance.

In the Upper Muschelkalk formation, three units have been investigated. These units are differentiated on the basis of their bedding spacing (thinly bedded with bedding spacing less than 0.10m; medium bedded with bedding spacing 0.10-0.50m; thickly bedded with bedding spacing over 0.50m). An additional notable difference is the occurrence of shales in the thinly and medium bedded units. These shales closely resemble the harder shales as found in the Keuper series (e.g. Box 8, page 83), and show similar decay development with marked pelitoclastesis.

Since the shale layers belonging to the Upper Muschelkalk have a limited thickness, usually of several centimetres only, the effects of this and the resulting differential erosion are not as marked as observed in the Keuper limestone unit, where the shale layers can have a considerably larger thickness. Differential weathering and erosion do occur however, especially

in the thinly bedded unit with bedding spacing less than 0.10m, in which shale intercalations are most abundant. An example of this is given in Figure 38. Note especially the marked difference between the generally jagged slope surface (exposed for approximately 50 years) and the relatively smooth back surface of the small wedge failure visible in the centre of the photograph (exposed for approximately 15 years). Because of the abundance of shales in the thinly bedded unit, and their almost complete absence in the thickly bedded unit, decay in engineering lifetimes of slopes mainly affects the thinly bedded unit.

Figure 38 – Slope in Upper Muschelkalk limestone near Tivissa (N4546160/E309940), excavated in 1950's (September 2004).

Weathering effects can also be recognized in the dolomitized limestone itself. As Adhikari (2002) described, this is especially apparent as an increase of secondary porosity of the material, most notably through crack formation resulting from dissolution attacking the most vulnerable layers present in the bedding structure of the limestone. This porosity increase is associated with a simultaneous increase of the clay content and a decrease of the slake durability when compared to the unweathered parent material.

4 Conceptual model for weathering and erosion

"If you don't know anything about computers, just remember that they are machines that do exactly what you tell them but often surprise you in the result." - Richard Dawkins, *The Blind Watchmaker.*

4.1 General

In paragraph 2.7, the different possible decay situations that may result from the balance between erosion and weathering are discussed; Table 5a/b gives a summary overview. To evaluate the development of such situations in slope decay, a two-dimensional model is derived. With this model the combined action and the respective importance of weathering and erosion can be evaluated for different locations on a slope.

As will be shown in chapter 5 and mentioned earlier in other parts of this thesis, geological and geotechnical data inevitably exhibit considerable scatter. This scatter resides in the variability of the subsoil materials themselves (in the Falset research area from hard limestones to friable mudstones, shales and clays), the variability of the rock mass architecture (e.g. bedding planes, bedding spacing, joints and faults) and in the semi-quantitative description of properties (e.g. strength and weathering classifications based on observations, limited in representativity by the limited number of outcrops, and blurred by artefacts such as quality of the classification and bias due to different observers).

A quantitative description based on empirical data alone therefore may lead –and indeed often will lead– to crude relations between relevant variables (Nieuwenhuis, 2006). Such relations, however valuable and cumbersome to

obtain, do not allow a physically acceptable analysis of the underlying process and the relative influence of important intervening parameters. The value of empirical descriptions for engineering practice, especially when due care has been taken to investigate the sources of scatter, stays of course beyond any doubt.

Perhaps even stronger than in exact disciplines characterized by controlled experiments, engineering geology is forced to consider natural processes with all their complexity. Support in the interpretation of such processes can be obtained by conceptual models. Such models are speculative and partly deductive by nature. They are based on assumptions, for example on weathering and erosion processes and their relations with relief and hydrology. Some of these relations (between weathering rate and depth for instance) have been investigated in some detail under controlled circumstances and for specific subsoils. Other relations remain unknown and have to be deduced. A conceptual model therefore has practical validity only if its computational results agree rather well with field observations. In addition to this, the value of conceptual models resides in the establishment of physically understandable relations between variables and parameters. It is for these two reasons, to find physical relations and to compare the outcome with available field data, that conceptual models are derived and applied in this thesis.

The conceptual model derived in this chapter combines the Bakker – Le Heux erosion model (see Appendix E) with a weathering penetration model in which the penetration rate is inversely proportional to the thickness of the weathering cover, on the basis of slope retreat measurements in the Gavadà study slope. Bakker and Le Heux (1946, 1952) formulated two models for slope evolution with time, in order to explain slope forms found in nature, in particular those in high mountain areas in Anatolia (Turkey) where the slopes are covered at their toe by pediments (Nieuwenhuis, 2006). In both models the down-wasted weathering products are deposited in the form of a growing scree slope at the original slope's toe. The nature of the down-wasting process (rolling downward, landslides, avalanches or

water/snow erosion) was not discussed. For the down-wasting of the exposed slopes two potential mechanisms were considered: parallel slope retreat through down-wasting of slices of constant thickness over the full slope height (Bakker and Le Heux, 1946), and rotating slope retreat through down-wasting of triangular slices that are thick at the top and thin at the toe (Bakker and Le Heux, 1952). The second mechanism results in a decreasing slope angle, and is described in more detail in Appendix E.

Whereas Bakker and Le Heux (1946) found that the parallel slope retreat mechanism appeared well applicable to the Anatolian mountains, the rotating slope retreat mechanism seems to be a better fit for Western European slopes (Hutchinson, 1988). In the investigated slopes of road cuts in the Falset research area, angular rotation of the retreating slope face has been observed. In view of this the rotating slope retreat model has been adopted here, and developed further.

The resulting set of equations can be solved numerically by time-stepping, and gives the slope profile as a function of time, as well as the penetration of the weathering front. Depending on erosion and weathering penetration rates, different decay situations such as listed in Table 5a/b are shown to occur at a given point in time for different locations along the slope profile, just as different situations occur for a given location along the slope profile for different exposure times.

Table 5a - Potential decay situations. See also Figure 18 - Figure 20, paragraph 2.7, for a graphical representation.

Balance	Processes	Situation at time of excavation	Decay situation
Imbalance favouring erosion	Only erosion, no weathering	No old weathering mantle or weathering zone from previous stage present	A1
		Old weathering mantle or weathering zone from previous stage present	A2
	Some weathering, but erosion penetrates faster than weathering	No old weathering mantle or weathering zone from previous stage present	B1
		Old weathering mantle or weathering zone from previous stage present	B2
Equilibrium of weathering and erosion	Erosion and weathering penetrate into the rock mass at equal rates	No old weathering mantle or weathering zone from previous stage present	C1
		Old weathering mantle or weathering zone from previous stage present	C2
Imbalance favouring weathering	Some erosion, but weathering penetrates faster than erosion	No old weathering mantle or weathering zone from previous stage present	D1
		Old weathering mantle or weathering zone from previous stage present	D2
	Only weathering, no erosion	No old weathering mantle or weathering zone from previous stage present	E1
		Old weathering mantle or weathering zone from previous stage present	E2

Table 5b – Effects of potential decay situations. See also Figure 18 - Figure 20, paragraph 2.7, for a graphical representation.

Decay situation	Weathering penetration depth	Weathering intensity on slope surface	Weathering intensity rate	
			Dynamic	Apparent
A1	Zero	Constant	Zero	Zero
A2	Decreases until mantle is eroded, then zero	Decreases until mantle is eroded, then constant	Negative until mantle is eroded, then zero	Negative until mantle is eroded, then tending to zero
B1	Zero	Constant	Zero	Zero
B2	Decreases until mantle is eroded, then zero	Decreases until mantle is eroded, then constant	Negative until mantle is eroded, then zero	Negative until mantle is eroded, then tending to zero
C1	Zero	Constant	Zero	Zero
C2	Constant, larger than zero	Constant (likely)		
D1	Increases	Increases	Positive (dynamic slope intensity rate, see paragraph 2.7)	Positive (apparent slope intensity rate, see paragraph 2.7)
D2	Increases	Increases		
E1	Increases	Increases	Positive and constant (dynamic reference intensity rate, see paragraph 2.7)	Positive and constant (apparent reference intensity rate, see paragraph 2.7)
E2	Increases	Increases		

4.2 Erosion

In Appendix E the Bakker – Le Heux model is presented, as discussed by Hutchinson (1998). The Bakker – Le Heux model describes the ultimate slope profile of a linearly retreating, initially straight slope, excluding erosion from the top surface. Basically, the model considers a decreasing angle of the apex line through the origin (the initial slope toe) and the upper section of the slope. A change in this angle results in a small increment of the eroded volume, and thus a corresponding small increment in the debris covering the toe of the slope in a scree wedge, while taking into account volume changes and erosion at the toe (see Figure 39, and refer to Appendix E).

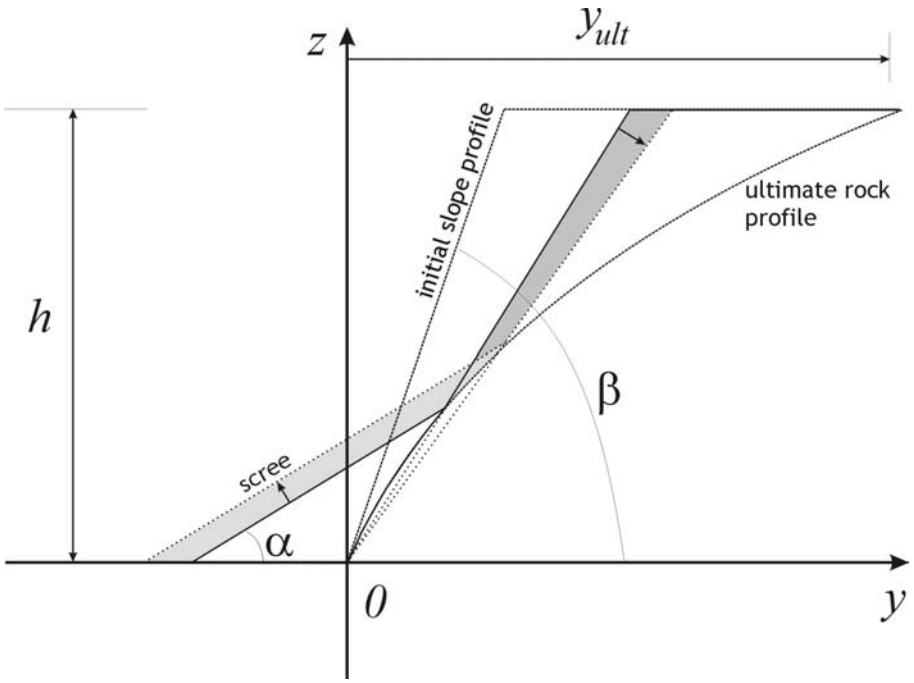

Figure 39 - Definition sketch of the Bakker - Le Heux model for slope retreat (after Hutchinson, 1998).

The limiting case of this slope development model is a convex, uneroded core of rock with a curve that has an inclination equal to the scree angle α at y_{ult} and equal to the initial slope angle β in the origin. The curved rock core is covered completely by scree inclined at angle α in this limiting case.

The model only describes this ultimate state of the eroded slope and gives an expression for the ultimate rock profile. The development of the slope profile in time can however be simulated quantitatively by assigning a time function to the inclination of the apex line through the origin (γ, Figure 40) and taking appropriately small time steps. Note that the situation sketched in Figure 40 omits erosion and weathering acting from the top surface for clarity. The sloep development is influenced if such erosion and weathering from the top occur (see remark with Equation (14), page 108).

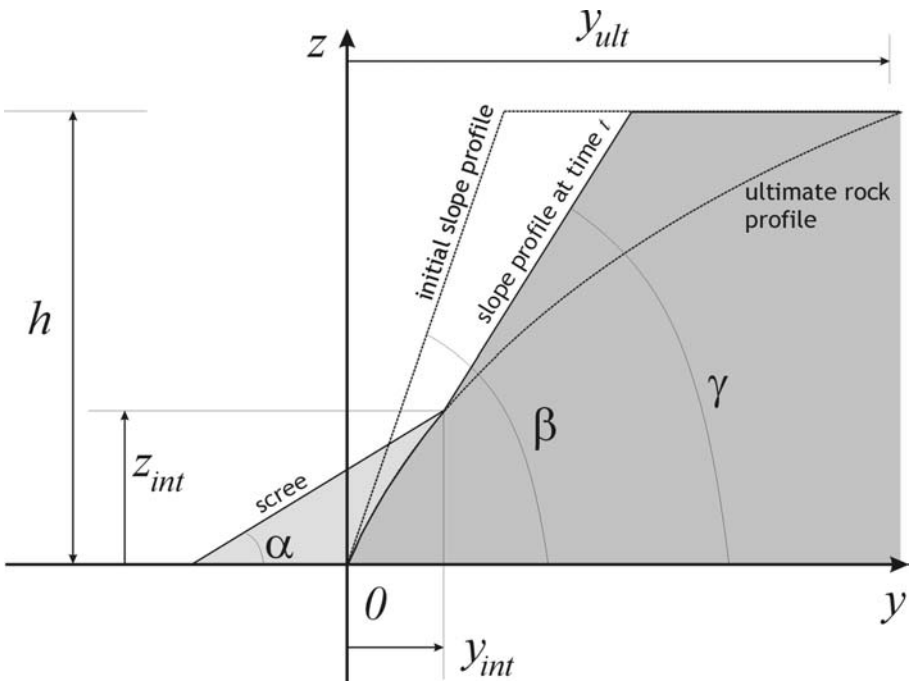

Figure 40 - Definition of parameters in time-dependent model for slope retreat.

Data from the study slope at Gavadà suggests that the slope retreat is linear in time for the first years after excavation[25] (see Box 10). If this observed trend for γ is extrapolated until the scree angle α is reached, then:

$$\begin{aligned} &\text{if } 0 \le t \le \frac{\beta - \alpha}{R_s} \quad \Rightarrow \quad \gamma = \beta - R_s t \\ &\text{if } t \ge \frac{\beta - \alpha}{R_s} \quad \Rightarrow \quad \gamma = \alpha \end{aligned} \tag{3}$$

With:

R_s	rate of angular slope retreat	[°/year]
t	time	[year]
α	stable slope angle for scree	[°]
β	initial slope angle at time of excavation	[°]
γ	inclination of the apex line through the crest and toe	[°]

In combination with equation (21) in Appendix E (which gives y, the depth from the original slope's toe, as a function of the height z, for the ultimate profile of the rock core), the angle defined by (3) gives the following expressions for the y_{int} and z_{int} (the coordinates where the surface of the scree wedge intercepts the intact rock, Figure 40):

$$y_{int} = \frac{z_{int}}{\tan(\gamma)} \tag{4}$$

$$z_{int} = \frac{h}{1-2c}\sqrt{(1-2c)\left(\mathrm{e}^{\frac{1-2c}{c-1}\ln\left(\frac{a\tan(\gamma)-1}{(a-b)\tan(\gamma)}\right)}-1\right)} \tag{5}$$

[25] *It should be noted that any function $\gamma(t)$ is allowed. The data reported by Hutchinson (1998) suggest that the rate of slope retreat decreases with longer exposure times. However, the time span covered by the study in the Falset area is too short to verify this. Therefore it cannot be proven that the observed trends remain valid for longer time intervals, and equation (3) should be considered as an example only. The methodology for derivation of the model is independent of equation (3).*

With:

a	cotangent of stable slope angle for scree, cot(α)	[-]
b	cotangent of initial slope angle at time of excavation, cot(β)	[-]
c	1-volume of rock/volume of scree	[-]
h	slope height	[m]
y_{int}	y-coordinate of interception between scree wedge and eroded rock	[m]
z_{int}	z-coordinate of interception between scree wedge and eroded rock	[m]

Starting at the point defined by the coordinates given by equations (4) and (5), the scree wedge stretches downward with an inclination equal to α and the rock face upward with an inclination γ (Figure 40).

At any time t, the profile of the eroded rock surface is given by:

$$\begin{aligned} &\text{if } 0 \le z \le z_{int} \quad \Rightarrow \quad y_e = az - (a-b)z\left[\frac{h^2 + (1-2c)z^2}{h^2}\right]^{\frac{c-1}{1-2c}} \\ &\text{if } z_{int} \le z \le h \quad \Rightarrow \quad y_e = \frac{z}{\tan(\gamma)} \end{aligned} \tag{6}$$

With:

y_e	y-coordinate of eroded rock profile	[m]
z	vertical coordinate	[m]

The profile of the overlying scree is given at any time t by:

$$if\ 0 \le z \le z_{int} \quad \Rightarrow \quad y_s = y_{int} - \frac{z_{int} - z}{\tan(\alpha)} \tag{7}$$

With:

y_s	y-coordinate of scree profile	[m]

In Equations (6) and (7), y_{int} and z_{int} are found by combining Equations (4) and (5) with (3). The slope profile and the profile of the eroded rock core that is covered by the scree is defined at any time t by equations (6) and (7), provided an expression for $\gamma(t)$ is known.

Box 10 – Linear slope retreat in the Gavadà slope

Since the excavation of the Gavadà slope in 1999, significant erosion has taken place. Figure 41 shows cross-sections measured by hand in consecutive years. At the foot of the slope, debris (pelitoclasts) accumulates, whereas the top of the slope recedes. When the inclination of the apex through the upper section of the slope (γ in Figure 40) is plotted against time, it is apparent that this angle decreases – at an approximately linear rate for the first five recorded years after excavation of 1.2°/year (Figure 42).

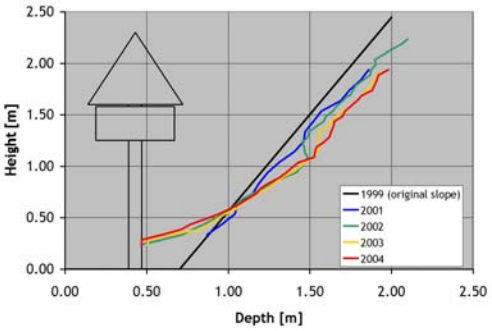

Figure 41 - Cross-sections of Gavadà slope at traffic sign. See also Figure 43.

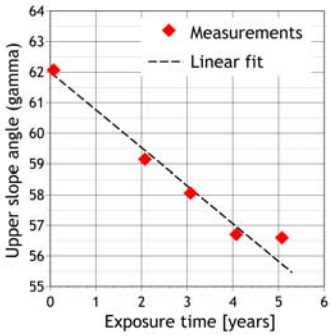

Figure 42 - Decrease in time of the slope angle of the apex through the upper section of the Gavadà slope, based on hand measurements.

A LIDAR scan was made in May 2004 (see also Box 9, page 90) of the section immediately left of the traffic sign, see Figure 43. The LIDAR results give erosion contours with respect to the original excavated slope surface of 1999 as displayed in Figure 44. Opposed to the Masriudoms slope, that shows distinctive rill erosion, this Gavadà slope has erosion contours that are approximately parallel to the toe of the slope. This indicates sheet-like linear retreat.

Figure 43 - Scanned section of Gavadà slope with coordinate system.

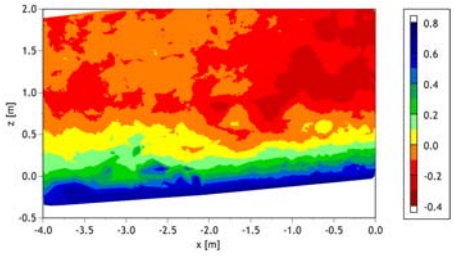

Figure 44 - Horizontal erosion in [m] calculated from LIDAR scanning results. Portrayed section left of traffic sign.

4.3 Penetration of the weathering front

Data by Heimsath (1997), presented in Appendix E, defines the penetration rate of a weathering front as a function of the thickness of the existing weathered zone with the following general equation:

$$\frac{dD_w}{dt} = \mathrm{e}^{A+BD_w} \tag{8}$$

With:

A	constant defining weathering penetration rate	[-]
B	constant defining weathering penetration rate	[1/m]
D_w	penetration depth of weathering (perpendicular to slope surface)	[m]
t	time	[year]

The differential equation (8) defines the weathering depth D_w as defined in Figure 45 as a function of time[26]. When considering a small time step Δt, the weathering depth at any height z can be calculated starting from a boundary condition (e.g. $t=0$: $D_w=0$) by:

$$\begin{aligned} &\text{Perpendicular to slope face} && D_w\big|_{t+\Delta t} = D_w\big|_t + \mathrm{e}^{A+BD_w|_t}\,\Delta t \\ &\text{In horizontal plane (y - direction)} && D_{w,y} = \frac{D_w}{\sin(\delta)} \\ & && \Rightarrow D_{w,y}\big|_{t+\Delta t} = \frac{D_w\big|_t + \mathrm{e}^{A+BD_w|_t}\,\Delta t}{\sin\left(\delta\big|_t\right)} \end{aligned} \tag{9}$$

With:

$D_{w,y}$	penetration depth of weathering (in direction of y)	[m]
δ	slope angle at the considered point	[°]

[26] *Note that if* $A=\ln(W_S)$ *and* $B=\frac{1}{W_S}$, *with* W_S *a penetration rate coefficient other than 0, this can be simplified to* $\frac{dD_W}{dt}=\frac{W_S}{1+t}$. *In that case, the weathering depth at any time t can be directly computed from* $D_W = W_s \ln(1+t)$ *and* $D_{W,y}=\frac{D_W}{\sin(\delta)}=\frac{W_S \ln(1+t)}{\sin(\delta)}$.

The slope angle δ of the intact rock profile depends on z and is given by:

$$\text{if } 0 \le z \le z_{int} \quad \Rightarrow \quad \delta\big|_t = \operatorname{atan}\left(\frac{S}{aS + ah^2\left(\frac{-S}{h^2}\right)^{\frac{1-c}{2c-1}} - ay^2\left(\frac{-S}{h^2}\right)^{\frac{1-c}{2c-1}} - bh^2\left(\frac{-S}{h^2}\right)^{\frac{1-c}{2c-1}} + by^2\left(\frac{-S}{h^2}\right)^{\frac{1-c}{2c-1}}} \right) \tag{10}$$

$$\text{if } z_{int} \le z \le h \quad \Rightarrow \quad \delta\big|_t = \gamma\big|_t$$

With:

S $\quad -h^2 - y^2 + 2cy$ [m²]

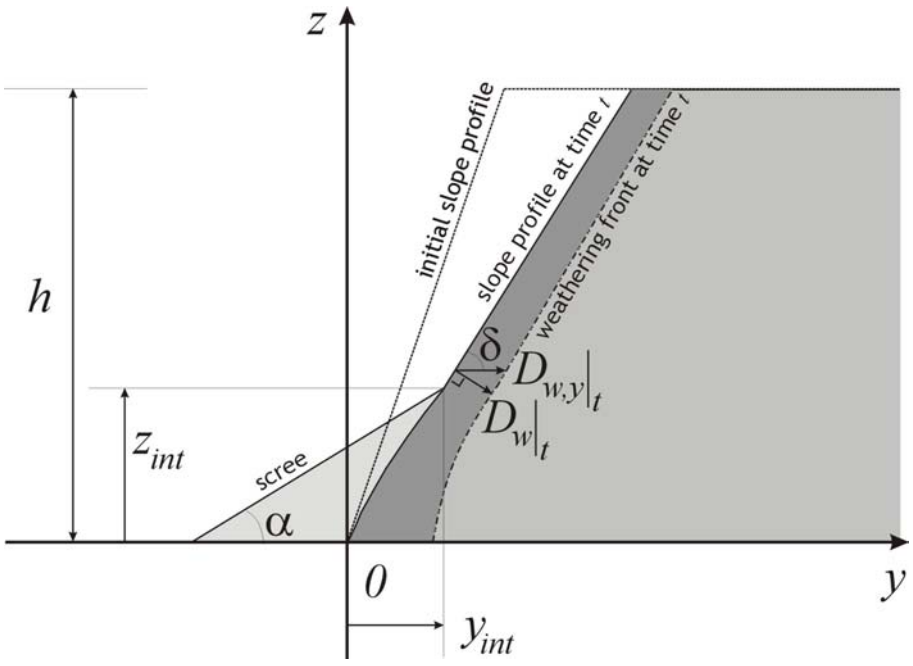

Figure 45 - Definition of the weathering penetration profile at time t. $D_w|_t$, $D_{w,y}|_t$ and δ are all functions of z.

4.4 Combined effect of weathering and erosion

Consider a time interval Δt starting at time t, with a weathered zone having thickness $D_w|_t$. During the interval Δt, some erosion will occur above the point of intercept of the scree cover and the rock core. The slope profile will be changing as described by the following equations:

$$\begin{cases} \text{if } z > z_{int} \begin{cases} y_e\big|_t = \dfrac{z}{\tan\left(\delta\big|_t\right)} \\ y_e\big|_{t+\Delta t} = \dfrac{z}{\tan\left(\delta\big|_{t+\Delta t}\right)} \\ \Delta y_e = y_e\big|_{t+\Delta t} - y_e\big|_t = \dfrac{z}{\tan\left(\delta\big|_{t+\Delta t}\right)} - \dfrac{z}{\tan\left(\delta\big|_t\right)} \end{cases} \\ \text{if } z \le z_{int} \begin{cases} y_e\big|_{t+\Delta t} = y_e\big|_t \\ \Delta y_e = y_e\big|_{t+\Delta t} - y_e\big|_t = 0 \end{cases} \end{cases} \tag{11}$$

The slope angle δ depends on the vertical location, z, and is defined by Equation (10). Simultaneously, some small penetration of the weathering front will occur in that same interval, on top of the penetration that had already been achieved at time t. The erosion during Δt will however remove some of the weathered material that was present at time t and therefore the additional weathering penetration leads to a smaller depth than suggested by Equation (9), on the basis of the weathering depth $D_w|_t$ alone. Depending on how much of the weathered material is removed by erosion (none, some or all), the maximum increase of the weathering depth at any height z as given by Equation (9) is only partially obtained:

$$
\begin{aligned}
D_{w,y}\big|_{t+\Delta t} &= \frac{D_w\big|_t + \mathrm{e}^{A+BD_w|_t}\,\Delta t}{\sin\left(\delta\big|_t\right)} - \Delta y_e && \text{if } \frac{\mathrm{e}^{A+BD_w|_t}\,\Delta t}{\sin\left(\delta\big|_t\right)} - \Delta y_e > 0 \\
D_{w,y}\big|_{t+\Delta t} &= D_{w,y}\big|_t = \frac{D_w\big|_t}{\sin\left(\delta\big|_t\right)} && \text{if } \frac{\mathrm{e}^{A+BD_w|_t}\,\Delta t}{\sin\left(\delta\big|_t\right)} - \Delta y_e = 0 \\
D_{w,y}\big|_{t+\Delta t} &= \max\left(0; \frac{D_w\big|_t + \mathrm{e}^{A+BD_w|_t}\,\Delta t}{\sin\left(\delta\big|_t\right)} - \Delta y_e\right) && \text{if } \frac{\mathrm{e}^{A+BD_w|_t}\,\Delta t}{\sin\left(\delta\big|_t\right)} - \Delta y_e < 0
\end{aligned}
\tag{12}
$$

The first line in Equation (12) represents a case where penetration of weathering can exceed erosion, the second exact equilibrium, and the third a case where erosion exceeds penetration of weathering (refer back to paragraph 2.7). Since the weathering depth cannot become negative, the weathering depth in the latter case is restricted to values larger than or equal to zero.

In terms of (*y*-)coordinates, the weathering front is defined by:

$$y_w\big|_{t+\Delta t} = y_e\big|_{t+\Delta t} + D_{w,y}\big|_{t+\Delta t} \tag{13}$$

With:

y_w *y*-coordinate of weathering penetration front [m]

Using Equation (13) the profile of the weathering front can be calculated through an iterative procedure with the boundary condition:

$$D_w\big|_{t=0} = 0 \Rightarrow y_w\big|_{t=0} = y_e\big|_{t=0} \tag{14}$$

In a similar way, the weathering penetration extending vertically downward from the (assumed) horizontal surface above the slope can be taken into account. Penetration of a weathering profile from the top surface predating the excavation can also be included by taking a boundary condition with non-zero weathering depth at $t=0$. Any weathering depth along the slope profile predating excavation can also be incorporated by adapting the boundary condition of Equation (14) to reflect the pre-existing weathering profile.

In the above equations it is assumed that the coefficients A and B are not influenced by the presence of a scree cover, in other words that for the rock covered by scree and for the rock that is not yet covered, the same coefficients A and B can be used. If weathering penetration rates are changed due to the influence of a scree cover (see footnote 14 on page 57), this can be included in the iteration by defining A_c and B_c in Equation (12) for all $z<z_{int}$, and A_s and B_s for all $z \geq z_{int}$ ($A_c \neq A_s$ and $B_c \neq B_s$, with the indices $_c$ and $_s$ indicating "covered by scree" and "slope surface", respectively).

4.5 Example of modelling results

Figure 46 and Figure 48 show results of a numerical calculation based on the model described above for the Gavadà case study slope. The example calculations exclude weathering from the top surface for ease of interpretation. If this is included, the top parts of the slope will be affected by it and weathering depths calculated for the top of the slope will be larger than on the basis of weathering from the slope surface alone.

Model parameter values used for these graphs are given in Table 6. These have been determined for the Gavadà study slope to fit repetitive slope profile measurements (Box 10, page 104) and estimated weathering depths found through excavation (Box 8, page 83). Figure 46 shows the calculated slope profile at different exposure times, with the eroded rock core, a scree cover, and the weathering penetration front.

Table 6 - Model parameters used for results shown in Figure 46.

Parameter	Symbol	Value	Unit
Stable angle of scree	α	35	[°]
Initial slope angle	β	62	[°]
Slope height	h	2.05	[m]
$1-\frac{\text{volume of rock}}{\text{volume of scree}}$	c	-1.0	[-]
Rate of slope retreat	R_s	1.2	[°/yr]
Weathering penetration parameter	A_s	-2.30	[-]
Weathering penetration parameter	B_s	-10	[1/m]
Weathering penetration parameter	A_c	-2.30	[-]
Weathering penetration parameter	B_c	-10	[1/m]

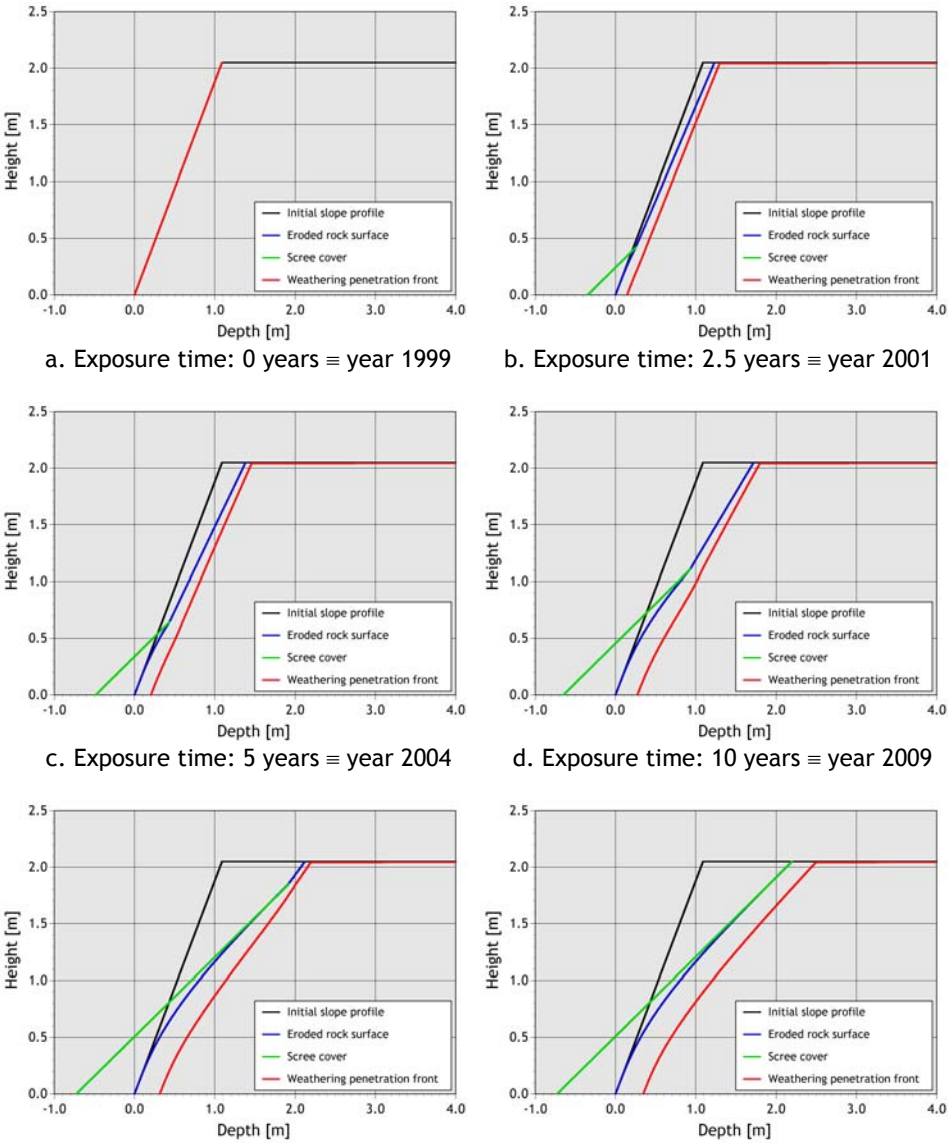

a. Exposure time: 0 years ≡ year 1999

b. Exposure time: 2.5 years ≡ year 2001

c. Exposure time: 5 years ≡ year 2004

d. Exposure time: 10 years ≡ year 2009

e. Exposure time: 15 years ≡ year 2014

f. Exposure time: 20 years ≡ year 2019

Figure 46 – Example of modelling results for Gavadà slope, for different exposure times and corresponding years (excavation in 1999). Origin at original slope toe.

Figure 46 shows the development of this modelled slope through the years and indicates that after 20 years a situation willl be reached in which the final convex shape of the rock core is reached, the whole slope is covered by scree, and erosion has come to an end. Before this occurs, the section of the eroded rock face that is not covered by scree extends linearly upward, creating a knick point at the intersection with the convex section underneath the scree cover, and the surface of the scree itself. This same knick point is reflected in the weathering penetration front; this is most clear in Figure 46d. To compare the modelling results of Figure 46 directly with the observed slope profile, Figure 47 shows the measured and modelled slope profiles in 2004 (refer back to Box 10, page 104). The position of the rock core was not measured; the dotted line shows the model prediction.

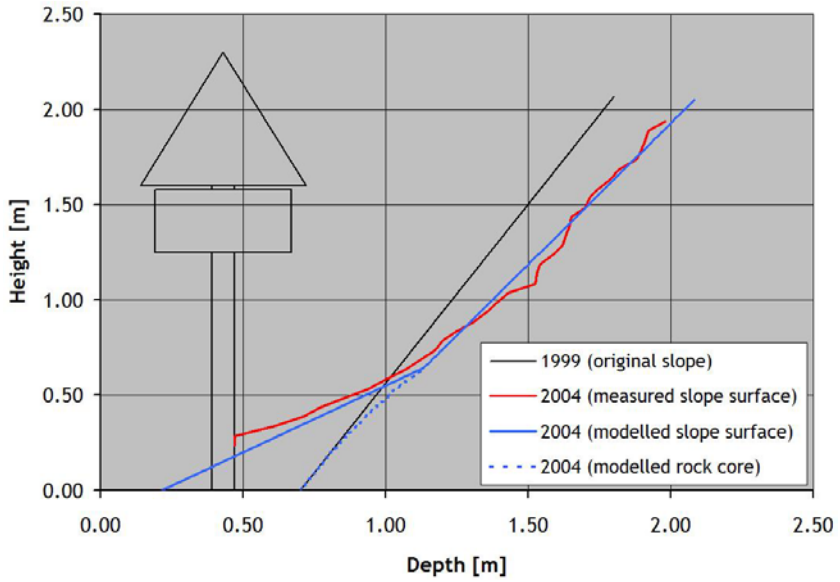

Figure 47 - Measured and modelled slope surface for the Gavadà slope in 2004.

Although cross-sections as in Figure 46 are visually appealing, a better insight into the fine balance between erosion and weathering is obtained in the graphs in Figure 48, which show the thickness of the weathered layer perpendicular to the slope surface as a function of (exposure) time. In the equations in the previous paragraphs 4.3 and 4.4, this is the parameter D_w.

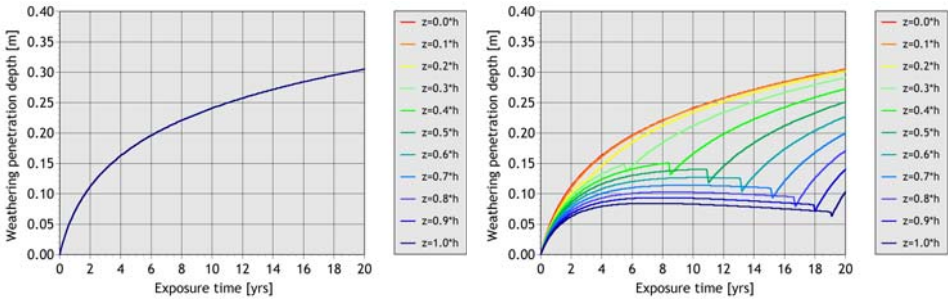

a. (rate of slope retreat 0° /yr) b. (rate of slope retreat 1° /yr)

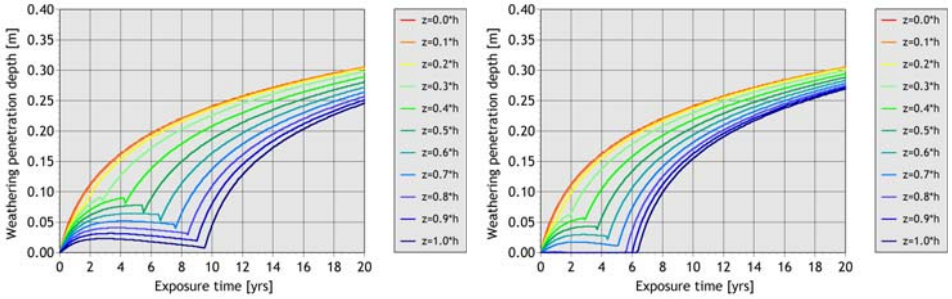

c. (rate of slope retreat 2° /yr) d. (rate of slope retreat 3° /yr)

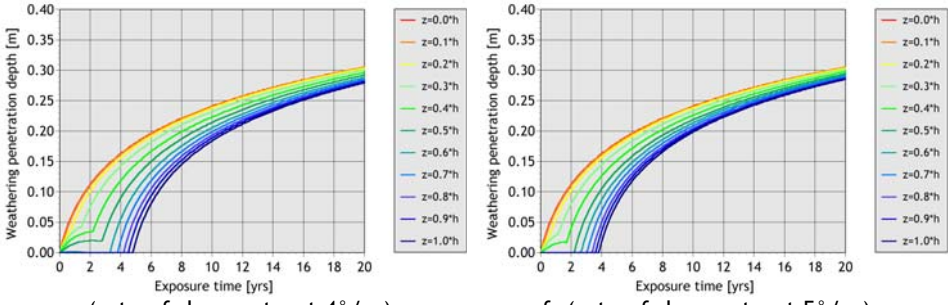

e. (rate of slope retreat 4° /yr) f. (rate of slope retreat 5° /yr)

Figure 48 – Example of modelling results: weathering depths changing in time, for different rates of slope retreat (R_s).

Figure 48a shows the result for the case where the rate of slope retreat is set at 0°/year; this effectively resembles decay situation E1 (refer back to Table 5a/b, page 98). A single curve is found representing points at all heights throughout the slope profile; this curve is given by the solution to the differential equation (8) and describes what in paragraph 2.6 was called the *reference penetration*. For the simplified case with $A=\ln(W_s)$ and $B=1/W_s$, with W_s a penetration rate coefficient in [m] other than zero, this solution is given by (see footnote 26, page 105):

$$D_w = W_s \ln(1+t) \tag{15}$$

Figure 48b-f present cases where erosion rates in terms of slope angle decrease are larger than zero, and therefore describe what in paragraph 2.5 was called the *slope weathering penetration rate*. Points at different heights in the slope profile now show different curves; lines are given for points at *0.0*h*, *0.1*h*, *0.2*h*, …, *1.0*h* (with *h* the slope height). At the foot of the slope (height *0.0*h*), no erosion occurs and the same curve as in Figure 48a is obtained; this is the limiting situation, visible in all graphs of Figure 48b-f. The curves representing the development of a weathered layer at the other points do however show clear differences.

In the graphs of Figure 48b and c, a weathering layers develops at the start of the decay processes at all heights in the slope profile; this can be recognized as an increase in the weathering thickness (rising curves) although not as fast as in the limiting case for the curve representing height *0.0*h*. These initially rising curves represent decay situations where some erosion occurs, but an imbalance favouring weathering exists (D1/D2, Table 5, page 98). The curves for points higher in the slope profile tend to become horizontal after some time; this signifies equilibrium between erosion and weathering penetration, resulting in a constant thickness of the weathered zone (C2, Table 5). Some curves even develop a negative slope signifying a decrease in the thickness of the weathered zone, and therefore an imbalance favouring erosion (B2, Table 5); this may even extend to the case where the weathered layer disappears altogether with D_w becoming zero (situation B1).

All curves finally trend upward again after a sudden knickpoint[27]; this knickpoint occurs at the time at which the scree extends to the height that is represented by each curve, resulting in erosion coming to an end at that particular height (E2, Table 5). In the limiting case of $t \rightarrow \infty$ all curves tend to become equal to the curve for *0.0*h*, implying that the whole slope is covered by scree and that erosion has ended.

Figure 48d-f show the same basic decay situations existing at various times and locations; however, in these three cases where erosion rates are relatively high, the curves for the upper section of the slope profile show a zero thickness of the weathered zone until the scree has built up to that particular height. These horizontal curves at $D_w=0$ represent decay situation B1 (Table 5). With an increase in erosion rates, the knickpoints at which the scree wedge passes the height represented by each curve shift to the left, towards shorter exposure times. In the limiting case for $R_s \rightarrow \infty$ all curves will fall on the same line again[28], represented by the upper bound curve for *0.0*h*.

Figure 49 summarizes the possible decay development types, from weathering without erosion (Figure 49a) to dominant erosion with a weathering profile developing only after erosion processes have come to an end (Figure 49f). This model with linear slope retreat clearly shows the complications for practical observations on decay in slopes. Points at different heights in the slope profile will be in different decay situations at the same time, and the decay situation at a specific location may change in time. The most homogeneous slope development will occur with either very small (relative to weathering penetration rates) erosion rates, or with very large erosion rates (again relative to weathering penetration rates). With intermediate combinations of erosion and weathering penetration rates, the

[27] *The small sharp step visible in most curves at this point results from the step-wise change of the slope angle at this specific point in time, which causes the weathering depth perpendicular to the slope to have a discontinous first order derivative.*

[28] *For $R_s \rightarrow \infty$, the final slope profile is reached after an infinitely short time, after which decay situation E1 occurs at all heights.*

upper slope will tend to show an imbalance favouring erosion wheres the lower slope will show imbalance favouring weathering.

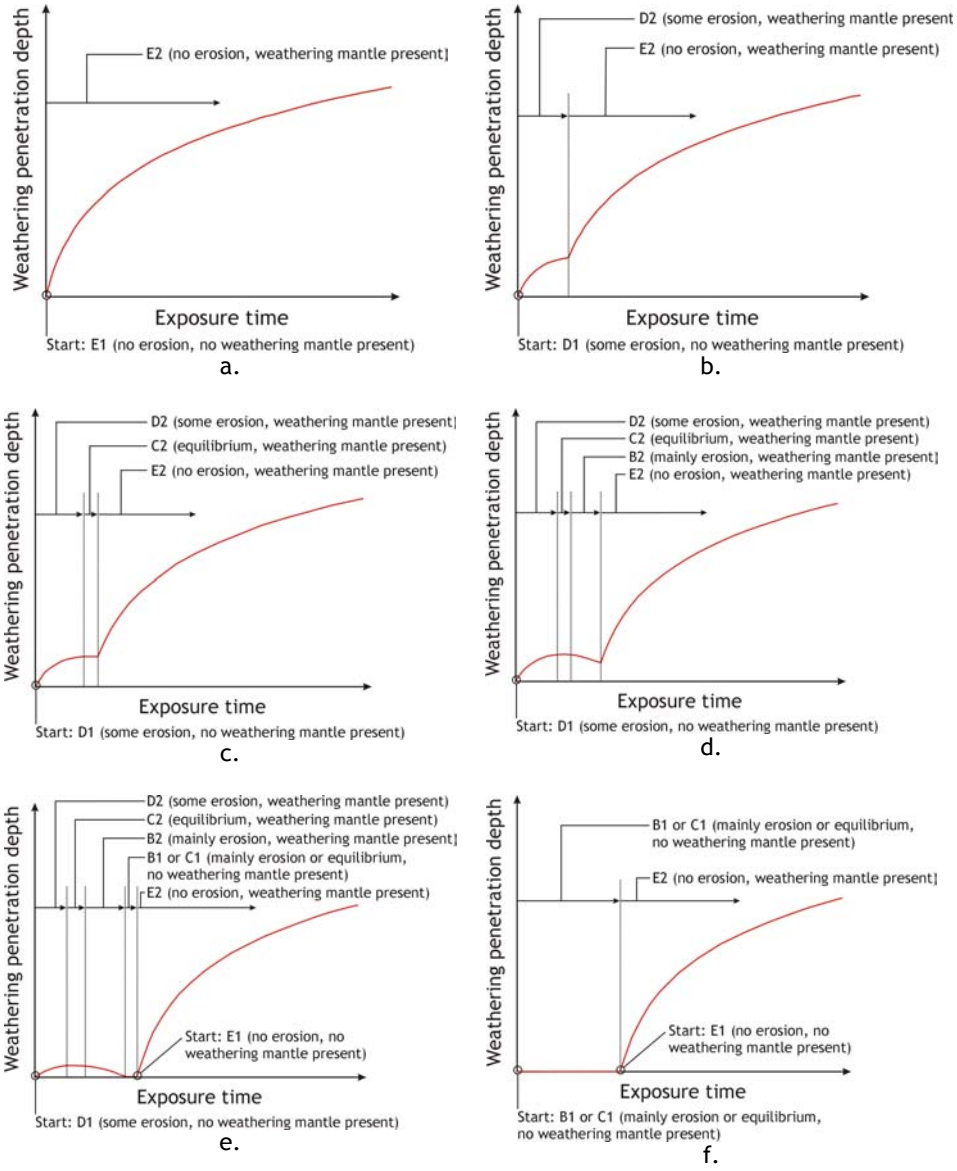

Figure 49 – Possible decay development types, depending on balance between erosion and weathering penetration rates.

5 Time-dependent weathering intensity: empirical results

"It is only shallow people who do not judge by appearances. The true mystery of the world is the visible, not the invisible." – Oscar Wilde, *The Picture of Dorian Gray*.

5.1 General trends for weathering intensity and rate

The rate of change of weathering intensity as observed on the slope surface is a reflection of the balance between erosion and rate of weathering penetration into the rock mass, and is one of the primary indicators of rock mass decay in slopes.

To assess the development of the weathering intensity in time for the various units regarded in this research, the field observations of the data set given in Appendix H can be used. The data set consists of classifications done using the SSPC system including weathering intensity classifications (see Table 3, page 50). These classifications give the value for *WE* at the time of observation, and for most cases the initial *WE* at the time of excavation can be estimated or is known exactly.

The value of *WE* decreases during the elapsed time of exposure of a slope, and the value of $(WE_{init}-WE_t)$ therefore increases with time – but is observed to do so at a decreasing rate on a linear time scale. The increase is however approximately linear when plotted against a logarithmic time scale. An example of $(WE_{init}-WE_t)$-values plotted against a logarithmic time scale is given in Figure 50.

Results as in Figure 50 and similar relations previously reported by Woldearegay and Onrust (2002) support the assumption that $(WE_{init}-WE_t)$ is linearly correlated with logarithmic time[29], although there is evident scatter caused by a combination of factors (mainly influences of other variables and the fact that only discrete values are assigned to *WE*).

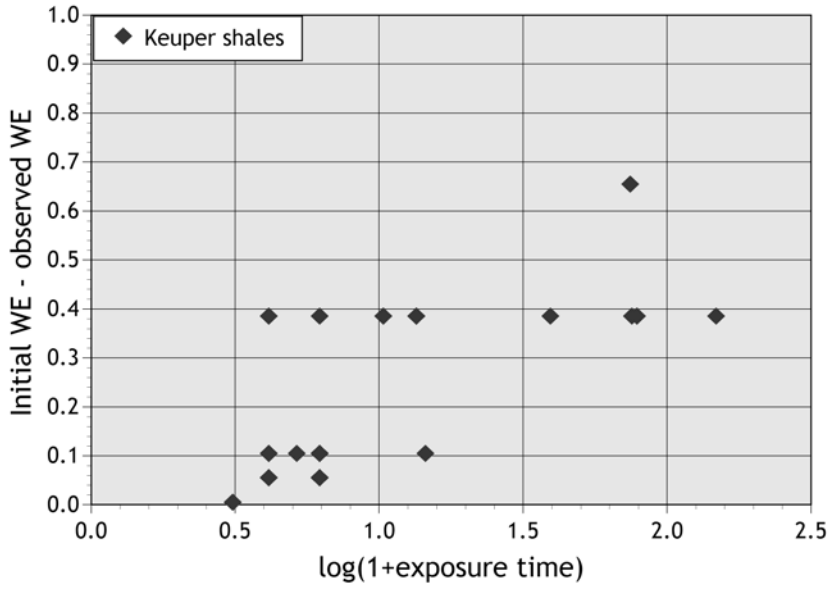

Figure 50 - Example of decrease in *WE* with increasing exposure time (in years). Data for Keuper shales.

Apparent weathering intensity rates according to equation (1) have been calculated for all individual data points[30]. Average, maximum and minimum

[29] This assumption was used in paragraph 2.5 in order to define the apparent weathering intensity rate (equation (1), page 55).

[30] In this analysis, the apparent weathering rate is used rather than the dynamic weathering rate (paragraph 2.5, equations (1) and (2)), since in most cases no time series of weathering observations in one unit and in one slope is available. Such a time series is required to calculate dynamic rates, but most data only consist of single and independent observations.

rates per unit are given in Table 7. Formations such as siltstones and shales have the highest average weathering intensity rates, up to about five times higher than those found for the limestones of the Upper Muschelkalk and Keuper formations. All units show a significant variation in the individual rates, with standard errors that are about 50% of the averages (Table 7), corresponding with the large amount of scatter that is apparent in plots such as Figure 50. Next to intrinsic variability and disturbing factors such as described in paragraph 2.5[31], the variation is likely to have a physical background, linked to the influence of the internal, external and geotechnical weathering conditions that were described in paragraph 2.2.3. This influence is thought to be most important in the units that have a high susceptibility to weathering, in which relatively small differences in conditions can be emphasized by the intensity of weathering: the Keuper shales and Middle Muschelkalk siltstones.

One particular geotechnical condition that has been investigated before and is found to be of great importance is the influence of the slope orientation on weathering processes occurring in that slope (Huisman et al., 2006). On a material scale the influence of orientation has been investigated by analysing the decay of gravestone inscriptions (e.g. Robinson and Williams, 1996; Williams and Robinson, 2000) or rock tablets (e.g. Matsukura and Hirose, 1999). On a rock mass scale, Nicholson (2001a) tried to extend such research to actual slopes; both types of study suggested that a delicate balance exists between exposure to sunlight, to wind, and to rain.

Next to slope orientation, excavation damage also has a notable influence on weathering susceptibility of a rock mass exposed in an artificial slope (Chhetri, 2005). This wil be addressed further in paragraph 5.4.

[31] *Especially the fact that in a classification WE is only determined as a discrete value out of the five possible values (see Table 3, page 50), and not as the normally distributed stochastic variable that it actually is (Hack, 1998).*

Table 7 - Apparent weathering intensity rates for the different geotechnical units

Formation (code)	Unit	R^{app}_{WE} [1/log (year)]	
Keuper (Tg3)	Shales	**Average**	**0.181**
		Minimum	*0.000*
		Maximum	*0.631*
		Standard error	*0.147*
	Limestones	**Average**	**0.067**
		Minimum	*0.000*
		Maximum	*0.166*
		Standard error	*0.024*
Middle Muschelkalk (Tg22)	Siltstones	**Average**	**0.325**
		Minimum	*0.064*
		Maximum	*0.692*
		Standard error	*0.170*
	Gypsum	**Average**	**0.123**
		Minimum	*0.000*
		Maximum	*0.241*
		Standard error	*0.064*
Upper Muschelkalk (Tg23)	Bedding spacing <0.10m	**Average**	**0.051**
		Minimum	*0.023*
		Maximum	*0.143*
		Standard error	*0.028*
	Bedding spacing 0.10-0.50m	**Average**	**0.042**
		Minimum	*0.019*
		Maximum	*0.105*
		Standard error	*0.018*
	Bedding spacing >0.50m	**Average**	**0.038**
		Minimum	*0.019*
		Maximum	*0.105*
		Standard error	*0.016*

5.2 Influence of slope orientation on weathering intensity rates

5.2.1 Probabilistic trend analysis

Observations made on slopes with different exposure times can be compared directly to assess the influence of slope orientation, if weathering intensity rates as defined by equation (1) (page 55) are considered instead of the weathering intensity itself. In addition to an analysis of the observations themselves, a bootstrap approach can be followed in order to include the possible variation in the underlying parameters *WE*, slope orientation, and exposure time, and to smooth out extremes and errors caused by singular observations. For this, Latin Hypercube simulations have been made for every data point, varying the *WE* coefficient, the slope aspect, and the exposure time[32]. The bootstrapping methodology is described by Chernick (1999), and Efron and Tibshirani (1998). A summary of the technique and associated sampling procedures is included in Appendix F.

Figure 51 through Figure 57 show the resulting apparent weathering intensity rates in radar plots, with the apparent weathering intensity rate as the distance from the origin and the slope dip direction as the orientation in each chart[33]. Results are presented for both the observed data (Figure 51a

[32] *In these simulations, WE is taken from a normal distribution with averages according to Table 3 and standard errors after Hack (1998); the slope aspect is taken from a normal distribution with averages equal to the recorded value and a standard error of 5° (Hack, 1998); and the exposure time is taken from a triangular distribution with the most likely value equal to the estimated exposure time, and maximum and minimum at ±10% of this estimate. See Appendix F.*

[33] *For this, the data set for each analyzed unit is subdivided into eight subsets, one per slope orientation interval of 45° with midpoints on the principal directions North, Northeast, East, Southeast, South, Southwest, West, and Northwest. Maximum, minimum and average apparent weathering rates as well as bootstrap percentiles are determined for these eight directions. For visualisation purposes the corresponding*

- Figure 57a) and the bootstrap results (Figure 51b - Figure 57b). It should be noted that in these latter figures, the percentages do not indicate confidence levels, but the fractions of the simulated data. Values plotted in these graphs are given in Table 8 through Table 10. A comparison between observed rates and rates predicted on the basis of the simulations show that the 50% percentiles give the best estimate when used to make the predictions (Figure 65, page 142).

The asymmetry observed in the graphs of Figure 51 - Figure 57 indicates that the slope aspect does indeed influence the weathering intensity rate. This in itself is not surprising; authors such as Williams and Robinson (2000) have already shown that the orientation of headstones on graveyards plays a role in weathering. The climate seems to be a governing factor in this relationship between weathering and orientation. It was, for example, found by Cantón et al. (2001) that exposure of gypsiferous mudstones to cyclic wetting and drying determines the rate and extent of weathering. Indeed, even seasonal variations in precipitation can be directly linked to the decay of some rock masses (Regüés et al., 1995). It is, therefore, necessary to relate the graphs for the different units to the prevailing climate in the research area before an interpretation of the results can be made. This task is facilitated by highly detailed climate data available through XMET (Appendix B). Results are discussed in paragraph 5.3.

The apparent weathering intensity rates show clear differences between the units, both in terms of weathering intensity rates (that are a measure for the weathering susceptibility), and the dependency of these rates on slope orientation. The results suggest that decay in the majority of the investigated slopes is erosion delimited, with an imbalance favouring weathering (situations D and E, Table 5, page 98). Only in these situations,

rates for intermediate orientations are found by linear interpolation. Note that for clear demonstration of the influence of slope orientation, the apparent weathering rate is shown at different scales in the different figures.

approximately constant apparent weathering intensity rates larger than zero will be found, as discussed in paragraph 2.7.

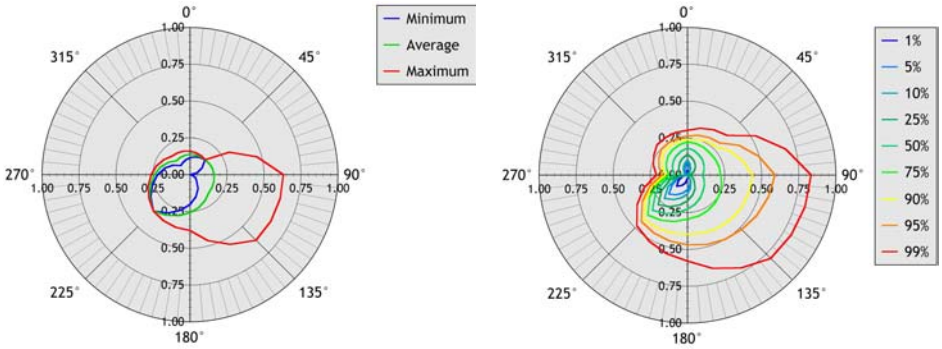

a. b.

Figure 51 – Apparent weathering intensity rates $R^{app}{}_{WE}$ for Keuper shale unit: based on observed data (a) and 2000 Latin Hypercube simulations (b). Angles indicate slope orientation.

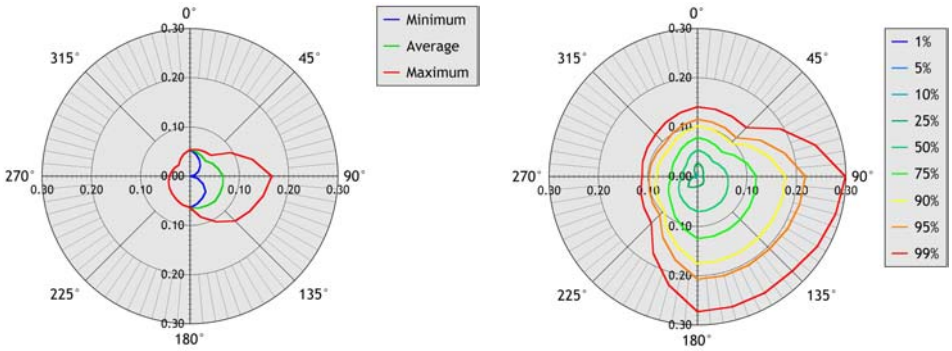

a. b.

Figure 52 – Apparent weathering intensity rates $R^{app}{}_{WE}$ for Keuper limestone unit: based on observed data (a) and 2000 Latin Hypercube simulations (b). Angles indicate slope orientation.

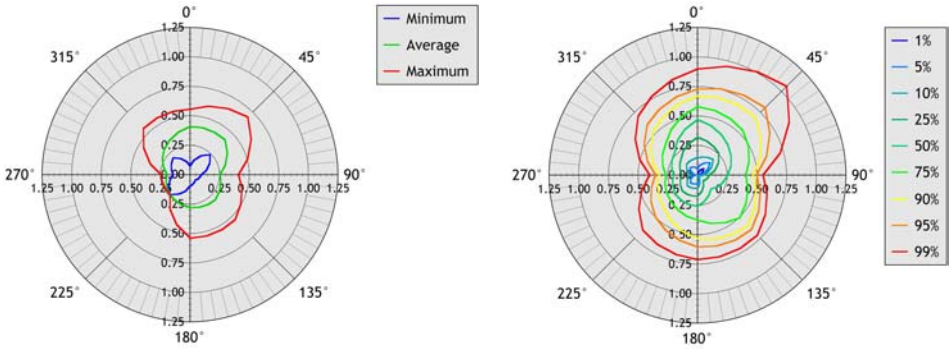

a. b.

Figure 53 – Apparent weathering intensity rates $R^{app}{}_{WE}$ for Middle Muschelkalk siltstone unit: based on observed data (a) and 2000 Latin Hypercube simulations (b). Angles indicate slope orientation.

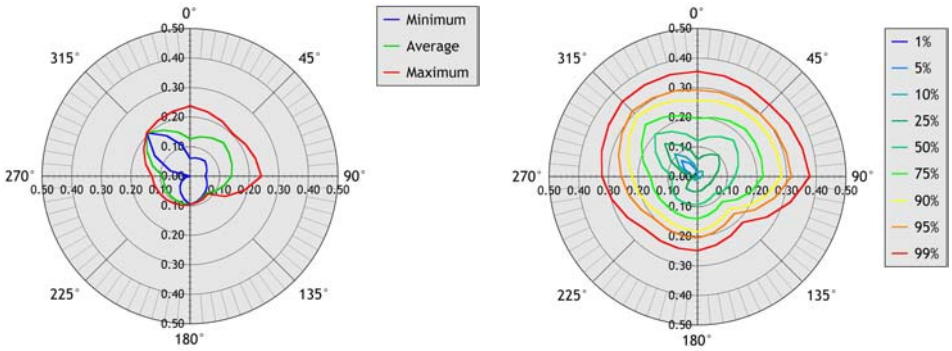

a. b.

Figure 54 – Apparent weathering intensity rates $R^{app}{}_{WE}$ for Middle Muschelkalk gypsum unit: based on observed data (a) and 2000 Latin Hypercube simulations (b). Angles indicate slope orientation.

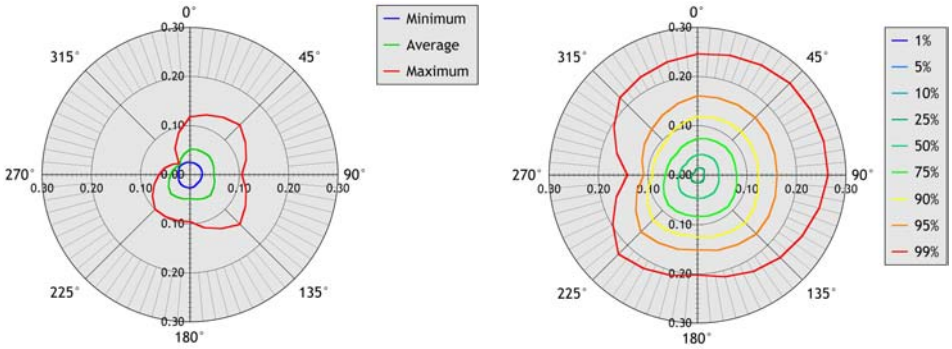

a. b.

Figure 55 – Apparent weathering intensity rates $R^{app}{}_{WE}$ for Upper Muschelkalk limestone unit with bedding spacing <0.10m: based on observed data (a) and 2000 Latin Hypercube simulations (b). Angles indicate slope orientation.

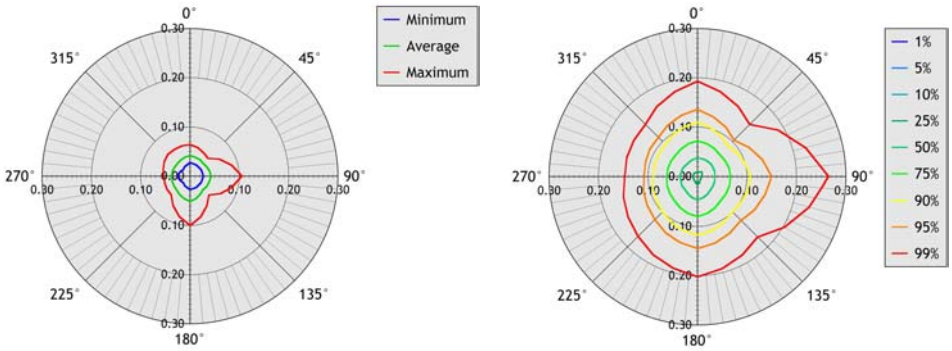

a. b.

Figure 56 – Apparent weathering intensity rates $R^{app}{}_{WE}$ for Upper Muschelkalk limestone unit with bedding spacing 0.10-0.50m: based on observed data (a) and 2000 Latin Hypercube simulations (b). Angles indicate slope orientation.

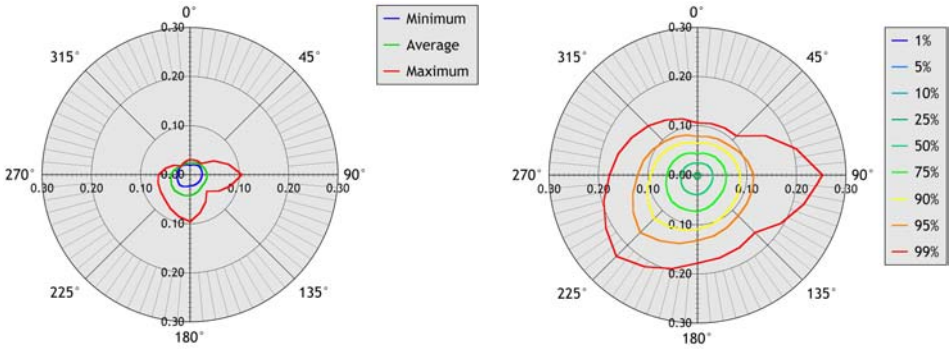

a. b.

Figure 57 – Apparent weathering intensity rates $R^{app}{}_{WE}$ for Upper Muschelkalk limestone unit with bedding spacing >0.50m: based on observed data (a) and 2000 Latin Hypercube simulations (b). Angles indicate slope orientation.

Table 8 - Orientation dependent weathering intensity rates $R^{app}{}_{WE}$ for Keuper units.

		Observed data			Bootstrap percentiles (2000 LHS runs)						
Unit		min	avg	max	5%	10%	25%	50%	75%	90%	95%
Keuper Shale	N	*0.115**	*0.138**	*0.160**	0.083	0.100	0.139	0.183	0.225	0.241	0.264
	NE	0.143	0.143	0.143	0.000	0.016	0.077	0.143	0.211	0.271	0.307
	E	0.000	0.164	0.631	0.000	0.000	0.000	0.101	0.224	0.437	0.589
	SE	0.064	0.178	0.631	0.000	0.005	0.067	0.147	0.263	0.417	0.515
	S	0.202	0.257	0.380	0.095	0.124	0.171	0.226	0.294	0.397	0.469
	SW	0.350	0.350	0.350	0.177	0.220	0.279	0.333	0.378	0.417	0.440
	W	*0.219**	*0.241**	*0.263**	0.000	0.009	0.045	0.085	0.126	0.150	0.172
	NW	0.087	0.132	0.176	0.008	0.035	0.081	0.134	0.184	0.225	0.249
Keuper Limestone	N	0.054	0.054	0.054	0.000	0.006	0.028	0.054	0.079	0.102	0.116
	NE	0.030	0.044	0.060	0.000	0.000	0.016	0.043	0.070	0.096	0.111
	E	0.000	0.067	0.166	0.000	0.000	0.010	0.062	0.119	0.178	0.218
	SE	0.045	0.072	0.129	0.000	0.000	0.017	0.069	0.122	0.174	0.206
	S	0.064	0.064	0.064	0.000	0.000	0.018	0.070	0.125	0.176	0.207
	SW	0.051	0.051	0.051	0.000	0.005	0.027	0.051	0.075	0.096	0.108
	W	*0.042**	*0.042**	*0.042**	0.000	0.000	0.004	0.030	0.052	0.083	0.098
	NW	0.032	0.032	0.032	0.000	0.000	0.006	0.032	0.058	0.080	0.094

** No field data available for these orientations; indicated values are averages of rates observed for the two bordering orientation classes.*

Table 9 – Orientation dependent weathering intensity rates R^{app}_{WE} for Middle Muschelkalk units.

		Observed data			Bootstrap percentiles (2000 LHS runs)						
Unit		min	avg	max	5%	10%	25%	50%	75%	90%	95%
Middle Muschelkalk Siltstone	N	0.072	0.408	0.556	0.056	0.144	0.319	0.469	0.579	0.670	0.729
	NE	0.241	0.419	0.692	0.148	0.186	0.255	0.361	0.537	0.690	0.806
	E	0.096	0.254	0.411	0.013	0.043	0.101	0.256	0.407	0.468	0.499
	SE	0.064	0.302	0.540	0.000	0.007	0.067	0.160	0.504	0.599	0.644
	S	0.096	0.280	0.539	0.069	0.107	0.175	0.259	0.376	0.535	0.604
	SW	0.239	0.239	0.239	0.085	0.121	0.183	0.246	0.315	0.397	0.500
	W	0.143	0.194	0.244	0.018	0.058	0.131	0.202	0.267	0.322	0.354
	NW	0.201	0.306	0.556	0.088	0.129	0.194	0.271	0.377	0.525	0.600
Middle Muschelkalk Gypsum	N	0.060	0.127	0.237	0.000	0.011	0.058	0.121	0.196	0.257	0.292
	NE	0.072	0.160	0.204	0.000	0.025	0.101	0.172	0.227	0.272	0.298
	E	0.052	0.140	0.241	0.000	0.013	0.057	0.127	0.221	0.283	0.316
	SE	0.074	0.080	0.085	0.000	0.008	0.042	0.080	0.118	0.153	0.175
	S	0.096	0.096	0.096	0.000	0.007	0.049	0.093	0.141	0.184	0.206
	SW	*0.048**	*0.094**	*0.113**	0.000	0.017	0.054	0.101	0.141	0.176	0.202
	W	0.000	0.091	0.129	0.000	0.000	0.000	0.085	0.159	0.221	0.257
	NW	0.207	0.207	0.207	0.076	0.108	0.156	0.202	0.248	0.288	0.312

** No field data available for these orientations; indicated values are averages of rates observed for the two bordering orientation classes.*

Table 10 - Orientation dependent weathering intensity rates R^{app}_{WE} for Upper Muschelkalk units.

		Observed data			Bootstrap percentiles (2000 LHS runs)						
Unit		min	avg	max	5%	10%	25%	50%	75%	90%	95%
Upper Muschelkalk BS < 0.10m	N	0.025	0.052	0.118	0.000	0.000	0.014	0.041	0.074	0.119	0.161
	NE	0.025	0.054	0.143	0.000	0.000	0.017	0.046	0.080	0.125	0.165
	E	0.025	0.048	0.105	0.000	0.000	0.013	0.043	0.079	0.123	0.161
	SE	0.023	0.059	0.143	0.000	0.000	0.016	0.048	0.088	0.136	0.168
	S	0.027	0.049	0.096	0.000	0.000	0.014	0.046	0.083	0.124	0.151
	SW	0.027	0.055	0.100	0.000	0.000	0.016	0.047	0.084	0.128	0.162
	W	0.023	0.039	0.063	0.000	0.000	0.012	0.037	0.065	0.091	0.109
	NW	0.027	0.029	0.032	0.000	0.000	0.007	0.032	0.060	0.093	0.131
Upper Muschelkalk 0.10 < BS < 0.50m	N	0.027	0.042	0.064	0.000	0.000	0.007	0.037	0.072	0.110	0.136
	NE	0.025	0.037	0.051	0.000	0.000	0.013	0.037	0.063	0.087	0.104
	E	0.027	0.043	0.105	0.000	0.000	0.008	0.035	0.067	0.107	0.150
	SE	0.025	0.038	0.054	0.000	0.000	0.008	0.037	0.067	0.100	0.124
	S	0.027	0.051	0.100	0.000	0.000	0.015	0.046	0.080	0.118	0.145
	SW	0.019	0.039	0.054	0.000	0.000	0.010	0.036	0.067	0.100	0.122
	W	0.025	0.037	0.053	0.000	0.000	0.009	0.035	0.062	0.089	0.108
	NW	0.019	0.036	0.063	0.000	0.000	0.009	0.033	0.062	0.092	0.112
Upper Muschelkalk BS > 0.50m	N	0.019	0.025	0.031	0.000	0.000	0.004	0.023	0.043	0.064	0.078
	NE	0.025	0.029	0.032	0.000	0.000	0.005	0.028	0.051	0.073	0.087
	E	0.025	0.035	0.105	0.000	0.000	0.006	0.031	0.058	0.087	0.114
	SE	0.023	0.034	0.048	0.000	0.000	0.007	0.033	0.061	0.093	0.116
	S	0.023	0.043	0.096	0.000	0.000	0.008	0.039	0.073	0.109	0.132
	SW	0.030	0.045	0.072	0.000	0.000	0.007	0.039	0.074	0.124	0.164
	W	0.025	0.038	0.064	0.000	0.000	0.006	0.033	0.062	0.095	0.121
	NW	0.025	0.025	0.025	0.000	0.000	0.005	0.028	0.053	0.078	0.096

5.2.2 Data distribution and orientation classes

The treatment of the degree of weathering, exposure time and slope orientation as stochastic parameters (see also Appendix F) is implicit in the bootstrap results as presented in Figure 51b - Figure 57b. The raw data itself gives results as included in Figure 51a - Figure 57a; however, for several units raw data is not available in all orientation classes. The overall number of data points, 426, is distributed in terms of slope orientation as noted in Table 11.

Table 11 - Distribution of data points over identified orientation classes.

Unit	N*	NE*	E*	SE*	S*	SW*	W*	NW*	Total
Keuper shales	0	1	15	25	4	1	0	2	48
Keuper limestones	1	4	34	29	2	1	0	1	72
Middle Muschelkalk siltstones	7	5	2	2	8	1	2	8	35
Middle Muschelkalk gypsum	10	3	4	3	1	0	5	1	27
Upper Muschelkalk BS<0.10m	5	13	15	23	16	7	12	2	93
Upper Muschelkalk 0.10<BS<0.50m	6	7	12	14	23	9	12	3	86
Upper Muschelkalk BS>0.50m	2	2	13	13	22	3	9	1	65

** All orientation classes are 45° wide: N (337.5°-022.5°), NE (022.5°-067.5°), E (067.5°-112.5°), SE (112.5°-157.5°), S (157.5°-202.5°), SW (202.5°-247.5°), W (247.5°-292.5°), and NW (292.5°-337.5°).*

Especially in the Keuper units, the data is distributed unevenly over the orientation classes. This is a direct result of the scarcity of good outcrops and (relatively) recent cuts in these units, as was described earlier in paragraph 3.2.

In the probabilistic approach followed to derive the bootstrap percentiles however, information for the orientation classes in which no raw data exists is gathered from data in the surrounding classes that have a probability distribution exceeding the orientation class limits. This is shown in Table 12, considering a 2σ (95% probability) interval around all data points.

Table 12 – Number of data points within a 2σ (95% probability) interval for identified orientation classes.

Unit	N*	NE*	E*	SE*	S*	SW*	W*	NW*	Total
Keuper shales	1	1	25	31	9	2	1	2	72
Keuper limestones	1	5	48	39	8	1	1	1	104
Middle Muschelkalk siltstones	10	8	4	4	8	6	3	11	54
Middle Muschelkalk gypsum	11	3	4	3	1	1	5	2	30
Upper Muschelkalk BS<0.10m	6	15	22	27	21	11	13	4	119
Upper Muschelkalk 0.10<BS<0.50m	6	9	15	22	27	12	15	9	115
Upper Muschelkalk BS>0.50m	2	2	19	26	23	6	11	3	92

** All orientation classes are 45° wide: N (337.5°-022.5°), NE (022.5°-067.5°), E (067.5°-112.5°), SE (112.5°-157.5°), S (157.5°-202.5°), SW (202.5°-247.5°), W (247.5°-292.5°), and NW (292.5°-337.5°).*

Although quantitative predictions of weathering rates in classes with no raw data points should be made with care and due consideration of the added uncertainty in these cases, the trends with asymmetrical distribution of weathering rates over the orientation classes, that are indicated by the bootstrap percentiles in Figure 51b - Figure 57b, are without exception homogeneous and show no local extremes. The gradual nature of these trends is identified in all units, also those with ample field data in each orientation class. Although singularities cannot be ruled out without a full coverage of all possible orientations by field data, this is in line with the expectation that any influence of slope orientation on weathering rate will be continuous with smooth transitions.

The observed trends remain if broader orientation classes are considered for the units with few or no data points in the 45° wide orientation classes. For example, Figure 58a gives the bootstrap percentiles derived for the Keuper shales using a limited number of four 90° wide orientation classes, with raw data in each of those classes. Qualitative results are similar to those that were displayed in Figure 51b for eight 45° wide orientation classes, although quantitative differences do exist. These are partially related to the choice of orientation classes, with the extremes plotted on the 90° class middles and necessarily no details within the quadrants. For comparison, Figure 58b gives the bootstrap percentiles derived for four 90° wide orientation classes

with boundaries that are shifted 45° from those in Figure 58a. The overall trend is similar with highest weathering rates in the southeast quadrant but inevitably the trend is shifted in accordance with the shift in orientation class boundaries. This shows that a sensitive trade-off between detail in observed trends and reliability of the results exists, for units with data unevenly distributed over the orientation classes.

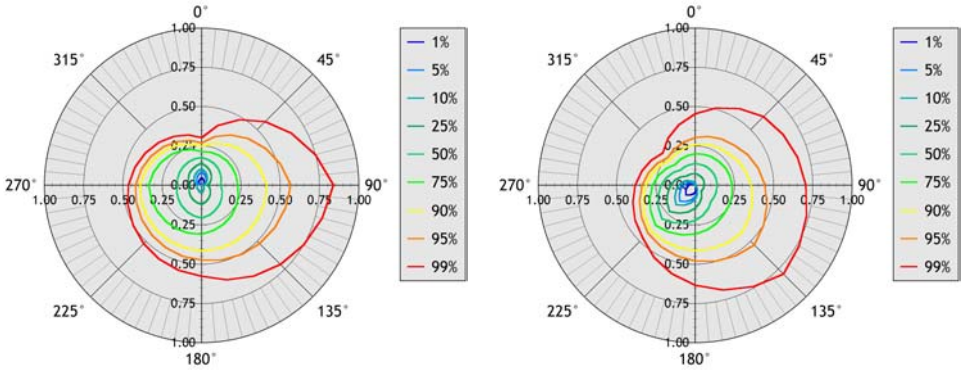

Figure 58 - Weathering intensity rate percentiles for Keuper shales, subdivided into four 90° wide orientation classes N (315°-045°), E (045°-135°), S (135°-225°), and W (225°-315°) (a) and NE (000°-090°), SE (090°-180°), S (180°-270°), and W (270°-360°) (b). Results based on 2000 Latin Hypercube simulations.

5.2.3 Subjectivity in weathering intensity classification

All bootstrap percentiles presented in Figure 51b - Figure 57b and Table 8 - Table 10 are determined based on *WE*-variation within the *observed* weathering class. However, as indicated earlier in Box 5 (page 51), subjectivity in weathering classification adds a variability to this parameter. Hack (1998) quantified this variability due to subjective observations using a box-type probability distribution and took into account the possibility of an observation error of one weathering degree off from the real weathering degree.

The extent and influence of this additional variability can also be estimated on the basis of the results with student reference groups, as described in Box 5, page 52, in which the subjective variability in weathering intensity observations was addressed. The influence of this subjectivity on the bootstrap analysis results can be assessed by including an additional uncertainty for the observed *WE* value in the data simulation routine, defined by:

- A probability pWE_{low}: the probability that the true *WE* value is (one class) lower than the observed *WE* value (so: the weathering intensity is underestimated).
- A probability pWE_{cor}: the probability that the true *WE* value is equal to the observed *WE* value (so: the weathering intensity is estimated correctly).
- A probability pWE_{high}: the probability that the true *WE* value is (one class) higher than the observed *WE* value (so: the weathering intensity is overestimated).

This variability has not been quantified for all possible combinations of units and weathering intensities. As an indication however, the distribution found for the Keuper shales in the Gavadà slope (see Box 5) can be used as an example. In that particular case, the true weathering degree at the time of observation was considered "highly weathered", corresponding to a *WE* value of 0.62. Based on the (limited) test discussed in Box 5, pWE_{low} is taken as 0.24, pWE_{cor} as 0.72, and pWE_{high} as 0.04 (refer to distribution given in Figure 12, Box 5, page 52). The difference of resulting bootstrap percentiles with the results that are found if no subjectivity is included is displayed in Figure 59.

Due to the added uncertainty in *WE* values, the outermost percentiles shift further away from the origin, and therefore the corresponding weathering intensity rates are higher. The influence is strongest in the higher single-sided probability values. Next to the influence on the percentiles for the apparent weathering intensity rate in a given orientation, the asymmetry is

less marked. However, qualitative agreement between Figure 59a and Figure 59b is good. The standard deviations given by Hack (1998) that are used for the variation of the parameter *WE* already include some proportion of the influence of subjectivity, since they are derived from a population in which this subjectivity also exists. Therefore the variability used to obtain Figure 59b is possibly exaggerated. Still, the qualitative relation between slope orientation and weathering rate remains well visible.

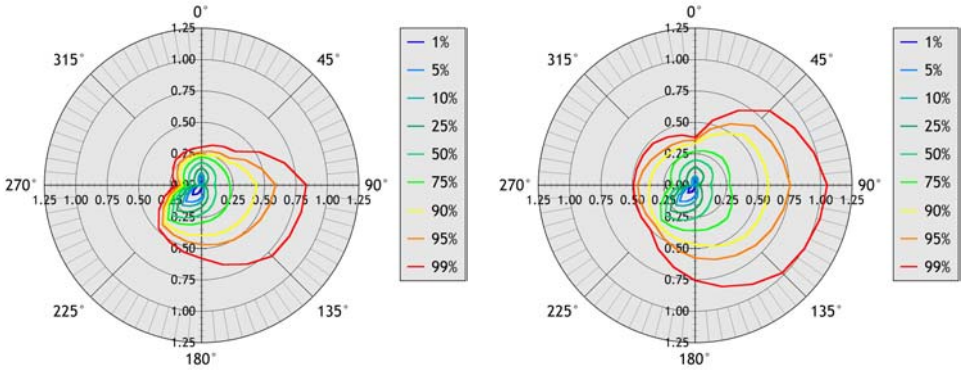

a. b.

Figure 59 – Weathering intensity rate percentiles for Keuper shales, without observation subjectivity (a, see also Figure 51b), and with estimated subjectivity as defined in text (b). Results based on 2000 Latin Hypercube simulations.

5.3 Influence of climate on weathering intensity rates

An analysis has been made of the prevailing wind direction and the wind velocity during rainfall events on the basis of the available XMET data for the year 2003 (Appendix B). Figure 77 gives the distribution of wind directions for various precipitation classes[34] for the XMET stations in Falset and Botarell. Although the overall prevailing wind direction through the year is from the northwest, this changes to the southeast when rainfall intensity increases. Figure 78 shows that the average wind velocity for the wind directions from the southeast increases with increasing precipitation rate. In short: when it rains, the wind tends to blow from the southeast with an increasing velocity with increasing precipitation.

Based on the results of Figure 77 (Appendix B), the graphs in Figure 51 - Figure 57 reveal the influences of the climate conditions on the weathering processes in the various rock masses. It is clear that the weathering intensity rates found for the Keuper shales and limestones (Figure 51 and Figure 52), which are usually interbedded with shaley material, correspond as far as their preferential orientation is concerned to the wind directions during precipitation events and directions with most intense solar radiation. In slopes facing the sund and wind during such events, wetting and drying cycles and associated swelling and shrinking will be most intense and pronounced, a factor which will lead to higher mechanical weathering intensity rates in these slopes. This corresponds to results found by Cantón

[34] *After Selby (1993):*

Precipitation intensity	Precipitation [mm/hr]
Drizzle	0.25 - 1.02
Light rain	1.02 - 3.81
Moderate rain	3.81 - 15.24
Heavy rain	15.24 - 40.64
Very heavy rain	40.64 - 101.60
Torrential rain	>101.60

et al. (2001). An important additional factor to note is the presence of small amounts of swelling clays in the Keuper shales (based on XRF/XRD tests approximately 4% by volume, with a total clay amount of 25-30%). Kühnel (2002) described the importance even of small amounts of swelling clays, and the associated cyclic swelling and shrinking is in such materials a dominant decay process (e.g. Pejon and Zuquette, 2002).

In contrast with the Keuper shales, the gypsum parts of the Middle Muschelkalk tend to weather fastest in slopes facing towards the north, relatively sheltered from the sun and wind during rainfall (Figure 54). The Middle Muschelkalk siltstones, that also contain some gypsum (approximately 10% by volume), show highest weathering intensity rates in east-facing slopes (Figure 53), which corresponds to the preferential wind direction during rainfall. The similarity to the precipitation data is however less than for the Keuper shales.

Water retention plays an important role here, especially for the gypsum unit itself. In slopes sheltered from the wind, drying out of the material directly after rainfall is slower, water is retained longer, and in soluble materials such as gypsum this may give rise to faster (chemical) weathering. In the Middle Muschelkalk siltstones, this effect will still exist because of the gypsum present as cement between the grains, but as Figure 53 suggests the physical weathering by wetting and drying of the clays present in the material (as in the Keuper shales, 25-30% by volume) is dominant leading to highest weathering intensity rates in slopes that face more towards the wind during rainfall.

An additional effect that may play a role in the gypsum units is the possible development of a crust by case hardening on slopes that face into prevailing wind directions during rainfall events (and thus experience more intense wetting and drying cycles), as suggested for sandstone by Robinson and Williams (1996). Although case hardening is commonly associated with sandstone weathering (e.g. Winkler, 1997), it can occur in any weathering process that involves the solution of material components and subsequent

redeposition and concentration of soluble material transported from inside a rock mass to the slope surface. Observations on slopes in the Middle Muschelkalk, especially near the town of Colldejou (e.g. datapoint D18, N4551480/E322770, Figure 60), have shown that thin crusts of up to 1mm are sometimes present. Such features of case hardening protect the slopes on which they occur from further weathering, and will lead to lower observed weathering intensity rates for the slope orientations in which they are found.

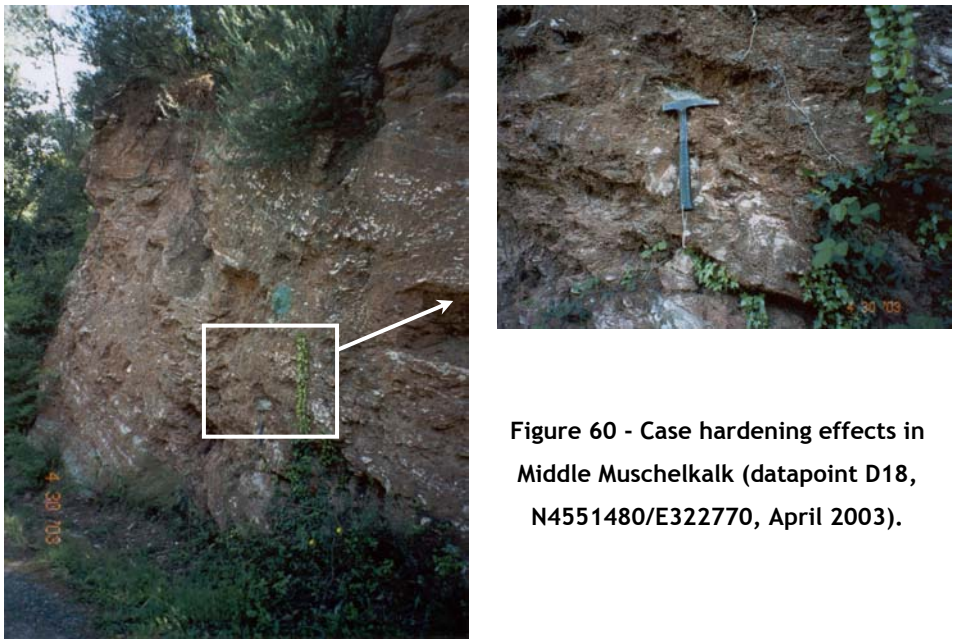

Figure 60 - Case hardening effects in Middle Muschelkalk (datapoint D18, N4551480/E322770, April 2003).

The limestone units of the Upper Muschelkalk have a low susceptibility to weathering and consequently show the smallest weathering intensity rates. Preferential directions are not as obvious as in the Keuper and Middle Muschelkalk rock masses, especially when looking at the 50% percentiles (Figure 55b - Figure 57b) that are close to circular. In the thinly bedded unit with a bedding spacing less than 10cm the influence of slope aspect is most pronounced, again indicating highest weathering intensity rates in east- to southeast facing slopes. This is explained by the regular occurrence of shales intercalated with the limestones in this unit.

The maximum weathering intensity rate decreases in a sequence of units from the Keuper limestones, via the Upper Muschelkalk with bedding spacing <0.10m, the Upper Muschelkalk with bedding spacing 0.10-0.50m, to the the Upper Muschelkalk with bedding spacing >0.50m (Figure 61). This sequence of units generally also corresponds to a decreasing amount of shales intercalated with the limestones.

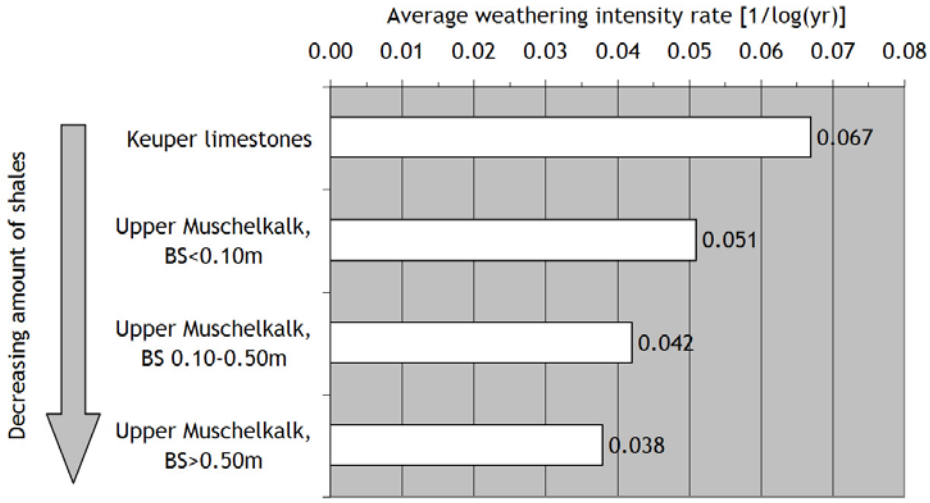

Figure 61 - Average weathering intensity rates for limestone units.

The importance of the intercalated shales can also be observed from the marked asymmetry in weathering intensity rates for Keuper limestones, when plotted against the slope orientation (Figure 52, page 123); it appears that the materials more resistant to weathering (the limestones) tend to "follow" the more susceptible materials present in a rock mass (the shales, compare Figure 51, page 123). A similar but less pronounced asymmetry can still be observed in the bootstrap results for the Upper Muschelkalk limestones with bedding spacing <0.10m (Figure 55, page 125); the medium- to thickly bedded units in the Upper Muschelkalk, in which the shale intercalations are of less importance, do not show this asymmetry.

5.4 Influence of excavation method on weathering intensity rates

5.4.1 Observed decay characteristics in Bhutan

Bhutan, with its capital Thimphu, is bordered by India towards its east, south and south-west and Tibet towards its north, in the great Himalayas. This south-eastern part of the Himalayas sees the highest precipitation during the monsoon season. The precipitation peaks during this season contribute to the rock mass weathering and erosion in the area.

Although the old crystalline basements of the Himalayas are metamorphosed to various degrees and have been subject to the Himalayan orogeny, they have preserved much of their original composition (Gansser, 1964). The data from Bhutan presented in this paragraph has been collected in the Thimphu area, in rocks of the so-called "Thimphu Group" (Bhargava, 1995). Data was gathered from two main litho-stratigraphic units (after Chhetri, 2005):

- Gneisses of the "Takhtsang formation" (Gansser, 1964). The gneisses are mostly feldspathic biotite-muscovite gneisses, fine to medium grained and foliated. Quartz veins are also seen in some of the exposures. Thin to medium bands of schists occur within the gneissic rocks in the section along the Simtokha – Dochu La road. The general strike of the rock layers is from northwest to southeast, with north-easterly dips ranging from 10° to 35°.
- Metamorphic rocks (mostly quartzites) belonging to the "Naspe formation". These are high grade metasediments and are mostly affected by faulting and folding.

Chhetri (2005) made a total of 100 SSPC classifications as part of M.Sc. research[35], 87 of which are in the gneisses of the Takhtsang formation.

[35] *As the SSPC has been validated for the Falset research area in Spain, one of the objectives of the project was to verify its applicability in the Bhutanese Himalayas. Since the SSPC correction factors for the method of excavation (*ME*) and the degree of*

Although this data set is by no means as extensive as that for the Falset area in Spain, the data can be used to obtain an indication of the influence of parameters other than slope orientation on weathering rates. A bootstrap analysis on the results for the Takhtsang gneisses similar to that presented in paragraph 5.2 results in Figure 62. In line with the results from the Falset area in Spain, a clear asymmetry is found with in this case south-east facing slopes showing notably higher apparent weathering intensity rates than north-west facing slopes. Although the specific climate data is less detailed than is available for the Falset area, this corresponds with the prevailing wind directions, especially in the monsoon season, when winds tend to blow from the south-east (Chhetri, 2005).

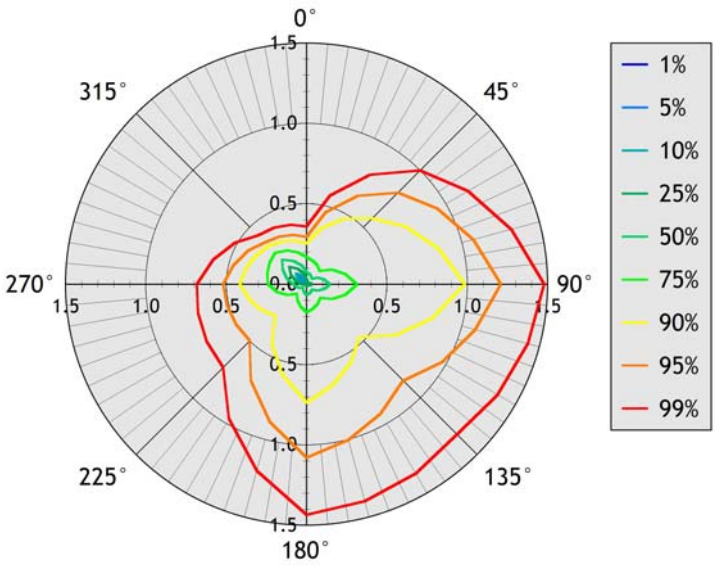

Figure 62 - Bootstrap percentiles for the apparent weathering intensity rates, Takhtsang gneiss (data from Chhetri, 2005). Angles indicate slope orientation.

*weathering (*WE*) are derived from Falset data only, the presented results shall be treated qualitatively rather than quantitatively.*

5.4.2 Relations with excavation damage

To verify the influence of excavation damage on the weathering susceptibility of rocks exposed in slopes, a subdivision of the Takhtsang gneiss data set into slopes with different excavation methods has been made to identify the possible influence of the excavation method on weathering susceptibility. Figure 63 shows the result for this subset of natural and blasted slopes, with a further division of the blasted slopes into classes with increasing damage to the rock mass during excavation (excavation classes after Hack, 1998), and with apparent weathering rates relative to the 99% percentile as found in Figure 62. As can be seen in the figure, blasted slopes tend to have higher weathering intensity rates in any orientation than natural slopes. For south-east facing slopes, an approximately five-fold increase in weathering rates is observed from natural to blasted slopes.

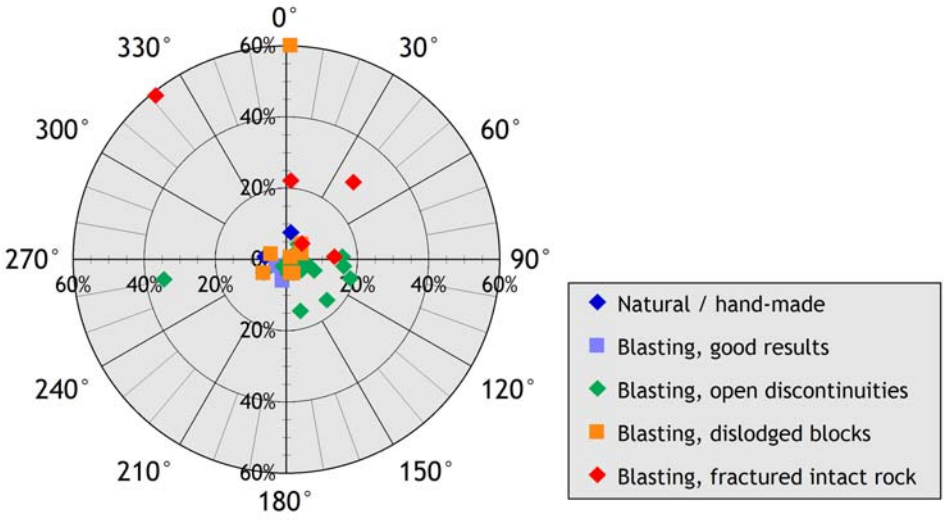

Figure 63 - Apparent weathering intensity rates for different excavation qualities, relative to corresponding 99% percentile of Figure 62.

The relation between the amount of damage due to blasting and apparent weathering intensity rates can be further refined by correcting for the asymmetry as observed in Figure 62. By grouping the data into two subsets,

one with orientations 090°-180° (according to Figure 62 the orientations that show highest weathering intensity rates), and one with orientations 225°-045° (the orientations that show smallest weathering intensity rates), and averaging the data for each identified blasting damage class, Figure 64 is obtained. This confirms the influence of excavation damage on weathering intensity rates in the Bhutanese setting, with a distinct decrease of the average apparent weathering intensity rates with decreasing excavation damage due to blasting.

Note that Figure 64 seems to suggest little difference between weathering rates in orientation class 090°-180° and orientation class 225°-045°. This results from the fact that Figure 64 gives average weathering rates; as can be seen in Figure 62, the 50% percentiles (that will be close to the average rates, see paragraph 6.1.1) indeed show only a small asymmetry. The asymmetry in Figure 62 is clearer in the higher percentiles.

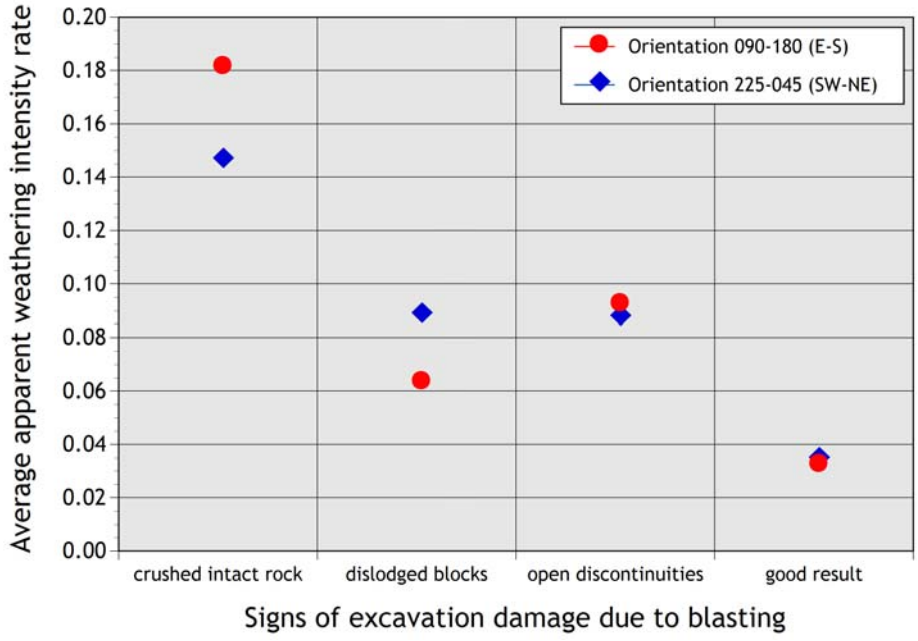

Figure 64 - Relation between blasting damage (represented by *ME*) and average apparent weathering intensity rate, Takhtsang gneiss (data from Chhetri, 2005).

6 Applications and limitations

"And yet: nature proposes, but fate disposes." - Simon Winchester, *Krakatoa - The day the world exploded.*

6.1 Prediction of weathering intensity

6.1.1 Results from research area

The results obtained for the data set collected in the Falset research area give bootstrap percentiles for the apparent weathering intensity rates shown in Figure 51b (page 123) to Figure 57b (page 126), for the seven investigated engineering geological units. From the weathering intensity rate percentiles, the anticipated degree of weathering or weathering intensity can be calculated easily by rearranging equation (1) (page 55). This gives the SSPC *WE*-parameter as a function of time for a given slope orientation and initial degree of weathering:

$$WE(t) = WE_{init} - R_{WE}^{app} \log(1+t) \tag{16}$$

An example of such a prediction is given in Box 11. Since these results are derived from a statistical analysis, due care should obviously be taken when applying the findings that describe *populations* to a specific case which involves an individual *sample*. Bootstrap percentiles as presented in the radar plots referred to above describe the likelihood of behaviour for a great number of data points, observed as well as simulated. In practical terms, this means that whereas the bootstrap percentiles describe the likelihood for population behaviour based on the simulated data sets, an individual slope may very well behave differently than expected based on those percentiles, and even the comparison of a small number of slopes may give opposing or

ambiguous results. However, *on average* (or for a certain likelihood), a large number of slopes will ideally show the anticipated behaviour.

This can be illustrated by comparing observed weathering intensities, as recorded in the data set given in Appendix H, to the weathering intensities that can be inferred from the bootstrap percentiles for the apparent weathering intensity rates that have been derived for the respective engineering geological units. On the basis of the empirical relations resulting from the bootstrap analyses, the expected *WE* values for all data points can be calculated from the resulting bootstrap percentiles for the apparent weathering intensity rates, and compared to the actually observed *WE* values. Figure 65 gives the resulting bootstrap probability distribution for the average error of the expected *WE* per unit. The graph shows that the 50% percentiles have an average error close to 0 for most units; only for the Keuper shales, the 50% percentile gives on average an overestimate of *WE*. Inevitably, reliability intervals for the units that are most susceptible to weathering (Keuper shales, and Middle Muschelkalk siltstones and gypsum) are widest, reflecting the larger standard deviation that is associated with *WE* values for higher weathering intensities (Hack, 1998).

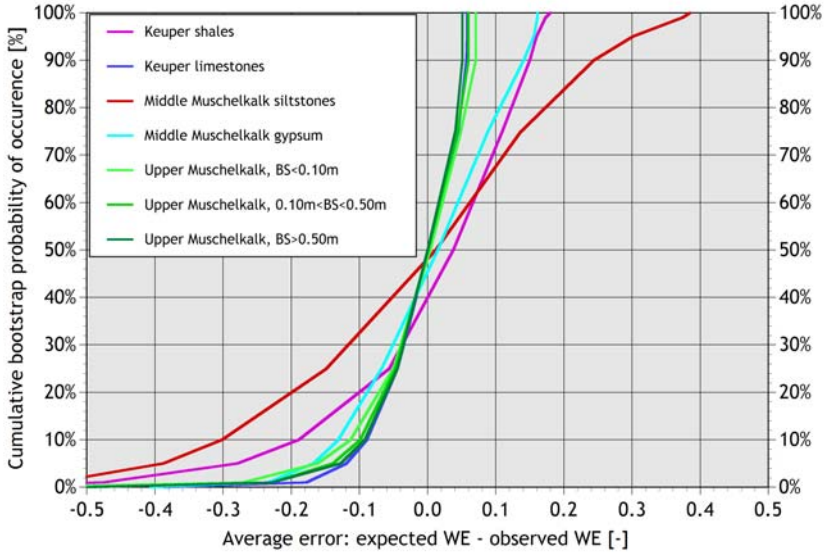

Figure 65 - Average error of expected WE value.

Box 11 – Prediction of weathering intensity for the Masriudoms slopes: influence of slope aspect

The two slopes of the road cut near Masriudoms (Appendix G) show clear signs of decay. The average slope angles in both slopes have been decreasing since the time of excavation, indicating that the slope angle as excavated is not sustainable in this unit. This was a continuous and gradual process until 2004, when a section of the north facing slope underneath an electricity pole failed (see Figure 66). This event turned the continuous process of decay into an episodic one.

Figure 66 - Slump type failure in slope near Masriudoms, May 2004.

The collapse occurred within a week after a period with considerable rainfall. The trigger for the slide is thought to be weakening of the clays in the slope by wettening after penetration of water, rather than water pressures sensu stricto. This also accounts for the delayed effects of wettening with failure occurring some time after rather than during a rainfall event. The likely importance of this process was postulated by Hack (1998) and is shown quantitatively by Jaboyedoff et al. (2004). The latter found that pore water pressures in gouge materials did not markedly rise before slide events, but that sliding in such materials is linked to material weakening and is delayed to some time after actual wetting of the clays.

It is interesting to hypothesize on the reasons for failure only of this section of the north facing slope. First of all, this section is relatively close to the old land surface as it was before 1992. In the situation until 1992 a small depression existed in the eastern hillside adjacent to the present slope. Therefore the part of the north facing slope closest to this depression may have been more affected by previous weathering than the rest of it, which had been at a larger distance from the old land surface. Furthermore, as can be observed in Figure 53 (page 124), the Middle Muschelkalk siltstones tend to weather faster when exposed in N- to SE-facing slopes than in S- to NW-facing slopes. Therefore, starting from what was probably a slightly variable but similar initial state of weathering, the decay by weathering will likely have affected the north facing slope more than the south facing slope, and will have penetrated deeper into its rock mass. ➲

To predict the weathering intensity in terms of its effect on slope stability, as defined by the WE parameter in the SSPC system, the bootstrap percentiles as given in Figure 53b can be used. Figure 67 gives the resulting distributions for the apparent weathering intensity rates ($R^{app}{}_{WE}$), as derived for the actual slope orientations (being 198° for the north slope, and 020° for the south slope) from Figure 53b.

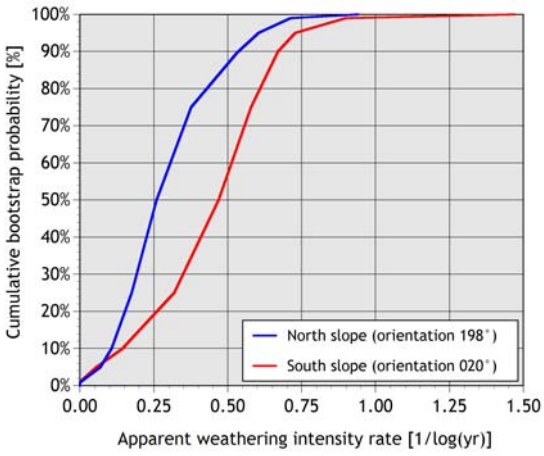

Figure 67 - Bootstrap probability distributions for $R^{app}{}_{WE}$, Masriudoms slopes.

By using equation (16) (page 141), the weathering intensity parameter WE can be directly predicted as a function of time, given the initial degree of weathering. For the Masriudoms road cut, this initial degree of weathering is estimated to have been "slightly weathered" for both slopes, corresponding to a WE value of 0.95. The resulting predictions for WE based on the different intensity rate probabilities given in Figure 67 are presented in Figure 68. For all intensity rate probabilities, the expected weathering intensity rates for the north facing slope are markedly higher than for the south facing slope. Therefore the expected WE parameter at a given moment in time is lower for the north facing slope.

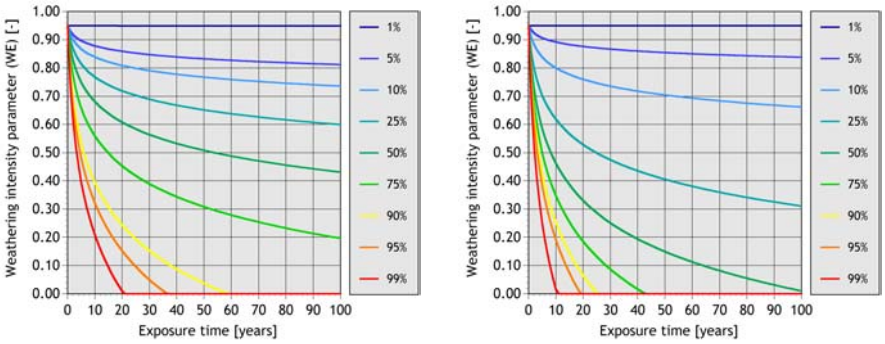

a. b.

Figure 68 – Prediction of weathering intensity parameter WE for the Masriudoms slopes: south facing (north) slope (a) and north facing (south) slope (b).

6.1.2 Considerations for exporting results

The results from the Falset research area indicate that the use of an apparent weathering intensity rate such as defined by equation (1) (page 55) is a useful indicator for the magnitude of rock mass decay, and facilitates establishing the influence of other (geotechnical) parameters on that decay. The data from the Falset area shows this for the influence of slope orientation. Data from Bhutan, presented in paragraph 5.4.1, has been used similarly to indicate the influence of excavation damage on rock mass decay in slopes.

As was mentioned in paragraph 5.2, the results obtained by using this apparent weathering intensity rate suggest that the rock mass decay in the Falset research area:

a) is a process which acts on an (approximately) logarithmic timescale;
b) is erosion delimited in the majority of the investigated slopes, with an imbalance favouring weathering (situations D and E, Table 5, page 98).

The apparent weathering intensity rates do however show a considerable scatter, even when taking into account the slope orientation as influencing parameter. As the results from Bhutan (paragraph 5.4.1) show, other geotechnical parameters such as excavation damage can affect the weathering susceptibility and therefore both the weathering intensity and penetration rates of a rock mass. Qualitatively, this has been shown for the damage due to excavation for blasted slopes.

In general terms, the results from the Falset area strongly suggest that similar engineering geological units[36] show maximum apparent weathering intensity rates of a similar magnitude. The Keuper shales and Middle Muschelkalk siltstones have the highest rates, in the order of 0.2-0.3 [1/log(yr)], and the dolomitised limestones of the Keuper and Upper

[36] *Defined by rock mass strength properties, such as the reference rock mass cohesion and friction angles in the SSPC system.*

Muschelkalk the smallest, in the order of 0.04-0.07 [1/log(yr)]. The Middle Muschelkalk gypsum shows intermediate weathering intensity rates, up to approximately 0.12 [1/log(yr)], half that of the most susceptible units. This implies that in practice the units that are most susceptible to weathering show considerably faster decay than the most resistant units. The weathering intensity rates can be included in the slope stability calculation of the SSPC system, to give time-dependent slope stability predictions (see paragraph 6.2.1 and Box 12).

The shales of the Keuper, the siltstones of the Middle Muschelkalk and the gypsum unit and gypsum-containing layers of the Middle Muschelkalk are affected by different principal weathering processes[37]. As a result the relation of the weathering intensity rates with the local climate differs for these units. The Keuper shales, with slaking as the dominant weathering process, show highest weathering intensity rates in slope orientations that face the sun and dominant wind during rainfall and are therefore exposed to the most pronounced wetting and drying cycles (corresponding to results found by Cantón et al., 2001).

The Middle Muschelkalk gypsum shows highest weathering intensity rates in slopes on the lee-side of hills during rainfall, corresponding to the importance of water retention for the static dissolution process. The Middle Muschelkalk siltstones, in which decay is caused by a combination of these two processes, highest weathering intensity rates are observed for intermediate orientations. The limestone units of the Upper Muschelkalk and Keuper show the smallest weathering intensity rates, but there is a trend that the weathering rate increases with an increasing amount of intercalated shales. It is likely that the higher the amount of such

[37] *The Keuper shales weather mainly by slaking caused by cyclic wetting and drying. Similar slaking combined with dissolution of gypsum cement are the dominant weathering processes in the Middle Muschelkalk siltsones. The Middle Muschelkalk gypsum is primarily weathered by dissolution of gypsum in the presence of water. See chapter 3.*

intercalated shales, the more predominant slaking becomes, with a tendency for highest weathering rates in slopes facing dominant wind directions during rainfall.

It is expected that similar qualitative results hold for other climatic environments as well, although this cannot be proven on the basis of the existing data. However, it should be noted that freeze-thaw weathering, with (diurnal) temperature changes as the driving mechanism, can obscure the influences of rainfall and water action. In the Falset research area, freeze-thaw weathering is not an important issue[38], but in a weathering environment where freeze-thaw is equally or even more important for rock mass decay than cyclic wetting and drying, slope orientations facing the midday sun (south facing on the northern hemisphere, north facing on the southern hemisphere) will suffer more from it. Depending on preferential wind directions during rainfall, freeze-thaw action may in such cases coincide with and emphasize the influence of slaking or chemical weathering through water. In the other extreme the influences of rainfall, wetting, drying, and water retention on one hand and freeze-thaw on the other may as well cancel each other.

If freeze-thaw action and other influences such as disturbances from agriculture, industry or urbanization (e.g. Inkpen and Jackson, 2000) can be neglected it is recommended to assume highest weathering intensity rates in slopes that are wind-facing during rainfall for rock masses where slaking is the dominant weathering process, and highest weathering intensity rates in slopes that are wind sheltered during rainfall, or carry water for the longest time, for rock masses where chemical reactions such as dissolution are the dominant weathering process. For weathering-resistant materials that are interbedded with more susceptible materials, highest weathering intensity rates can be expected in slope orientations for which the more

[38] *Although some freeze-thaw action is expected for the Thimphu area in Bhutan, the observed weathering phenomena in the Bhutanese data do not indicate it to be the principal decay process.*

susceptible material will show highest rates: rainfall-facing for shales and similar slaking materials, sheltered for materials in which dissolution and similar processes are dominant. These trends, as observed in the Falset area, are summarized in Figure 69.

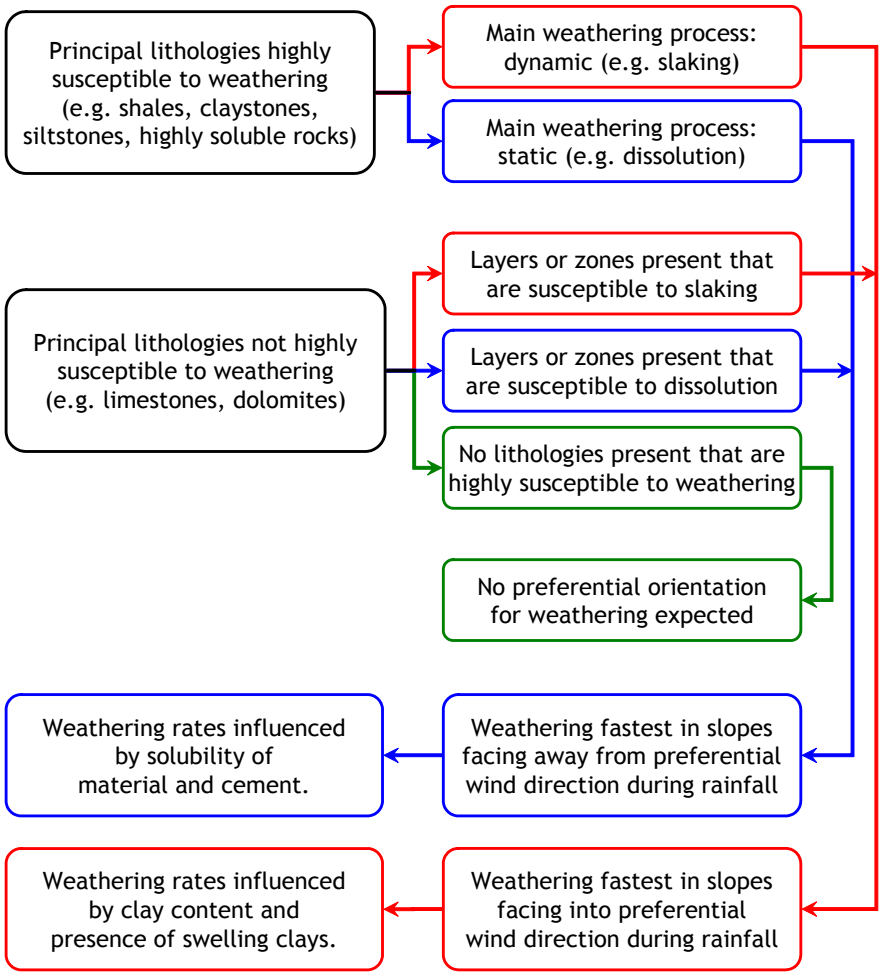

Figure 69 - Guideline for predicting qualitative behaviour with respect to weathering and slope orientation.

6.2 Prediction of slope stability

6.2.1 Slope stability prediction using the SSPC

In the SSPC system, the *WE* parameter predicted on the basis of the bootstrap percentiles for apparent weathering intensity rates for the different engineering geological units (see equation (16), page 141) can be directly incorporated in the stability models that are included in the SSPC.

The SSPC calculates slope stability probabilities as a function of slope geometry and rock mass characteristics that include *WE* (Hack, 1998; Hack et al., 2003). By defining *WE* as a function of time, as can be done with a prediction of the weathering intensity rate, the slope stability probability also becomes a function of time. In addition, since a prediction of weathering intensity is associated with a certain bootstrap percentile, the estimated probability of such time-dependent slope stability is quantified, and slope stability predictions can be made for different probabilities of occurrence (e.g. Tegtmeier, 2005). By additionally incorporating a time dependent slope angle based on an average decrease of the slope angle according to equation (3) (page 102), the effect of erosion can also be assessed. An example of such an analysis is given in Box 12. Tegtmeier (2005) further included progressive weakening of the weathered zone to arrive at a situation where the strength of a rock mass varies throughout the slope and with time, with a simultaneous change of slope geometry in time (through erosion).

Since such slope stability prediction may include an extrapolation of the data set on which it is based into the future, the results should then be treated as such. As was shown in paragraph 6.1.1, the 50% bootstrap percentiles for weathering *rates*, when converted to weathering *intensities*, have the best agreement *on average* with the actual observations. Therefore, the 50% percentile lines are believed to give the most reliable prediction of slope stability changes in the future – qualitative if not quantitative. As Box 12 demonstrates, a particular slope design can be evaluated through such calculations with respect to its influence on future slope stability.

Box 12 – Stability development of the Masriudoms slopes

In Box 11 on page 143, the prediction of weathering intensities as functions of time for the two opposing slopes at the Masriudoms study site are discussed. Using these, the slope stability probability can be predicted for any time, with the SSPC system. Based on an initial slope angle of 50°, and a decrease of the slope angle of 1°/year (until a final slope angle of 35° is reached; according to equation (3), page 102, and corresponding to field observations), results for the orientation independent stability probability (refer to Hack, 1998) based on an initial slope angle of 50° are given in Figure 70, with different curves representing different bootstrap percentiles for the apparent weathering intensity rate, $R^{app}{}_{WE}$.

In both graphs, the (stabilising) influence of the decreasing slope angle is visible during the first 15 years, after which a stable slope angle is reached. This culminates in a marked peak in most curves. Ultimately, weathering and associated rock mass weakening inevitably lead to a decrease of the stability for all percentile curves >5%. An important difference between the results for the two slopes is found and this is most notable when looking at the threshold for orientation independent stability (OIS) of 50% (corresponding approximately to a factor of safety of 1, in deterministic terms). The 50% bootstrap percentile for the south facing (north) slope remains above this threshold throughout the considered time interval, whereas for the north facing (south) slope this line indicates a minimum OIS of 40% within the first years following excavation. The lower stability of the south slope as observed in reality (see Box 11, page 143) corresponds to these findings.

The same stability prediction can also be used to assess the influence of slope design on current and future slope stability. Graphs similar to those in Figure 70, but now for an initial slope angle of 40° instead of 50°, are given in Figure 71. It is clear from the higher expected stability probabilities that the stability of this slope could have been considerably higher, had the slope been designed with a smaller slope angle.

A comparison of the development of these two slopes since their excavation back in 1992, as discussed earlier in Box 11, shows the intricate and in some respects episodic behaviour of the various decay processes. These are influenced by the history of the site, the local climate, the slope orientation, the material exposed in it, and by discrete events such as intense rainfall. Although the interference of these influences generally complicates the interpretation of the decay, the observations made in these slopes can be well explained and are in agreement with the results of this study.

It should be considered however that these particular slopes were in a very similar situation to begin with at the time of excavation and have been observed throughout their exposure time. In situations where starting conditions differ, or in older slopes where the various processes have been working for a longer time span, the influences of internal, external, and geotechnical weathering parameters may be more obscured.

➲

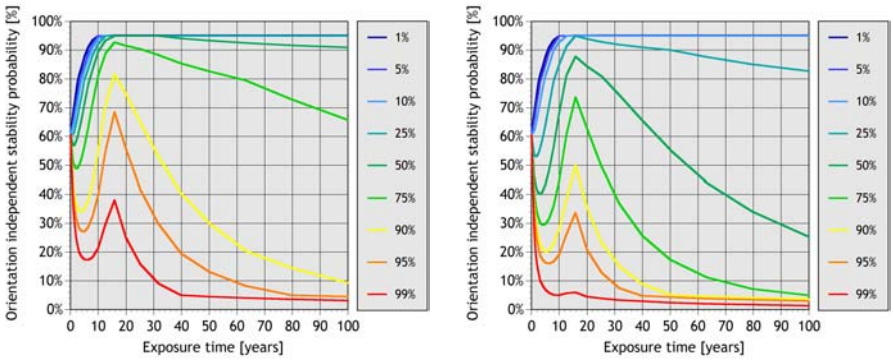

a. b.

Figure 70 – Prediction of orientation independent stability probability for the Masriudoms slopes, for an initial slope angle of 50°: south facing (north) slope (a) and north facing (south) slope (b).

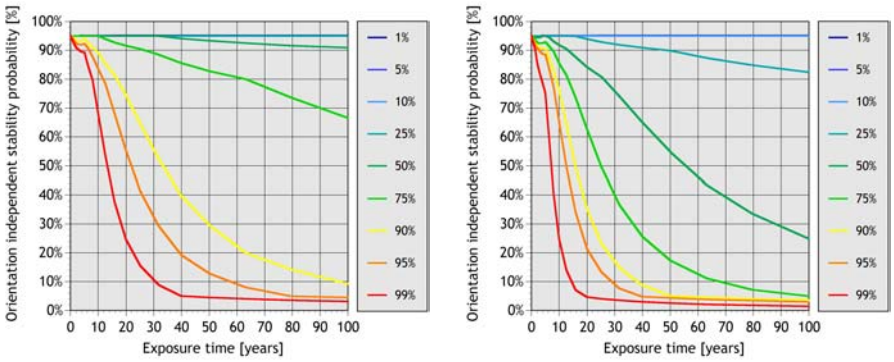

a. b.

Figure 71 – Prediction of orientation independent stability probability for the Masriudoms slopes, for an initial slope angle of 40°: south facing (north) slope (a) and north facing (south) slope (b).

6.2.2 Interpretation of probabilistic models

Alternative approaches exist to slope stability assessment: deterministic, partial-factor principle, and probabilistic. To obtain the best possible basis for evaluation it is useful to include a probabilistic analysis (Nilsen, 2000), but a common problem with probabilistic methods is their interpretation. Instead of an apparently simple black-and-white deterministic answer[39], probabilistic methods yield a greyscale picture where it is not immediately clear if a calculated probability for a certain type of performance is satisfactory or not. The same is true for defining target values of such probabilities, for design stages. As with deterministic approaches, the desired target values for stability probabilities depend on the effects that unsatisfactory performance would have; as an example, target design stabilities for major highway road cuts will be higher than for secondary backcountry roads that see far less traffic.

General target values for the probability of "unsatisfactory performance" are defined for example by the US Army Corps of Engineers in Anon. (1995), see Table 13. The probability of unsatisfactory performance is defined as *"the probability that the value of performance function will approach the limit state, or that an unsatisfactory event will occur"* (Anon., 1995). If for example the performance function is defined in terms of slope stability, and the probability of unsatisfactory performance is 0.023, then 23 of every 1000 slopes will show instability phenomena.

The values listed in Table 13 seem to be quite small and therefore very strict for geotechnical applications such as slope stability. As with all such guidelines, it has to be considered what an "unsatisfactory event" in the

[39] *Deterministic methods may appear to give such a clear black-and-white result, but uncertainty is an important concept even in such deterministic approaches. This is usually dealt with by introducing an appropriately large factor of safety into deterministic calculation methods. Because of this, outcomes of deterministic methods and the conclusions based upon these are fuzzier than they may appear on first sight.*

above quoted definition is – e.g. a major catastrophe with a full-scale slope collapse without warning, an increased requirement for roadside maintenance because of small toppling blocks, or problems during slope constructions that necessitate re-designing the slope. It seems that the target probabilities listed in Table 13 are for events of the first category. An example to put the figures into perspective, a poor result would be obtained if 2.3% gives unsatisfactory performance. Considering a major road construction or realignment program with, say, 20 slopes to be cut, this would correspond to approximately half a slope giving unsatisfactory performance. In such a large scale project, this outcome would not likely be considered as poor, but remediated during the construction stage. Note that redesign during construction actually improves the stability probability because the uncertainties of the underlying data (rock mass characteristics etc.) are continuously reduced when an increasing amount of data becomes available.

In terms of SSPC slope stability probability, the likeliness of failure is defined as any instability event happening, ranging from individual failing blocks to deep-seated large volume slope failure. With failures of the first kind, a 95% stability probability (translating to a single slope out of the 20 in the example above showing some rockfall) would in most cases qualify as an agreeable result. This example underlines that still, engineering wisdom has to be applied in setting target probabilities, and in differentiating the impact of satisfactory performance in different cases.

Table 13 - Target design probabilities as maintained by the U.S. Army Corps of Engineers (Anon., 1995).

Expected performance level	Probability of unsatisfactory performance [-]
High	0.0000003
Good	0.00003
Above average	0.001
Below average	0.006
Poor	0.023
Unsatisfactory	0.07
Hazardous	0.16

6.3 Implications of decay for geotechnical engineering

Fookes and Sweeney (1976), Fookes and Weltman (1989a and 1989b) and Shakoor (1995) describe practical engineering problems that can arise if a slope and the rock mass exposed in it are subject to decay by weathering, and the remedial works that may be required to limit the consequences of this. Weathering decay is particularly responsible for relatively small failures and rock falls with a high repetition frequency, but can also lead to large scale failure of a slope as a whole.

Stabilizing measures that are possible in various stages of the project are described by the authors mentioned above, and in detail by Ortigao and Sayao (2004). It is beyond the scope of this research to address possible slope stabilisation measures in detail. With respect to rock mass decay, general considerations for remedial measures are given in Table 14.

Fookes and Sweeney (1976) made the important observation that basic design decisions in complex situations should only be made as the slope face is exposed. The realignment of the N-420 section between Coll Negre and Coll Teixeta that commenced in 2000 is an example where this would have reduced construction costs considerably. As it was, predefined designs were maintained during excavation and construction of the slopes in question, calling for expensive remedial measures and re-excavation in a later stage. (Box 3, page 24). Shakoor (1995) dealt specifically with the effects of and possible remedial measures against differential weathering and erosion, such as described for example in Box 4, page 35.

Table 14 - Remedial measures for slope instability due to rock mass decay.

Stage	Action
Before excavation	• Mapping of geotechnical features, site investigation • Shield or strengthen structures against blast damage • Temporary or permanent protection from rock fall at the slope toe • Prevent continuous water flow over face (usually by crest drains)
During excavation	• Slope design depends on rock type, mass properties, site properties, economical boundary conditions (for excavation as well as long-term maintenance) • Monitor overbreak and fracturing with the applied blasting technique (if any), preferably in trial blasts • As excavation proceeds, detailed mapping of the geological structure • Decide on required stabilization measures • On existing slopes, removal of individual blocks may be an inexpensive alternative to stabilization measures.

After excavation	• Monitoring of deformation and slope processes
	• Evaluation of design based on the exposed geological structure as compared to the expected structure used in the design phases
	• Consider remedial measures if necessary. Options are:
	  ○ Mechanical reinforcement (e.g. bolting, grouting), in order to prevent failure;
	  ○ Measures that limit effects of failure (e.g. collectors, netting), in order to decrease the hazard associated with failure, rather than the vulnerability;
	  ○ Measures that decrease decay influences (e.g. drainage, grouting), in order to stop weathering and erosion affecting the slope;
	  ○ Measures that limit the influences of decay on slope stability (e.g. benching), in order to avoid stability decrease by (allowed) decay.

7 Conclusions

"'Forty-two!' yelled Loonquawl. 'Is that all you've got to show for seven and a half million years' work?'" – Douglas Adams, *The Hitchhiker's Guide to the Galaxy*.

Decay of rock and unconsolidated soil masses underlying artificial slopes can greatly affect the geotechnical mass properties within engineering timescales. This may induce a rapid change in mass strength, from initial rock-like properties in a fresh state to soil-like properties in a completely weathered state. For the safe construction of a road cut with respect to its envisaged engineering lifetime, it is therefore of vital importance to incorporate in the initial design not only the present-day geotechnical characteristics, but also the dominant time-related processes that control the engineering behaviour of soil and rock masses as well as the rate of decay of the geotechnical properties.

The three main processes that are involved in the decay of slopes in engineering timescales are:

- **Relaxation** or redistribution of stress and strain following excavation leading to loss of structural integrity;
- **Weathering** of the slope material;
- (Subsequent) **erosion** of the slope material.

These processes are mostly restricted to a relatively shallow zone in the rock mass close to the slope surface, and such shallow surface/sub-surface processes are usually not taken into account in slope stability assessments that commonly address deep-seated instability.

The processes that determine the decay of the material as well as the mass quality of rock and soil slopes can be of external as well as internal nature, and act on a wide range of scales from molecular to many metres. This range in scales, the many different processes that are involved, and the inhomogeneity of most rock and soil masses make weathering and decay in general notoriously difficult to predict.

Of the three processes that constitute decay in general, weathering is the least difficult to quantify. Assessment of weathering intensity is possible through a verbally descriptive approach (commonly a description according to a standardized classification system), measuring mechanical index properties, or determining chemical indices. Although direct measurements through index testing gives an objective measure for the weathering intensity, they have the disadvantage of being totally dependent on the nature of the (primary) weathering process. Results for a different parent material, a different weathering environment and so on cannot be compared conclusively. In that respect the resulting indices are very specific parameters that are a good *quantitative* measure for one specific combination of material and weathering environment, but a poor *qualitative* measure to compare different materials, or different environments (and therefore sites).

It is for this reason that classification systems are still often preferred over measurable parameters for assessing weathering intensity, even though classification results may show considerable variability (scatter). Such variability is due to more than artefacts alone; apart from subjectivity of the person who made the classification and variation introduced by conceptual errors in the appreciation of the data's behaviour in the real world, the intrinsic variability of the data itself also contributes to it. If variability is appreciated as an inevitable part of the data and even as part of the information it provides, a probabilistic evaluation can yield results that show trends and details that remain hidden in a deterministic approach. The opposite is also true: deterministic analysis in general can show trends difficult to detect from a probabilistic approach. At the current stage of

knowledge on rock mass decay, the broad lines that are detectable by probabilistic analysis need to be considered first before individual parameters can be isolated and their influence can be deduced in a deterministic way.

Weathering intensity and the rates of change thereof may be estimated from geological materials (possibly used as construction materials), in-situ observations, mass-balances for catchment areas, or from laboratory tests, which often give ambiguous results when regarded quantitatively. From a stability point of view, weathering intensity classification should ideally not just describe the fraction of a mass affected by weathering, but that fraction in relation to the mass actually determining stability. In discontinuity controlled stability this implies that the weathering depth in relation to the discontinuity roughness is a more important indicator of the intensity of weathering than the amount of the total material which is weathered. The latter however is a common denominator of weathering intensity in classification systems, such as the British Standard BS5930.

As a part of the SSPC classification system that has been used to gather the data used in this research, the parameter *WE* (Hack, 1998) represents the weathering intensity of the rock mass that is actually determining slope stability. Generally, the intensity of weathering will change in depth, with a weathering front penetrating into the rock mass underlying a slope. Therefore, it is expected that the weathering degree gradually decreases with depth. Hence the question of which *WE* to assign to the rock mass does not only depend on the intensity of weathering itself, but also on what penetration depth of a particular weathering degree is of engineering significance with respect to slope stability.

Any definition of the weathering intensity rate should describe the ratio of the change in the state of weathering and (a function of) the time required for that change. Ideally, it would be possible to quantify this change dynamically in time – this is to say that the change, and the rate of change, can be defined at any moment. In the real world of slopes, this would mean

that the state of weathering of a particular unit in a particular slope would have to be described during a number of years, and the change from each observation to the next divided by the elapsed time (or a function of it) would give this "dynamic" weathering intensity rate. However, most often no time series of weathering observations in one unit and in one slope would be available; most data will consist of single and independent observations. In that case, the apparent rate, quantified by the change in weathering from the initial state divided by a function of the total exposure time, is a useful alternative to the dynamic rate. Based on the results of this research, the following definitions are used for the weathering intensity rates:

Apparent weathering intensity rate:

$$R_{WE}^{app} = \frac{WE_{init} - WE_t}{\log(1+t)}$$

Dynamic weathering intensity rate:

$$R_{WE}^{dyn} = \frac{\Delta WE}{\Delta \log(1+t)} \approx \frac{WE_{t-\Delta t} - WE_t}{\log(1+t) - \log(1+(t-\Delta t))}$$

With the logarithmic time scale used for the equations above, the apparent weathering intensity rate is approximately constant for a particular slope material in an unchanging setting.

Weathering penetration will occur in a slope with a rate that not only depends on the weathering susceptibility of the mass in question, but also the amount of erosion that occurs simultaneously with weathering. As long as the weathering products on the slope surface remain undisturbed by erosion, the weathering front penetrates at a continuously decreasing rate when regarded on a linear time scale. Since this is the result of weathering alone, this is defined as the *reference weathering penetration rate*. If the weathered cover is partially or completely being eroded, this will lead to an equilibrium between weathering and erosion, or tend towards a prevailing of one of these processes. In that case, the penetration rate of a weathering

front is for any given penetration depth smaller than in a situation without erosion, defined as the *slope weathering penetration rate*.

Following primary relaxation after excavation, the decay of a rock mass is a process seeking equilibrium between weathering and erosion whilst under the influence of on-going stress and strain redistribution in the form of secondary relaxation. The extent to which such equilibrium is actually reached determines the outcome of the decay process and the effects that the decay has on the geotechnical properties of the resulting rock mass, and thus, ultimately, the slope stability. Three main situations can be distinguished:

- Imbalance favouring erosion (i.e. weathering-delimited).
- Equilibrium between weathering and erosion.
- Imbalance favouring weathering (i.e. erosion-delimited).

An overview of the possible decay situations was given in Table 5a/b (page 98), repeated below. Two more definitions are of importance in this respect. In the situation that erosion occurs at a slower penetration rate than weathering, the degree of weathering as observed in the slope surface and the weathering penetration depth will increase (situation D1 and D2). Since part of the weathering penetration is simultaneously being eroded, the apparent weathering intensity rate is not as high as possible in situation E1 and E2 (see below). The resulting apparent weathering intensity rate is termed the *apparent slope weathering intensity rate*.

In situations E1 and E2 the weathering penetration rate is the highest possible since no erosion affects the material being weathered. The apparent and dynamic weathering intensity rates are therefore defined as the *apparent* and *dynamic reference weathering intensity rates*, respectively.

Table 5a - Potential decay situations. See also Figure 18 - Figure 20, paragraph 2.7, for a graphical representation.

Balance	Processes	Situation at time of excavation	Decay situation
Imbalance favouring erosion	Only erosion, no weathering	No old weathering mantle or weathering zone from previous stage present	A1
		Old weathering mantle or weathering zone from previous stage present	A2
	Some weathering, but erosion penetrates faster than weathering	No old weathering mantle or weathering zone from previous stage present	B1
		Old weathering mantle or weathering zone from previous stage present	B2
Equilibrium of weathering and erosion	Erosion and weathering penetrate into the rock mass at equal rates	No old weathering mantle or weathering zone from previous stage present	C1
		Old weathering mantle or weathering zone from previous stage present	C2
Imbalance favouring weathering	Some erosion, but weathering penetrates faster than erosion	No old weathering mantle or weathering zone from previous stage present	D1
		Old weathering mantle or weathering zone from previous stage present	D2
	Only weathering, no erosion	No old weathering mantle or weathering zone from previous stage present	E1
		Old weathering mantle or weathering zone from previous stage present	E2

Table 5b – Effects of potential decay situations. See also Figure 18 - Figure 20, paragraph 2.7, for a graphical representation.

Decay situation	Weathering penetration depth	Weathering intensity on slope surface	Weathering intensity rate	
			Dynamic	Apparent
A1	Zero	Constant	Zero	Zero
A2	Decreases until mantle is eroded, then zero	Decreases until mantle is eroded, then constant	Negative until mantle is eroded, then zero	Negative until mantle is eroded, then tending to zero
B1	Zero	Constant	Zero	Zero
B2	Decreases until mantle is eroded, then zero	Decreases until mantle is eroded, then constant	Negative until mantle is eroded, then zero	Negative until mantle is eroded, then tending to zero
C1	Zero	Constant	Zero	Zero
C2	Constant, larger than zero	Constant (likely)		
D1	Increases	Increases	Positive (dynamic slope intensity rate, see paragraph 2.7)	Positive (apparent slope intensity rate, see paragraph 2.7)
D2	Increases	Increases		
E1	Increases	Increases	Positive and constant (dynamic reference intensity rate, see paragraph 2.7)	Positive and constant (apparent reference intensity rate, see paragraph 2.7)
E2	Increases	Increases		

The relative rates of penetration of each process into the rock mass following excavation of the slope determine the behaviour of the slope with respect to stability and the maximum sustainable slope height and slope angle. The data collected in the Falset research area suggest that in that area, rock mass decay is erosion delimited in the majority of the investigated slopes, with an imbalance favouring weathering (situations D1, D2, E1, and E2).

Even if the classification describes the engineering-wise appropriate weathering degree perfectly, the outcome will be a discontinuous transition from one weathering degree to another at a specific time, rather than a continuous process, since the weathering degree can only be described as one out of a limited number of options. Further uncertainty resulting from personal bias or intrinsic variability reflects itself in a probability distribution with non-zero variance for the weathering data, rather than a single discrete value.

Results of this study indicate that if uncertainty is appreciated as an inevitable part of the data and even as part of the information it provides, a probabilistic evaluation can yield results that show trends and details that remain hidden in a deterministic approach. The opposite is also true: a deterministic approach can show trends difficult to detect from a probabilistic approach. However, at the current stage of knowledge the broad lines as can be found by probabilistic analysis need to be detected first before individual parameters can be isolated and their influence can be found in a deterministic way.

In order to find physical relations and to compare the outcome with available field data a conceptual model has been derived and applied in this thesis. This combines the Bakker – Le Heux erosion model (with rotating slope retreat mechanism) with a weathering penetration model in which the penetration rate is inversely proportional to the thickness of the weathering cover, on the basis of slope retreat measurements in the Gavadà study slope. The resulting set of equations has been solved numerically by time-stepping,

and gives the slope profile as a function of time, as well as the penetration of the weathering front. Depending on erosion and weathering penetration rates, the different possible decay situations are shown to occur at a given point in time for different locations along the slope profile, just as different situations occur for a given location along the slope profile for different exposure times. In this thesis this is demonstrated for a linear decrease of the slope angle with time; the qualitative results are independent of the precise nature of this particular trend.

The most homogeneous slope development will occur with either very small (relative to weathering penetration rates) or zero erosion rates, or with very large erosion rates (again relative to weathering penetration rates). Intermediate combinations of erosion and weathering penetration rates will cause the upper parts of a slope to show imbalance favouring erosion whereas the lower parts of that same slope will show imbalance favouring weathering. It has to be noted though that the lower part of a slope may be covered by scree after some time, which may affect the rate of weathering penetration in that part.

By considering weathering intensity rates, rather than weathering intensity, observations made on slopes with different exposure times can be compared directly. The results of classifications made in the Falset area suggest that similar engineering geological units show maximum apparent weathering intensity rates of a similar magnitude. The Keuper shales and Middle Muschelkalk siltstones have the highest rates, in the order of 0.2-0.3 [1/log(yr)], and the dolomitised limestones of the Keuper and Upper Muschelkalk the smallest, in the order of 0.04-0.07 [1/log(yr)]. The Middle Muschelkalk gypsum shows intermediate weathering intensity rates, up to approximately 0.12 [1/log(yr)], half that of the most susceptible units.

In order to include the possible variation in the underlying parameters *WE*, slope orientation, and exposure time, and to smooth out variations caused by singular observations, a bootstrap analysis has been applied to the available classification data. With this method, statistical properties of the

true data can be assessed with, in many cases, a much greater reliability than would be possible on the basis of the true data alone. The technique that has been applied here shows the influence of slope orientation and excavation damage on the apparent weathering intensity rate.

The trends derived from bootstrapping results indicate that the relation of the weathering intensity rates with the local climate differs for these units. The Keuper shales, with slaking as the dominant weathering process, show highest weathering intensity rates in slope orientations that face the sun and dominant wind during rainfall, and are therefore exposed to the most pronounced wetting and drying cycles. The Middle Muschelkalk gypsum shows highest weathering intensity rates in slopes on the lee-side of hills during rainfall and sheltered from the sun, corresponding to the importance of water retention for the static dissolution process. The Middle Muschelkalk siltstones, in which decay is caused by a combination of these two processes, highest weathering intensity rates are observed for intermediate orientations. In the limestone units of the Upper Muschelkalk and Keuper, that show the smallest weathering intensity rates, the weathering rate increases with an increasing amount of intercalated shales, with an increasing tendency for highest weathering rates in slopes facing dominant wind directions during rainfall. The quantitative reliability of these trends is to some extent limited by an uneven data distribution and considerations regarding subjectivity of observations. A trade-off exists between the detail in observed trends as described above and the reliability of the results, for units with data unevenly distributed over the orientation classes. Therefore one of the aims of further research shall be to gather evenly distributed data sets for validation which is not biased by the presence of one or more preferential orientations in the data set.

In addition to the influence of local climate, damage to the mass underlying the slope caused by the excavation method is shown to affect the weathering susceptibility of that mass. Data gathered in the Bhutanese Himalaya shows a distinct decrease of the average apparent weathering intensity rates with decreasing excavation damage due to blasting.

Appendices

Is it the flag that moves? Is it the wind?
Neither: it is your mind.
- Hui-Neng (6th Ch'an Buddhist Patriarch of China)

A Geology of Falset research area

"We learn geology the morning after the earthquake." – Ralph Waldo Emerson.

A.1 General

The Catalan Coastal Ranges form a system of ridges and depressions parallel to the Catalan coast trending from the southwest to the northeast, in the south-eastern edge of the Ebro Basin (Masana, 1994). (Figure 72). The highest point is approximately 1,700 m above sea level.

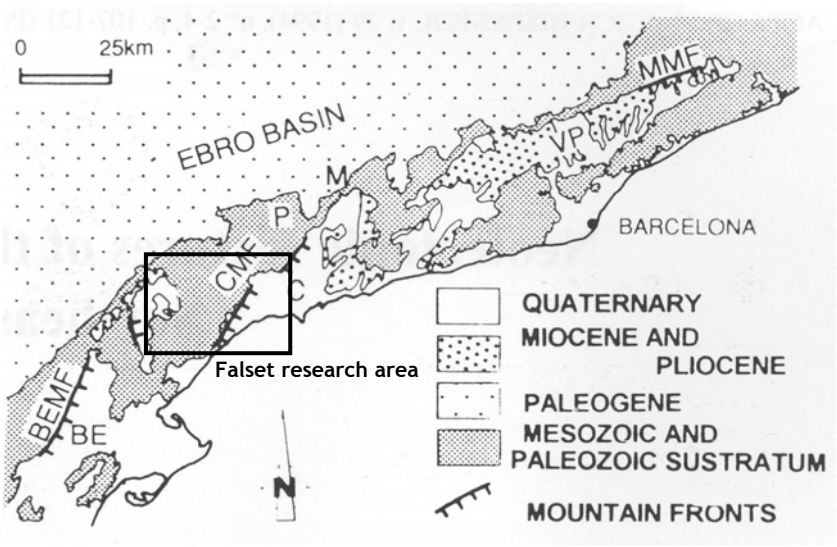

Figure 72 - Mountain fronts in the Catalan Coastal Ranges (from Masana, 1994). MMF: Montseny Mountain Front, CMF: El Camp Mountain Front, BEMF: Baix Ebre Mountain Front, BE: Baix Ebre basin, C: El Camp basin, VP: Vallès-Penedès basin, P: Prades range, M: Miramar range.

The stratigraphy of the research area consists of a sedimentary sequence of Devonian through to Quaternary age. Several igneous rocks occur, intruded into Carboniferous and Lower Muschelkalk formations as granodiorite bodies and aplitic dykes. The majority of the intrusions are from Carboniferous to Permian age and possibly associated with the Hercynian orogeny; minor intrusive phases occurred during the Alpine orogeny. The data used in this study was collected in the Triassic sediments of the Middle Muschelkalk, Upper Muschelkalk and Keuper, which correspond to the Germanic facies (Krömmelbein 1976). These Germanic facies types of the formations deposited in the Triassic, from the Buntsandstein up to the Keuper, have received a good deal of attention in the literature (e.g. Lopez-Gomez et al., 1993; Morad et al., 1995; Vecsei, 1998; Vescsei and Mandau, 2002).

This Triassic sequence is characterized by massive or very thick bedded sandstones with some conglomerate beds at the base (Buntsandstein), followed by thick bedded limestones and dolomites (Lower Muschelkalk), partly deformed sandy clayey siltstone with gypsum (Middle Muschelkalk), limestones and dolomites with marly intercalations (Upper Muschelkalk), and a series of shales and siltstones, in the lower part interbedded with limestones and dolomites (Keuper). On top of the Keuper, as the youngest formation in the Triassic, undifferentiated dolomites occur.

A.2 Studied formations

The stratigraphy, tectonical development, structural geology and formations distinguished in the area are described in geological maps by the IGME. A brief description of the formations investigated for this research is given below.

A.2.1 Middle Muschelkalk

In the Catalan coastal mountain range, of which the research area around Falset is part, the Middle Muschelkalk includes sandstone, mudstone, anhydrite and minor carbonate layers, deposited during a regressive period on the edge of a relatively flat continent in a fluvial or evaporitic lagoon

regime. In the north-eastern part of the basin, interbedded sandstones and mudstones formed by terminal alluvial fan deposits are dominant. In the south-western part of the basin, in and around the Falset research area, the Middle Muschelkalk is characterized by interbedded evaporites and mudstones that have been deposited in sabhka and mudflat environments (Morad et al., 1995).

In the Falset area the amount of evaporitic gypsum varies considerably throughout the formation. In locations where high amounts are present, small quarries have been exploited (most notably in the vicinity of Pradell de la Teixeta and Masriudoms). The formation as a whole is generally valley forming and often used for agriculture.

Sediments are classified as mudstones when they contain at least 50% of siliclastic material finer than 63 micrometres (Wetzel and Einsele, 1991) and the Middle Muschelkalk siltstones fall into this category. The siltstones classify as a low to medium plasticity clayey silt according to BS5930 (Hernandez, 2002).

A.2.2 Upper Muschelkalk

The Upper Muschelkalk consists of limestones that are often dolomitized; characteristics, sedimentary environments and the diagenesis processes that have affected this formation in the area are extensively described by López-Gómez et al. (1993). The Upper Muschelkalk shows an increasing thickness from north to south, from 110 to 200 metres. At the top weak intercalations of red clays occur before the transition towards the Keuper.

A.2.3 Keuper

This formation increases in thickness towards the south-southeast, and contains red and greenish shales with intercalated gypsum layers. These gypsum layers can reach considerable thickness, for example near the “Coll del Guix” (“gypsum pass”) near Colldejou. Intercalated dolomites occur as well. The incompetent nature of this formation has caused considerable deformation during the tectonically active stages in the geological past,

where this formation just as the Middle Muschelkalk has acted as detachment plane for the folding. The formation is generally valley forming and often used for agriculture.

A.3 Tectonical development

Several deformation phases occurred during the Carboniferous/Permian. During these phases, slatey cleavage developed in the sedimentary rocks, and intrusive rocks penetrated into the metamorphosed Carboniferous sedimentary formations.

In the early Triassic, the Buntsandstein covered the erosion surface that was left after the Permian. The base of this formation is formed by conglomerates, followed by red sandstones and then shales that may contain some gypsum. The whole Triassic is of a more continental development type than for example in the Alps. On the Buntsandstein, the Lower Muschelkalk was deposited in a transgressive phase with a warm climate, in a slightly deeper marine sedimentary environment. This was followed by a regressive phase, still with a warm climate but now with a more continental and evaporitic environment: the Middle Muschelkalk. Another transgression leads to deposition of the Upper Muschelkalk, with considerably more clay influx than in the Lower Muschelkalk. Some reefs are found as well. Then, again a regression, and more continental influx, led to the deposition of the Keuper.

The next major transgression starts the Jura sequence, which ends with an unconformity. During the Cretaceous, the Albian sandstones are deposited during a regressive phase followed by another transgression, during which limestones and dolomites are deposited.

The Tertiary is linked with upheaval, deformation, erosion, and the deposition of conglomerates. Due to the enormous influx of eroded material, these conglomerates can achieve considerable thickness (e.g. the Montsant ridge). Offshore from Tarragona, some oil deposits were found that date from the Tertiary, and therefore some deep seismic data is available for this

area. The deformations during the Tertiary have resulted in the general trend in the research area of northwest dipping strata. In the Quaternary a variety of colluvial, alluvial and aeolian soils was deposited and partly cemented.

A.4 Seismicity

The seismicity in the Valencia trough is moderate. Epicentres are concentrated in three zones (the Eastern Pyrenees, the Catalan Coastal Ranges and the Betic range), with almost total absence of earthquakes between the last two zones (Masana, 1994).

Seismic events in the research area are infrequent and seldom in historical time, but not unheard of. The last major earthquake in the area itself had a Mercalli intensity of VIII-IX and occurred on the 3rd of October 1845 with its epicentre near Tivissa, reportedly causing landslides and the collapse of buildings in villages in the area (such as Pratdip). In 1927 another major earthquake occurred to the north of Barcelona, with its epicentre near Montseny. These and a number of additional seismic events with smaller intensity have been recorded in the Valles region of Catalunya (Bertran i Duarte and Tarragó i Vidal, 2002). Geological and morphological investigations have revealed a potential for even stronger seismic events with a low repeat frequency (e.g. Masana, 1994). The present-day morphology however does not show immediate signs of earthquake influences other than the ancient fault reported by Masana (1994).

In general, the northern half of the Catalan Coastal Ranges has a higher concentration of epicentres than the southern half. In the north, more seismic events occur but with limited intensity (generally up to magnitude 4), whereas in the south fewer earthquakes occur, but on average with higher intensity (around magnitude 4). Hypocentres have a depth of up to 15 kilometres (Masana, 1994).

B Climate of Falset research area

"Climate is what we expect, weather is what we get." – Mark Twain.

B.1 Temperature

The climate in the Falset research area is characterized by dry, hot summers (with temperatures ranging from 15° to 35°C) and moderate winters (with average daytime temperatures of 10° to 15°C), in which temperatures may occasionally drop below 0°C in the mountains. The average annual temperature in the area varies with the elevation and distance from the coast, but is generally around 15°C with January and February being the coldest and July and August the warmest months.

The mean annual precipitation is given in Figure 73; average monthly precipitations for six villages in the research area are given in Figure 74.

B.2 Precipitation

Rainfall is mainly concentrated in the autumn, especially around the end of September and beginning of October. Rivers and streams in the area are mostly dry from March until October/November. It may also rain for long periods during the winter, and even up to March/April although this is not typical. Snowfall in winter is rare, but not unknown in the villages at higher altitudes, such as Colldejou.

The mean annual precipitation is given in Figure 75; average monthly precipitations for six villages in the research area are given in Figure 76.

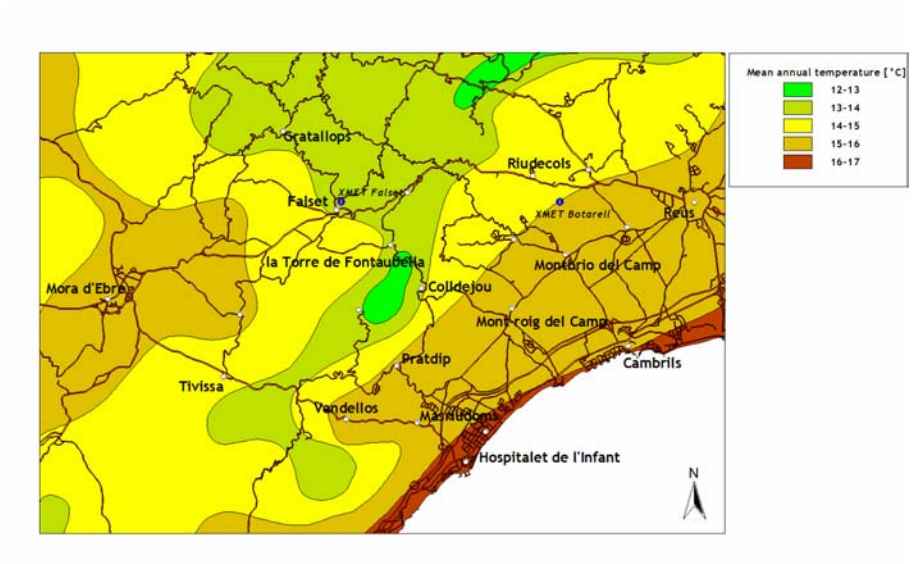

Figure 73 - Mean annual temperature in the Falset research area (temperature data updated 23/12/1996, from http://mediambient.gencat.net/; data digitised from *Atles climàtic de Catalunya*, 1st edition, ICC, Barcelona, 1996).

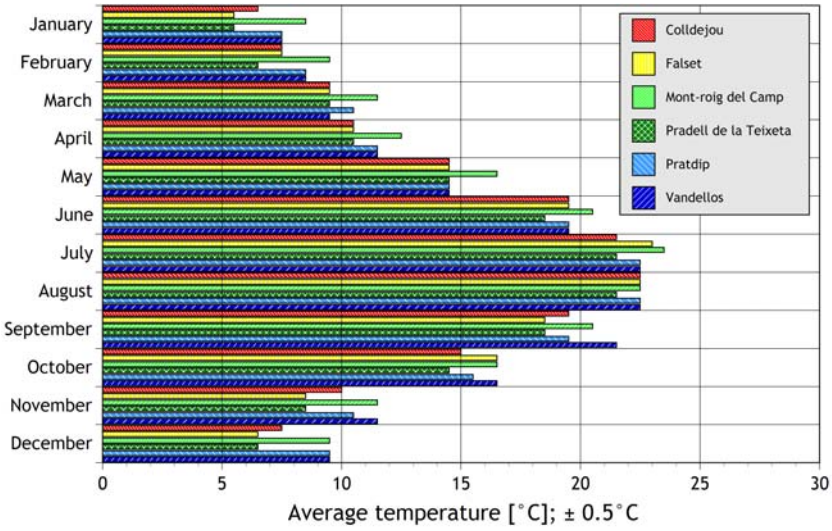

Figure 74 - Average temparatures per month for six villages in the Falset research area (temperature data updated 23/12/1996, from http://mediambient.gencat.net/; underlying data digitised from *Atles climàtic de Catalunya*, 1st edition, ICC, Barcelona, 1996).

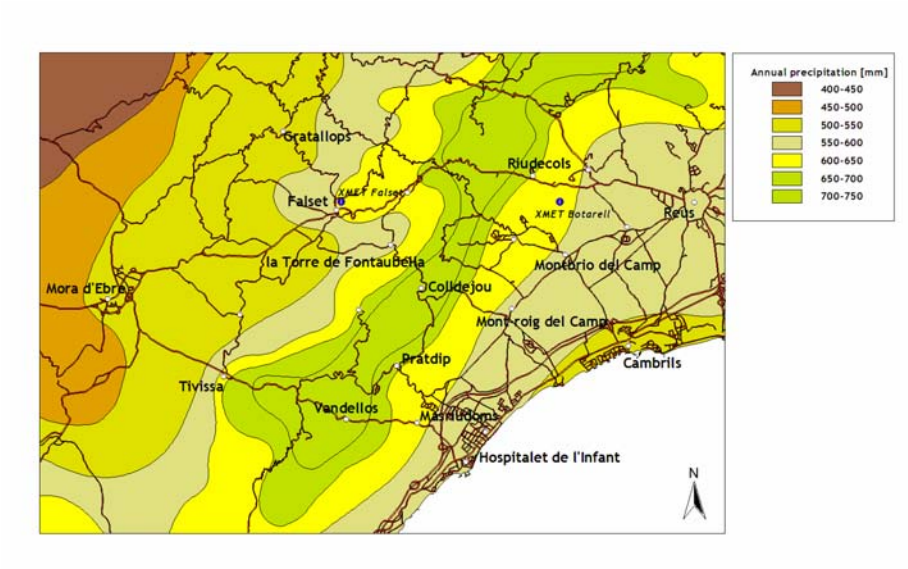

Figure 75 - Mean annual precipitation in the Falset research area (precipitation data updated 16/12/1996, from http://mediambient.gencat.net/; data digitised from *Atles climàtic de Catalunya*, 1st edition, ICC, Barcelona, 1996).

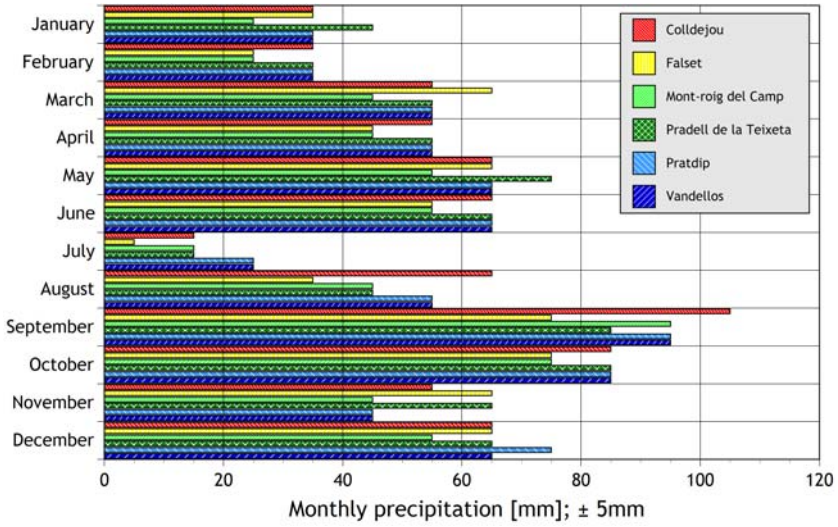

Figure 76 - Average monthly precipitation for six villages in the Falset research area (precipitation data updated 16/12/1996, from http://mediambient.gencat.net/; underlying data digitised from *Atles climàtic de Catalunya*, 1st edition, ICC, Barcelona, 1996).

B.3 Wind direction and velocity

Very detailed climate data has become available in recent years through the XMET network[40]. XMET stands for a network of automated meteorological stations distributed over Catalunya. All stations deliver their data to the central server of the Servei Meteorològic in Barcelona. In 2003, a total of 58 stations was active of which 54 had their data available in real-time through internet. The parameters measured are:

- Wind velocity and direction at 10m above ground level;
- Solar radiation at 2.0m above ground level;
- Precipitation, temperature and relative humidity at 1.5m above ground level;
- Air pressure.

The data is available as averages for every half-hour interval. Two XMET stations are located in the Falset research area: one near the town of Falset itself, the other near Botarell, on either side of the El Camp mountain front. Their precise locations are given in Figure 73 and Figure 75.

With the available data for the year 2003 an analysis was made of the prevailing wind direction during rainfall events, as well as the wind velocity during those events. Figure 77 gives the distribution of wind directions for four precipitation classes[41]. Although the overall prevailing wind direction

[40] *XMET data can be accessed through the internet:*
http://www.gencat.net/servmet/marcs/marcos_observacio/marcs_dades.htm

[41] *After Selby (1993):*

Precipitation intensity	Precipitation [mm/hr]
Drizzle	0.25 - 1.02
Light rain	1.02 - 3.81
Moderate rain	3.81 - 15.24
Heavy rain	15.24 - 40.64
Very heavy rain	40.64 - 101.60
Torrential rain	>101.60

through the year is from the northwest, this changes to the southeast when rainfall increases. As Figure 78 shows, the average wind velocity for the winds from the southeast increases with increasing precipitation rate.

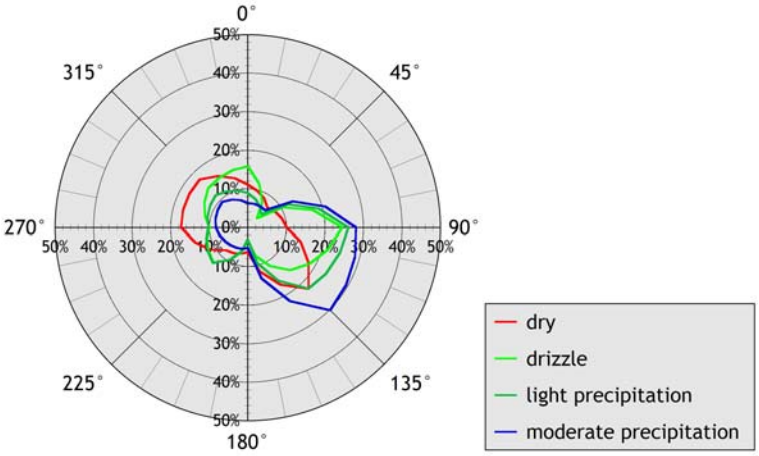

a.

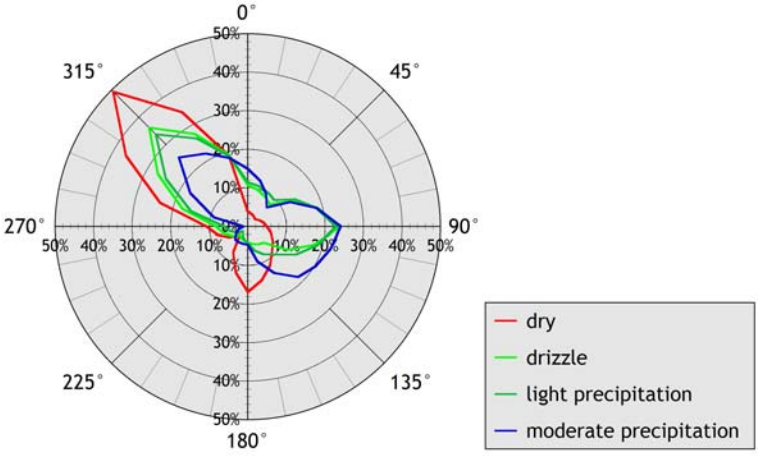

b.

Figure 77 – Wind directions as fraction of all data for four precipitation intensity classes; data for the Falset (a) and Botarell (b) XMET stations, 2003.

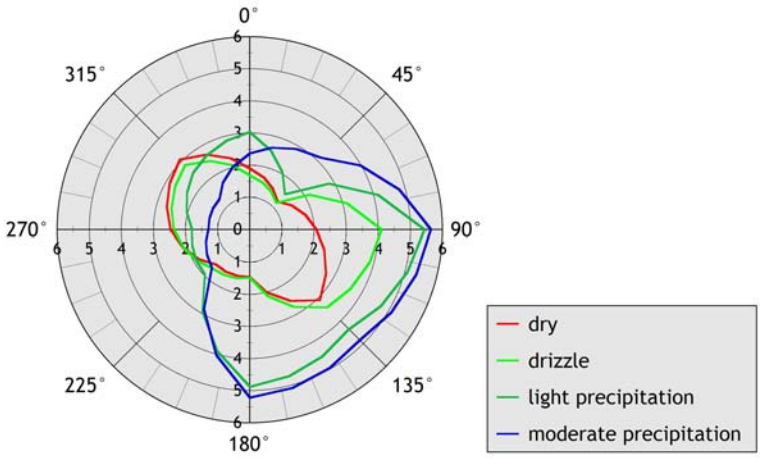

a.

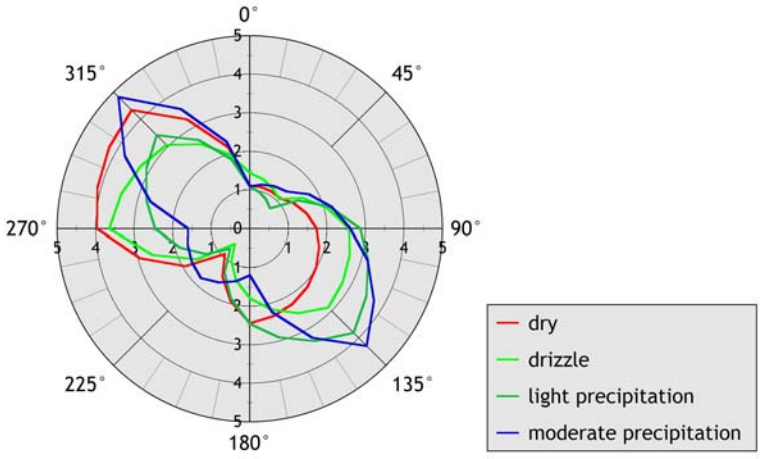

b.

Figure 78 – Average wind velocities for three precipitation classes; data for the Falset (a) and Botarell (b) XMET stations, 2003.

C Weathering processes

"I have always looked upon decay as being just as wonderful and rich an expression of life as growth." – Henry Miller.

C.1 General

The weathering processes that affect slopes in the way as described in this thesis occur near the earth's surface, under surface conditions. In particular chemical processes that occur at considerable depth, e.g. in deep water bearing faults under high pressure, may be different. Several mechanical processes that are described in this appendix only occur at or near the surface, where cyclic behaviour is often dominant.

C.2 Mechanical weathering processes

Mechanical weathering is often the most perceptive decay process in rock masses. A definition of the term should be wide enough to include all processes in which breakdown of the material is brought about by natural mechanical processes[42]. In many cases mechanical weathering is related to periodical changes in the conditions to which a material is exposed, with cyclic loading as a result; however, also static loads caused by mechanical weathering processes may be high enough to fracture intact rock (Table 15).

[42] *This does for example also include root action, a process sometimes described under the header "biological weathering". Weathering by biological means however also acts on a material by mechanical and/or chemical processes. Therefore, biological weathering is not treated as a separate phenomenon here.*

Table 15 - Pressures typically generated by some mechanical weathering processes (after Fookes et al., 1988).

Mechanical weathering process	Resulting pressure [MPa]
Freezing (max. at -20°C)	200
Hydration of salts	100
Crystallization of salts	2-20
Clay expansion	2

Cyclic processes involved in mechanical weathering are:

- **Wetting and drying / slaking**

  Due to wetting and drying cycles, rock material may swell and shrink repeatedly because of a varying quantity of water present in the material, or varying quantities of water bonded to or incorporated in minerals. The associated volume changes will lead to weakening of the material by the repeated tensile and compressive stresses. This will ultimately result in the material falling apart, commonly known as *slaking*. Weak rocks such as marls and clays, especially when some amount of swelling clay is present (Kühnel, 2002), are most vulnerable to this process. Dissolved salts such as sodium sulphate may also worsen the effects of wetting and drying.

- **Insolation weathering**

  Differential rates and amounts of thermal expansion and contraction in rock and soil forming materials will cause tensile stresses within the mass. Thus, diurnal temperature changes will for example lead to cyclic tensile stresses and ultimately fracturing. Causes for this may be:

  - The low thermal conductivity of rock materials in general will lead to an inhomogeneous temperature distribution in the material and therefore differential stresses. Examples of this are higher expansion at the surface than in the interior, or variable expansion because of differential exposure of different parts of the rock mass or slope to the sun. Different colours of rock minerals may play a role in this, with dark-coloured minerals absorbing more energy than light-reflecting light-coloured minerals;

  - Differential thermal conductivity within the rock mass, due to the presence of different material (e.g. lithologies) within one rock mass exposed in a slope. Composition, porosity etc. of the different materials all play a role.
  - Differential thermal conductivity within the rock material itself, because of structural and mineralogical variability. Therefore cracking may occur along mineral boundaries.
  - The presence of trapped water, or saturated pores with very low permeability, will lead to stresses resulting from differential thermal expansion and contraction of the rock material and the water during temperature changes. The volume increase for water and rock can differ by a factor of 10 for temperature changes of around 30°C and because of this theoretically pressures in the order of 18 MPa can be generated (Winkler, 1994).

- **Freeze and thaw**

  When liquid water freezes into ice, a volume increase occurs of up to 9%. Therefore freezing of water in pores, fractures, discontinuities or other openings in a rock material or mass causes tensile stresses that may well be high enough to fracture intact rock (refer to Table 15). Of course this is most relevant in temperate and arctic climates, but during glaciation periods in the geological past this may have affected rock masses that are in more moderate climates today. As in wetting and drying and insolation weathering, the most detrimental effect comes from cyclic freezing and thawing, with repeated loading.

Static loads leading to mechanical weathering and breakdown of the rock may result from:

- **Crystallization**

  A process similar to freezing of water is the crystallization of salts, although this is usually not a cyclic process. The volume increase during crystallization of salts may amount up to 5%. This leads to smaller stresses than the volume increase in the case of freezing

water (Table 15), but those are still high enough to cause fracturing of intact rock or opening of existing fractures or discontinuities.

- **Abrasion**
  When two rock surfaces are in contact during translational movement, those surfaces will wear by grinding. This may occur on a large scale along discontinuities if a rock mass is deformed as a whole, or on a small scale during erosional transport.
- **Tectonic stress release / spalling**
  Rocks that are exposed at the Earth's surface today were generally formed under high pressures at large depths. During their migration to the surface following tectonic uplift and erosion of overlying materials, the confining stresses have been decreased. This unloading leads to stress-strain redistribution through the rock mass and associated volume changes. This causes fracturing of the rock along planes that are generally parallel to the local topography, and perpendicular to the direction of greatest stress reduction. The fracture spacing usually decreases towards the surface. Spalling is a term also used in this context, and describes the fractures resulting from bending stresses in unloaded layers of rock.
  Often a decrease in bedding spacing towards the top of current day-topography is attributed to this phenomenon, but it should be noted that it may well occur due to other reasons than unloading alone. Figure 79 shows as an example an outcrop of the Lower Muschelkalk limestones in the Falset area, close to the town of Torre de Fontaubella, with the almost complete stratigraphical sequence of this formation. The upper part of the Lower Muschelkalk represents a shallowing-upward sequence (López-Gómez et al., 1993) that has led to a closer bedding spacing; in combination with unloading following uplift of the limestones this is expressed today as seen in Figure 79. The closer bedding spacing seen in this outcrop, close to surface, might on first glance be attributed to stress release but in fact it is the expression of a property of the rock mass which was already present before uplift and erosion of overlying strata.

Figure 79 – Lower Muschelkalk outcrop, near Torre de Fontaubella.

Note the similarities between the tectonic stress release in this context, and in stress release because of excavation. In tectonic stress release and spalling, otherwise intact material is fractured along planes of weakness. In stress release following excavation, the decrease of normal stress on existing discontinuities is a governing factor. Obviously the time scales of these two processes are completely different.

- **Biological action**

  The actions of animals and vegetation can cause breaking of particles, opening of existing discontinuities, or fracturing of intact rock; an example of this is damage caused by roots growing into joints. The influences of the biological weathering environment are complex; this is described by several authors, and discussed in paragraph 2.8.

C.3 Chemical weathering

Chemical weathering is a descriptive term for a range of chemical processes that may encompass a phase change (dissolution into ionic components), or a change of mineral type and structure. As for mechanical weathering, chemical weathering of materials exposed at the Earth's surface can be caused by biological conditions (e.g. lichens, vegetation influencing groundwater pH), environmental conditions (e.g. local hydrology, temperatures, rainfall), or a combination of both; in some cases it might be hard to determine where "biology" ends and "environment" begins.

An extensive description of chemical weathering processes can be found in the literature on this subject (e.g. Ollier, 1975 and Bland and Rolls, 1998) and a schematical representation of some processes and products is given in Figure 80. Below typical weathering types are described:

- **Dissolution**
  During dissolution, ions are released after a reaction of minerals with water. Generally, dissolution is enhanced by low pH values, and mainly affects carbonates and evaporites, such as gypsum: $CaSO_4 \cdot 2\ H_2O \rightarrow Ca^{2+} + SO_4^{2-} + 2H_2O$
- **Oxidation / reduction**
  Oxidation implies the loss of electrons from elements, and results in oxides, or hydroxides if water is present. As an example, the oxidation reaction to form hematite from pyroxene is: $4FeSiO_3 + O_2 \rightarrow 2Fe_2O_3 + 4SiO_4$
  Reduction is the reversal of oxidation: the addition of electrons to elements.
- **Hydrolysis**
  During hydrolysis acids react with silicate minerals, releasing silica and metal cations. An example is the change of orthoclase into kaolinite:
  $2KALSi_3O_8 + 2H^+ + 9H_2O \rightarrow H_4AL_2Si_2O_9 + 4H_4SiO_4 + 2K^+$

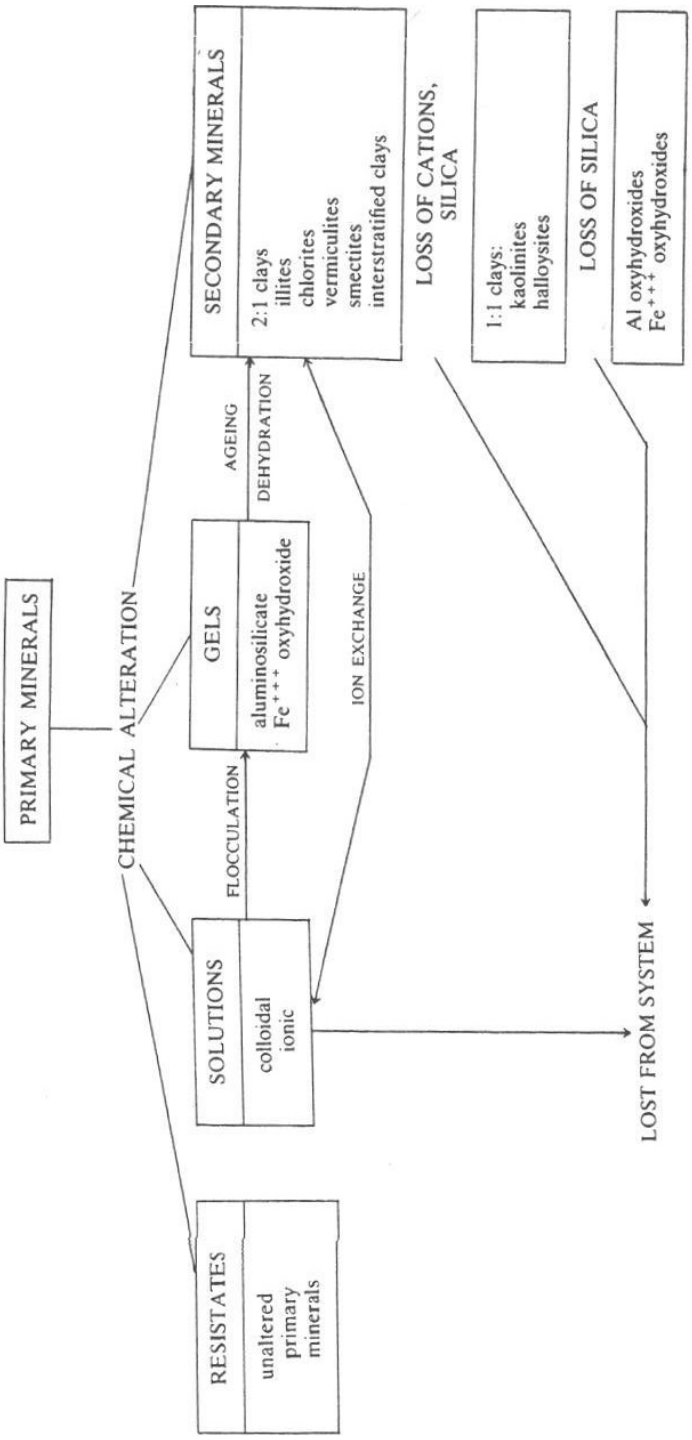

Figure 80 - Processes and products of chemical alteration of aggregates in unbound pavement construction (Mellon, 1985; reproduced from Smith and Collis, 1993).

- **Hydration / dehydration**
  Hydration involves the addition of water molecules to molecules, usually ferric oxides; an example is the reaction of hematite and water to form goethite:
  $Fe_2O_3 + H_2O \rightarrow 2FeOOH$
  Dehydration is commonly used to describe the loss of water from molecules, usually evaporitic minerals. An example is dehydration of gypsum, resulting in water and anhydrite:
  $CaSO_4 \cdot 2\ H_2O \rightarrow CaSO_4 + 2\ H_2O$
- **Ion exchange**
  In this process, cations present in a solution in contact with clay minerals are exchanged with cations present in the clay lattices. This leads to a change in the type of clay mineral and the material properties. An example is the exchange of sodium by calcium in montmorillonite clay, greatly reducing the plasticity and swelling capacity:
  Na-montmorillonite + $Ca^{2+} \rightarrow$ Ca-montmorillonite + Na^{+}
- **Chelation**
  Chelation occurs in silicate minerals, and describes the bonding of metal ions to ring-structured organics; it is therefore related to biological activity.

D Erosion processes

"Constant dropping wears away stones." – Benjamin Franklin.

D.1 Wet erosion

In the presence of water, erosion may occur because of *impact* (rainsplash) or *flow* (sheet wash, rill and gully erosion). Commonly erosion by flow directly follows that by impact but they are not invariably linked; flow erosion can occur without rainfall if water flows over the slope surface from other sources than rain, and in steep slopes particles loosened by the impact of rain may be transported by falling (gravity) rather than by transport in flow (e.g. Fornis et al., 2005). Wet erosion is mainly restricted to unconsolidated soils and very weak rocks.

Rainsplash is related to the kinetic energy of the impacting water droplets, which is the product of their impact speed and weight (Table 16). The impact speed is a combination of wind speed and fall velocity, which is strongly affected by aerodynamic resistance. The wind speed has a twofold influence on the kinetic energy: although it will increase the impact speed, turbulence will cause a reduction of the diameter of large droplets down to 3-5 mm (Roose, 1996). Furthermore, wind will cause the falling raindrops to deviate from the vertical, which enables them to affect otherwise sheltered parts of a slope.

The kinetic energy of impacting raindrops is dissipated in several ways:

a) **Compression of the surface** (in unconsolidated soils), following rapidly after moistening of the surface;

b) **Crushing and shear stresses**, leading to separation of aggregated particles into smaller aggregates or elementary particles (e.g. individual grains);
c) **Displacement of particles**: projection of particles in a crown formation on flat soil and displacement in all directions but most effectively downhill on slopes. These particles may be elementary, or aggregates or clods;
d) **Noise** of the impact of the drops on resistant material.
e) **Heat**, warming up the water, soil and air.

Table 16 - Raindrop velocity and kinetic energy (after Selby, 1993)

Rainfall type	Median droplet diameter [mm]	Fall velocity [m/s]	Intensity [mm/hr]	Kinetic energy [J/mm^2 per mm of rain]
Fog	0.01	0.0	0.05	0.52
Mist	0.10	0.2	0.13	4.14
Drizzle	0.96	4.1	0.25	6.61
Light rain	1.24	4.8	1.02	11.95
Moderate rain	1.60	5.7	3.81	16.94
Heavy rain	2.05	6.7	15.24	22.17
Very heavy rain	2.40	7.3	40.64	25.92
Torrential rain - 1	2.85	7.9	101.60	29.42
Torrential rain - 2	4.00	8.9	101.60	29.42
Torrential rain - 3	6.00	9.3	101.60	29.42

Particles displaced by rainsplash are transported over a short initial distance as a result of the kinetic energy transferred to them by the impact of raindrops. After this, they may be deposited, carried off as sediment in water flow, or fall down a slope under the influence of gravity. Although research has shown that splash erosion requires rainfall of a high intensity (>25mm/hr) to have a significant effect on its own, it is likely that rain of lower intensity does also adversely affect the surface of slopes in unconsolidated soils and very weak rocks by enhancing weathering (notably slaking), decreasing strength parameters (such as cohesion and internal friction in the case of undrained deformation), increasing pore pressures, seepage, and developing a relatively impermeable crust on the slope surface which enhances future runoff (Roose, 1996).

Sheet runoff only starts if rainfall exceeds infiltration. With gentle slope angles of up to 10°, water flow will be of relatively small velocity because of the roughness of the slope surface. Flow velocities in this range can carry off fine sediment loosened by rainsplash. If runoff attains higher velocities than an approximate threshold of 25cm/s, the flow might not only transport loosened particles, but also erode the slope surface in the form of rills or gullies. In such channels, the flow will be localized along flow lines rather than distributed as a sheet over the whole slope surface. This leads to a subsequent increase in velocity, to further erosion, and the formation of rills or, with progressing erosion and higher flow velocities, gullies. This erosion mechanism along distinct lines of flow is termed linear erosion and is capable of not only transporting clay and silts, but also sand, gravel, pebbles and (in more extreme cases with high flow velocities) boulders.

Different levels of linear erosion are distinguished based on the dimensions of the flow channels formed, as depicted in Table 17.

Table 17 - Different types of linear erosion (after Roose, 1996).

Linear erosion type	Dimensions of flow channel
Groove erosion	Up to 10 cm deep
Rill erosion	Over 10 cm deep, but narrow
Gullying sheet erosion	10 to 20 cm deep, up to several m wide
Gully erosion	Over 50 cm deep

E Weathering and erosion models in literature

"Everything has been thought of before, but the problem is to think of it again." – Johann Wolfgang Von Goethe.

E.1 Weathering intensity and rates of change

Time functions for weathering intensity are commonly empirical and based on experimental results. Often such functions are taken as power functions with the general form (e.g. Colman, 1981; White and Brantley, 2003):

$$I = Kt^n \tag{17}$$

With:

I	parameter for weathering intensity	[-]
K	coefficient	[-]
n	exponent, generally <1	[-]
t	time	[year]

A graphically similar general empirical relation to describe the intensity of weathering as a function of time as suggested by Colman (1981) is:

$$\frac{P}{P_0} = c_1 + c_2 \log\left(1 + t\right) \tag{18}$$

With:

P	property (glass amount) at some time t	[-]
P_0	initial property (glass amount)	[-]
c_1	coefficient	[-]
c_2	coefficient	[-]

An example of such a relation is given in Figure 81, for the decay of volcanic ash in time, with solid lines representing a logarithmic relationship and dotted lines an exponential relationship (Colman, 1981).

In equation (18) the ratio P/P_0 represents a decrease of some property with respect to the fresh state, and c_1 and c_2 are constants. In terms of weathering, P/P_0 is exactly what WE stands for, and equation (18) can be converted to:

$$WE(t) = WE_{init} - R_{WE}^{app} \log(1+t) \Rightarrow R_{WE}^{app} = \frac{WE_{init} - WE(t)}{\log(1+t)} \tag{19}$$

With:

$R^{app}{}_{WE}$	apparent weathering intensity rate	[1/log (year)]
WE_{init}	*WE* at time of excavation	[-]
WE(t)	*WE* after time *t*	[-]
t	exposure time of slope	[years]

This particular rate is used in this thesis for the *apparent weathering intensity rate* (see paragraph 2.5).

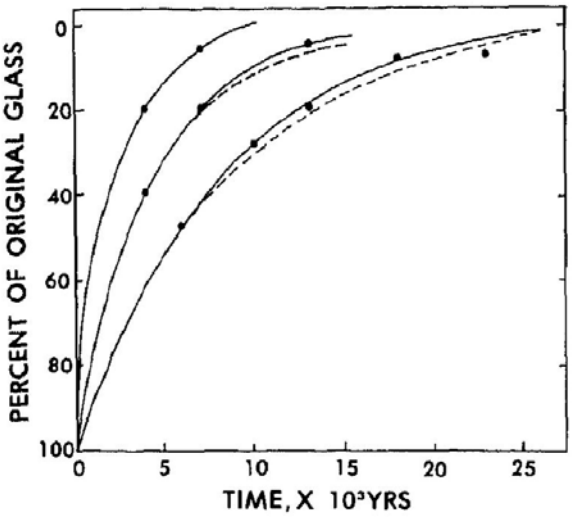

Figure 81 - Weathering of glass in volcanic ashes, at three locations in New Guinea. Original data collected by Ruxton (1968). Solid lines represent a *log(1+t)* type relationship suggested by Colman, dotted lines original relations suggested by Ruxton. Figure from Colman (1981).

E.2 Weathering penetration

One of the few examples of a quantified relation for weathering depth and time is given by Heimsath et al. (1997), who determined soil production rates (calculated from in-situ produced cosmogenic ^{10}Be and ^{26}Al in bedrock samples) as a function of the thickness of the weathered soil cover for

hillslopes in northern California[43]. The resulting data is shown in Figure 82 together with the curve fit such as reported by Heimsath et al. (1997).

The soil production rate, which is equal to the increase of the thickness of the weathered zone in time, is shown to decrease with an increasing thickness of that same weathered zone. The derived empirical relation is presented in Figure 82 and has the following general shape and defines the weathering depth as a function of time:

$$\frac{dD_w}{dt} = \mathrm{e}^{A+BD_w} \tag{20}$$

With:

D_w	Depth (thickness) of weathered layer
t	time
A, B	constants

Figure 82 - Data and empirical relation by Heimsath defining soil production rate as a function of weathered soil thickness (after Heimsath et al., 1997).

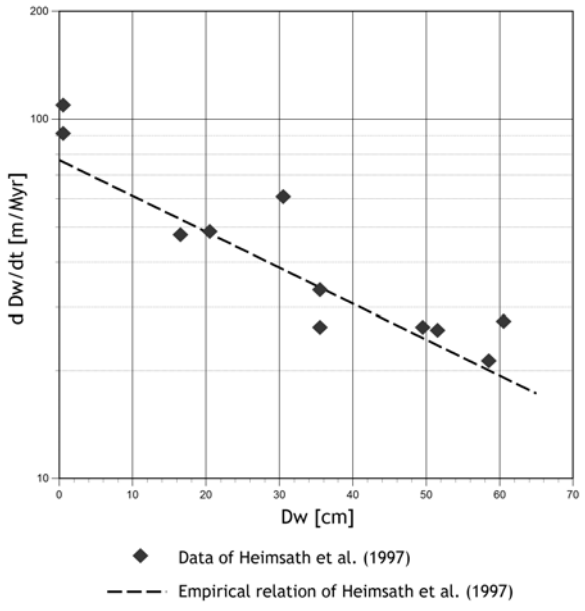

[43] *With soil defined as distinct colluvial material, lacking relict rock structure and derived from underlying bedrock.*

E.3 Erosion and slope retreat

The Bakker – Le Heux model for idealised linear slope retreat assumes the following points as summarized by Hutchinson (1998):

- An initially straight slope of uniform material of inclination β exists, steep enough for debris removal not to be transport-limited;
- The slope has horizontal ground at its toe and past its crest;
- No standing water is present at the foot;
- In a given time, weathering causes retreat of all parts of the exposed free face due to the erosion of fine debris, which can be approximated theoretically by infinitesimal increments; larger falls, where volumes larger than the individual particles are affected, are not considered;
- The resulting debris accumulates contemporaneously at the cliff foot as a rectilinear scree with a constant slope angle α ($\alpha<\beta$);
- Beneath the accumulating scree, the rock surface is protected from further erosion, while the rock face above continues to retreat;
- Thus, with time, a convex-outward shape is produced in the surface of the intact rock beneath the scree. Ultimately the original cliff develops into a straight slope inclined with the scree angle α, to which, in its last formed upper part, the underlying convex rock core is tangential.

The definition of the model is given in Figure 83. The ultimate profile of the convex rock core underneath the scree is given by the following expression for c≠½:

$$y = az - (a-b)z\left[\frac{h^2 + (1-2c)z^2}{h^2}\right]^{\frac{c-1}{1-2c}} \qquad (21)$$

With y=0 and z=0 at the foot of the initial slope profile, and:

a $\cot(\alpha)$

b $\cot(\beta)$

c $1-\frac{\text{volume of rock}}{\text{volume of scree}}$

A ratio of the volumes of rock to scree smaller than 1 (c>0) indicates a volume increase of material during erosion and sedimentation. A value larger than 1 (c<0) indicates removal of sediment at the foot of the slope. The model is not defined for c=0.5.

Equation (21) gives y, the depth from the original slope's toe, as a function of the height z, for the ultimate profile of the rock core. For intermediate slope profiles the angle of the slope's upper part, which is not yet covered by scree, defines the coordinates of the point on the slope surface where the surface of the scree wedge intercepts the intact rock core.

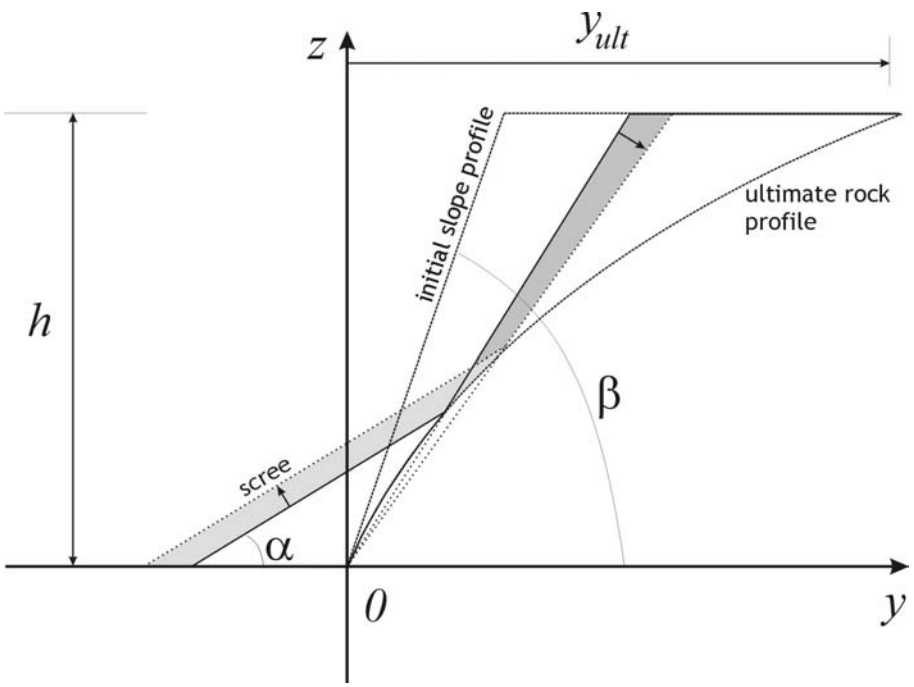

Figure 83 - Definition sketch of the Bakker - Le Heux model for slope retreat (after Hutchinson, 1998).

E.4 Generalized erosion and weathering penetration models

The total volumes of weathered and eroded material on a slope may be modelled as functions of time, and this has been done during this research to study the development of equilibrium between weathering penetration and erosion (Nieuwenhuis, 2004).

In Figure 84 three different volumes are defined:

- V_1 Volume of material weathered after excavation and still present on slope
- V_2 Volume of material weathered after excavation and eroded from slope
- V_0 Total volume of material weathered after excavation = V_1+V_2

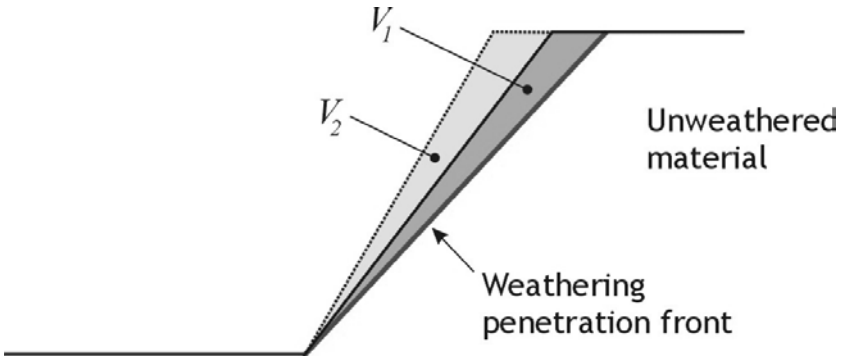

Figure 84 - Definition sketch for generalised weathering and erosion model.

Colman (1981) gives possible differential equations that describe this situation. The basic model proposed by Colman (1981) rests on the following assumptions:

- Erosion can affect both weathered and unweathered material.
- The weathering penetration rate is inversely proportional to the volume V_1 of the cover of weathered material on the slope face.

The basic volume balance for the situation defined above is:

$$\frac{dV}{dt} = \phi_{V,in} - \phi_{V,out} + P_V \tag{22}$$

With:

ϕ_V	Volume flux of weathered material in or out of the model
P_V	Production of weathered material in the model

When the model encompasses the slope as a whole, the influx of weathered material is zero. The outflux results from erosion, and the production term represents the weathering of material in the slope. A prospective analysis of this situation has been described by Colman (1981), for the case that the erosion rate is independent from the cover of weathered material. Under the assumptions that the weathering intensity rate in terms of volume is inversely proportional to the volume V_1 of the cover of weathered material on the slope face, the following equations can be defined on any time t:

$$V_0 = V_1 + V_2 \tag{23}$$

$$\frac{dV_0}{dt} = \frac{a^*}{V_1} \tag{24}$$

$$\frac{dV_2}{dt} = b^* \tag{25}$$

In these, a^* and b^* are constant coefficients. Equation (24) describes the penetration[44] of the weathering front[45] into the slope as an increase in the total volume of weathered material, V_0; equation (25) describes the erosion of weathered material from the slope as an increase of the volume of weathered material eroded from the slope, V_2.

The volume of eroded material V_2 can be determined directly as:

$$V_2 = b^* t \tag{26}$$

[44] *Colman (1981) considered any inverse of possible positive functions. In this example, the description is limited to the inverse linear relation of equation (24).*

[45] *The boundary between weathered material and unweathered material, separating V_1 from the unweathered rock mass.*

For the weathered volume still present on the slope, the assumption of constant erosion rate b^* gives:

$$\left.\begin{aligned} \frac{dV_1}{dt} &= \phi_{V_1,in} - \phi_{V_1,out} + P_{V_1} \\ \phi_{V_1,out} &= \frac{dV_2}{dt} \\ P_{V_1} &= \frac{dV_0}{dt} \end{aligned}\right\} \Rightarrow \frac{dV_1}{dt} = \frac{a^*}{V_1} - b^* \tag{27}$$

Equation (27) can be solved since the resulting differential equation is separable (Boyce and DiPrima, 1986) and gives the following result in terms of $t(V_1)$, using the boundary condition $t=0$: $V_1=0$:

$$t = \frac{a^* \ln a^* - b^* V_1 - a^* \ln\left(-b^* V_1 + a^*\right)}{b^{*2}} \tag{28}$$

This translates to:

$$V_1 = \frac{-b^{*2}t + a^* \ln\left(a^*\right) - a^* \ln\left(\mathrm{W}\left(\frac{-\mathrm{e}^{\frac{-b^{*2}t + a^* \ln\left(a^*\right) - a^*}{a^*}}}{a^*} \right) \right)}{b^*} \tag{29}$$

With:

$W(x)$ Inverse function of xe^x

For this situation, the (ultimate) equilibrium value for V_1 is equal to a^*/b^*.

A more elaborate model has been derived by Nieuwenhuis (2004), based on the boundary condition $t=0$: $V_0=V_1=V_2=0$ and the following, slightly stricter assumptions:

- Erosion only affects weathered material.
- Weathering penetration rate is inversely proportional to the volume V_1 of the cover of weathered material on the slope face.
- Erosion rate is linearly proportional to the volume V_1 of the cover of weathered material on the slope face.

Under the assumptions that the weathering penetration rate in terms of volume is inversely proportional to the volume V_1 of the cover of weathered

material on the slope face, the erosion rate is linearly proportional to the volume V_1 of the cover of weathered material on the slope face, and erosion does not affect unweathered material, the following equations describe the volume balance on any time *t*:

$$V_0 = V_1 + V_2 \tag{30}$$

$$\frac{dV_0}{dt} = \frac{a^{**}}{V_1} \tag{31}$$

$$\frac{dV_2}{dt} = b^{**}V_1 \tag{32}$$

In Equations (31) and (32), a^{**} and b^{**} are constant coefficients. Equation (31) describes the penetration of the weathering front into the slope as an increase in the total volume of weathered material, V_0; equation (32) describes the erosion of weathered material from the slope as an increase of the volume of weathered material eroded from the slope, V_2. The difference in assumptions between this model and the basic model by Colman (1981) is apparent when comparing the equations (25) and (32).

The volume V_1 is the volume of weathered material still present on the slope, and is therefore linked to the weathering degree as would be recognized in the field in an actual slope; the change in V_1 with time thus signifies a weathering penetration rate as would be found based on actual field classifications. If penetration of the weathering front and erosion of weathered material are in equilibrium, V_1 will remain constant while both V_0 and V_2 will change. In such a case, weathering will still act on the slope, but the amount of weathered material present on the slope will not change and based on field observations, a weathering penetration as well as intensity rate will be found equal to 0. If the penetration of the weathering front exceeds the erosion of weathered material, V_1 will increase, whilst if the erosion of weathered material exceeds the penetration of the weathering front, V_1 will decrease[46].

[46] *The latter situation cannot arise under the assumptions made here. The reason for this is that only weathered material can be eroded according to Equation (32).*

A volume balance for V_1 gives:

$$\left.\begin{aligned} \frac{dV_1}{dt} &= \phi_{V_1,in} - \phi_{V_1,out} + P_{V_1} \\ \phi_{V_1,out} &= \frac{dV_2}{dt} \\ P_{V_1} &= \frac{dV_0}{dt} \end{aligned}\right\} \Rightarrow \frac{dV_1}{dt} = \frac{a^{**}}{V_1} - b^{**}V_1 \tag{33}$$

Equation (33) can be solved:

$$\frac{dV_1}{dt} = \frac{a^{**}}{V_1} - b^{**}V_1 \Leftrightarrow V_1\frac{dV_1}{dt} = a^{**} - b^{**}V_1^2 \Leftrightarrow \frac{dV_1^2}{dt} = 2a^{**} - 2b^{**}V_1^2 \tag{34}$$

Substitution of $y = V_1^2$ gives:

$$\frac{dy}{dt} + 2b^{**}y = 2a^{**} \tag{35}$$

The solution to equation (35) is, using the boundary condition *t=0*: $V_1=0$:

$$y = V_1^2 = \frac{a^{**}}{b^{**}}\left(1 - e^{-2b^{**}t}\right) \Rightarrow V_1 = \sqrt{\frac{a^{**}}{b^{**}}\left(1 - e^{-2b^{**}t}\right)} \tag{36}$$

Combining equations (32) and (36) results in:

$$\frac{dV_2}{dt} = b^{**}V_1 = b^{**}\sqrt{\frac{a^{**}}{b^{**}}\left(1 - e^{-2b^{**}t}\right)} \tag{37}$$

Integrating equation (37) using the boundary condition *t=0*: $V_2=0$ gives:

$$V_2 = -\sqrt{\frac{a^{**}}{b^{**}}}\left[\sqrt{1 - e^{-2b^{**}t}} - \operatorname{atanh}\left(\sqrt{1 - e^{-2b^{**}t}}\right)\right] \tag{38}$$

The expression for the total volume of weathered material as a function of time can be found by substituting equations (36) and (38) in equation (30):

$$V_0 = \sqrt{\frac{a^{**}}{b^{**}}}\operatorname{atanh}\left(\sqrt{1 - e^{-2b^{**}t}}\right) \tag{39}$$

The results are summarised below:

Total weathered volume	Volume	$V_0 = \sqrt{\frac{a^{**}}{b^{**}}}\,\mathrm{atanh}\left(\sqrt{1-e^{-2b^{**}t}}\right)$
	Rate	$\frac{dV_0}{dt} = \frac{b^{**}}{\sqrt{\frac{a^{**}}{b^{**}\left(1-e^{-2b^{**}t}\right)}}}$
Weathered material still present on slope	Volume	$V_1 = \sqrt{\frac{a^{**}}{b^{**}}\left(1-e^{-2b^{**}t}\right)}$
	Rate	$\frac{dV_1}{dt} = \frac{b^{**}e^{-2b^{**}t}}{\sqrt{\frac{a^{**}}{b^{**}\left(1-e^{-2b^{**}t}\right)}}}$
Weathered material eroded from slope	Volume	$V_2 = -\sqrt{\frac{a^{**}}{b^{**}}}\left[\sqrt{1-e^{-2b^{**}t}} - \mathrm{atanh}\left(\sqrt{1-e^{-2b^{**}t}}\right)\right]$
	Rate	$\frac{dV_2}{dt} = b^{**}\sqrt{\frac{a^{**}}{b^{**}}\left(1-e^{-2b^{**}t}\right)}$

F Data simulation and bootstrapping

"We demand rigidly defined areas of doubt and uncertainty." – Douglas Adams, *The Hitchhiker's Guide to the Galaxy*.

F.1 Introduction

The data based simulation method for statistical inference described in this chapter is the mathematical equivalent to pulling oneself up by one's bootstrap (Efron and Tibshirani, 1998). Starting from a limited amount of observed data, a larger set of hypothetical but still realistic data is generated. Based on the distribution of this simulated data, statistical properties of the true data can be assessed with, in many cases, a much greater reliability than would be possible on the basis of the true data alone. This reliability of the results largely depends on the validity of the assumptions that are applied in the data simulation, and these should be made with care.

Paragraphs F.2 and F.3 are based on the literature on this subject (Efron and Tibshirani, 1998; Chernick, 1999). The applications to rock and soil mass decay and slope stability are developed during this research.

F.2 Data simulation techniques

F.2.1 Pure Monte Carlo Sampling (MCS), with replacement

In pure Monte Carlo sampling, a series of n random numbers between 0 and 1 is generated. For each of those random numbers, the corresponding parameter value is calculated with the inverse of the cumulative probability function. The procedure is illustrated in Figure 85, for $N = 5$. Out of the five

random numbers p_1, p_2, ..., and p_5, five parameter values x_1, x_2, ..., and x_5 are calculated. These simulated parameter values are consequently unsorted.
In the generation of random numbers, there is no restriction by the numbers that were generated in previous steps, and therefore two or more identical parameter values may be generated (the i^{th} and j^{th} simulations are identical if p_i=p_j).

Schematically, the simulation procedure for N = 5 is:

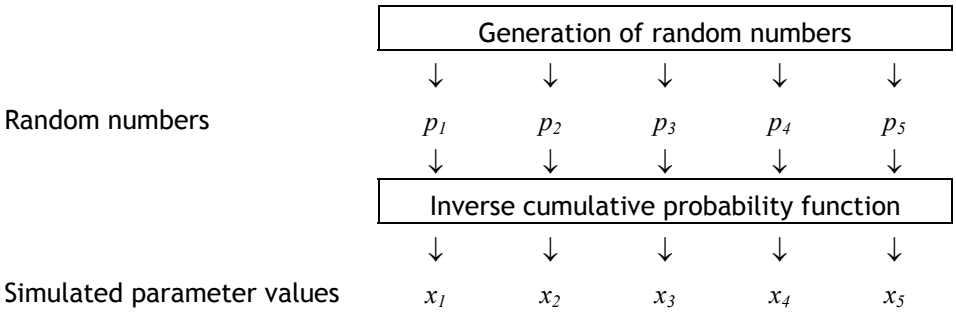

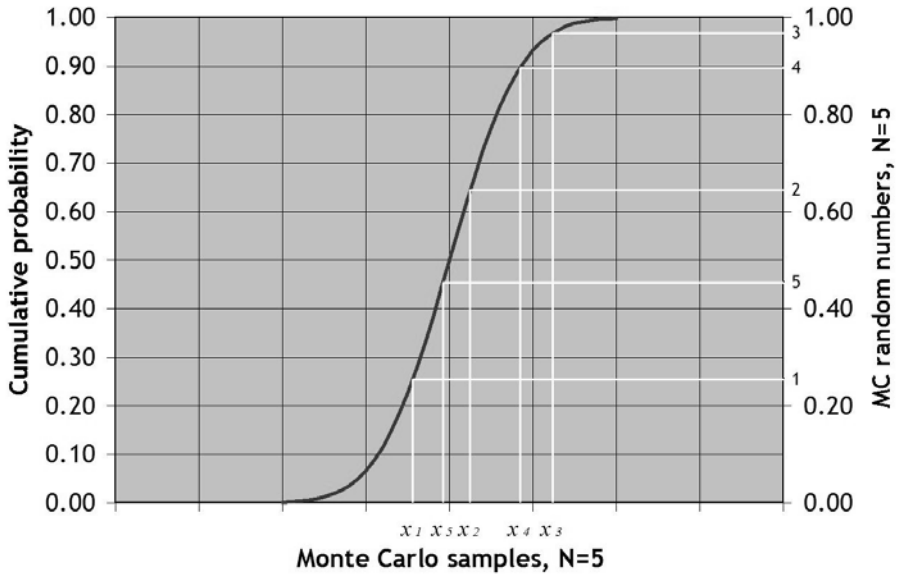

Figure 85 - The principle of Monte Carlo Sampling with replacement; in this example, 5 samples are taken.

F.2.2 Latin Hypercube Sampling (LHS), without replacement

In the stratified Latin Hypercube sampling method, the interval [0;1] is divided into N intervals of equal size $\frac{1}{N}$. The next step is to generate a random number in every interval $\left[\frac{i}{N};\frac{i+1}{N}\right]_{i=0}^{N-1}$ for a random order of i. This procedure gives N simulated parameter values in random order; see Figure 86. In each of the unique Latin Hypercube intervals, only one random number and therefore only one simulated parameter value is generated.

Schematically, the simulation procedure is as follows:

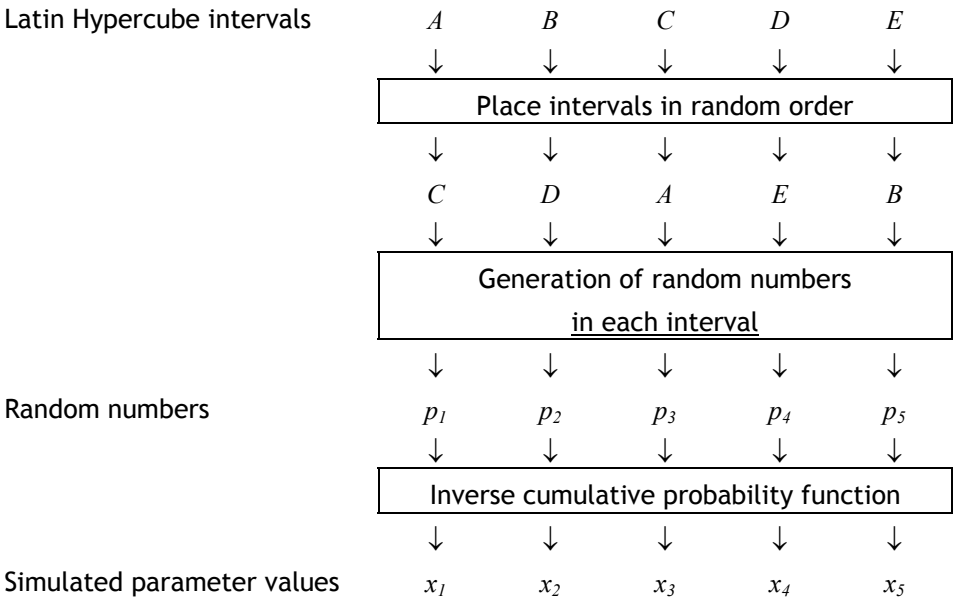

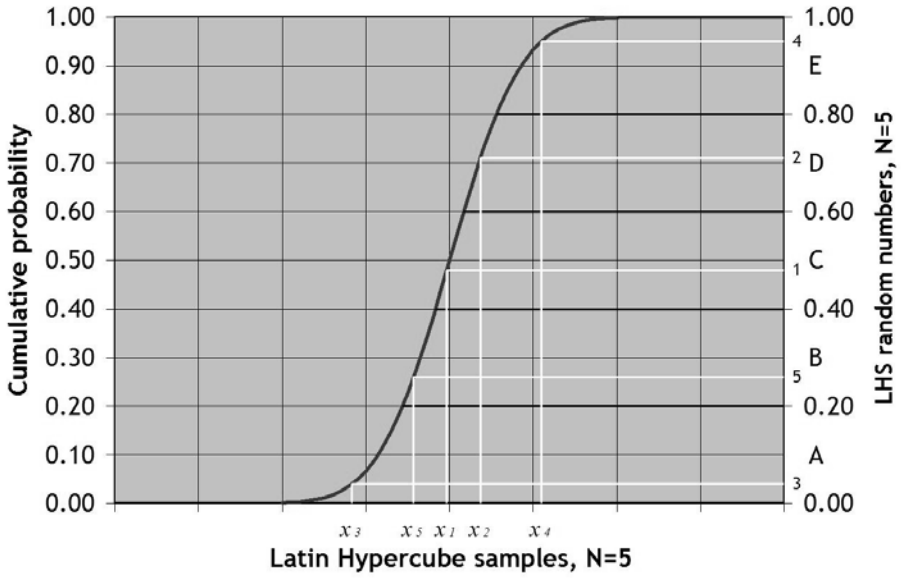

Figure 86 - The principle of Latin Hypercube Sampling without replacement; in this example, 5 samples are taken.

F.3 Bootstrapping[47]

In statistical analysis, the bootstrap generates a large amount of imaginary yet realistic data from a limited set of samples, enabling us to quantify statistical parameters that can only be determined with difficulty, or not at all, from the original samples (Efron and Tibshirani, 1998).

In Figure 87 the general line of bootstrapping is explained. In real life, observations that compose a data set x result from the (unknown) probability distribution(s) P of the stochastic variable(s) that compose x. In a three-sample problem a data "point" x_i is an observation consisting of three variables, in a general form $x_i=(a,b,c)$. $\hat{\theta}$ is a statistical variable derived from the dataset x and thus also depends on the probability model that forms the basis for x.

[47] *The explanation of the bootstrap calculation methods is after Efron and Tibshirani (1998).*

The bootstrap model of reality is in itself rather similar, with the estimation of the probability model the most critical. Based on that estimated probability model $\hat{P}$ a hypothetical or simulated data set x^* is created, consisting of data points x_i^* that each consist of estimates for the composing stochastic variables (e.g. a simulated aspect, exposure time, and weathering degree). As many data points can be simulated as desired, and therefore it is possible to generate a simulated data set $\hat{\theta}^*$ larger the "real" data set $\hat{\theta}$.

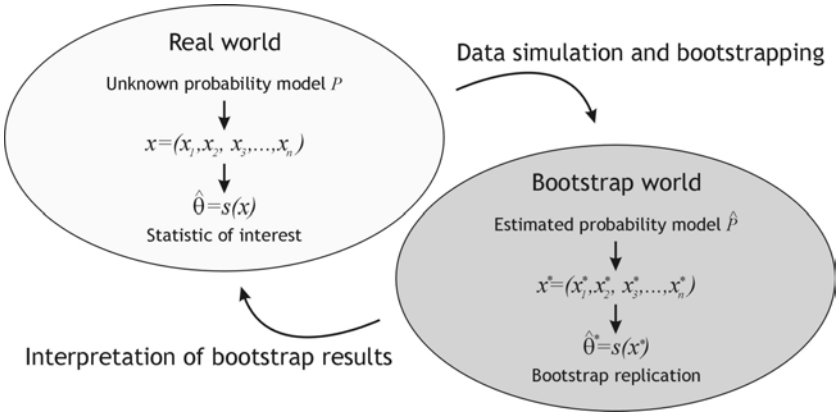

Figure 87 – Schematic diagram of the bootstrap methodology (after Efron and Tibshirani, 1998). Data simulation takes place in the "bootstrap world", to generate a number of hypothetical data sets x^* that are combined into $s(x^*)$.

To apply the bootstrap method to the research subject of rock mass decay in artificial slopes, probability distributions have to be assigned to some or all of the input variables. In this research, three parameters are treated as stochastic variables: the recorded *WE*, exposure time and slope aspect. Various alternative probability distributions can be assigned, such as a normal distribution (quantified with mean and standard deviation), a block distribution (quantified with upper and lower boundaries), and a triangular distribution (quantified with lower, most likely and upper values). The normal distribution and similar types do not have a fixed upper or lower boundary; in theory, any value is possible (albeit with a very small

probability for extremely low or high values), whereas the block and triangular distributions do have a fixed upper and lower limit.

A bootstrap analysis starts with a data simulation process (see section F.2), generating an imaginary data set. From this data set, the set of resulting variables such as the weathering intensity rate is calculated. The bootstrap percentiles such as used in this study are the contours that indicate the fractions of this resulting variable, and are an effective method to determine reliability intervals (e.g. Chernick, 1999). Following the notation by Efron and Tibshirani (1998) and Figure 87, the percentiles are derived from a set of B bootstrap replications that make up $\hat{\theta}^{*}(B)$. This itself is of course derived from B simulated data points x^{*1}, x^{*2}, x^{*3}, …, x^{*B}. If $\hat{\theta}_{B}^{*(\alpha)}$ is the α-percentile ($0 \le \alpha \le 1$), that is, the $\alpha * B^{th}$ value in the ordered vector $\hat{\theta}^{*}(B)$, then $\hat{\theta}_{B}^{*(\alpha)}$ gives the single-sided bootstrap percentile for α, and the interval $\left[\hat{\theta}_{B}^{*(\alpha)}, \hat{\theta}_{B}^{*(1-\alpha)}\right]$ gives the two-sided bootstrap percentiles for $1-2\alpha$. These single- and two-sided percentiles are the bootstrap estimates for the respective single- and two-sided confidence limits (Efron and Tibshirani, 1998).

F.4 Application to rock mass decay data

F.4.1 Input probability distributions: WE

For the bootstrap process that generates a set of simulations for the parameter defined by the degree of weathering, *WE*, a normal distribution is applied in accordance with Hack (1998). The characteristics of the normal distributions for each weathering degree are given in Table 18 and plotted in Figure 88 for the parameter WE_{mass}. This is the average of the reduction parameters for the rock mass cohesion and the rock mass friction angle (see Hack, 1998).

Table 18 - Mean values and standard errors for WE_{mass} (Hack, 1998)

Degree of rock mass weathering (BS5930, 1981)	WE_{mass}	
	Mean value	Standard error
Fresh	1.00	0.00
Slightly weathered	0.95	0.06
Moderately weathered	0.90	0.07
Highly weathered	0.62	0.12
Completely weathered	0.35	0.11

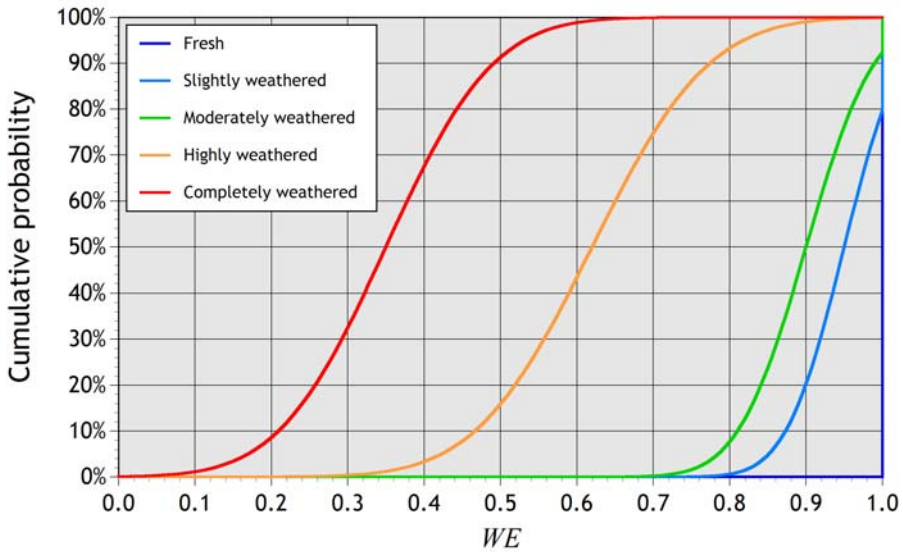

Figure 88 - Normal cumulative probability distributions for the possible degrees of weathering (Hack, 1998); see also Table 18.

F.4.2 Input probability distributions: exposure time

For the exposure time a symmetrical triangular distribution has been defined, limiting the minimum and maximum values to ±10% of the estimated age of a slope. The cumulative probability distribution for these limiting boundaries is given in Figure 89 for a normalized exposure time equal to the true exposure time divided by the estimated exposure time, having a maximum and minimum at 1.10 and 0.90.

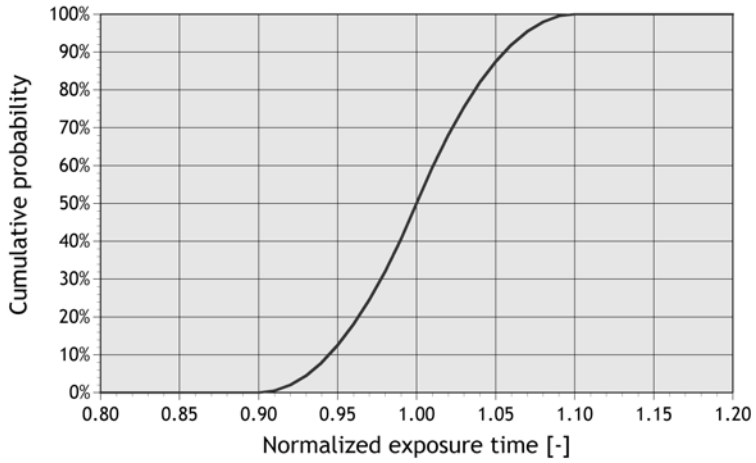

Figure 89 - Triangular cumulative probability distribution for a normalised exposure time; recorded value equals 1, the horizontal axis indicates relative variation of up to ±10%.

F.4.3 Input probability distribution: slope aspect

The probability distribution for the slope aspect is chosen according to Hack (1998) as normal, with a standard error of 5°. This distribution is shown in Figure 90.

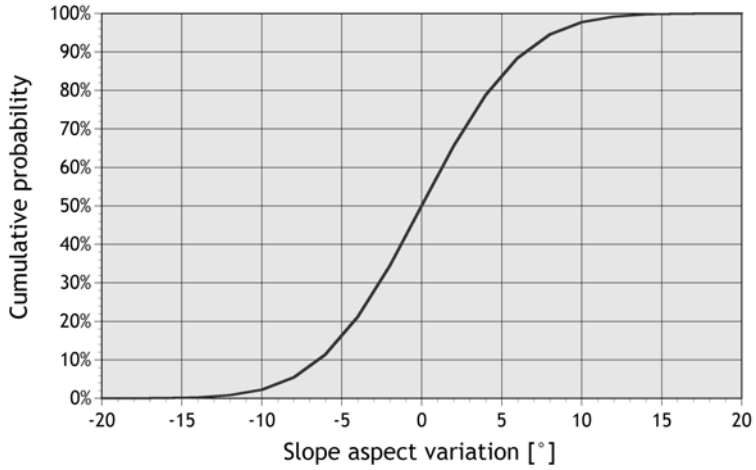

Figure 90 - Normal cumulative probability distribution for the slope aspect; 0° indicates the recorded value. Standard error = 5° (Hack, 1998).

F.4.4 Procedure

In order to determine the bootstrap percentiles for the weathering intensity rate R^{app}_{WE}, the following schematic procedure is used as a flow scheme for the Mathcad 8 Professional script developed for this procedure (Figure 98):

1. The original data is read; for each unit, the data consists of:
    a. The observed degree of weathering after the estimated exposure time
    b. The initial degree of weathering at the time of excavation
    c. The estimated exposure time
    d. The slope aspect

2. For each data point, the following probability intervals are determined:
    a. The standard deviation around the observed degree of weathering (see F.4.1)
    b. The upper and lower limits of the triangular interval around the estimated exposure time (see F.4.2)
    c. The standard deviation around the estimated slope orientation (see F.4.3)

3. For each data point, a random value is taken according to the Monte Carlo or the Latin Hypercube procedures from the following distributions:
    a. The observed degree of weathering after the estimated exposure time
    b. The estimated exposure time
    c. The slope orientation

    This is repeated for the desired number of data simulations (see F.5), giving the bootstrap replications.

4. For all the bootstrap replications, the apparent weathering intensity rate is calculated.

5. The data set of bootstrap replications is subdivided into eight subsets, one per (simulated) slope orientation interval of 45°:
   a. North 337.5° - 22.5°
   b. Northeast 22.5° - 67.5°
   c. East 67.5° - 112.5°
   d. Southeast 112.5° - 157.5°
   e. South 157.5° - 202.5°
   f. Southwest 202.5° - 247.5°
   g. West 247.5° - 292.5°
   h. Northwest 292.5° - 337.5°

6. These eight subsets are each sorted in ascending order based on the weathering intensity rate calculated from the simulated data.

7. For the desired percentile values (e.g. 5%, 10%, 25%, 50%, 75%, 90%, and 95%) the corresponding weathering intensity rates are determined from these sorted subsets for each orientation interval.

8. The end result is a table giving the weathering intensity rate for a specific percentile probability and an orientation interval.

F.5 Convergence of simulation methods

The main practical difference between the Monte Carlo and Latin Hypercube data simulation procedures is the rate of convergence to a stable bootstrap result. The number of simulations required to reach a stable end result is less for the Latin Hypercube because in that procedure simulations are made for the whole range of possible values including the extremes, whereas the Monte Carlo method may need more samples to accurately describe the extremes of the resulting probability distribution (on average, the probability of simulating a particular value is the same).

The question of when to stop data simulation, or in other words with what number of data simulations a satisfactory and robust result is created, has received quite some attention (e.g. Dagum et al., 2000), but the answer

remains a difficult one. A common measure for the conversion of the simulation process is the Standard Error of the Mean (SEM) which has been applied here. To quantify the convergence of the simulations that result in bootstrap percentiles for the apparent weathering intensity rate $R^{app}{}_{WE}$ (see paragraph 5.2), the average simulated weathering intensity rate has been determined for each of the eight slope orientation classes. This has been repeated 50 times for each unit, and for an increasing number of data simulations. Figure 91 to Figure 97 give the standard error (as percentage of the average: the **S**tandard **E**rror of the **M**ean, SEM) of those 50 average rates for each unit and orientation plotted against the number of simulations. Note that the analysis has been carried out for discrete numbers of simulations only. Therefore the lines in the graphs represent the interpolations between these discrete points.

All figures show a faster convergence towards a small SEM for the Latin Hypercube procedure. Differences between the various slope orientations result from the fact that each orientation class contains different amounts of original input data. In general, the SEM is around 1% of the mean or less with 2000 Latin Hypercube simulations and it is this procedure which has been applied for the $R^{app}{}_{WE}$ -simulations.

Figure 98 gives as an example the resulting polar plots of weathering intensity rate percentiles for Keuper shales with different amounts of Latin Hypercube simulations per data point. Although the exact percentiles do change slightly with an increase of the number of simulations, the observed trend is independent from this. With 2000 simulations, there is no significant change in the percentiles anymore and a robust solution is obtained.

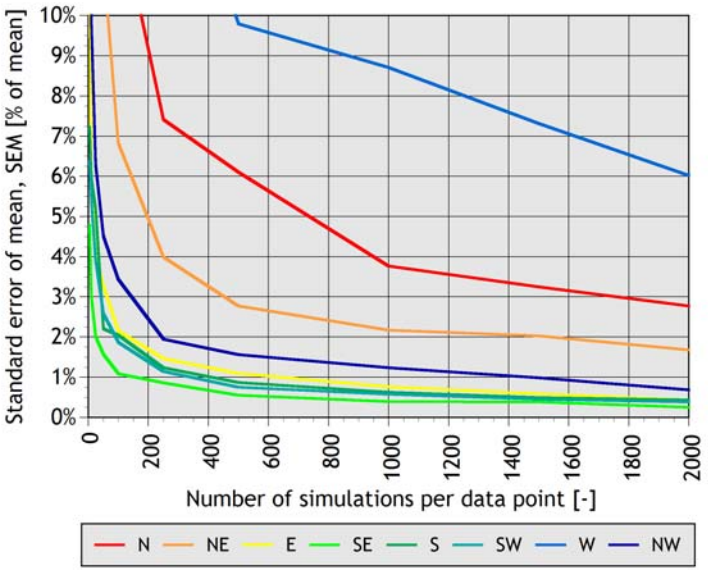

a.

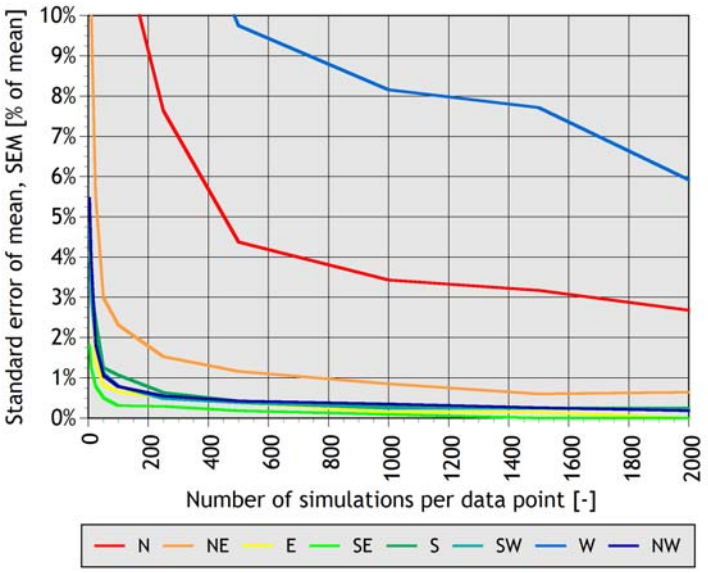

b.

Figure 91 – Convergence of simulation procedure for Keuper shales (a. for Monte Carlo and b. for Latin Hypercube).

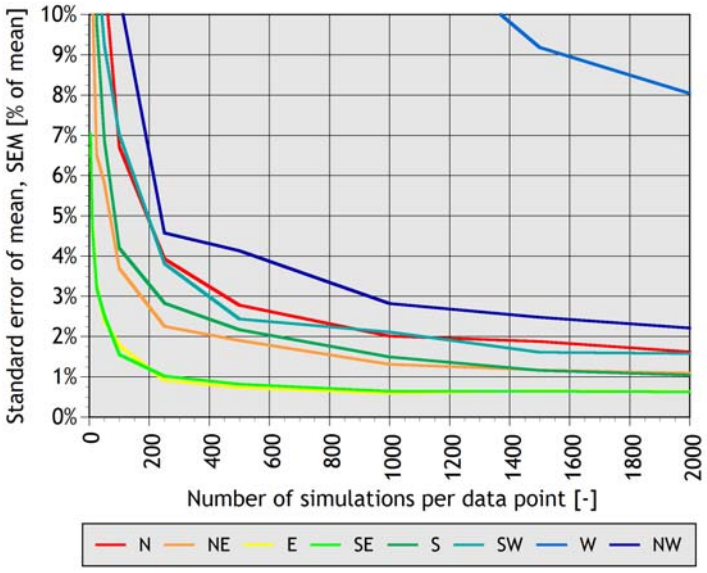

a.

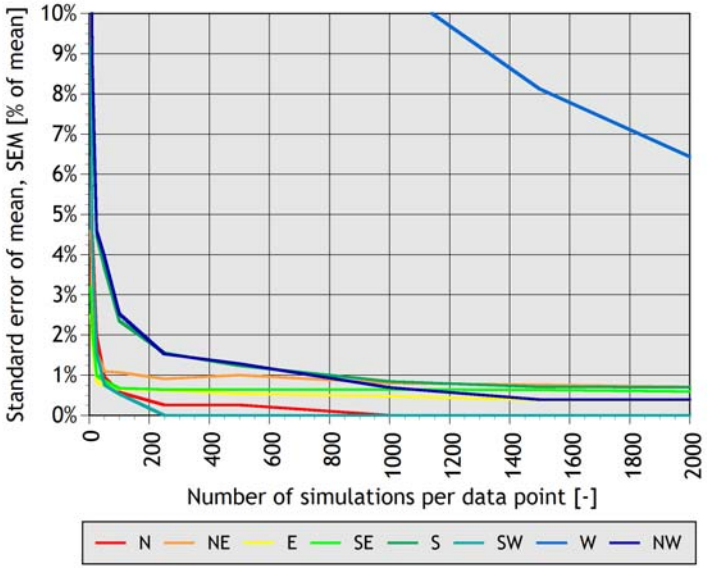

b.

Figure 92 – Convergence of simulation procedure for Keuper limestones (a. for Monte Carlo and b. for Latin Hypercube).

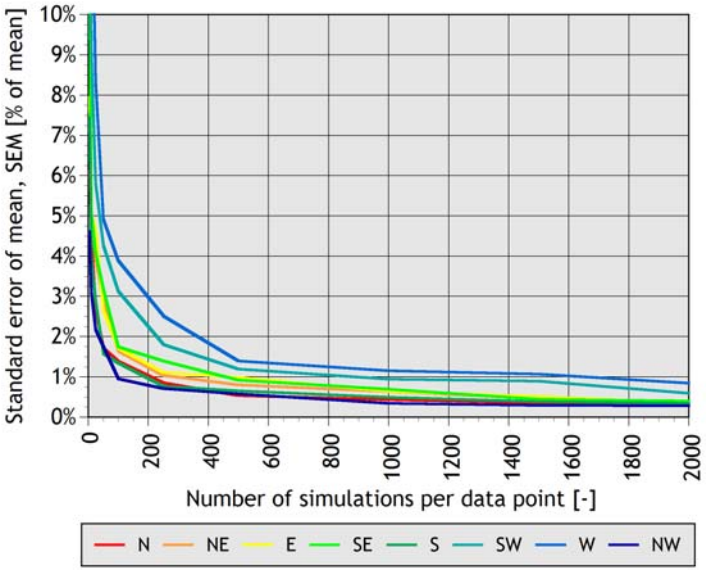

a.

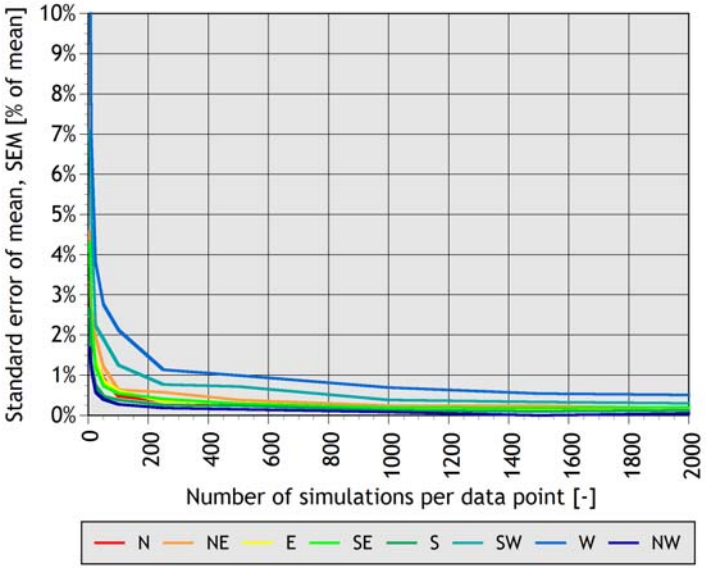

b.

Figure 93 – Convergence of simulation procedure for Middle Muschelkalk siltstones (a. for Monte Carlo and b. for Latin Hypercube).

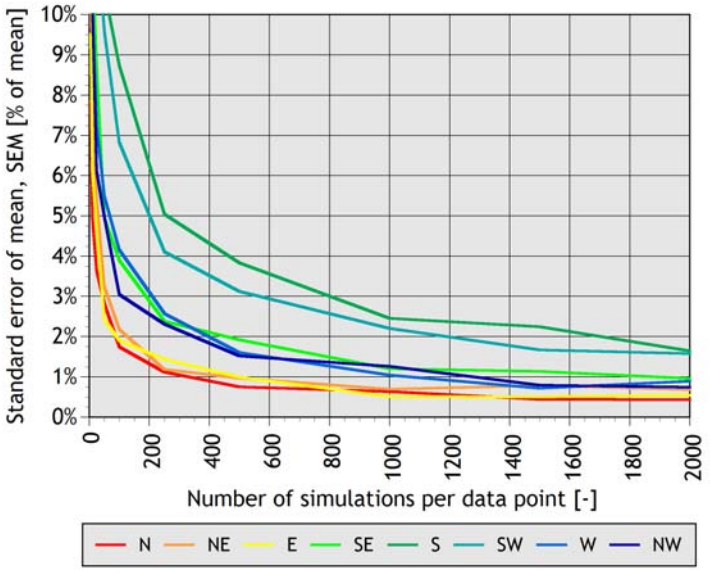

a.

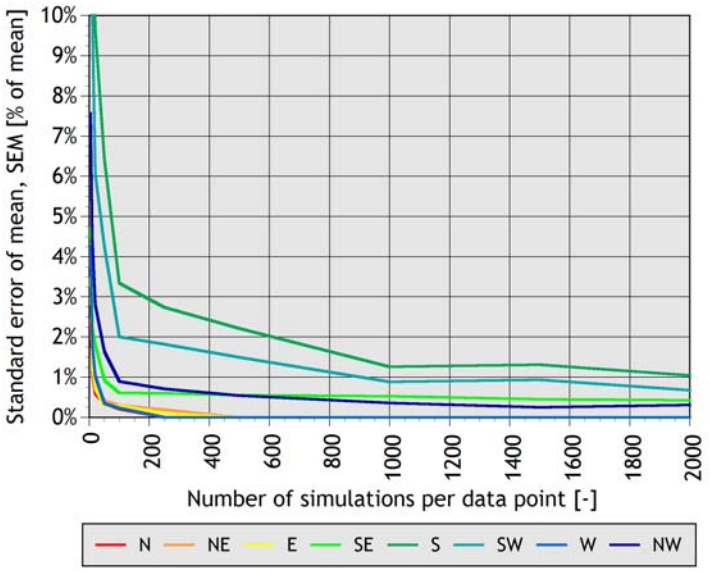

b.

Figure 94 – Convergence of simulation procedure for Middle Muschelkalk gypsum (a. for Monte Carlo and b. for Latin Hypercube).

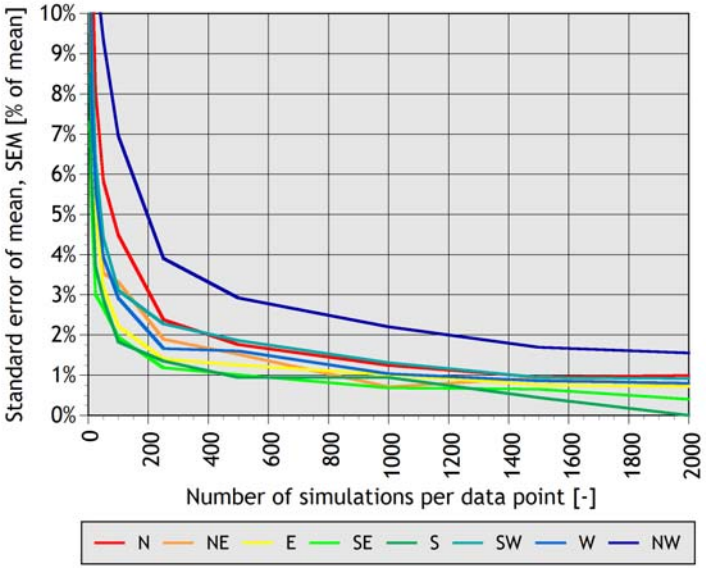

a.

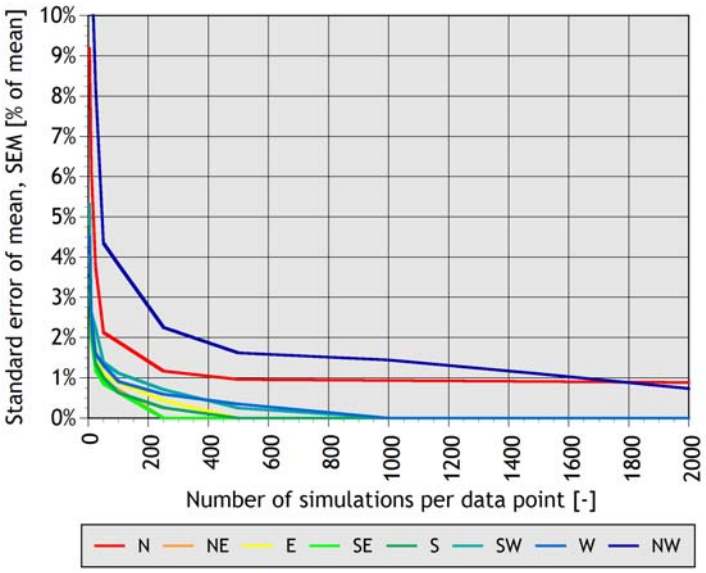

b.

Figure 95 – Convergence of simulation procedure for Upper Muschelkalk with bedding spacing <0.10m (a. for Monte Carlo and b. for Latin Hypercube.

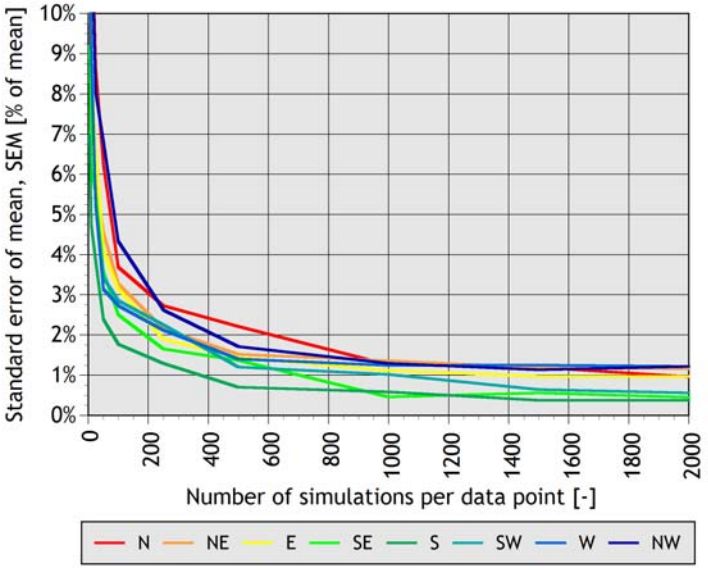

a.

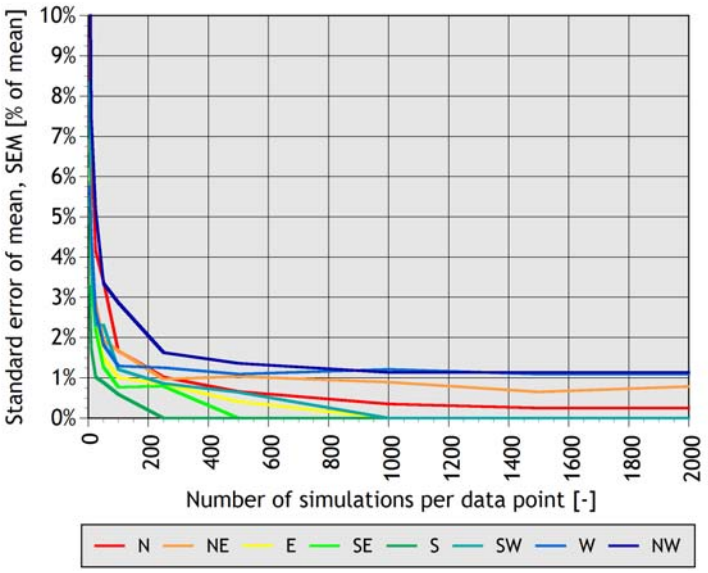

b.

Figure 96 – Convergence of simulation procedure for Upper Muschelkalk with bedding spacing 0.10-0.50m (a. for Monte Carlo and b. for Latin Hypercube).

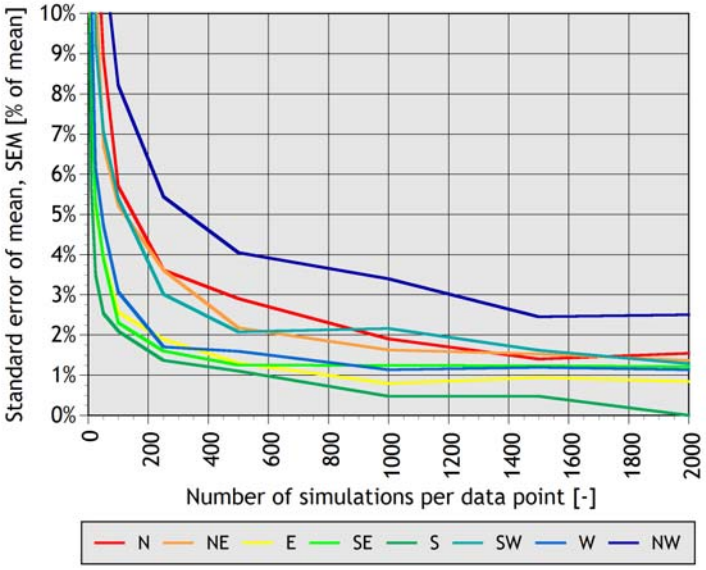

a.

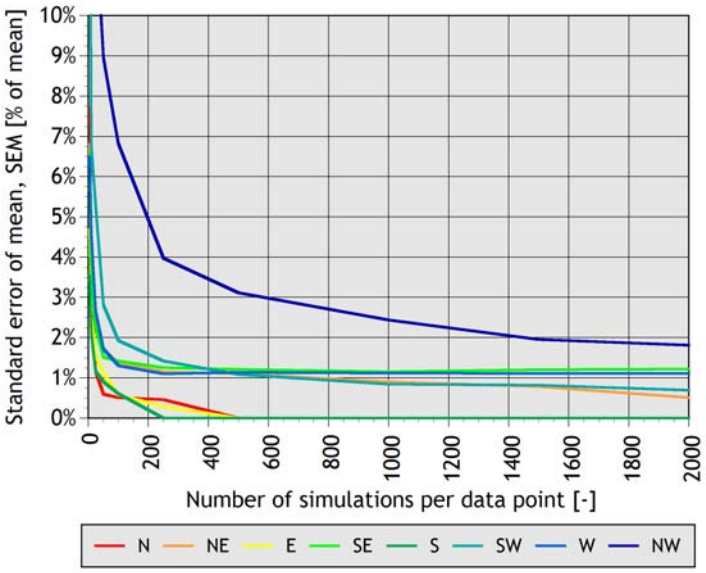

b.

Figure 97 – Convergence of simulation procedure for Upper Muschelkalk with bedding spacing >0.50m (a. for Monte Carlo and b. for Latin Hypercube).

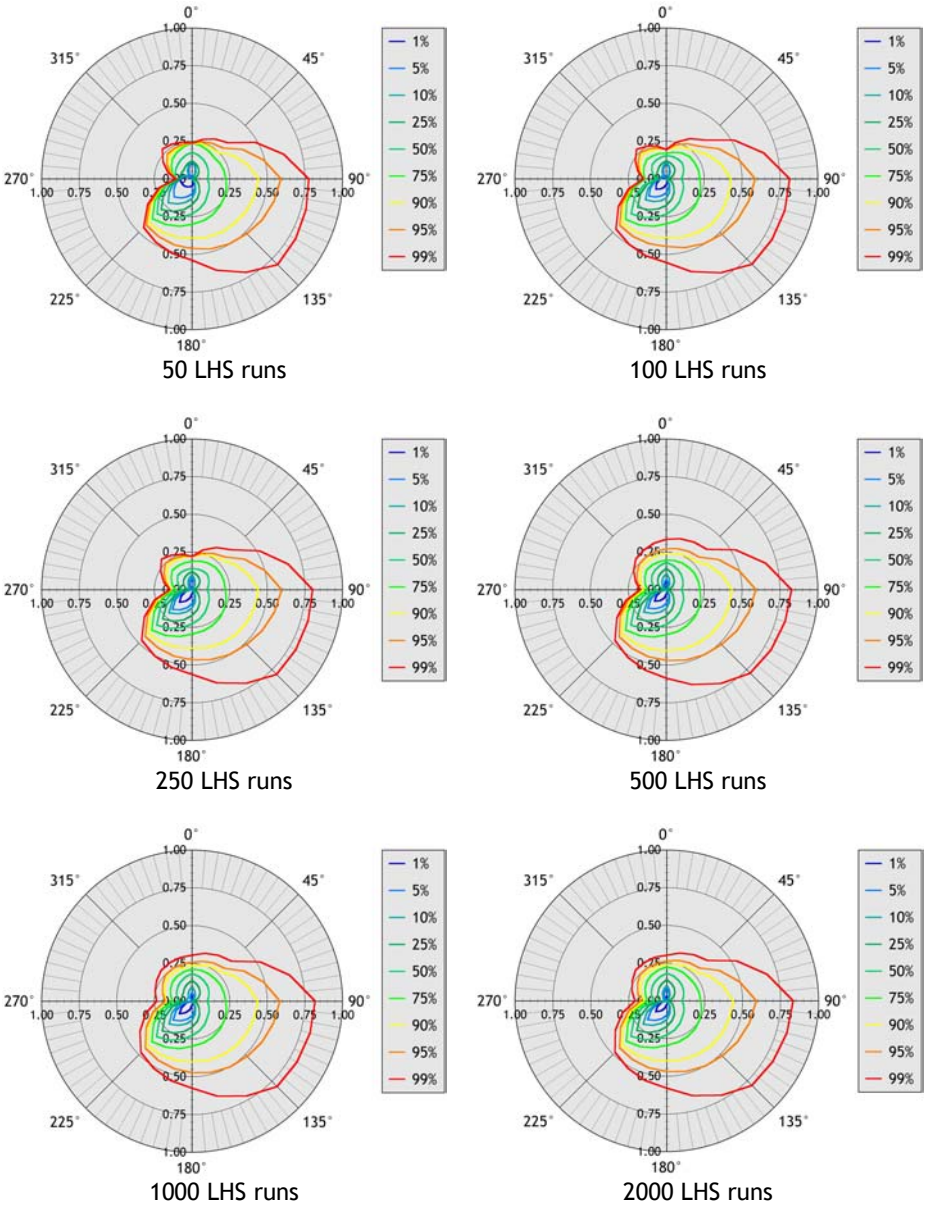

Figure 98 - Example of change in results with an increasing number of Latin Hypercube simulations per data point (results for Keuper shales).

Script 1 - Mathcad 8 Professional script for data simulation (example data set).

First, several input parameters are defined. The parameter lhsruns defines the number of LHS runs - this is the number of simulations per data point:

$lhsruns := 2000$

$lhsstep := \frac{1}{lhsruns}$

Standard deviation of orientation distribution (5° according to Hack, 1998):

$orsdv := 5.0$

Uncertainty in exposure time (plus or minus Tunc %):

$Tunc := 10$

The input data: columns in "D" are slope orientation, orientation code, exposure time, WE, WE initial

$$D := \begin{bmatrix} 0 & 1 & 10 & 0.9 & 1 \\ 45 & 2 & 10 & 0.9 & 1 \\ 90 & 3 & 10 & 0.9 & 1 \\ 135 & 4 & 10 & 0.9 & 1 \\ 180 & 5 & 10 & 0.9 & 1 \\ 225 & 6 & 10 & 0.9 & 1 \\ 270 & 7 & 10 & 0.9 & 1 \\ 315 & 8 & 10 & 0.9 & 1 \end{bmatrix}$$

$datapoints := rows(D)$

In a matrix S, the following data is stored:
1st column slope aspect
2nd column orientation code
3rd column recorded exposure time - Tunc%
4th column recorded exposure time
5th column recorded exposure time + Tunc%
6th column Initial WE (at time of excavation)
7th column recorded WE
8th column standard error of recorded WE (Hack, 1998)

$i := 0 .. (datapoints - 1)$

$$S_{i,0} := D_{i,0} \qquad S_{i,1} := D_{i,1} \qquad S_{i,5} := D_{i,4} \qquad S_{i,6} := D_{i,3}$$

$$S_{i,7} := \begin{cases} 0.0001 & if\ D_{i,3} = 1.00 \\ 0.06 & if\ D_{i,3} = 0.95 \\ 0.07 & if\ D_{i,3} = 0.90 \\ 0.12 & if\ D_{i,3} = 0.62 \\ 0.11 & if\ D_{i,3} = 0.35 \end{cases}$$

$$S_{i,2} := \left(1 - \frac{Tunc}{100}\right) \cdot D_{i,2} \qquad S_{i,3} := D_{i,2} \qquad S_{i,4} := \left(1 + \frac{Tunc}{100}\right) \cdot D_{i,2}$$

The following are three routines that build three matrices "T", "WE" and "OR" with the data simulations for exposure time, WE and slope aspect, respectively. The structure of the routines is similar, but the inverse probability distribution depends on the variable: triangular for "T", normal for "WE" and "OR".
In accordance with the LHS procedure, first a random order of the "lhsruns" segments is determined by sorting a matrix with sequential indices for the segments in the first column and random numbers in the second column, based on those random numbers. Then, a second random number determines the probability falling within the segments for which the inverse probability distribution gives the variable value.
Care has to be taken with the WE parameters: if the recorded WE is 1, the standard error is 0 so the simulation will always be equal to the recorded value of 1. The simulated WE values are limited to be >=0 and <=1, with a maximum equal to the initial WE. This is a limiting "cap" for the normal probability distributions, similar to the procedure followed by Hack. The maximum of WEinit automatically includes the condition that WE-simulations >1 are to be reset at 1.
The resulting matrices are of the dimensions "datapoints" x "lhsruns", so every row contains all the simulations for one data point.

$$Tlhs(A,B) := \left| \begin{array}{l} \text{for } i \in 0..(A-1) \\ \quad \left| \begin{array}{l} \text{for } k \in 0..(B-1) \\ \quad \left| \begin{array}{l} SEG_{k,0} \leftarrow k \\ SEG_{k,1} \leftarrow rnd(1) \end{array} \right. \\ SEGs \leftarrow csort(SEG,1) \\ \text{for } j \in 0..(B-1) \\ \quad \left| \begin{array}{l} p \leftarrow SEGs_{j,0} \cdot lhsstep + rnd(1) \cdot lhsstep \\ MTlhs_{i,j} \leftarrow if\left[p < \frac{\left(S_{i,3} - S_{i,2}\right)}{\left(S_{i,4} - S_{i,2}\right)}, S_{i,2} + \sqrt{\left(S_{i,3} - S_{i,2}\right) \cdot \left(S_{i,4} - S_{i,2}\right) \cdot p}, S_{i,4} - \left[\sqrt{\left(S_{i,4} - S_{i,3}\right) \cdot \left(S_{i,4} - S_{i,2}\right) \cdot (1-p)} \right] \right] \end{array} \right. \end{array} \right. \\ MTlhs \end{array} \right.$$

$$WElhs(A,B) := \left| \begin{array}{l} \text{for } i \in 0..(A-1) \\ \quad \left| \begin{array}{l} \text{for } k \in 0..(B-1) \\ \quad \left| \begin{array}{l} SEG_{k,0} \leftarrow k \\ SEG_{k,1} \leftarrow rnd(1) \end{array} \right. \\ SEGs \leftarrow csort(SEG,1) \\ \text{for } j \in 0..(B-1) \\ \quad \left| \begin{array}{l} p \leftarrow SEGs_{j,0} \cdot lhsstep + rnd(1) \cdot lhsstep \\ MWElhs_{i,j} \leftarrow \left| \begin{array}{l} 1 \text{ if } S_{i,6} = 1 \\ 0 \text{ if } qnorm\left(p, S_{i,6}, S_{i,7}\right) < 0 \\ S_{i,5} \text{ if } qnorm\left(p, S_{i,6}, S_{i,7}\right) > S_{i,5} \\ qnorm\left(p, S_{i,6}, S_{i,7}\right) \text{ otherwise} \end{array} \right. \end{array} \right. \end{array} \right. \\ MWElhs \end{array} \right.$$

$$ORlhs(A,B) := \left| \begin{array}{l} \text{for } i \in 0..(A-1) \\ \quad \left| \begin{array}{l} \text{for } k \in 0..(B-1) \\ \quad \left| \begin{array}{l} SEG_{k,0} \leftarrow k \\ SEG_{k,1} \leftarrow rnd(1) \end{array} \right. \\ SEGs \leftarrow csort(SEG,1) \\ \text{for } j \in 0..(B-1) \\ \quad \left| \begin{array}{l} p \leftarrow SEGs_{j,0} \cdot lhsstep + rnd(1) \cdot lhsstep \\ MORlhs_{i,j} \leftarrow qnorm\left(p, S_{i,0}, orsdv\right) \end{array} \right. \end{array} \right. \\ MORlhs \end{array} \right.$$

$$T := Tlhs(datapoints, lhsruns)$$

$$WE := WElhs(datapoints, lhsruns)$$

$$OR := ORlhs(datapoints, lhsruns)$$

These three matrices "T", "WE" and "OR" are then combined into a matrix "OUT". Simulated aspects (1st column) are reset to fall in the interval 0<=aspect<=360, since simulations may be <0 or >360. The corresponding orientation codes are determined as well (2nd column). Other columns contain simulations for the exposure time (3rd column), log of exposure time (4th column), initial WE (5th column), simulated WE (6th column) and weathering rate (7th column) as defined by WEinit-WE/log(exposure time).

$n := 0 .. lhsruns - 1$

$o := 0 .. datapoints - 1$

$$OUT_{n\cdot(datapoints)+o,0} := \begin{cases} OR_{o,n} & if\ 0 \le OR_{o,n} \le 360 \\ OR_{o,n} - 360 & if\ OR_{o,n} > 360 \\ 360 + OR_{o,n} & if\ OR_{o,n} < 0 \end{cases}$$

$$OUT_{n\cdot(datapoints)+o,1} := \begin{cases} 1 & if\ 337.5 < OUT_{n\cdot(datapoints)+o,0} \le 360 \\ 1 & if\ 0 \le OUT_{n\cdot(datapoints)+o,0} \le 22.5 \\ 2 & if\ 22.5 < OUT_{n\cdot(datapoints)+o,0} \le 67.5 \\ 3 & if\ 67.5 < OUT_{n\cdot(datapoints)+o,0} \le 112.5 \\ 4 & if\ 112.5 < OUT_{n\cdot(datapoints)+o,0} \le 157.5 \\ 5 & if\ 157.5 < OUT_{n\cdot(datapoints)+o,0} \le 202.5 \\ 6 & if\ 202.5 < OUT_{n\cdot(datapoints)+o,0} \le 247.5 \\ 7 & if\ 247.5 < OUT_{n\cdot(datapoints)+o,0} \le 292.5 \\ 8 & if\ 292.5 < OUT_{n\cdot(datapoints)+o,0} \le 337.5 \end{cases}$$

$$OUT_{n\cdot(datapoints)+o,2} := T_{o,n}$$

$$OUT_{n\cdot(datapoints)+o,3} := log\left(1 + T_{o,n}\right)$$

$$OUT_{n\cdot(datapoints)+o,4} := D_{o,4}$$

$$OUT_{n\cdot(datapoints)+o,5} := WE_{o,n}$$

$$OUT_{n\cdot(datapoints)+o,6} := \frac{D_{o,4} - WE_{o,n}}{log\left(1 + T_{o,n}\right)}$$

Next, 8 lines are added to the matrix "OUT" that will later on be used to separate the subsets with different orientation classes, with a value in the weathering rate column of -99. This will make sure that every orientation class will contain at least one row. After that the matrix "OUT" is sorted based on the orientation code, giving a matrix "OUTsort".

$i := 1 .. 8$

$$OUT_{lhsruns\cdot datapoints+i-1,1} := i$$

$$OUT_{lhsruns\cdot datapoints+i-1,6} := -99$$

$$OUTsort := csort(OUT, 1)$$

A similar procedure is followed for a much smaller matrix containing the same variables as "OUT", but now based on the exact recorded values instead of the data simulations. This is to compare the bootstrap percentiles to maximum, minimum and average recorded values.

$i := 0 .. datapoints - 1$

$$real_{i,0} := D_{i,0} \qquad real_{i,1} := D_{i,1} \qquad real_{i,2} := D_{i,2} \qquad real_{i,6} := \frac{\left(D_{i,4} - D_{i,3}\right)}{log\left(1 + D_{i,2}\right)}$$

$$real_{i,3} := log\left(1 + D_{i,2}\right) \qquad real_{i,4} := D_{i,4} \qquad real_{i,5} := D_{i,3}$$

$j := 1 .. 8$

$$real_{datapoints+j-1,1} := j$$

$$real_{datapoints+j-1,6} := -99$$

$$realsort := csort(real, 1)$$

To determine how many rows the subsets for each orientation class contain, a histogram is made for both the matrix "OUTsort" (simulated data) and the matrix realsort (recorded data). The histogram classes are equal to the orientation codes (with the addition of 9).

$$codes := \begin{bmatrix} 1 \\ 2 \\ 3 \\ 4 \\ 5 \\ 6 \\ 7 \\ 8 \\ 9 \end{bmatrix}$$

$$codesd := hist(codes, OUTsort^{\langle 1 \rangle})$$

$$codesr := hist(codes, realsort^{\langle 1 \rangle})$$

The histogram outcome is used to construct two matrices codesdata and codesreal that contain the orientation code (1st column), number of rows for that orientation code's subset (2nd column) and the cumulative number of rows (3rd column).

$i := 1 .. 8$

$codesdata_{i-1,0} := codes_{i-1}$ $\quad$ $codesreal_{i-1,0} := codes_{i-1}$

$codesdata_{i-1,1} := codesd_{i-1}$ $\quad$ $codesreal_{i-1,1} := codesr_{i-1}$

$codesdata_{i-1,2} := \Sigma submatrix(codesd, 0, i-1, 0, 0)$ $\quad$ $codesreal_{i-1,2} := \Sigma submatrix(codesr, 0, i-1, 0, 0)$

The subsets are extracted from the matrices "OUTsort" and "realsort" and sorted based on the weathering rate. For the matrices based on the recorded values, the fake line with weathering rate equal to -99 is deleted if there are more data points within a particular orientation class. If that fake line is the only one in a class, it is kept.

$$OUTsort1 := csort(submatrix(OUTsort, 0, codesdata_{0,2} - 1, 0, 6), 6)$$

$$OUTsort2 := csort(submatrix(OUTsort, codesdata_{0,2}, codesdata_{1,2} - 1, 0, 6), 6)$$

$$OUTsort3 := csort(submatrix(OUTsort, codesdata_{1,2}, codesdata_{2,2} - 1, 0, 6), 6)$$

$$OUTsort4 := csort(submatrix(OUTsort, codesdata_{2,2}, codesdata_{3,2} - 1, 0, 6), 6)$$

$$OUTsort5 := csort(submatrix(OUTsort, codesdata_{3,2}, codesdata_{4,2} - 1, 0, 6), 6)$$

$$OUTsort6 := csort(submatrix(OUTsort, codesdata_{4,2}, codesdata_{5,2} - 1, 0, 6), 6)$$

$$OUTsort7 := csort(submatrix(OUTsort, codesdata_{5,2}, codesdata_{6,2} - 1, 0, 6), 6)$$

$$OUTsort8 := csort(submatrix(OUTsort, codesdata_{6,2}, codesdata_{7,2} - 1, 0, 6), 6)$$

$$rsort1 := csort(submatrix(realsort, 0, codesreal_{0,2} - 1, 0, 6), 6)$$

$$rsort2 := csort(submatrix(realsort, codesreal_{0,2}, codesreal_{1,2} - 1, 0, 6), 6)$$

$$rsort3 := csort(submatrix(realsort, codesreal_{1,2}, codesreal_{2,2} - 1, 0, 6), 6)$$

$$rsort4 := csort(submatrix(realsort, codesreal_{2,2}, codesreal_{3,2} - 1, 0, 6), 6)$$

$$rsort5 := csort(submatrix(realsort, codesreal_{3,2}, codesreal_{4,2} - 1, 0, 6), 6)$$

$$rsort6 := csort(submatrix(realsort, codesreal_{4,2}, codesreal_{5,2} - 1, 0, 6), 6)$$

$$rsort7 := csort(submatrix(realsort, codesreal_{5,2}, codesreal_{6,2} - 1, 0, 6), 6)$$

$$rsort8 := csort(submatrix(realsort, codesreal_{6,2}, codesreal_{7,2} - 1, 0, 6), 6)$$

$realsort1 := if(rows(rsort1)=1, rsort1, submatrix(rsort1, 1, rows(rsort1)-1, 0, 6))$

$realsort2 := if(rows(rsort2)=1, rsort2, submatrix(rsort2, 1, rows(rsort2)-1, 0, 6))$

$realsort3 := if(rows(rsort3)=1, rsort3, submatrix(rsort3, 1, rows(rsort3)-1, 0, 6))$

$realsort4 := if(rows(rsort4)=1, rsort4, submatrix(rsort4, 1, rows(rsort4)-1, 0, 6))$

$realsort5 := if(rows(rsort5)=1, rsort5, submatrix(rsort5, 1, rows(rsort5)-1, 0, 6))$

$realsort6 := if(rows(rsort6)=1, rsort6, submatrix(rsort6, 1, rows(rsort6)-1, 0, 6))$

$realsort7 := if(rows(rsort7)=1, rsort7, submatrix(rsort7, 1, rows(rsort7)-1, 0, 6))$

$realsort8 := if(rows(rsort8)=1, rsort8, submatrix(rsort8, 1, rows(rsort8)-1, 0, 6))$

With the vector "perc" the bootstrap percentiles are defined; these percentiles will define the weathering rates corresponding to the fractions given in perc of the complete (simulated) data set:

$perc := (0 \;\; 0.01 \;\; 0.05 \;\; 0.1 \;\; 0.25 \;\; 0.5 \;\; 0.75 \;\; 0.9 \;\; 0.95 \;\; 0.99 \;\; 1)$ $\qquad percpoints := cols(perc)$

The bootstrap percentiles are determined for each subset containing the data for a particular weathering class. If the only data in the subset is the fake line, with weathering rate -99, that value of -99 is taken as percentile. Otherwise that line is discarded and the nth line is taken, n corresponding to a fraction of the data set as defined in perc. That means that if there are no simulations falling within a particular weathering class, all weathering rate percentiles for the percentages listed in perc will be set at -99.

$i := 0 .. percpoints - 1$

$percentiles1_{0,i} := if\left[max\left(OUTsort1^{\langle 6\rangle}\right) < 0, OUTsort1_{trunc\left[perc_{0,i}\cdot(rows(OUTsort1)-1)\right],6}, OUTsort1_{1+trunc\left[perc_{0,i}\cdot(rows(OUTsort1)-2)\right],6}\right]$

$percentiles2_{0,i} := if\left[max\left(OUTsort2^{\langle 6\rangle}\right) < 0, OUTsort2_{trunc\left[perc_{0,i}\cdot(rows(OUTsort2)-1)\right],6}, OUTsort2_{1+trunc\left[perc_{0,i}\cdot(rows(OUTsort2)-2)\right],6}\right]$

$percentiles3_{0,i} := if\left[max\left(OUTsort3^{\langle 6\rangle}\right) < 0, OUTsort3_{trunc\left[perc_{0,i}\cdot(rows(OUTsort3)-1)\right],6}, OUTsort3_{1+trunc\left[perc_{0,i}\cdot(rows(OUTsort3)-2)\right],6}\right]$

$percentiles4_{0,i} := if\left[max\left(OUTsort4^{\langle 6\rangle}\right) < 0, OUTsort4_{trunc\left[perc_{0,i}\cdot(rows(OUTsort4)-1)\right],6}, OUTsort4_{1+trunc\left[perc_{0,i}\cdot(rows(OUTsort4)-2)\right],6}\right]$

$percentiles5_{0,i} := if\left[max\left(OUTsort5^{\langle 6\rangle}\right) < 0, OUTsort5_{trunc\left[perc_{0,i}\cdot(rows(OUTsort5)-1)\right],6}, OUTsort5_{1+trunc\left[perc_{0,i}\cdot(rows(OUTsort5)-2)\right],6}\right]$

$percentiles6_{0,i} := if\left[max\left(OUTsort6^{\langle 6\rangle}\right) < 0, OUTsort6_{trunc\left[perc_{0,i}\cdot(rows(OUTsort6)-1)\right],6}, OUTsort6_{1+trunc\left[perc_{0,i}\cdot(rows(OUTsort6)-2)\right],6}\right]$

$percentiles7_{0,i} := if\left[max\left(OUTsort7^{\langle 6\rangle}\right) < 0, OUTsort7_{trunc\left[perc_{0,i}\cdot(rows(OUTsort7)-1)\right],6}, OUTsort7_{1+trunc\left[perc_{0,i}\cdot(rows(OUTsort7)-2)\right],6}\right]$

$percentiles8_{0,i} := if\left[max\left(OUTsort8^{\langle 6\rangle}\right) < 0, OUTsort8_{trunc\left[perc_{0,i}\cdot(rows(OUTsort8)-1)\right],6}, OUTsort8_{1+trunc\left[perc_{0,i}\cdot(rows(OUTsort8)-2)\right],6}\right]$

These eight matrices (or vertices, rather) are combined into 1 matrix containing one row for each orientation class, with the percentiles corresponding to the fractions of perc in the consecutive columns:

$i := 1 .. cols(perc)$

$percentiles_{0,i} := perc_{0,i-1}$ (This gives a header row with the percentile fractions)

$percentiles_{1,i} := percentiles1_{0,i-1}$ $\qquad percentiles_{2,i} := percentiles2_{0,i-1}$

$percentiles_{3,i} := percentiles3_{0,i-1}$ $\qquad percentiles_{4,i} := percentiles4_{0,i-1}$

$percentiles_{5,i} := percentiles5_{0,i-1}$ $\qquad percentiles_{6,i} := percentiles6_{0,i-1}$

$percentiles_{7,i} := percentiles7_{0,i-1}$ $\qquad percentiles_{8,i} := percentiles8_{0,i-1}$

$j := 1 .. 8$

$percentiles_{j,0} := j$ (This gives a header column with the orientation classes)

A similar procedure is followed for the recorded values. Note that fake lines with -99 as the rate were discarded if there were data points falling in a class; now, the maximum, minimum and average rate are taken for each class. If the fake line was not discarded, meaning that there was no data for that class, these rates come out as the fake value of -99:

$k := 1 .. 8$

$minavgmax_{k-1,0} := k$ (This gives a header column with the orientation classes)

$minavgmax_{0,1} := min(realsort1^{\langle 6 \rangle})$ $minavgmax_{0,2} := mean(realsort1^{\langle 6 \rangle})$ $minavgmax_{0,3} := max(realsort1^{\langle 6 \rangle})$

$minavgmax_{1,1} := min(realsort2^{\langle 6 \rangle})$ $minavgmax_{1,2} := mean(realsort2^{\langle 6 \rangle})$ $minavgmax_{1,3} := max(realsort2^{\langle 6 \rangle})$

$minavgmax_{2,1} := min(realsort3^{\langle 6 \rangle})$ $minavgmax_{2,2} := mean(realsort3^{\langle 6 \rangle})$ $minavgmax_{2,3} := max(realsort3^{\langle 6 \rangle})$

$minavgmax_{3,1} := min(realsort4^{\langle 6 \rangle})$ $minavgmax_{3,2} := mean(realsort4^{\langle 6 \rangle})$ $minavgmax_{3,3} := max(realsort4^{\langle 6 \rangle})$

$minavgmax_{4,1} := min(realsort5^{\langle 6 \rangle})$ $minavgmax_{4,2} := mean(realsort5^{\langle 6 \rangle})$ $minavgmax_{4,3} := max(realsort5^{\langle 6 \rangle})$

$minavgmax_{5,1} := min(realsort6^{\langle 6 \rangle})$ $minavgmax_{5,2} := mean(realsort6^{\langle 6 \rangle})$ $minavgmax_{5,3} := max(realsort6^{\langle 6 \rangle})$

$minavgmax_{6,1} := min(realsort7^{\langle 6 \rangle})$ $minavgmax_{6,2} := mean(realsort7^{\langle 6 \rangle})$ $minavgmax_{6,3} := max(realsort7^{\langle 6 \rangle})$

$minavgmax_{7,1} := min(realsort8^{\langle 6 \rangle})$ $minavgmax_{7,2} := mean(realsort8^{\langle 6 \rangle})$ $minavgmax_{7,3} := max(realsort8^{\langle 6 \rangle})$

The resulting matrices for the bootstrap percentiles and the minimum, average and maximum recorded rates are (note: the first row in the matrix "percentiles" contains the bootstrap probabilities; the first column in both matrices contains the orientation codes):

$$percentiles = \begin{bmatrix} 0.000 & 0.000 & 0.010 & 0.050 & 0.100 & 0.250 & 0.500 & 0.750 & 0.900 & 0.950 & 0.990 & 1.000 \\ 1.000 & 0.000 & 0.000 & 0.000 & 0.010 & 0.050 & 0.096 & 0.141 & 0.182 & 0.207 & 0.249 & 0.332 \\ 2.000 & 0.000 & 0.000 & 0.000 & 0.010 & 0.051 & 0.096 & 0.141 & 0.183 & 0.208 & 0.257 & 0.318 \\ 3.000 & 0.000 & 0.000 & 0.000 & 0.010 & 0.050 & 0.096 & 0.142 & 0.182 & 0.207 & 0.251 & 0.341 \\ 4.000 & 0.000 & 0.000 & 0.000 & 0.010 & 0.051 & 0.096 & 0.142 & 0.182 & 0.205 & 0.253 & 0.328 \\ 5.000 & 0.000 & 0.000 & 0.000 & 0.010 & 0.050 & 0.096 & 0.141 & 0.182 & 0.207 & 0.253 & 0.387 \\ 6.000 & 0.000 & 0.000 & 0.000 & 0.010 & 0.050 & 0.096 & 0.142 & 0.183 & 0.206 & 0.252 & 0.329 \\ 7.000 & 0.000 & 0.000 & 0.000 & 0.010 & 0.051 & 0.096 & 0.141 & 0.182 & 0.206 & 0.252 & 0.327 \\ 8.000 & 0.000 & 0.000 & 0.000 & 0.010 & 0.051 & 0.096 & 0.141 & 0.183 & 0.207 & 0.253 & 0.337 \end{bmatrix}$$

$$minavgmax = \begin{bmatrix} 1 & 0.096 & 0.096 & 0.096 \\ 2 & 0.096 & 0.096 & 0.096 \\ 3 & 0.096 & 0.096 & 0.096 \\ 4 & 0.096 & 0.096 & 0.096 \\ 5 & 0.096 & 0.096 & 0.096 \\ 6 & 0.096 & 0.096 & 0.096 \\ 7 & 0.096 & 0.096 & 0.096 \\ 8 & 0.096 & 0.096 & 0.096 \end{bmatrix}$$

G Case study slopes

"It is a capital mistake to theorise before one has data. Insensibly one begins to twist facts to suit theories, instead of theories to suit facts." - Sir Arthur Conan Doyle, *A Scandal in Bohemia.*

In the following table (overleaf), the case study slopes referred to in the text are presented with short descriptions and photographs.

Gavadà – Keuper shales
A small road leading from the C-233 at the Coll de Fatxes to the south, past the farm locally known as Geinessies towards the settlement of Gavadà and the Coll d'Aumet, was reconstructed and widened in 1999, and a number of small road cuts had to be made. This reconstruction handed the rare opportunity to see and watch relatively intact Keuper shales and their decay. A small cut around N4543330/E314815 was investigated in detail for this.

Right: orthophoto and oblique photo of slope

Masriudoms – Middle Muschelkalk siltstones
At the western edge of the village of Masriudoms around N4543282/E322140, a road cut comprising two opposite slopes was excavated in Middle Muschelkalk siltstones in 1992, during reconstruction of the C-233 road that leads inland from Hospitalet de l'Infant to Mora de l'Ebre. The slope on the north side of the road has an orientation of 198°, whereas the south slope is orientated towards 020°. The photo shows this south slope.

Right: orthophoto and oblique photo of slope

La Torre de Fontaubella – Upper Muschelkalk ("Cindarto slope")
The so-called "Cindarto-slope" (named after Cindarto, 1992) is located along the TV-3001 between La Torre de Fontaubella and Marçà, at N4554790/E318020 and is excavated in Upper Muschelkalk limestones. The road cut had been a liability for block slide failure ever since its excavation in the 1950/60's because of a day-lighting bedding plane dip angle of 37° directly towards the road. In 1991 such a failure indeed occurred. In the following years the slope was investigated in detail. The geometry was recorded using triangulations and over the years several rock mass characterisations and classifications were made, and samples were taken for laboratory testing.

Right: orthophoto and oblique photo of slope

Hostal – Keuper shales and limestones
The example described here is located along the N-420 road, around the coordinates N4557925/E320500. The slope length and height are 225m and 40m, respectively. It faces approximately east (110°) and was constructed with an average slope angle of 70°. The initial excavation for realignment of the N-420 was made in 1988; since then, the slope geometry has changed somewhat because of erosion and mass movement of weak layers and rock fall as well as periodic re-excavation works.

Right: orthophoto and oblique photo of slope

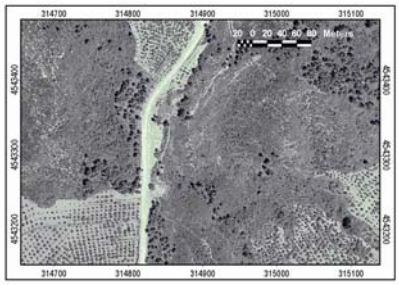






H Data

"Those whom devotion to abstract discussions has rendered unobservant of the facts are too ready to dogmatize on the basis of a few observations." - Aristotle, *De Generatione et Corruptione*.

H.1 Classification data set

The classification data used in this research has been gathered during engineering geological mapping fieldworks in the Falset area by students and staff from ITC and the Delft University of Technology, in the period of 1990 until 2004. Previous compilations of this data were made by Kouokam (1993), Hack (1998), Chapagain (2001), Hernandez (2002) and De Jong (2003). Until 1996, the fieldwork classification data was used to verify, adapt and validate the SSPC classification system by Hack (1996 and 1998) and since then, the final version of the SSPC system has been used throughout the fieldworks.

From the resulting set of fieldwork data, classifications for the studied units[48] were extracted and verified by desk study and field checks, and revised where necessary. Selected data sets were created for the studied units and managed in a GIS, containing classification information on:

- Coordinates (UTM)
- Road No.
- Slope orientation, angle and height
- Year of exposure / excavation

[48] *Keuper shales and limestones, Middle Muschelkalk siltstones and gypsum, and Upper Muschelkalk limestones with bedding spacings 0-0.10m, 0.10-0.50m, and >0.50m.*

- Year of observation
- Exposure time
- WE (SSPC) at the time of observation
- WE (SSPC) at the time of excavation (estimated)
- Weathering intensity rate as defined by equation (1) (page 55)
- Bedding spacing
- Bedding dip direction
- Bedding dip
- Apparent dip of bedding planes in cross-section (AP in SSPC)
- Intact rock material strength at the time of observation (IRS in SSPC)
- Mean annual precipitation (see Appendix B)
- Mean annual evapotranspiration (see Appendix B)
- Mean annual temperature (see Appendix B)

H.2 Data verification

For all the classifications of which the data has been used for this research, a check was made on the exact unit which had been classified. In most cases the unit was gathered from notes on the field forms describing the material classified, or photographs in the mapping reports. In cases where field form notes were not clear about the precise unit and where photographs were lacking, field checks were made in 2003 and 2004 by the author and dr. H.R.G.K. Hack. During these field checks, the exposure times for all road sections and slopes involved in the classifications have been estimated, based on direct historical data, visible signs of excavation methods, the width and state of the roads, et cetera.

An example of such a check and the way data has been gathered from existing slopes is represented in Figure 99 for a slope originally described in 1992, in the Upper Muschelkalk. Different weathering grades were observed in this particular slope and in 1992, a remark had already been made on the field form that parts of the slope had been re-excavated. During a field check this was confirmed, and four different data points were defined for the unit

exposed in this slope (Upper Muschelkalk with bedding spacing 0.10-0.50m) based on different weathering grades and exposure times.

a. b.

Figure 99 - Slope in Upper Muschelkalk near Figuera, at N4565700/E309937; September 2004. Not interpreted (a) and interpreted with data points (b).

After the verification of all classifications, a total of 426 reliable data points remained, distributed over the different units as follows (Table 19).

Table 19 - Number of data points per unit.

Unit	Data points
Keuper shales	48
Keuper limestones	72
Middle Muschelkalk siltstones	35
Middle Muschelkalk gypsum	27
Upper Muschelkalk, bedding spacing < 0.10m	93
Upper Muschelkalk, 0.10m < bedding spacing < 0.50m	86
Upper Muschelkalk, bedding spacing > 0.50m	65
Total	**426**

An overview of all data points is included in Table 20-Table 26.

H.3 Statistical considerations

Apart from limitations arising from the amount of data per unit and the fact that only sedimentary rocks have been studied in detail, an important consideration is possible bias in the input data. If parameters influencing weathering and erosion behaviour are not independent, this may reflect

itself in the results and observed relationships. The most notable possible bias stems from the structural geological boundary conditions in the Falset area, where the general dip of bedding planes is towards the northwest due to regional tilting. This means that the separate influences of apparent dip angle of the main discontinuities[49] and the orientation of a slope with respect to the prevailing climate[50] are statistically very hard to separate. Due to the on average northwest dip, most southeast facing slopes will have a negative apparent dip (*AP*, *AP* <0 indicates a dip *into* the slope) whereas most northwest facing slopes will have a positive apparent dip (*AP* >0 indicates a dip *out of* the slope).

In principle, the average coincidence of south-eastward slope orientations with negative AP values for the bedding, and the opposite for north-westward slope orientations, means that trends observed in weathering and erosion behaviour with respect to slope orientation will statistically show trends with apparent dip too. Vice versa, influences of the apparent dip may be obscured by effects of the slope orientation. It is assumed here that the clear trends observed for the influence of slope orientation on weathering indeed result from the orientation, rather than the dependent variable apparent dip, for two reasons:

- Since the observed trends for orientation correspond to anticipated weathering processes and the influence thereupon of orientation-related conditions.
- Because similar relations are found in (albeit less extensive) data sets that do not show such a bias (data from Bhutan, paragraph 5.4).

[49] *In the studied units Keuper, Middle Muschelkalk and Upper Muschelkalk, these are generally the bedding planes.*

[50] *Most notably prevailing wind directions, rainfall, and exposure to the sun, but also conditions such as vegetation.*

Table 20 - Weathering data for Keuper shales.

Data point	Easting [m]	Northing [m]	Exposure time [years]	WE observed [-]	WE at excavation [-]	Slope orientation [°]
A1	320570	4557920	2	1.00	1.00	100
A2	320570	4557920	2	1.00	1.00	100
A3	320475	4557800	3	0.95	1.00	100
A4	320475	4557800	3	0.90	1.00	100
A5	320475	4557800	3	0.95	1.00	100
A6	320475	4557800	3	0.90	1.00	100
A7	320368	4557714	3	0.90	1.00	104
A8	320368	4557714	3	0.62	1.00	110
A9	320368	4557714	3	0.95	1.00	110
A10	320368	4557714	3	0.95	1.00	120
A11	320368	4557714	3	0.62	1.00	120
A12	310393	4545780	4	0.90	1.00	62
A13	320420	4557750	5	0.95	1.00	112
A14	320420	4557750	5	0.95	1.00	100
A15	320420	4557750	5	0.95	1.00	140
A16	320420	4557750	5	0.95	1.00	140
A17	320420	4557750	5	0.90	1.00	152
A18	320420	4557750	5	0.95	1.00	117
A19	320420	4557750	5	0.90	1.00	132
A20	320420	4557750	5	0.95	1.00	120
A21	320420	4557750	5	0.95	1.00	132
A22	320420	4557750	5	0.95	1.00	125
A23	320368	4557714	5	0.62	1.00	98
A24	320457	4557835	5	0.95	1.00	100
A25	320457	4557835	5	0.95	1.00	100
A26	320460	4557607	5	0.90	1.00	124
A27	320460	4557607	5	0.90	1.00	132
A28	320460	4557607	5	0.90	1.00	122
A29	320460	4557607	5	0.90	1.00	122
A30	320460	4557607	5	0.90	1.00	120
A31	320460	4557607	5	0.90	1.00	122
A32	320460	4557607	5	0.90	1.00	122
A33	320460	4557607	5	0.90	1.00	134
A34	320460	4557607	5	0.90	1.00	150
A35	320350	4557700	9	0.62	1.00	152

Data point	Easting [m]	Northing [m]	Exposure time [years]	WE observed [-]	WE at excavation [-]	Slope orientation [°]
A36	320350	4557700	9	0.62	1.00	160
A37	320350	4557570	12	0.62	1.00	110
A38	320350	4557700	12	0.62	1.00	150
A39	320450	4557750	12	0.62	1.00	130
A40	320450	4557750	12	0.62	1.00	138
A41	320450	4557750	12	0.62	1.00	130
A42	319502	4557582	13	0.90	1.00	300
A43	308208	4562075	37	0.62	1.00	200
A44	321085	4542662	71	0.35	1.00	228
A45	321836	4548216	72	0.62	1.00	170
A46	320271	4548824	75	0.62	1.00	170
A47	319929	4546820	75	0.62	1.00	154
A48	308584	4563556	142	0.62	1.00	330

Table 21 - Weathering data for Keuper limestones.

Data point	Easting [m]	Northing [m]	Exposure time [years]	WE observed [-]	WE at excavation [-]	Slope orientation [°]
B1	320570	4557920	2	1.00	1.00	100
B2	320475	4557800	3	0.95	1.00	100
B3	320475	4557800	3	0.90	1.00	100
B4	320475	4557800	3	0.95	1.00	100
B5	320475	4557800	3	0.95	1.00	100
B6	320475	4557800	3	0.95	1.00	100
B7	320475	4557800	3	0.95	1.00	100
B8	320475	4557800	3	0.95	1.00	100
B9	320475	4557800	3	0.95	1.00	100
B10	320368	4557714	3	0.95	1.00	90
B11	320368	4557714	3	0.95	1.00	90
B12	320367	4557714	3	0.95	1.00	89
B13	320368	4557714	3	0.95	1.00	89
B14	320368	4557714	3	0.95	1.00	110
B15	320368	4557714	3	0.95	1.00	120
B16	320368	4557714	3	0.95	1.00	120
B17	320420	4557750	5	0.95	1.00	112
B18	320420	4557750	5	0.95	1.00	140
B19	320420	4557750	5	0.95	1.00	140
B20	320420	4557750	5	0.95	1.00	152

Data point	Easting [m]	Northing [m]	Exposure time [years]	WE observed [-]	WE at excavation [-]	Slope orientation [°]
B21	320420	4557750	5	0.95	1.00	117
B22	320420	4557750	5	0.95	1.00	130
B23	320420	4557750	5	0.95	1.00	120
B24	320420	4557750	5	0.95	1.00	132
B25	320420	4557750	5	0.95	1.00	125
B26	320457	4557835	5	0.95	1.00	100
B27	320457	4557835	5	0.95	1.00	90
B28	320457	4557835	5	0.95	1.00	100
B29	320457	4557835	5	0.95	1.00	100
B30	320457	4557835	5	0.95	1.00	90
B31	320457	4557835	5	0.95	1.00	90
B32	320460	4557607	5	0.95	1.00	124
B33	320460	4557607	5	0.95	1.00	156
B34	320460	4557607	5	0.90	1.00	156
B35	320460	4557607	5	0.95	1.00	132
B36	320460	4557607	5	0.95	1.00	122
B37	319888	4557349	5	0.95	1.00	122
B38	320460	4557607	5	0.95	1.00	122
B39	320460	4557607	5	0.95	1.00	155
B40	320460	4557607	5	0.95	1.00	120
B41	320460	4557607	5	0.95	1.00	122
B42	320460	4557607	5	0.95	1.00	122
B43	320460	4557607	5	0.90	1.00	134
B44	320460	4557607	5	0.95	1.00	122
B45	320460	4557607	5	0.95	1.00	122
B46	320460	4557607	5	0.95	1.00	122
B47	320460	4557607	5	0.90	1.00	148
B48	320460	4557607	5	0.95	1.00	154
B49	320457	4557835	5	0.95	1.00	180
B50	320457	4557835	5	0.95	1.00	180
B51	320350	4557570	12	0.95	1.00	110
B52	320350	4557570	12	0.95	1.00	90
B53	320350	4557570	12	0.95	1.00	95
B54	320350	4557570	12	0.90	1.00	110
B55	320350	4557570	12	0.90	1.00	90
B56	320350	4557570	12	0.95	1.00	105
B57	320350	4557570	12	0.95	1.00	110

Data point	Easting [m]	Northing [m]	Exposure time [years]	WE observed [-]	WE at excavation [-]	Slope orientation [°]
B58	320350	4557570	12	0.95	1.00	110
B59	320350	4557570	12	0.95	1.00	110
B60	320350	4557570	12	0.95	1.00	112
B61	320350	4557570	12	0.95	1.00	110
B62	320350	4557570	12	0.95	1.00	100
B63	320350	4557570	12	0.95	1.00	118
B64	320350	4557570	12	0.90	1.00	125
B65	308675	4563168	37	0.95	1.00	300
B66	320430	4557775	45	0.95	1.00	52
B67	320350	4557570	45	0.95	1.00	52
B68	320350	4557570	45	0.90	1.00	52
B69	321464	4542623	71	0.90	1.00	39
B70	321085	4542662	71	0.90	1.00	10
B71	322049	4548100	72	0.90	1.00	75
B72	318665	4554854	93	0.90	1.00	215

Table 22 - Weathering data for Middle Muschelkalk siltstones.

Data point	Easting [m]	Northing [m]	Exposure time [years]	WE observed [-]	WE at excavation [-]	Slope orientation [°]
C1	319796	4543388	2	0.62	0.95	25
C2	319493	4557488	4	0.90	1.00	250
C3	319690	4543059	4	0.90	0.95	340
C4	322074	4543129	4	0.62	0.95	20
C5	322620	4559600	5	0.95	1.00	132
C6	322140	4543282	5	0.62	0.95	180
C7	320180	4543225	6	0.62	0.95	325
C8	320600	4557600	10	0.90	1.00	87
C9	322100	4559150	10	0.90	1.00	160
C10	320180	4543225	11	0.62	0.95	325
C11	322074	4543129	11	0.35	0.95	20
C12	321904	4543284	11	0.35	0.95	346
C13	321801	4543221	11	0.35	0.95	321
C14	321513	4543238	11	0.35	0.95	23
C15	321201	4543238	11	0.35	0.95	16
C16	310848	4545896	11	0.62	0.95	30
C17	322140	4543282	12	0.35	0.95	198
C18	322620	4559600	15	0.35	1.00	132

Data point	Easting [m]	Northing [m]	Exposure time [years]	WE observed [-]	WE at excavation [-]	Slope orientation [˚]
C19	320680	4546610	17	0.62	1.00	310
C20	325981	4549696	17	0.62	1.00	60
C21	320680	4546610	18	0.35	0.62	310
C22	320680	4546610	21	0.35	0.62	310
C23	323140	4552510	35	0.62	1.00	250
C24	322930	4551460	35	0.62	1.00	190
C25	313562	4552547	36	0.62	1.00	300
C26	319494	4557508	37	0.62	1.00	320
C27	310091	4566902	37	0.35	1.00	356
C28	310133	4567124	37	0.35	1.00	82
C29	309687	4567114	37	0.62	1.00	180
C30	308397	4560705	37	0.62	1.00	60
C31	309837	4556885	38	0.62	1.00	218
C32	321278	4543229	43	0.62	1.00	340
C33	322222	4547561	46	0.62	0.90	160
C34	322130	4547554	46	0.35	0.90	200
C35	325722	4549954	75	0.62	1.00	200

Table 23 - Weathering data for Middle Muschelkalk gypsum.

Data point	Easting [m]	Northing [m]	Exposure time [years]	WE observed [-]	WE at excavation [-]	Slope orientation [˚]
D1	321930	4558920	2	1.00	1.00	280
D2	322260	4543065	4	0.95	1.00	40
D3	322080	4543199	4	0.95	1.00	260
D4	321376	4543192	5	0.90	1.00	0
D5	321376	4543192	5	0.90	1.00	0
D6	322214	4543249	5	0.90	1.00	10
D7	322214	4543249	5	0.90	1.00	10
D8	322214	4543249	5	0.90	1.00	10
D9	322446	4543272	5	0.90	1.00	271
D10	321975	4543147	5	0.90	0.95	0
D11	322446	4543272	5	0.90	1.00	271
D12	322446	4543272	5	0.90	1.00	271
D13	322380	4543110	8	0.95	1.00	90
D14	321790	4547490	10	0.90	1.00	200
D15	320675	4546623	14	0.90	1.00	145
D16	320667	4546612	16	0.90	1.00	134

Data point	Easting [m]	Northing [m]	Exposure time [years]	WE observed [-]	WE at excavation [-]	Slope orientation [°]
D17	320667	4546612	21	0.90	1.00	124
D18	322770	4551480	35	0.90	1.00	350
D19	309720	4566904	37	0.62	1.00	100
D20	322837	4544452	39	0.90	1.00	94
D21	322705	4551500	39	0.62	1.00	350
D22	322680	4551500	46	0.90	1.00	347
D23	309684	4557356	68	0.62	1.00	330
D24	321976	4547805	72	0.62	1.00	90
D25	320221	4547164	72	0.62	1.00	50
D26	320221	4547165	72	0.62	1.00	50
D27	325600	4549600	75	0.62	1.00	0

Table 24 - Weathering data for Upper Muschelkalk, BS < 0.10m.

Data point	Easting [m]	Northing [m]	Exposure time [years]	WE observed [-]	WE at excavation [-]	Slope orientation [°]
E1	321200	4558450	2	0.95	1.00	96
E2	321207	4558300	4	0.90	1.00	115
E3	311440	4545089	4	0.90	1.00	50
E4	311440	4545089	4	0.95	1.00	50
E5	312025	4545125	4	0.95	1.00	140
E6	310601	4545674	4	0.95	1.00	230
E7	314365	4545128	5	0.95	1.00	90
E8	314507	4545288	5	0.95	1.00	90
E9	322574	4542971	6	0.90	1.00	340
E10	309937	4565700	7	0.95	1.00	50
E11	321473	4558384	9	0.90	1.00	140
E12	321473	4558384	9	0.90	1.00	145
E13	321050	4558200	9	0.95	1.00	140
E14	321050	4558200	9	0.95	1.00	140
E15	321050	4558200	9	0.95	1.00	180
E16	321473	4558384	9	0.90	1.00	228
E17	320600	4557600	10	0.95	1.00	75
E18	320600	4557600	10	0.95	1.00	140
E19	321050	4558200	10	0.90	1.00	160
E20	321050	4558200	10	0.95	1.00	180
E21	321050	4558200	10	0.95	1.00	180
E22	321050	4558200	10	0.95	1.00	180

Data point	Easting [m]	Northing [m]	Exposure time [years]	WE observed [-]	WE at excavation [-]	Slope orientation [°]
E23	321050	4558200	12	0.95	1.00	120
E24	321827	4558888	12	0.95	1.00	148
E25	321050	4558200	12	0.90	1.00	140
E26	321050	4558200	12	0.90	1.00	180
E27	321050	4558200	12	0.90	1.00	170
E28	321890	4558938	12	0.95	1.00	186
E29	321206	4558485	35	0.90	1.00	60
E30	321041	4558175	35	0.90	1.00	102
E31	320227	4557608	35	0.95	1.00	134
E32	320155	4557588	35	0.95	1.00	150
E33	320948	4558124	35	0.90	1.00	134
E34	321210	4558428	37	0.90	1.00	60
E35	321220	4558387	37	0.90	1.00	85
E36	321220	4558387	37	0.90	1.00	85
E37	321078	4558659	37	0.90	1.00	155
E38	309231	4567067	37	0.90	1.00	352
E39	309155	4567123	37	0.95	1.00	195
E40	309458	4567150	37	0.95	1.00	180
E41	309458	4567150	37	0.95	1.00	180
E42	309260	4567161	37	0.95	1.00	230
E43	308403	4565405	37	0.95	1.00	320
E44	309197	4567020	37	0.95	1.00	272
E45	309197	4567020	37	0.90	1.00	272
E46	307492	4560542	38	0.90	1.00	280
E47	307498	4560592	38	0.95	1.00	250
E48	307498	4560592	38	0.95	1.00	250
E49	310425	4555182	38	0.95	1.00	75
E50	310257	4555336	38	0.90	1.00	205
E51	321625	4558750	40	0.95	1.00	180
E52	309101	4545748	41	0.95	1.00	161
E53	309988	4545932	41	0.95	1.00	223
E54	321050	4558200	42	0.95	1.00	90
E55	321158	4558207	42	0.95	1.00	186
E56	318190	4546857	42	0.90	1.00	142
E57	318275	4548246	42	0.95	1.00	120
E58	321050	4558200	43	0.90	1.00	230
E59	321050	4558200	43	0.90	1.00	280

Data point	Easting [m]	Northing [m]	Exposure time [years]	WE observed [-]	WE at excavation [-]	Slope orientation [°]
E60	321050	4558200	43	0.95	1.00	280
E61	321050	4558200	43	0.95	1.00	280
E62	321050	4558200	45	0.90	1.00	60
E63	320350	4557570	45	0.95	1.00	130
E64	309937	4565700	67	0.95	1.00	50
E65	314646	4542477	71	0.90	1.00	25
E66	314461	4542290	71	0.95	1.00	111
E67	314837	4543667	71	0.95	1.00	93
E68	314773	4542828	71	0.95	1.00	247
E69	314844	4542964	71	0.95	1.00	275
E70	320611	4547938	72	0.90	1.00	110
E71	320917	4542825	72	0.95	1.00	0
E72	322565	4548423	72	0.95	1.00	45
E73	319484	4542723	72	0.95	1.00	350
E74	314912	4543601	72	0.95	1.00	132
E75	322627	4551195	75	0.95	1.00	82
E76	318600	4542400	75	0.95	1.00	320
E77	319370	4542430	75	0.95	1.00	60
E78	318920	4542670	75	0.95	1.00	140
E79	319340	4541850	75	0.95	1.00	250
E80	323024	4550017	75	0.95	1.00	180
E81	306837	4562334	92	0.95	1.00	340
E82	300329	4562475	92	0.95	1.00	90
E83	309035	4562218	92	0.90	1.00	270
E84	309937	4565700	67	0.90	1.00	50
E85	319063	4554823	93	0.95	1.00	90
E86	317867	4554914	93	0.95	1.00	130
E87	322764	4542826	96	0.95	1.00	40
E88	322595	4542849	96	0.90	1.00	140
E89	322229	4542515	96	0.90	1.00	180
E90	321050	4558200	150	0.95	1.00	275
E91	321050	4558200	150	0.95	1.00	128
E92	309937	4565700	492	0.90	1.00	50
E93	319577	4546264	500	0.62	1.00	156

Table 25 - Weathering data for Upper Muschelkalk, 0.10m < BS < 0.50m.

Data point	Easting [m]	Northing [m]	Exposure time [years]	WE observed [-]	WE at excavation [-]	Slope orientation [°]
F1	321200	4558450	2	0.95	1.00	96
F2	321207	4558300	4	0.95	1.00	110
F3	322747	4542998	5	0.95	1.00	22
F4	319093	4548575	7	0.95	1.00	10
F5	321050	4558200	9	0.95	1.00	98
F6	321369	4558341	9	0.95	1.00	134
F7	321400	4558500	9	0.95	1.00	130
F8	321369	4558341	9	0.95	1.00	120
F9	321373	4558391	9	0.90	1.00	200
F10	321473	4558384	9	0.90	1.00	170
F11	321473	4558384	9	0.90	1.00	170
F12	321050	4558200	9	0.95	1.00	158
F13	321050	4558200	9	0.95	1.00	170
F14	321050	4558200	9	0.95	1.00	160
F15	320600	4557600	10	0.95	1.00	140
F16	320600	4557600	10	0.95	1.00	128
F17	321050	4558200	10	0.95	1.00	160
F18	321050	4558200	10	0.95	1.00	180
F19	321050	4558200	10	0.95	1.00	180
F20	321050	4558200	10	0.95	1.00	180
F21	321050	4558200	10	0.95	1.00	210
F22	319111	4548460	10	0.95	1.00	290
F23	319162	4548760	10	0.95	1.00	270
F24	318950	4557410	11	0.95	1.00	220
F25	320350	4557570	12	0.95	1.00	340
F26	321050	4558200	12	0.95	1.00	185
F27	321050	4558200	12	0.95	1.00	220
F28	321913	4558982	12	0.95	1.00	249
F29	321100	4558280	35	0.95	1.00	100
F30	320845	4558072	35	0.95	1.00	146
F31	313660	4552554	36	0.95	1.00	0
F32	309347	4567008	37	0.95	1.00	155
F33	309247	4567016	37	0.95	1.00	170
F34	309948	4565007	37	0.95	1.00	100
F35	308380	4561516	37	0.95	1.00	130

Data point	Easting [m]	Northing [m]	Exposure time [years]	WE observed [-]	WE at excavation [-]	Slope orientation [°]
F36	308421	4565374	37	0.95	1.00	275
F37	310533	4555275	38	0.90	1.00	170
F38	310534	4555275	38	0.90	1.00	170
F39	310234	4555297	38	0.90	1.00	300
F40	317760	4554822	38	0.95	1.00	100
F41	320550	4546598	41	0.95	1.00	146
F42	321050	4558200	42	0.95	1.00	220
F43	317638	4546196	42	0.90	1.00	110
F44	318172	4546486	42	0.95	1.00	176
F45	318443	4548203	42	0.95	1.00	245
F46	321050	4558200	45	0.95	1.00	60
F47	321050	4558200	45	0.95	1.00	290
F48	319162	4548760	45	0.95	1.00	290
F49	319079	4548406	45	0.95	1.00	340
F50	309893	4556627	68	0.95	1.00	180
F51	309785	4556908	68	0.90	1.00	222
F52	309841	4556774	68	0.95	1.00	270
F53	319748	4546217	71	0.90	1.00	138
F54	320020	4546357	71	0.95	1.00	190
F55	320020	4546357	71	0.95	1.00	190
F56	320611	4547938	72	0.95	1.00	110
F57	321347	4547451	72	0.95	1.00	84
F58	321347	4547451	72	0.95	1.00	135
F59	321347	4547451	72	0.95	1.00	160
F60	321837	4548478	72	0.95	1.00	40
F61	316958	4547813	72	0.95	1.00	20
F62	319484	4542723	72	0.95	1.00	248
F63	322626	4551195	75	0.95	1.00	110
F64	322627	4551195	75	0.95	1.00	82
F65	320580	4542550	75	0.95	1.00	170
F66	320480	4542700	75	0.95	1.00	280
F67	320850	4542870	75	0.95	1.00	310
F68	319659	4546235	75	0.90	1.00	180
F69	319407	4546309	75	0.90	1.00	190
F70	320109	4546711	75	0.95	1.00	130
F71	325892	4549689	75	0.95	1.00	60
F72	325681	4549811	75	0.90	1.00	290

Data point	Easting [m]	Northing [m]	Exposure time [years]	WE observed [-]	WE at excavation [-]	Slope orientation [˚]
F73	318600	4542400	75	0.95	1.00	100
F74	310528	4564592	92	0.95	1.00	270
F75	310538	4564862	92	0.90	1.00	280
F76	310494	4556481	93	0.95	1.00	50
F77	318076	4555821	93	0.95	1.00	125
F78	310265	4556639	93	0.95	1.00	150
F79	322260	4559590	93	0.90	1.00	203
F80	317848	4554936	93	0.90	1.00	34
F81	317849	4554937	93	0.90	1.00	34
F82	317851	4554938	93	0.90	1.00	34
F83	322015	4542481	97	0.90	1.00	180
F84	321461	4558234	147	0.95	1.00	215
F85	314194	4545262	497	0.95	1.00	230
F86	313767	4544531	497	0.95	1.00	302

Table 26 - Weathering data for Upper Muschelkalk, BS > 0.50m.

Data point	Easting [m]	Northing [m]	Exposure time [years]	WE observed [-]	WE at excavation [-]	Slope orientation [˚]
G1	320570	4557920	2	0.95	1.00	100
G2	322764	4542957	4	0.95	1.00	220
G3	315058	4544865	5	0.95	1.00	250
G4	319134	4548713	7	0.95	1.00	280
G5	321473	4558384	9	0.95	1.00	170
G6	321473	4558384	9	0.95	1.00	170
G7	320600	4557600	10	0.95	1.00	142
G8	320600	4557600	10	0.95	1.00	142
G9	320600	4557600	10	0.95	1.00	122
G10	320600	4557600	10	0.95	1.00	142
G11	321050	4558200	10	0.95	1.00	160
G12	320600	4557600	10	0.95	1.00	172
G13	321050	4558200	10	0.95	1.00	180
G14	321050	4558200	10	0.95	1.00	180
G15	321400	4558500	10	0.90	1.00	160
G16	321050	4558200	10	0.95	1.00	160
G17	321050	4558200	10	0.95	1.00	160
G18	320600	4557600	10	0.95	1.00	288
G19	320350	4557570	12	0.95	1.00	174

Data point	Easting [m]	Northing [m]	Exposure time [years]	WE observed [-]	WE at excavation [-]	Slope orientation [°]
G20	321878	4558913	12	0.95	1.00	170
G21	321050	4558200	12	0.95	1.00	170
G22	321050	4558200	12	0.95	1.00	170
G23	321206	4558485	35	0.95	1.00	60
G24	320525	4557793	35	0.95	1.00	100
G25	320371	4557691	35	0.95	1.00	108
G26	320826	4558092	35	0.95	1.00	112
G27	321041	4558175	35	0.95	1.00	102
G28	320309	4557628	35	0.95	1.00	125
G29	320866	4558095	35	0.95	1.00	130
G30	320814	4558103	35	0.95	1.00	155
G31	320866	4558085	35	0.95	1.00	130
G32	320749	4558193	35	0.95	1.00	164
G33	320824	4558087	35	0.95	1.00	178
G34	320671	4558072	35	0.95	1.00	180
G35	320525	4557793	35	0.95	1.00	290
G36	318950	4555100	35	0.95	1.00	162
G37	318950	4555100	35	0.95	1.00	162
G38	321100	4558497	37	0.95	1.00	90
G39	309137	4567096	37	0.95	1.00	242
G40	309197	4567020	37	0.95	1.00	272
G41	318950	4555100	40	0.95	1.00	162
G42	318092	4546091	41	0.95	1.00	200
G43	323816	4543730	42	0.95	1.00	0
G44	321262	4558249	42	0.95	1.00	90
G45	321050	4558200	42	0.95	1.00	170
G46	321050	4558200	42	0.95	1.00	268
G47	321050	4558200	43	0.95	1.00	230
G48	321050	4558200	45	0.95	1.00	90
G49	318489	4546252	45	0.95	1.00	90
G50	319288	4542928	71	0.95	1.00	110
G51	325602	4547560	72	0.95	1.00	110
G52	322626	4551195	75	0.95	1.00	110
G53	321180	4542760	75	0.95	1.00	270
G54	320066	4546753	75	0.95	1.00	120
G55	306915	4563622	92	0.95	1.00	295
G56	309943	4565609	92	0.95	1.00	50

Data point	Easting [m]	Northing [m]	Exposure time [years]	WE observed [-]	WE at excavation [-]	Slope orientation [°]
G57	308881	4562180	92	0.95	1.00	80
G58	308167	4565863	92	0.95	1.00	120
G59	310538	4564862	92	0.95	1.00	280
G60	309325	4563540	92	0.95	1.00	270
G61	310706	4555703	93	0.95	1.00	120
G62	321369	4558341	147	0.95	1.00	120
G63	321480	4558484	147	0.95	1.00	195
G64	321400	4558500	150	0.95	1.00	128
G65	314051	4544168	497	0.95	1.00	0

References

Adhikari, G.P. (2002): *Weathering processes in the Upper Muschelkalk of the Tarragona province (Spain) in relation with material composition*. M.Sc. thesis, ITC, Delft.

Aghamiri, R.; Schwartzman, D.W. (2002): Weathering rates of bedrock by lichens: a mini watershed study. *Chemical Geology*, **188**, pp. 249-259.

Amenta, R.V. (2001): Three-dimensional computer modeling of fabric evolution in igneous rocks. *Computers & Geosciences*, **27**, pp. 477-483.

Anon. (1995): *Introduction to probability and reliability methods for use in geotechnical engineering*. Technical letter ETL 1110-2-547, September 30 1995, U.S. Army Corps of Engineers, Washington DC.

Anon. (1996): *Atles climàtic de Catalunya* (climatic atlas of Catalunya), 1st edition, ICC, Barcelona.

Auvray, C.; Homand, F.; Sorgi, C. (2004): The aging of gypsum in underground mines. *Engineering Geology*, **74**, pp. 183-196.

Ayalew, L. (2000): *Weathered rock mass characterization considering uncertainty, with an example from Gilgel Gibe hydropower project in Ethiopia*. Ph.D. thesis TU Clausthal, Shaker Verlag, Aachen.

Azzoni, A.; Bailo, F.; Rondena, E. Zaninetti, A. (1996): Assessment of texture coefficient for different rock types and correlation with uniaxial compressive strength and rock weathering. *Rock Mechanics and Rock Engineering*, **29**(1), pp. 39-46.

Bakker, J.P.; Le Heux, J.W.N. (1946): Projective-geometric treatment of O. Lehmann's theory of the transformation of steep mountain slopes. *Proceedings Koninklijke Nederlandse Akademie van Wetenschappen (KNAW)*, **49**(5), pp. 533-547.

Bakker, J.P.; Le Heux, J.W.N. (1952): A remarkable new geomorphological law. The law of the denudation slope with recti-linear cross-profile I-III. *Proceedings Koninklijke Nederlandse Akademie van Wetenschappen (KNAW)*, **55**(4), pp. 399-410 and 554-571.

Barton, M.E.; Coles, B.J. (1984): The characteristics and rates of the various slope degradation processes in the Barton Clay Cliffs of Hampshire. *Quarterly Journal of Engineering Geology*, **17**, pp. 117-136.

Barton, N.; Lien, R.; Lunde, J. (1974): Engineering classification of rock masses for design of tunnel support. *Rock Mechanics*, **6**(4), pp. 189-236.

Battany, M.C.; Grismer, M.E. (2000): Rainfall runoff and erosion in Napa Valley vineyards: effects of slope, cover and surface roughness. *Hydrological Processes*, **14**, pp. 1289-1304.

Bauluz, B.; Mayayo, M.J.; Fernandez-Nieto, C.; Gonzalez Lopez, J.M. (2000): Geochemistry of Precambrian and Paleozoic siliciclastic rocks from the Iberian Range (NE Spain): implications for source-area weathering, sorting, provenance, and tectonic setting. *Chemical Geology*, **168**, pp. 135-150.

Bertran i Duarte, J.; Tarragó i Vidal, M. (2002): Els terratrèmols. El risc sísmic al Vallès i al litoral maresmenc i Barceloní. *Monographíc*, **17**, pp. 145-164.

Bhargava, O.N. (1995): The Bhutan Himalaya: A geological account. *Geological Survey of India, Special Publication No. 29.* pp. 13-14, 89-108.

Bland, W.; Rolls, D. (1998): *Weathering – An introduction to the scientific principles*. Arnold Publishers, London.

Boeglin, J.-L.; Probst, J.-L. (1998) Physical and chemical weathering rates and CO2 consumption in a tropical lateritic environment: the upper Niger basin. *Chemical Geology*, **148**, pp. 137-156.

Bouchard, M.; Jolicoeur, S. (2000): Chemical weathering studies in relation to geomorphological research in southeastern Canada. *Geomorphology*, **32**, pp. 213-238.

Boyce, W.E.; DiPrima, R.C. (1986): *Elementary differential equations and boundary value problems*. John Wiley and Sons, New York.

Brabb, E.E.; Harrod, B.L. (1989): *Landslides: extent and economic significance*. Balkema, Rotterdam.

Bryan, R.B. (2000): Soil erodibility and processes of water erosion on hillslope. *Geomorphology*, **32**, pp. 385-415.

Bryan, R.B.; Rockwell, D.L. (1998): Water table control on rill initiation and implications for erosional response. *Geomorphology*, **23**, pp. 151-169.

BS5930 (1981): *Code of practice for site investigations*. British Standards Institution, London.

BS5930 (1999): *Code of practice for site investigations*. British Standards Institution, London.

Calcaterra, D.; Gili, J.A.; Iovinelli, R. (1998): Shallow landslides in deeply weathered slates of the Sierra de Collcerola (Catalonian Coastal Range, Spain). *Engineering Geology*, **50**, pp. 283-298.

Cantón, Y.; Solé-Benet, A.; Queralt, I.; Pini, R. (2001): Weathering of a gypsum-calcareous mudstone under semi-arid environment at Tabernas, SE Spain: laboratory and field-based experimental approaches. *Catena*, **44**, pp. 111-132.

Cerdà, A.; García-Fayos, P. (1997): The influence of slope angle on sediment, water and seed losses on badland landscapes. *Geomorphology*, **18**, pp. 77-90.

Chandler, R.J.; Apted, J.P. (1988): The effect of weathering on the strength of London Clay. *Quarterly Journal of Engineering Geology*, **21**, pp. 59-68.

Chapagain, B. (2001): *Degradation of geotechnical properties of rock masses in engineering time: Tg22, Tg23, and Tg3*. M.Sc. thesis, ITC, Delft.

Chernick, M.R. (1999): *Bootstrap methods: a practitioner's guide*. Wiley, New York.

Chertkov, V. Y.; Ravina, I. (2000): Shrinking–swelling phenomenon of clay soils attributed to capillary-crack network. *Theoretical and Applied Fracture Mechanics*, **34**, pp. 61-67.

Chhetri, I.K. (2005): *Influence of method of excavation on weathering*. M.Sc. thesis, ITC, Enschede.

Chigira, M.; Nakamoto, M.; Nakata, E. (2002): Weathering mechanisms and their effects on the landsliding of ignimbrite subject to vapor-phase crystallization in the Shirakawa pyroclastic flow, northern Japan. *Engineering Geology*, **66**, pp. 111-125.

Chigira, M.; Oyama, T. (1999): Mechanism and effect of chemical weathering of sedimentary rocks. *Engineering Geology*, **55**, pp. 3-14.

Cindarto (1992). *Rock slope stability*. M.Sc. thesis, ITC, Delft.

Colman, S.M. (1981): Rock-weathering rates as functions of time. *Quaternary Research*, **15**(3), pp. 250-264.

Cooper, A.H.; Waltham, A.C. (1999): Subsidence caused by gypsum dissolution at Ripon, North Yorkshire. *Quarterly Journal of Engineering Geology*, **32**, pp. 305-310.

Curtis, C.D. (2003): The aqueous geochemistry of metals in the weathering environment: strengths and weaknesses in our understanding of speciation and process. *Mineralogical Magazine*, **67**(2), pp. 235-246.

Czerewko, M.A.; Cripps, J.C. (2001): Assessing the durability of mudrocks using the modified jar slake index test. *Quarterly Journal of Engineering Geology and Hydrogeology*, **34**, pp. 153-163.

Dagum, P.; Karp, R.; Luby, M.; Ross, S. (2000): An optimal algorithm of Monte Carlo estimation. *Siam Jornal of Computing*, 29(5), pp. 1484-1496.

Dearman, W.R. (1995): Description and classification of weathered rocks for engineering purposes: the background to the BS5930:1981 proposals. *Quarterly Journal of Engineering Geology*, **28**, pp. 267-276.

Dick, J.C.; Shakoor, A. (1995): Characterizing durability of mudrocks for slope stability purposes. In: Haneberg, W.C.; Anderson, S.A. (eds.): *Clay and Shale Slope Instability - Reviews in Engineering Geology Volume X*. The Geological Society of America, Boulder (Co.), pp. 121-130.

Dubelaar, C.W.; Koch, R.; Lorenz, H.G. (1997): Weathering of travertine in temperate humid climate, National Monument, Amsterdam, Netherlands. In: Marinos, P.G.; Koukis, G.C.; Tsiambaos, G.C.; Stournaras, G.C. (eds.): *Proceedings International Symposium on Engineering Geology and the Environment*. A.A. Balkema, Rotterdam, pp. 3135-3141.

Dupré, B.; Dessert, C.; Oliva, P.; Goddéris, Y.; Viers, J.; François, L.; Millot, R.; Gaillardet, J. (2003): Rivers, chemical weathering and Earth's climate. *Comtes Rendus Géoscience*, **335**, pp. 1141-1160.

Efron, B.; Tibshirani, R. (1998): *An introduction to the bootstrap*. Chapman & Hall/CRC, Boca Raton.

Ehlen, J. (1999): Fracture characteristics in weathered granites. *Geomorphology*, **31**, pp. 29-45.

Fan, J.-C.; Wu, M.-F. (2001): Effects of soil strength, texture, slope steepness and rainfall intensity on interrill erosion of some soils in Taiwan. In: Stott, D.E.; Mohtar, D.H.; Steinhardt, G.C. (eds.): *Sustaining the Global Farm. Selected papers from the 10th International Soil Conservation Organization Meeting, May 24-29, 1999.* International Soil Conservation Organization (http://www.iscohome.org/).

Feng, J.; Chuhan, Z.; Gang, W.; Guanglun, W. (2003): Creep modeling in excavation analysis of a high rock slope. *Journal of Geotechnical and Geoenvironmental Engineering*, **129**(9), pp. 849-857.

Fookes, P.G.; Dearman, W.R.; Franklin, J.A. (1971): Some engineering aspects of rock weathering with field examples from Dartmoor and elsewhere. *Quarterly Journal of Engineering Geology*, **4**, pp. 139-185.

Fookes, P.G.; Gourley, C.S.; Ohikere, C. (1988): Rock weathering in engineering time. *Quarterly Journal of Engineering Geology*, **21**, pp. 33-57.

Fookes, P.G.; Hawkins, A.B. (1988): Limestone weathering: its engineering significance and a proposed classification scheme. *Quarterly Journal of Engineering Geology*, **21**, pp. 7-31.

Fookes, P.G.; Sweeney, M. (1976): Stabilization and control of local rock falls and degrading rock slopes. *Quarterly Journal of Engineering Geology*, **9**, pp. 37-55.

Fookes, P.G.; Weltman, A.J. (1989a): Rock slopes: stabilization and remedial measures against degradation in weathered and fresh rock. *Proceedings of the Institution of Civil Engineers, Part 1*, **86**, pp. 359-380.

Fookes, P.G.; Weltman, A.J. (1989b): Discussion - Rock slopes: stabilization and remedial measures against degradation in weathered and fresh rock. *Proceedings of the Institution of Civil Engineers, Part 1*, **86**, pp. 1209-1211.

Fornis, R.;Vermeulen, H.R.; Nieuwenhuis, J.D. (2005): Kinetic energy-rainfall intensity relationship for Central Cebu, Philippines for soil erosion studies. *Journal of Hydrology*, **300**, pp. 20-32.

Francis, S.C. (1987): Slope development through the threshold concept. In: Anderson, M.G.; Richards, K.S. (eds.): *Slope stability*. John Wiley & Sons, London, pp. 601-624.

Franco Rodriguez, D.Y. (2001): *Slope stability and differential weathering along the road N420 near Tarragona, modelled in GIS*. M.Sc. thesis, ITC, Delft

Franks, C.A.M. (1999): Characteristics of some rainfall-induced landslides on natural slopes, Lantau Island, Hong Kong. *Quarterly Journal of Engineering Geology*, **32**, pp. 247-259.

Freyssenet, P.; Farah, A.S. (2000): Geochemical mass balance and weathering rates of ultramafic schists in Amazonia. *Chemical Geology*, **170**, pp. 133-151.

Gabbard, D.S.; Huang, C.; Norton, L.D.; G. C. Steinhardt, G.C. (1998): Landscape position, surface hydraulic gradients and erosion processes. *Earth Surface Processes and Landforms*, **23**(1), pp. 83-93.

Gabeta, E.J.; Burbanka, D.W.; Putkonen, J.K.; Pratt-Sitaulaa, B.A.; Ojhac, T. (2004): Rainfall thresholds for landsliding in the Himalayas of Nepal. *Geomorphology*, **63**, pp. 131-143.

Gansser, A. (1964). *Geology of the Himalaya*. Interscience, London.

Garcia-Vallès, M.; Topal, T.; Verndrell-Saz, M. (2003): Lichenic growth as a factor in the physical deterioration or protection of Cappadocian monuments. *Environmental Geology*, **43**, pp. 776-781.

Gardner, R.; Walsh, N. (1996): Chemical weathering of metamorphic rocks from low elevations in the southern Himalaya. *Chemical Geology*, **127**, pp. 161-176.

Geological Society Engineering Group Working Party Report (1995): The description and classification of weathered rocks for engineering purposes. *Quarterly Journal of Engineering Geology*, **28**, pp. 207-242.

Gökceoğlu, C.; Resat Ulusay, R.; Sönmez, H. (2000): Factors affecting the durability of selected weak and clay-bearing rocks from Turkey, with particular emphasis on the influence of the number of drying and wetting cycles. *Engineering Geology*, **57**, pp. 215-237.

Goodman, R.E. (1980): *Introduction to rock mechanics*. Wiley, New York.

Goudie, A.S. (1999): A comparison of the relative resistance of limestones to frost and salt weathering. *Permafrost and Periglacial Processes*, **10**, pp. 309-316.

Govindaraju, R.S. (1998): Effective erosion parameters for slopes with spatially varying properties. *Journal of Irrigation and Drainage Engineering*, **124** (2), pp. 81-88.

Grainger, P.; Harris, J. (1986): Weathering and slope stability on Upper Carboniferous mudrocks in south-west England. *Quarterly Journal of Engineering Geology*, **19**, pp. 155-173.

Guan, P.; Ng, C.W.W.; Sun, M.; Tang, W. (2001): Weathering indices for rhyolitic tuff and granite in Hong Kong. *Engineering Geology*, **59**, pp. 147-159.

Gupta, A.S.; Rao, K.S. (2000): Weathering effects on the strength and deformational behaviour of crystalline rocks under uniaxial compression state. *Engineering Geology*, **56**, pp. 257-274.

Gupta, A.S.; Rao, K.S. (2001): Weathering indices and their applicability for crystalline rocks. *Bulletin of Engineering Geology and the Environment*, **60**, pp. 201-221.

Hack, H.R.G.K. (1996): *Slope Stability Probability Classification*. Ph.D. thesis, ITC, Delft.

Hack, H.R.G.K. (1998): *Slope Stability Probability Classification,* 2nd edition. Ph.D. thesis, ITC, Delft.

Hack H.R.G.K.; Huisman M. (2002): Estimating the intact rock strength of a rock mass by simple means. In: Rooy, J.L. van; Jermy, C.A. (eds.) (2002): *Engineering Geology for Developing Countries - Proceedings of 9th Congress of the International Association for Engineering Geology and the Environment*. Durban, South Africa, 16 - 20 September 2002, pp. 1971-1977.

Hack, H.R.G.K.; Price, D.G. (1997): Quantification of weathering. In: Marinos, P.G.; Koukis, G.C.; Tsiambos, G.C.; Stournaras, G.C. (eds.): *Proceedings International Symposium on Engineering Geology and the Environment*. A.A. Balkema, Rotterdam, pp. 145-150.

Hack, H.R.G.K.; Price, D.G.; Rengers, N. (2003): A new approach to rock slope stability - a probability classification (SSPC). *Bulletin of Engineering Geology and the Environment,* **62**, article: pp. 167-184 & erratum: pp 185-185.

Hawkins, A.B. (1979): Case histories of some effects of solution/dissolution in the Keuper rocks of the Severn Estuary region. *Quarterly Journal of Engineering Geology*, **12**, pp. 31-40.

Heimsath, A.M.; Dietrich, W.E.; Nishiizumi, K.; Finkel, R.C. (1997): The soil production function and landscape equilibrium. *Nature*, **388**, pp. 358-361.

Hencher, S.R.; McNicholl, D.P. (1995): Engineering in weathered rock. *Quarterly Journal of Engineering Geology*, **28**, pp. 253-266.

Hernandez, E. (2002): *Rock mass classification, rock mass degradation and slope stability in the Middle Muschelkalk, in Tarragona province, Spain*. M.Sc. thesis, ITC, Delft.

Hodson, M.E.; Langan, S.J.; Kennedy, F.M.; Bain, D.C. (1998): Variation in soil surface area in a chronosequence of soils from Glen Feshie, Scotland and its implications for mineral weathering rate calculations. *Geoderma*, **85**, pp. 1-18.

Huisman, M. (2001): Case: Reconstruction of the N420 road in the province of Tarragona, Spain. *Ingeokring Newsletter*, nr. 9, Summer 2001, pp. 17-25.

Huisman, M.; Hack, H.R.G.K. (2002): Quantifying slope stability decrease in engineering lifetimes using bootstrap percentiles. In: Dinis da Gama, C.; Ribeiro e Sousa, L. (eds.): *Proceedings Eurock 2002 - I.S.R.M. International Symposium on Rock Engineering for Mountainous Regions, Madeira, Portugal, November 2002*, pp. 197-204. Publ. Sociedade Portuguesa de Geotecnia, Portugal.

Huisman, M.; Hack, H.R.G.K.; Nieuwenhuis, J.D. (2004): Observed rock mass degradation and resulting slope instability. In: Schubert, W. (ed.): *Rock Engineering – Theory and Practice. Proceedings of the ISRM Regional Symposium Eurock 2004 & 53rd Geomechanics Colloquy*. Verlag Glückauf, Essen, Germany, ISBN 3-7739-5995-8, pp. 449-452.

Huisman, M.; Hack, H.R.G.K.; Nieuwenhuis, J.D. (2006): Predicting rock mass decay in engineering lifetimes: The influence of slope aspect and climate. *Environmental & Engineering Geoscience*. **12** (1), pp. 39-51.

Hutchinson, J.N. (1998): A small-scale field check on the Fisher-Lehmann and Bakker-Le Heux cliff degradation models. *Earth Surface Processes and Landforms*, **23**, pp. 913-926.

Hutchinson, J.N. (2001): Reading the ground: Morphology and geology in site appraisal. *Quarterly Journal of Engineering Geology and Hydrogeology*, **34**, pp. 7-50.

IGME (Instituto Geologico y Minero de España): *Mapa geologico de España (1:50.000), Segunda serie, Primera edición.* Map sheets 444/32-17 (Flix) (1979), 445/33-17 (Cornudella) (1978), 471/32-18 (Mora de Ebro) (1981), 472/33-18 (Reus) (1980). IGME, Madrid.

Indraratna, B.; Ranjith, P.G.; Gale, W. (1999): Single phase water flow through rock fractures. *Geotechnical and Geological Engineering*, **17**, pp. 211-240.

Inkpen, R.J.; Jackson, J. (2000): Contrasting weathering rates in coastal, urban and rural areas in southern Britain: preliminary investigations using gravestones. *Eart Surface Processes and Landforms*, **25**, pp. 229-238.

Irfan, T.Y.; Dearman, W.R. (1978): Engineering petrography of a weathered granite. *Quarterly Journal of Engineering Geology*, **11**, pp. 233-244.

Jaboyedoff, M.; Baillifard, F.; Bardou, E.; Girod, F. (2004): The effect of weathering on Alpine rock instability. *Quarterly Journal of Engineering Geology and Hydrogeology*, **37**, pp. 95-103.

Jessel, M.; Bons, P.; Evans, L.; Barr, T.; Stüwe, K. (2001): Elle: the numerical simulation of metamorphic and deformation microstructures. *Computers & Geosciences*, **27**, pp. 17-30.

Jiang, K.; Esaki, T. (2002): Quantitative evaluation of stability changes in historical stone bridges in Kagoshima, Japan, by weathering. *Engineering Geology*, **63**, pp. 83-91.

Jong, G. de (2003): *The quantification of weathering and erosion in engineering time*. M.Sc. thesis, Delft University of Technology, Delft.

Katz, O.; Reches, Z.; Roegiers, J.-C. (2000): Evaluation of mechanical rock properties using a Schmidt Hammer. *International Journal of Rock Mechanics and Mining Sciences*, **37**, pp. 723-728.

Kemeny, J. (2004): Time-dependent drift degradation due to the progressive failure of rock bridges along discontinuities. *International Journal of Rock Mechanics and Mining Sciences*, **42**(1), pp. 35-46.

Kim, S.; Park, H.D. (2003): The relationship between physical and chemical weathering indices of granites around Seoul, Korea. *Bulletin of Engineering Geology and the Environment*, **62**, pp. 207-212.

Knott, D. (2004): Personal communication.

Kouokam, E. (1993): Compilation of all Falset data to final report on engineering geological map. M.Sc. thesis, ITC, Delft.

Krömmelbein, K. (ed.) (1976): *Brinkmanns Abriß der Geologie, Band II: Historische Geologie (10./11. Auflage).* Ferdinand Enke Verlag, Stuttgart.

Kuchitsu, N.; Ishizaki, T.; Nishiura, T. (1999): Salt weathering of the brick monuments in Ayutthaya, Thailand. *Engineering Geology*, **55**, pp. 91-99.

Kühnel, R.A. (2002): Driving forces of rock degradation. In: Galán and Zezza (eds.): *Proceedings Protection and Conservation of the Cultural Heritage of the Mediterranean Cities, Sevilla, Spain*, A.A. Balkema, Rotterdam, pp. 11-17.

Kühnel, R.A. (2003): Personal communication.

Kühnel, R.A. (2004): Cause and consequence: volume changes behind building material deterioration. *Materials Characterization*, **53**(2-4), pp. 171-180

Kühnel, R.A.; Gaast, S.J. van der; Brych, J.; Laan, G.J.; Kulnig, H. (1994): The role of clay minerals in durability of rocks: observations on basaltic rocks. *Applied Clay Science*, **9**, pp. 225-237.

Kühnel, R.A.; Tshibangu Katshi, J.-P. (1997): Causes of basalt degrading: methods of prediction of basalt durability. In: *Proceedings of the Sixth Euroseminar on Microscopy Applied to Building Materials, June 25-27, 1997, Reykjavik, Iceland*.

Kühnel, R.A.; Tshibangu Katshi, J.-P. (1999): Natural stone used for building, construction or monumental purposes: new trends in quality control. In: Petersen, H.S.; Larbi, J.A.; Janssen, H.H.A. (eds.): *Proceedings of the 7th Euroseminar on Microscopy Applied to Building Materials, June 29 – July 2, 1999, Delft, the Netherlands*.

Laubscher, D.H. (1990): A geomechanics classification system for the rating of rock mass in mine design. *Journal of the South African Institute of Mining and Metallurgy*, October 1990, pp. 257-272.

Lee S.G.; Freitas, M.H. De (1988): Quantitative definition of highly weathered granite using the slake durability test. *Geotechnique*, **38**, pp. 635-640.

Lindsay, P.; Anderson, J.; Bourke, F.; Campbell, R.N.; Clarke, L. (2000): Predicting slope stability in open pit gold and coal mines. In: *2000 New Zealand Minerals & Mining Conference Proceedings*. Crown Minerals, Wellington.

Lineback Gritzner, M.; Marcus, W.A.; Aspinall, R.; Custer, S.G. (2001): Assessing landslide potential using GIS, soil wetness modeling and topographic attributes, Payette River, Idaho. *Geomorphology*, **37**, pp. 149-165.

López-Gómez, J.; Mas, R.; Arche, A. (1993): The evolution of the Middle Triassic (Muschelkalk) carbonate ramp in the SE Iberian ranges, eastern Spain: sequence stratigraphy, dolomitization processes and dynamic controls. *Sedimentary Geology*, **87**, pp. 165-193.

Martin, R.P. (1986): Use of index tests for engineering assessment of weathered rocks. In: *Proceedings of the 5th International IAEG Congress, Buenos Aires 1986*. International Association of Engineering Geology and the Environment (IAEG). pp. 433-450.

Martin, Y. (2000): Modelling hillslope evolution: linear and nonlinear transport relations. *Geomorphology*, **34**, pp. 1-21.

Masana, E. (1994): Neotectonic features of the Catalan coastal ranges, northeastern Spain. *Acta Geologica Hispanica*, **29**(2-4), pp. 107-121.

Matsukura, Y. ; Hirose, T. (1999): Five year measurements of rock tablet weathering on a forested hillslope in a humid temperate region. *Engineering Geology*, **55**, pp. 69-76.

Matsukura, Y.; Takahashi, K. (1999): A new technique for rapid and non-destructive measurement of rock-surface moisture content; preliminary application to weathering studies of sandstone blocks. *Engineering Geology*, **55**, pp. 113-120.

Meisina, C. (2004): Swelling-shrinking properties of weathered clayey soils associated with shallow landslides. *Quarterly Journal of Engineering Geology and Hydrogeology*, **37**, pp. 77-94.

Mellon, P. (1985): *An investigation of altered basalts used for road aggregate in Ethiopia*. Ph.D. thesis, Hatfield Polytechnic, Hatfield.

Millot, R.; Gaillardet, J.; Dupré, B.; Allègre, C.J. (2002): The global control of silicate weathering rates and the coupling with physical erosion: new insights from rivers of the Canadian Shield. *Earth and Planetary Science Letters*, **196**, pp. 83-98.

Morad, S.; Al-Aasm, I.S. Longstaff, F.J.; Marfil, R.; Ros, L.F. de; Johansen, H.; Marzo, M. (1995): Diagenesis of a mixed siliclastic/evaporitic sequence of the Middle Muschelkalk (Middle Triassic), the Catalan coastal roange, NE Spain. *Sedimentology*, **42**, pp. 749-768.

Neil, D. (1989): Weathering rates of a subaerially exposed marble in eastern Australia. *Zeitschrift für Geomorphologie*, **33** (4), pp. 463-473.

Nicholson, D.T. (2001a): *Deterioration of excavated rockslopes: mechanisms, morphology and assessment*. Ph.D. thesis, University of Leeds, Leeds.

Nicholson, D.T. (2001b): Pore properties as indicators of breakdown mechanisms in experimentally weathered limestones. *Earth Surface Processes and Landforms*, **26**, pp. 819-838.

Nicholson, D.T. (2003): Breakdown mechanisms and morphology for man-made rockslopes in North West England. *North West Geography*, **3**, pp. 12-26.

Nicholson, D.T.; Lumsden, A.C. (2000): Excavation-induced deterioration of rock slopes. In: Bromhead, E.; Dixon, N.; Ibsen, M.L. (eds.): *Landslides in research, theory and practice – Proceedings of the 8th international symposium on landslides*, Thomas Telford, London, pp. 1105-1110.

Nicholson, D.T.; Nicholson, F.H. (2000): Physical deterioration of sedimentary rocks subjected to experimental freeze-thaw weathering. *Earth Surface Processes and Landforms*, **25**, pp. 1295-1307.

Nieuwenhuis, J.D. (1991a): *Variations in stability and displacements of a shallow seasonal landslide in varved clays*. Balkema, Rotterdam.

Nieuwenhuis, J.D. (1991b): *The lifetime of a landslide; investigations in the French Alps*. Balkema, Rotterdam.

Nieuwenhuis, J.D. (2002): Displacement observations of large land-slides and their interpretation. In: Barends, F.B.J.; Steijger, P.M.P.C. (eds.): *Learned and Applied - Soil Mechanics out of Delft,* Balkema, Rotterdam, pp. 195-200.

Nieuwenhuis, J.D. (2004): Personal communication.

Nieuwenhuis, J.D. (2006): Personal communication.

Nilsen, B. (2000): New trends in rock slope stability analyses. *Bulletin of Engineering Geology and the Environment*, **58**, pp. 173-178.

Nova, R. (1997): On the modelling of the mechanical effects of diagenesis and weathering. *ISRM News Journal*, **4** (2), pp. 15-20.

Ollier, C.D. (1975): *Weathering*. Longman Group Ltd., London.

Ortigao, J.A.R.; Sayao, A. (eds.) (2004): *Handbook of slope stabilisation*. Springer Verlag, Berlin.

Parker, D.B.; Michel, T.G.; Smith, J.L. (1995): Compaction and water velocity effects on soil erosion in shallow flow. *Journal of Irrigation and Drainage Engineering*, **121** (2), pp. 170-178.

Pejon, O.J.; Zuquette, L.V. (2002): Analysis of cyclic swelling of mudrocks. *Engineering Geology*, **67**, pp. 97-108.

Pera, E. Le; Sorriso-Valvo, M. (2000): Weathering and morphogenesis in a Mediterranean climate, Calabria, Italy. *Geomorphology*, **34**, pp. 251-270.

Pope, G.A.; Dorn, R.I., Dixon, J.C. (1995): A new conceptual model for understanding geographical variations in weathering. *Annals of the Association of American Geographers*, **85**(1), pp. 38-64.

Price, D.G. (1993): A suggested method for the classification of rock mass weathering by a ratings system. *Quarterly Journal of Engineering Geology*, **26**, pp. 69-76.

Price, D.G. (1995): Weathering and weathering processes. *Quarterly Journal of Engineering Geology*, **28**, pp. 243-252.

Raff, D.A.; Ramírez, J.A.; Smith, J.L. (2004): Hillslope drainage development with time: a physical experiment. *Geomorphology*, **62**, pp. 169-180.

Regüés, D.; Pardini, G.; Gallart, F. (1995): Regolith behaviour and physical weathering of clayey mudrock as dependent on seasonal weather conditions in a badland area at Vallcebre, Eastern Pyrenees. *Catena*, **25**, pp. 199-212.

Rengers, N.; Huisman, M.; Hack, H.R.G.K.; Rupke, J. (2001): Quantification of engineering geological parameters: GIS-based slope instability hazard and risk assessment. *Felsbau*, **19** (5), pp. 102-106.

Robinson, D.A.; Williams, R.B.G. (1996): An analysis of the weathering of Wealden sandstone churches. In: Smith, B.J.; Warke, P.A. (eds.): *Processes of urban stone decay*. Donhead Publishing, London, pp. 133-149.

Robinson, D.A.; Williams, R.B.G. (2000): Experimental weathering of sandstone by combinations of salts. *Earth Surface Processes and Landforms*, **25**, pp. 1309-1315.

Roose, E. (1996): *Land husbandry – Components and strategy*. FAO Soils Bulletin 50, Food and Agriculture Organization of the United Nations, Rome.

Rupke, J.; Cammeraat, E.; Seijmonsbergen, A.C.; Westen, C.J. van (1988): Engineering geomorphology of the Widentobel catchment, Appenzell and Sankt Gallen, Switzerland: a geomorphological inventory system applied to geotechnical appraisal of slope stability. *Engineering Geology*, **26**, pp. 33-68.

Ruxton, B.P. (1968): Rates of weathering of Quaternary volcanic ash in north-east Papua. *Journal of Geology*, 76, pp. 518-527.

Santi, P.M. (1995): Assessing the strength and durability properties of shales. In: Keefer, D.K.; Ho, C.L. (eds.): *Landslides Under Static and Dynamic Conditions - Analysis, Monitoring, and Mitigation*. ASCE Geotechnical Special Publication No. 52, pp. 37-55.

Saunders, M.K.; Fookes, P.G. (1970): A review of the relationship of rock weathering and climate and its significance to foundation engineering. *Engineering Geology*, **4**, pp. 289-325.

Selby, M.J. (1993): *Hillslope materials and processes*. Oxford University Press, Oxford.

Semhi, K.; Suchet, P.A.; Clauer, N.; Probst, J.-L. (2000): Impact of nitrogen fertilizers on the natural weathering-erosion processes and fluvial transport in the Garonne basin. *Applied Geochemistry*, **15**, pp. 865-878.

Shakoor, A. (1995): Slope stability considerations in differentially weathered mudrocks. In: Haneberg, W.C.; Anderson, S.A. (eds.): *Clay and Shale Slope Instability - Reviews in Engineering Geology Volume X*. The Geological Society of America, Boulder (Co.), pp. 131-138.

Shakya, N.M.; Chander, S. (1998): Modelling of hillslope runoff processes. *Environmental Geology*, **35**(2-3), pp. 115-123.

Sigaran, C. (2005): Personal communication.

Sjöberg, R.; Broadbent, N. (1991): Measurement and calibration of weathering using the Schmidt hammer, on wave washed moraines on the upper Norrland coast, Sweden. *Earth Surface Processes and Landforms*, **16**, pp. 57-64.

Slob, S.; Hack, H.R.G.K. (2004): 3D terrestrial laser scanning as a new field measurement and monitoring technique. In: Hack; H.R.G.K.; Azzam, R.; Charlier, R. (eds.): *Engineering Geology for Infrastructure Planning in Europe. A European Perspective*. Springer Verlag, Berlin, pp. 179-190.

Smith, B.J.; Warke, P.A.; Moses, C.A. (2000): Limestone weathering in contemporary arid environments: a case study from southern Tunisia. *Earth Surface Processes and Landforms*, **25**, pp. 1343-1354.

Smith, M.R.; Collis, L. (1993): *Aggregates – Sand, gravel and crushed rock for construction purposes*, 2nd edition. The Geological Society, London.

Smyth, C.G.; Royle, S.A. (2000): Urban landslide hazards: incidence and causative factors in Nitorói, Rio de Janeiro State, Brazil. *Applied Geography*, **20**, pp. 95-117.

Stewart, B.W.; Capo, R.C.; Chadwick, O.A. (2001): Effects of rainfall on weathering rate, base cation provenance, and Sr isotope composition of Hawaiian soils. *Geochimica et Cosmochimica Acta*, **65**, pp. 1087-1099.

Stomph, T.J.; Ridder, N. de; Giesen, N.C. van de (2001): A flume design for the study of slope length effects on runoff. *Earth Surface Processes and Landforms*, **26**, pp. 647-655.

Stonestrom, D.A.; White, A.F.; Akstin, K.C. (1998): Determining rates of chemical weathering in soils – solute transport versus profile evolution. *Journal of Hydrology*, **209**, pp. 331-345.

Stretch, R.C.; Viles, H.A. (2002): The nature and rate of weathering by lichens on lava flows on Lanzarote. *Geomorphology*, **47**, pp. 87-94.

Tang, T. (1998): Field Testing of Rock Hardness and Its Relationship to Limestone Dissolution in Guilin, Southern China. *Middle States Geographer*, **31**, pp. 15-22.

Taylor-Firth, A.; Laycock, E.A. (1999): Weathering simulation for durability assessment of the in-service performance of construction materials. *Quarterly Journal of Engineering Geology*, **32**, pp. 291-301.

Tegtmeier, W. (2005): *Numerical modelling of rock mass decay in road cuts*. M.Sc. thesis, Delft University of Technology, Delft.

Trudgill, S.T. (2000): Weathering overview – measurement and modelling. In: Viles, H.A. (ed.): Recent advances in field and laboratory studies of rock weathering. *Zeitschrift für Geomorphologie*, Supplementband, 120, pp. 187-193.

Trudgill, S.T.; Viles, H.A. (1998): Field and laboratory approaches to limestone weathering. *Quarterly Journal of Engineering Geology*, **31**, pp. 333-341.

Trudgill, S.T.; Viles, H.A.; Inkpen, R.J.; Moses, C.; Gosling, W.; Yates, T.; Collier, P.; Smith, D.I.; Cooke, R.U. (2001): Twenty-year weathering remeasurements at St. Paul's Cathedral, London. *Earth Surface Processes and Landforms*, **26**, pp. 1129-1142.

Vaughan, P.R.; Maccarini, M.; Mokhtar, S.M. (1988): Indexing the engineering properties of residual soil. *Quarterly Journal of Engineering Geology*, **21**, pp. 69-84.

Vecsei, A. (1998): A sandy tidal coast in the uppermost Muschelkalk and the origin of the Muschelkalk/Keuper boundary in the southwestern Germanic basin. *Geologischer Rundschau*, **86**, pp. 835-851.

Vecsei, A.; Mandau, T. (2002): Redbeds from the Middle Muschelkalk (Middle Triassic) of the SW Germanic Basin: arid environments from Pangea's interior. *International Journal of Earth Sciences (Geologischer Rundschau)*, **91**, pp. 111-122.

Vicente Silvestre, M.; Ribeiro e Sousa, L.; Hack, H.R.G.K. (2002): Laboratory study of geometrical and hydro-mechanical characteristics of discontinuities. International Society for Rock Mechanics (ISRM), News Journal, **7**(2), pp. 9-23.

Viles, H.A. (ed.) (2000): Recent advances in field and laboratory studies of rock weathering. *Zeitschrift für Geomorphologie,* Supplementband 120.

Wetzel, A.; Einsele, G. (1991): On the physical weathering of various mudrocks. *Bulletin of the International Association of Engineering Geology*, (44), pp. 89-99.

White, A.F.; Brantley, S.L. (2003): The effect of time on the weathering of silicate minerals: why do weathering rates differ in the laboratory and field? *Chemical Geology*, **202**, pp. 479-506.

Williams, D.M.; McNamara, K. (1992): Limestone to dolomite to dedolomite conversion and its effect on rock strength: a case study. *Quarterly Journal of Engineering Geology*, **24**, pp. 131-135.

Williams, R.G.B.; Robinson, D.A. (2000): Effects of aspect on weathering: anomalous behaviour of sandstone gravestones in southeast England. *Earth Surface Processes and Landforms*, **25**, pp. 135-144.

Winkler, E.M. (1997): *Stone in architecture: Properties and durability*, 3rd edition. Springer-Verlag, New York.

Woldearegay, K.; Onrust, R.T. (2002): Decay of geotechnical properties of slope rock mass within engineering lifetime. In: Ciesielczuk, J.; Ostaficzuk, S. (eds.): *Landslides: Proceedings of the Tenth International Conference and Fieldtrip on Landslides (ICFL), Polish Lowlands/Carpathians/Baltic Coast/Poland, September 6-16.* Mineral and Energy Economy Research Institute, Polish Academy of Sciences, Krakow, Poland, pp. 169-179.

Wüst, R.A.J.; McLane, J. (2000): Rock deterioration in the Royal Tomb of Seti I, Valley of the Kings, Luxor, Egypt. *Engineering Geology*, **58**, pp. 163-190.

Xie, Y.; Elsen, E. van den; Liu, B.Y.; Trouwborst, K.O.; Ritsema, C.J.; Wu, Y.Q.; Zhang, W.B. (2002): Soil moisture distribution and runoff generation in a gully system. In: *Proceedings of the 12th International Soil Conservation Organization (ISCO) Conference, May 26-31, 2002. Beijing, China, Volume II.* Ministry of Water Resources, Beijing, China.

Yeo, I.W.; Freitas, M.H. De; Zimmerman R.W. (1998): Effect of shear displacement on the aperture and permeability of a rock fracture. *International Journal of Rock Mechanics and Mining Sciences*, **35**, pp. 1051-1070.

Zhang, J.; Jiao, J.J.; Yang, J. (2000): In situ rainfall infiltration studies at a hillside in Hubei Province, China. *Engineering Geology*, **57**, pp. 31-38.

Symbols and abbreviations

A	constant defining weathering penetration rate	[-]
a	cotangent of stable slope angle for scree, cot(α)	[-]
a^*	coefficient	[-]
a^{**}	coefficient	[-]
B	constant defining weathering penetration rate	[1/m]
b	cotangent of initial slope angle at time of excavation, cot(β)	[-]
b^*	coefficient	[-]
b^{**}	coefficient	[-]
c	1-volume of rock/volume of scree	[-]
c_1	coefficient	[-]
c_2	coefficient	[-]
D_w	penetration depth of weathering (perpendicular to slope surface)	[m]
$D_{w,y}$	penetration depth of weathering (in direction of y)	[m]
h	slope height	[m]
I	parameter for weathering intensity	[-]
i	parameter defining LHS interval	[-]
K	coefficient	[-]
N	number of simulations per data point	[-]
n	exponent	[-]
P	property (glass amount) at some time t	[-]
P_0	initial property (glass amount)	[-]
P_v	production of weathered material	[m³/year]
pWE_{low}	probability that the true WE value is (one class) lower than the observed WE value	[-]
pWE_{cor}	probability that the true WE value is equal to the observed WE value	[-]
pWE_{high}	probability that the true WE value is (one class) higher than the observed WE value	[-]
$R^{app}{}_{WE}$	apparent weathering intensity rate	[1/log(year)]
$R^{dyn}{}_{WE}$	dynamic weathering intensity rate	[1/log(year)]
R_s	rate of angular slope retreat	[°/year]
S	$-h^2 - y^2 + 2cy$	[m²]

SWE	weathering intensity parameter for the SRM (defined in SSPC)	[-]
t	time	[year]
V	volume	[m^3]
V_0	total volume of material weathered after excavation	[m^3]
V_1	volume of material weathered after excavation and still present on slope	[m^3]
V_2	volume of material weathered after excavation and eroded from slope	[m^3]
W_s	coefficient for weathering penetration rate	[m]
$W(x)$	Inverse function of xe^x	
WE	weathering intensity parameter (defined in SSPC)	[-]
WE_{init}	initial weathering intensity parameter at time of excavation	[-]
WE_t	weathering intensity parameter after some time t	[-]
x	horizontal coordinate parallel to slope strike	[m]
y	horizontal coordinate perpendicular to slope strike	[m]
y_e	y-coordinate of eroded rock profile	[m]
y_{int}	y-coordinate of interception between scree wedge and eroded rock	[m]
y_s	y-coordinate of scree profile	[m]
y_{ult}	ultimate y-coordinate of slope crest after linear slope retreat	[m]
y_w	y-coordinate of weathering penetration front	[m]
z	vertical coordinate	[m]
z_{int}	z-coordinate of interception between scree wedge and eroded rock	[m]
α	stable slope angle for scree	[°]
β	initial slope angle at time of excavation	[°]
γ	inclination of the apex line through the crest and toe of the slope	[°]
δ	slope angle	[°]
σ	standard deviation	
ϕ_V	volume flux of weathered material in or out of control volume	[m^3/year]

BS	Bedding Spacing
ERM	Exposure Rock Mass (defined in SSPC)
GIS	Geographical Information System
GMT	Greenwich Mean Time
IAEG	International Association for Engineering Geology and the Environment
ICC	Institut Cartogràphic de Catalunya
IGME	Instituto Geologico y Minero de España
IDNDR	International Decade of Natural Disaster Reduction (1990-2000, instituted by United Nations)
IRS	Intact Rock Strength (defined in SSPC)
ISRM	International Society for Rock Mechanics
ITC	International Institute for Geo-information Science and Earth Observation
KNGMG	Koninklijk Nederlands Geologisch Mijnbouwkundig Genootschap (Royal Geological and Mining Society of the Netherlands)
LIDAR	LIght Detection And Ranging
MBA	Methylene Blue Adsorption
MRMR	Mining Rock Mass Rating
RMR	Rock Mass Rating
RQD	Rock Quality Designation
RRM	Reference Rock Mass (defined in SSPC)
SEM	Standard Error of the Mean
SRM	Slope Rock Mass (defined in SSPC)
SSPC	Slope Stability Probability Classification
UCS	Unconfined Compressive Strength
UTM	Universal Transverse Mercator projection
XRD	X-Ray Diffraction
XRF	X-Ray Fluorescence
XMET	Xarxes METeorològiques

Glossary

Bedding	
… planes	In sedimentary rocks, the planes separating the individual layers. Bedding planes follow the original sedimentation layering.
… spacing	The perpendicular distance between two bedding planes. Within a single engineering geological unit the characteristic bedding spacing is taken as the average perpendicular distance between each two neighbouring bedding planes in that unit.
Block size	The dimensions of the individual blocks that constitute a rock mass and are separated by discontinuities.
Bootstrap	A statistical method in which hypothetical data is generated with data simulation techniques such as Monte Carlo or Latin Hypercube sampling, based on a known or estimated probability distribution. The amount of hypothetical data is used to infer statistical properties of the original variable.
… percentiles	Fractions of the generated data or calculation outcome resulting from a bootstrap simulation.
Case hardening	A weathering process in which dissolves material constituents precipitate on the rock or soil surface where the water in which they were dissolved evaporates. This process builds a crust on the surface that is often stronger than the material underneath it (which is affected by dissolution weathering).
Classification	In the context of this research a systematic description of a rock mass, commonly with a geotechnical goal (such as estimating slope stability). The descriptions of a classification may be qualitative or quantitative. Qualitative descriptions (e.g. the weathering degree) are often standardized.

Data simulation	A process in which random data is generated based on a probability distribution. Large amounts of simulated data will show a population histogram that corresponds to the initial probability distribution.
Decay	The combined action of relaxation, weathering and erosion, leading to alteration and disintegration of materials and rock masses.
… situations	Since decay is a combination of several processes, various situations exist depending on the balance between the primary processes. In this thesis a differentiation is made into situations with an imbalance favouring erosion (erosion delimited), with equilibrium between weathering penetration and erosion, and an imbalance favouring weathering (weathering delimited).
Discontinuity	In the context of this thesis, a mechanical interface in a rock mass. This may be a bedding plane, joint plane, crack, etc. Next to mechanical discontinuities, so-called integral discontinuities may exist in a rock mass: planes of changing properties (e.g. material composition or strength) that have not yet developed into mechanical discontinuities.
… aperture	An often poorly defined parameter quantifying the "open-ness" of a discontinuity. Often a width of the discontinuity is taken as the aperture, but this is only a true descriptor if the discontinuity planes are parallel. In all other cases the width of a discontinuity will change along it, and this is directly linked to the discontinuity roughness. The aperture can also be defined in terms of hydraulic conductivity, although this is a combination of the geometry of the discontinuity planes (that influence flow resistance) and the factual "open-ness".
… spacing	The (average) shortest distance between discontinuities of one orientation set.

Dissolution	Chemical weathering process in which ions are released after a reaction of minerals with water. Generally, dissolution is enhanced by low pH values, and mainly affects carbonates and evaporites.
Engineering lifetime	The duration for which an engineering work shall remain serviceable.
Erosion	The removal and transport of material, destroying the rock mass structure, for example by water, gravity, or wind. Effects of natural erosion processes are most pronounced in soils and relatively weak rocks or rock masses with many discontinuities and a small block size.
… delimited	A decay situation in which both erosion and weathering occur, with an imbalance favouring weathering. The slope development is controlled by the prevailing erosion rate.
… rate	The rate of retreat of a (slope) surface due to erosion, usually expressed as change of depth per unit time, or eroded mass per unit time.
Excavation damage	The structural damage inflicted on the mass and material underlying a slope due to the method of excavation. Also known as back-break.
Exposure time	The duration over which a road cut has been exposed, equal to the time since excavation.
Factor of safety	A determistic parameter, in the context of this thesis quantifying slope stability. Defined as the ratio of forces or moments resisting movement and those promoting movement.
Freeze-thaw	Mechanical weathering process in which water repeatedly freezes and thaws, with associated expansion and contraction of the water and strains and stresses in the surrounding material.
Geotechnical soil	See soil.
Hydration	Chemical weathering process in which water molecules are added to molecules, usually ferric oxides.
De-…	Dehydration is a chemical weathering

	process in which water is released from molecules, usually evaporitic minerals. An example is dehydration of gypsum, resulting in water and anhydrite.
Hydrolysis	Chemical weathering process in which acids react with silicate minerals, releasing silica and metal cations.
Ion exchange	Chemical weathering process in which cations present in a solution in contact with clay minerals are exchanged with cations present in the clay lattices. This leads to a change in the type of clay mineral and the material properties. An example is the exchange of sodium by calcium in montmorillonite clay, greatly reducing the plasticity and swelling capacity.
Latin Hypercube sampling	A stratified sampling method in which hypothetical data is generated based on the unique combination of a cumulative probability and the variable value. The cumulative probability interval for a parameter is stratified, in each sub-interval a random probability is chosen, and the corresponding variable value taken as simulated data. In each of the sub-intervals intervals, only one random number and therefore only one simulated parameter value is generated.
LIDAR	LIght Detection And Ranging; a surface scanning method in which the reflection of a laser beam is recorded together with its travel time from the scanner and the direction in which the beam was transmitted. Together these give a three-dimensional coordinate of the reflection point. Modern LIDAR scanners produce a three-dimensional point cloud of the surroundings visible from the camera standpoint.
MBA	Methylene Blue Adsorption; a value registering the amount of Methylene Blue that can be adsorbed per unit mass of a material. This parameter is used for discerning clay types. Clays with higher swelling capacity show a higher MBA value.

Monte Carlo sampling	An unsorted sampling method in which hypothetical data is generated based on the unique combination of a cumulative probability and the variable value. By choosing a random probability, the corresponding variable value is taken as simulated data. Repeating this procedure generates a data set with ultimately the similar probability distribution as was used to generate the data. In the generation of random numbers, there is no restriction by the numbers that were generated in previous steps, and therefore two or more identical parameter values may be generated.
MRMR	Mining Rock Mass Rating; a classification system which is a further development of the RMR system (see RMR). Main use is determining rock mass quality for underground excavations.
Mudstone	In the context of this thesis, mudstone is used as a general term and includes clay, silt, siltstone, claystone, shale and argillite. The term mudstone is commonly applied to fine-grained rocks that rapidly decompose.
Oxidation	Chemical weathering process in which electrons are released from elements, resulting in oxides, or hydroxides if water is present. The reversal of reduction.
Pelitoclastesis	The formation of fine debris called pelitoclasts through the process of slaking, as a result of wetting and drying.
Permeability	The property of a porous medium that quantifies the resistance to the flow of a liquid through that medium.
Porosity	The fraction of a multiphase system occupied by voids.
Probability distribution	The relation between a particular value of a (stochastic) variable and the probability of its occurrence.

Q-system	A classification system expressing the quality of a rock mass with the computed Q-value. Originally developed to describe the quality of a rock mass for underground excavations with the specific goal of determining the support requirements.
Rebound	See relaxation
Reduction	Chemical weathering process in which electrons are added to elements. The reversal of oxidation.
Relaxation	The term used in this thesis to describe redistribution of stress and strain, leading to loss of structural integrity, following lowering of the confining stress level. The term rebound is frequently used in literature to describe (some of) the effects of relaxation.
RMR	Rock Mass Rating; a classification system developed to determine rock mass quality for underground excavations. The RMR is a point rating method with a final rating ranging from 0 (very poor rock for tunnelling) to 100 (very good rock for tunnelling).
Rock	In the context of this thesis lithified, cemented material, without necessarily referring to its unconfined compressive strength that is often the basis for the definition of rock in classification systems. This may include what is often described as "geotechnical" soils – materials that are rock according to classification systems, but geotechnically behave as a soil because of their small strength. Weathering intensity plasy a role in this; see soil.
RQD	Rock Quality Designation; a parameter used to quantify rock core recovery. RQD is defined as the cumulative length of all core fragments longer than 100mm divided by the total core length. Optimal core diameter for determining RQD is 47.5mm.
Safety factor	See factor of safety

Slake durability	The resistance of a material to slaking under the influence of wetting and drying, determined by an index test measuring the material loss after a number of wetting-drying cycles.
Slaking	The disintegration of a material (usually weak rock or soil containing clay) when saturated with water. Most detrimental with cyclic wetting and drying.
Slope	
… aspect	A term often used for the dip direction of the slope face.
… orientation	The dip direction of the slope face.
… retreat	The backward migration of a slope face because of erosion.
… stability	Qualitatively, the intrinsic resistance to mechanical failure of any scale. Qualtitatively, this may be expressed with a factor of safety or with a probability to be stable or unstable. Often, an ill-defined differentiation is made regarding the scale of failure that is regarded. Small failures are often not considered in describing slope stability and many stability assessment methods typically analyze deep-seated failure incorporating large volumes.
Soil	In the context of this thesis: unconsolidated material, or material in which cementation has been destroyed completely. The distinction between weak rock and soil is problematic since materials classified as weak rocks may behave as soils in several aspects. It has to be noted that with an increasing weathering intensity, a rock effectively is transformed into a soil. In the context of this thesis, reference is made to rocks (e.g. the Keuper shales) that may in fact behave as soils in all important aspects in the weathered state in which they are encountered in the field, but are rocks in their initial unweathered state.

SSPC	Slope Stability Probability Classification; a classification method yielding the data for a probabilistic slope stability analysis. This classification method is used to collect the data presented in this thesis.
Strain	A dimensionless quantity of deformation, either one-, two- or three-dimensional, defined as linear, areal, or volumetric compression or extension divided by original length, area or volume.
Unconsolidated soil	See soil.
Undercutting	The removal by erosion of weak layers underlying more competent layers.
Weathering	In general terms, alteration of a material or mass due to the exposure to certain physical or chemical conditions.
Biological …	Weathering under the influence of biological agents. This is often regarded as separate from mechanical and biological weathering, or at least separate enough to warrant a type of its own. Biological weathering processes however invariably consist of chemical or mechanical, or a combination of both.
Chemical …	Alteration by chemical processes.
Degree of …	A term describing the amount of alteration that a material or mass has undergone. Also often named weathering intensity.
… delimited	A decay situation in which both erosion and weathering occur, with an imbalance favouring erosion. The slope development is controlled by the prevailing weathering intensity and penetration rates.
… front	The boundary between material or mass altered by weathering, and that as yet unaffected by it. The weathering front penetrates into an exposed material or mass.
Insolation …	Mechanical weathering process in which differential rates and amounts of thermal expansion and contraction in rock and soil forming materials will cause tensile stresses and, ultimately, fracturing within the mass.

… intensity	A term describing the amount of alteration that a material or mass has undergone. Also often named degree of weathering.
… intensity rate	The rate of change of the amount of alteration for a given material or mass control volume.
Mechanical …	Alteration by mechanical processes.
… parameters	Factors that control weathering, of an internal, external, or geotechnical nature: **Internal**: Rock and soil material and mass properties such as porosity, permeability, discontinuities, and material composition. **External**: Parameters related to the weathering environment such as climate, topography, chemistry of weathering solutions, hydrology, and vegetation. **Geotechnical**: Slope design parameters such as aspect, slope angle, height, method of excavation, and drainage measures.
… penetration	The advancing of the weathering front into a material or mass.
… penetration rate	The rate of advance of the weathering front into a material or mass.
… rate	Although in fact incomplete, this is the usual term for weathering intensity rate.
Susceptibility to …	A term describing the resistance of a material or mass to weathering. A low resistance corresponds with a high weathering susceptibility.
Wetting-drying	Mechanical weathering process with repeated cycles of saturating and drying of a material. Commonly associated with clays, wetting-drying often leads to slaking.
Wind direction	In this thesis, the wind direction is defined as the direction from which the wind blows, as opposed to its heading.

Index

Curriculum Vitae

Marco Huisman was born on August 6, 1972 in Gouderak, the Netherlands. During the period of 1984-1990 he attended the Coornhert Gymnasium in Gouda. From 1990 until 1995 he was a student at the faculty of Mining and Petroleum Engineering of Delft University of Technology, where he graduated cum laude with a specialisation in Engineering Geology.

From 1995-1999, he was employed by WL|Delft Hydraulics as s consultant in the Division of Dredging and Tunnelling Technology. From 2000-2005, he was employed as assistant professor by the International Institute for Geo-information Science and Earth Observation (ITC), in the Section Engineering Geology and Division Earth Systems Analysis. His current employer is Bluewater Energy Services B.V., where he works as geotechnical engineer for the Section Civil & Subsea. The research of which this thesis is the result was primarily carried out during his employment by ITC.

Since 2003 Marco Huisman acts as the representative of the National Group of the Netherlands of the ISRM (International Society for Rock Mechanics) and as board member of the Ingeokring, the Dutch section of the IAEG (International Association for Engineering Geology and the Environment) and engineering geology section of the KNGMG, the Royal Geological and Mining Society of the Netherlands.

Marco Huisman currently lives in Vlaardingen and is married to Lisa Parman.